CONTROLLING THE INTERFACES OF SUPRAMOLECULAR HYDROGELS FOR TISSUE CULTURE APPLICATION

EFSTRATIOS D. SITSANIDIS

A thesis submitted in partial fulfilment of the requirements of the University of Kent and the University of Greenwich for the Degree of Doctor of Philosophy

July 2018

DECLARATION

"I certify that this work has not been accepted in substance for any degree, and is not concurrently being submitted for any degree other than that of Doctor of Philosophy being studied at the Universities of Greenwich and Kent. I also declare that this work is the result of my own investigations except where otherwise identified by references and that I have not plagiarised the work of others"

SIGNED BY STUDENT: 

SIGNED BY SUPERVISOR: 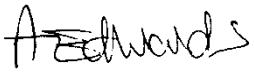

ACKNOWLEDGEMENTS

First and foremost, I would like to express my special appreciation to my supervisors, Dr Alison Edwards and Dr Andrew Hall for the opportunity they gave me to work on this project. Alison and Andy not only taught me scientific discipline but helped me become an independent researcher. I would like to thank them for their guidance, academic and moral support through this challenging three-year journey.

I would especially like to thank our collaborators in Diamond Light Source, Dr Giuliano Siligardi, Dr Tamas Javorfi and Dr Rohanah Hussain for all their insightful comments, training and support for the SRCD spectroscopy work.

My appreciation goes to the Universities of Kent and Greenwich for providing me the facilities for TEM, SEM, NMR, MS, CD and rheology experiments. Thank you to Dr Andrew Hurt, Mr Mark Allen, Dr Iain Goodall, Dr Bruce Alexander and Dr Jennifer Hiscock for their assistance and for being valuable advisors. I would especially like to express my gratitude to the University of Kent for offering me the Kent's 50th anniversary scholarship and supported me financially during my studies.

I am grateful to all of those whom I had the pleasure to work with at the Chemistry and Drug Delivery group (Dr Colin Moore, Dr Stefania Lettieri, Dr Giorgia Giovanini, Dr Filip Kunc, Dr Sounya Sasi) and especially Dr Carmen Piras for the collaborative hydrogel and CD work and Mrs Voula Kasapidou for the training, assistance, guidance and time she spent on the biocompatibility studies. I would like to thank also visiting students Violette, Holly, Carla and Alexandra for their hard work and valuable help on the synthesis and preparation of hydrogels.

A special thanks to my beloved parents and my sister's family whose love I always carry with me. I would like to thank them for their unconditional support and patience in whatever I pursue.

Last but not least, there are no words to express my love to my dear friend Agnie who taught me to be strong and enjoy the little things in life. It's so unfair she left us so soon. What a gentle soul and wonderful lady, such a fighter and full of positive thoughts. Knowing Agnie made me a better person. Thank you is not enough.

ABSTRACT

The research work undertaken focused on the preparation and characterization of novel low molecular weight (LMW) hydrogels as functional biomaterials for tissue culture applications. To achieve this objective, new LMW compounds (as potential hydrogelators) were synthesized bearing a galactosamine or glucosamine moiety. The incorporation of carbohydrates was anticipated to confer molecular recognition of certain biomolecules upon the formed supramolecular gels and therefore act as potential anchor sites for cell-binding. The synthesis was based on short synthetic routes and low-cost starting materials were used as supplied. The target compounds were not confined only to those containing carbohydrates. A cinnamoyl-protected diphenylalanine hydrogelator was prepared and the properties of its corresponding hydrogel were investigated.

Understanding the self-assembly mechanisms of supramolecular hydrogels is fundamental for the preparation and application of these novel materials. Therefore, a variety of techniques were employed for assessing and characterisation of gelation and to determine the configurational alignment of the formed fibres within the three-dimensional network of the gels. Specifically, the preparation and handling of hydrogels were optimized leading to robust gelation protocols. TEM and SEM microscopy revealed the size, shape and perplexing patterns of the fibres. XRD measurements verified polymorphism whereas rheology studies confirmed the viscoelastic properties of the gels. Non-covalent intermolecular interactions are the driving forces of the molecular packing, leading to higher order architectures. The combined spectroscopic analysis of the prepared hydrogels (by NMR, IR, UV-vis, CD) was advantageous to explore the nature of such interactions and allow the identification of key functional groups which actively participated in the self-assembly process. As a result of the CD work undertaken, utilisation of a synchrotron facility led to the establishment of a protocol for the evaluation of LMW hydrogels by SRCD spectroscopy, which was recently published. Finally, a preliminary biocompatibility study was undertaken to assess the toxicity of the hydrogels upon brain cancer cells.

This project therefore required an interdisciplinary approach which involved the synthesis of a number of LMW compounds where some were found to be hydrogelators. This led to the preparation of their corresponding hydrogels and the study of their microscopic/macroscopic properties for the development of novel biocompatible materials suitable for tissue culture applications.

CONTENTS

2. SYNTHESIS OF LMW HYDROGELATORS

3. CHARACTERIZATION OF LMW HYDROGELS

5. BIOCOMPATIBILITY STUDIES OF LMW HYDROGELS

6.CONCLUSIONS AND FUTURE WORK

***Supplementary information is provided in the appendix.**

LIST OF FIGURES

Chapter 1

Chapter 2

Chapter 5

LIST OF SCHEMES

Chapter 2

LIST OF TABLES

Chapter 1

Chapter 2

Chapter 3

Chapter 4

Chapter 5

LIST OF ABBREVIATIONS

A.U.: Arbitrary units

Abs: Absorbance

AFM: Atomic force microscopy

Anh: Anhydrous

Boc: *tert*-Butyloxycarbonyl

CB: Circular birefringence

CD: Circular dichroism

Cin: Cinnamic

DCM: Dichloromethane

DIC: *N, N'*-diisopropylcarbodiimide

DIPEA: *N,N*-Diisopropylethylamine

DMEM: Dulbecco's Modified Eagle Medium

DMF: Dimethylformamide

DMSO: Dimethyl sulfoxide

DPBS: Dulbecco's Phosphate Buffered Saline

DSC: Differential scanning calorimetry

DySA: Dynamic self-assembly

EA: Ethyl acetate

ECM: Extracellular matrix

EDC: *N*-(3-Dimethylaminopropyl)-*N'*-ethylcarbodiimide hydrochloride

Eq: Equivalents

ESA: Equilibrium self-assembly

EthD-1: Ethidium homodimer-1

Fmoc: Fluorenylmethyloxycarbonyl

FT: Furrier transform

GalNH: Galactosamine

GBM: Glioblastoma multiforme

GlcNH: Glucosamine

Hex: Hexane

HOAT: 1-hydroxy-7-azabenzotriazole

HOMO: Highest occupied molecular orbital

HPLC: High performance liquid chromatography

HR-MS: High resolution Mass spectroscopy

HV: High voltage

Ind: Indole

IR: Infrared

LB: Linear birefringence

LCPL: Left circularly polarized light

LD: Linear dichroism

LMW: Low molecular weight

LUMO: Lowest unoccupied molecular orbital

M.p: Melting point

MGC: Minimum gelation concentration

MTS: 3-(4,5-dimethylthiazol-2-yl)-5-(3-carboxymethoxyphenyl)-2-(4-sulfophenyl)-2H-tetrazolium

NHS: *N*-Hydroxysuccinimide

NMR: Nuclear magnetic resonance

OSu: Hydroxy-succinimide

PA: Peptide amphiphiles

PBS: Phosphate-buffered saline

PIFE: Primary inner filter effect

PMT: Photomultiplier tube

RCPL: Right circularly polarized light

R_f: Retention factor

Rt: room temperature

SEM: Scanning electron microscopy

SFM: Scanning force microscopy

SIFE: Secondary inner filter effect

SR: Synchrotron radiation

TBAF: tetrabutylammonium fluoride

TBTU: *O*-(Benzotriazol-1-yl)-*N*,*N*,*N*′,*N*′-tetramethyluronium tetrafluoroborate

*t*Bu: *tert*-butyl

TEM: Transmission electron microscopy

TFA: Trifluoroacetic acid

THF: tetrahydrofuran

TLC: Thin layer chromatography

UV: Ultra violet

XRD: X-ray diffraction

1. INTRODUCTION

1.1 Functionality and classification of gels

In Nature, higher order architectures stem from the hierarchical organization of simpler biomolecules (building blocks), namely nucleic acids, amino acids, sugars and lipids. Such supramolecular systems have a direct impact on emergence, homeostasis and advancement of life. The structure-functionality relationships of the self-assembled biomolecular building blocks has inspired the development of a plethora of materials with potential applications in different fields. Indeed, in recent years, the development of soft materials with desirable physical properties and tuneable characteristics has gained much attention, due to their use in areas such as catalysis,[1,2] sensing,[3-5] tissue engineering,[6-10] cell culture,[11-14] wound healing[15-18] and drug delivery.[19-23]As a result, different types of gel have been prepared, of which, supramolecular hydrogels have gained increased prominence.

Gelator molecules can have a range of applications due to their ability to self-assemble into aggregates, forming fibres which, when entangled, yield viscoelastic, semi-solid materials (gels). These heterogeneous systems consist of a solvent (liquid phase-major component) immobilized in an elastic, cross-linked, three-dimensional, fibrous network (solid phase-minor component). Depending upon their origin, composition, mode of self-assembly and the medium used, gels are classified in different categories (Figure 1.1).

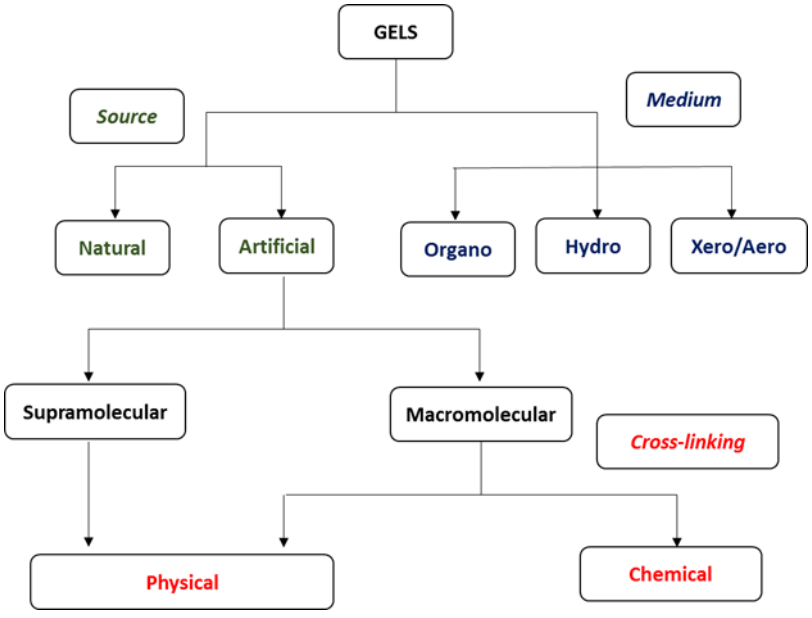

Figure 1.1 Classification of gels.

Based on the type of intermolecular interactions involved during the gelation process, gels are classified as physical (natural) or chemical (artificial). Supramolecular gels are physical gels which originate from the self-assembly of the gelator molecules through weak, intermolecular, non-covalent interactions. Hydrogen bonding, π-π stacking, donor-acceptor interactions, metal coordination, van der Waals forces and solvophobic effects, render a highly ordered molecular arrangement in such systems, leading to the formation of a three-dimensional fibrous network, capable of encapsulating and immobilizing solvent molecules. Conversely, polymeric gels are chemical gels which derive from a randomly cross-linked fibrous matrix formed through the development of strong covalent chemical bonds.[24] The tuneable characteristics of supramolecular gels are related to the chemical structure of their building blocks. The chemical modification of the gelator molecules governs the types of intermolecular forces involved during the gelation process, facilitating both the preparation and handling of such materials.

Depending on the solvent used, these materials can be classified as hydrogels[25] and organogels[26] while xerogels[27] and aerogels[28–30] derive from the previous two when processed under certain conditions. Hydrogels consist of a large amount of water encapsulated within a fibrous network. They have been used extensively for cell culture, tissue engineering and drug delivery applications. In organogels, the dispersion medium is an organic solvent. Due to their reversible nature, from free-flowing liquids to non-flowing materials, they are suitable for applications where on-demand flow is desirable (cosmetics, paints and inks).[26] Despite the high toxicity of organic solvents, there are cases where organogels have been used for drug delivery applications, in which the pharmacophore is administered via transdermal, oral and parenteral routes.[23] As reported by Miravet *et al.*, there are thermodynamic differences between organogels and hydrogels on the basis of gel solubilization. Although gelation is enthalpy driven within an organic solvent, in water the driving force of the hydrogelators self-assembly is entropic.[31]

Xerogels are obtained by evaporation of hydrogels or organogels and are widely used in adsorption and separation technologies. What is intriguing is that different preparation methods have a direct impact on their absorption capacity, surface area, pore size and volume.[32] Aerogels are solids derived from organogels or hydrogels after evaporation of their solvent under supercritical conditions. As reported by Shen *et al.*, due to their bulk properties, transitional density and enthalpy differences from liquids and gases, they are defined as a "state of matter" rather than functional materials.[29] Their high porosity, low

density, large surface area, low conductivity and high optical transparency make them suitable for use in sensing, acoustics, as thermal insulators, absorbents, catalytic systems, electronic devices and drug delivery systems.[28]

The current research work focuses on the design and synthesis of novel LMW gelators for the preparation of potential biocompatible hydrogels for tissue culture applications. Different classes of soft materials are described in the following sections with emphasis on LMW supramolecular gels.

1.2 Triggering gelation: self-assembly, non-covalent interactions and thermodynamics

LMW gelators self-assemble into aggregates in a hierarchical manner, leading to the formation of highly ordered architectures. This dynamic process is affected by the structural characteristics of the building blocks and by the nature of the gelation trigger. Certain functional groups and solvophobic effects, are responsible for the development of non-covalent forces which orientate the spatial arrangement of LMW gelators, determine the configuration and conformation of the formed supramolecular nanostructures and define their macroscopic properties.

Understanding the mechanisms and driving forces which shape the structural features of the fibrous network in supramolecular gels (thickness, length, branching of fibres), is essential in terms of controlling their properties. For example, the entanglement and branching of fibres determine the elasticity and coherence of supramolecular systems, while their stability, responsiveness and host-guest interactions are affected by energy transactions and the formation of either thermodynamically or kinetically favoured assemblies. As mentioned by Liu *et al*., the formation of a fibrous network in supramolecular systems should be approached beyond the molecular level, in which molecules arrange themselves via weak cohesive interactions. Therefore, its formation should be examined via the crystallization process which consists of a nucleation-fibre growth mechanism.[33]

Fibres originate form nucleation centres and their branching intensity dictates the rheological properties of the gels. As described by Liu *et al*. in the case of spherulitic fibre formation, fibres originate from spherulite centres and, as they grow, they penetrate to neighboring spherulites.[33] There are no clear boundaries and the fibre entanglement is responsible for the stiffness of the gels. In addition, the nucleation rate can be controlled by its thermodynamic driving force, in this case supersaturation and rate of cooling. Interestingly, by lowering the

thermodynamic driving force either *via* temperature control or the use of suitable additives, a small number of spherulites will be formed in a certain volume. This will create a coherent network of fibres, responsible for the elastic properties of the formed material. However, a lower driving force will lead to a lower fibre mass which does not support elasticity. Therefore, there should be an optimal thermodynamic driving force to combine these two opposite effects and yield a gel with the desirable elasticity.[33]

One of the latest reviews on supramolecular materials addresses the properties of LMW gels in relation to the modes of self-assembly.[34] Based on their thermodynamic profile, this process is classified either as an equilibrium self-assembly (ESA)[35] or as a non-equilibrium or dynamic self-assembly (DySA) .[36] ESA leads to stable nanostructures at lower energy states; no energy flow is observed (equilibrium) and the systems are characterized by a maximum entropic factor. DySA leads to the formation of a three-dimensional matrix at an energy state far from equilibrium, which is maintained by a supply of energy.

At an equilibrium state, the building blocks are organized into structures corresponding to the minimum energy state of a thermodynamic potential, such as the Gibbs free energy (G) ($G=H-TS$) (H is enthalpy and S is entropy) or the Helmholtz free energy (F) ($F=U-TS$) (U is the internal energy) accordingly. These potentials are determined by certain parameters which are kept constant during the process. For instance, when temperature (T), pressure (P) and number of molecules (N) are kept constant (isothermal, isobaric changes), then the building blocks are organized in structures corresponding to the minimum Gibbs free energy. In the case where the temperature (T), volume of the system (V) and number of molecules (N) are kept constant, then the formed supramolecular nanostructure corresponds to the minimum of Helmholtz free energy. For both cases, a negative Gibbs free energy ($\Delta G<0$) and negative Helmholtz energy ($\Delta F<0$) not only characterize the minimum energy state of the systems, but also determine the spontaneity of the self-assembly process.[35] Interestingly, such a process could be driven either by enthalpy ($\Delta H <0$ or $\Delta U<0$, $\sim\Delta S=0$) or entropy ($\Delta S>0$, $\Delta H =0$ or $\Delta U =0$) or both.

The DySA process is mainly observed in biological systems which can adapt the spatial organization of their supramolecular nanostructures according to external stimuli. From a thermodynamic perspective, such behaviour means that these metastable molecular arrangements depend on an external supply of energy. An interesting example, reported by Stupp *et al*.,[37] demonstrates that the energy landscapes of self-assembly and the functions of

supramolecular systems are linked together. In their work, they described the self-assembly of a peptide amphiphile which consists of β-sheet-domains (held together by H-bonds) and charged residues which promote electrostatic repulsion forces. Depending on intermolecular repulsion, different metastable assemblies were formed. The thermodynamic assembly promotes cell adhesion and thus cell survival, while the metastable product interferes with the adhesion mechanism and can lead to death. At low intermolecular repulsion, long fibres with β-sheets were thermodynamically favoured, whereas monodisperse shorter fibres represented a metastable state. At higher intermolecular repulsion forces, the thermodynamic product and the kinetically trapped assembly were separated by an energy barrier of 171 kJ mol^{-1} (Figure 1.2).[37] Additionally, Adams and co-workers in their review focused on the importance of self-assembly to control the properties of LMW gels. They describe that the process of gelation itself could follow different transitional pathways, depending on the applied trigger (heating-cooling, solvent change, pH changes, use of enzymes) and can be characterized as a kinetically trapped state rather than a thermodynamic minimum.[38]

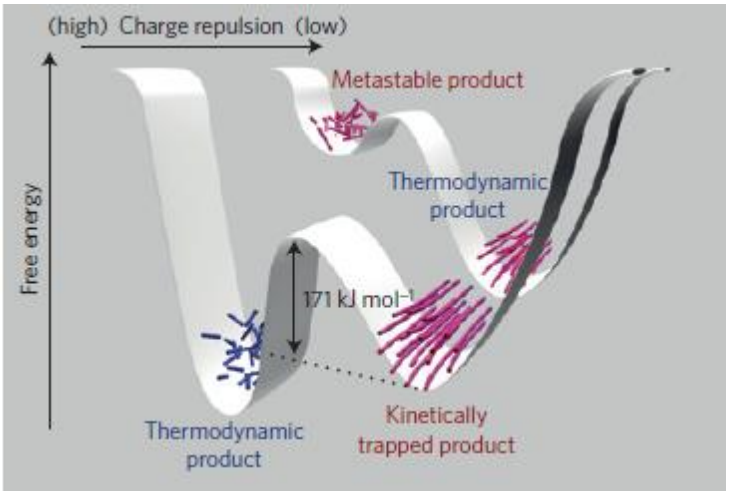

Figure 1.2 Free energy landscapes of peptide amphiphile assemblies under high (front) and low (back) charge repulsion between peptide amphiphile building blocks.[37]

In most cases, LMW gelators are amphiphiles and their gelation property is influenced by the interactions of solvent molecules with the solvophilic and solvophobic moieties of the supramolecular formed networks. A model representing gelator molecules as prisms with solvophobic and solvophilic faces was described by Ulijn and Tuttle, so as to investigate the self-assembly of LMW amphiphiles.[39] Based on the thermodynamic nature of the gels, the gel state could be either a kinetically trapped metastable state or a thermodynamic minimum. Both cases have been observed. The gel-to-crystal transition is akin to the first scenario and

is based on the high number of stabilizing forces in crystals compared to those present in the gel state. On the contrary, a preferential conformation of the fibres, due to the amphiphilic nature of their building blocks, can lead to thermodynamically stable states, corresponding to formations such as wormlike micelles (Figure 1.3). Their model showed that, depending on the specific characteristics of the supramolecular structure and the balance between solvophilicity and solvophobicity, both the gel state and crystal formation can represent a thermodynamic minimum.

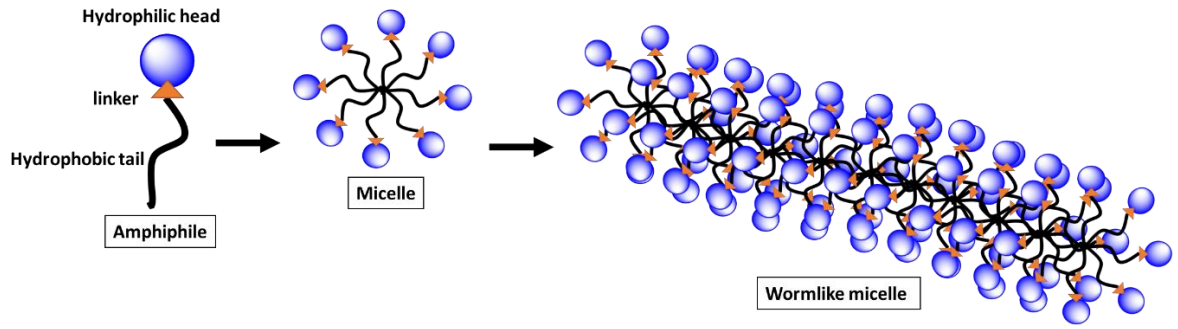

Figure 1.3 Wormlike micelles.

The effects of aromatic-aromatic interactions and other non-covalent forces on chemical and biological recognition, as reviewed by Diederich and co-workers, illustrate how such weak forces dictate the thermodynamics of the formed supramolecular systems.[40] *In silico* studies revealed the most stable configurations among functional groups and chemical moieties were those participating in arene-arene, perfluoroarene-arene, sulfur-arene complexes and in H-bonding and ion interactions with π systems.

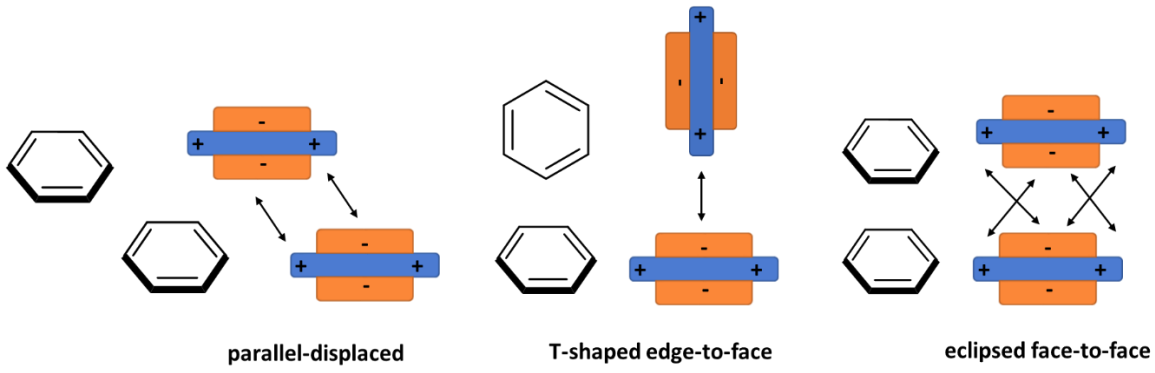

Figure 1.4 Benzene dimer interaction geometries.

Benzene dimers were used as a simple model for the investigation of aromatic ring interaction geometries, such as parallel-displaced, T-shaped edge-to-face and eclipsed face-

to-face (Figure 1.4). These are highly affected by the presence of heteroatoms within the rings since they promote their superimposition due to the introduction of charge polarization (δ+ and δ-) and through the presence of substituents with an electron donating or electron withdrawing effect.

C-H···π interactions are observed between non-aromatic moieties and aromatic rings. These weak forces contribute to the overall protein stability, the recognition and affinity of substrates to binding sites, reaction stereoselectivity and the conformation of supramolecular systems. As described by Martin *et.al.*, C-H···π contacts were found to be crucial for the chiral recognition process in host-guest systems. Their studies towards the quantification of these weak forces revealed which hydrogen atom of their host model participated in the interaction with the aromatic ring of the guest molecules. In addition, the contribution of such a single interaction to the overall chiral recognition was estimated to be approximately 70% of the whole enantioselection process.[41] Their main characteristic is a large charge dispersion and a weak electrostatic contribution which distinguishes C-H···π bonds from the classical H-bonds such as O-H···π and N-H···π[40] (Figure 1.5).

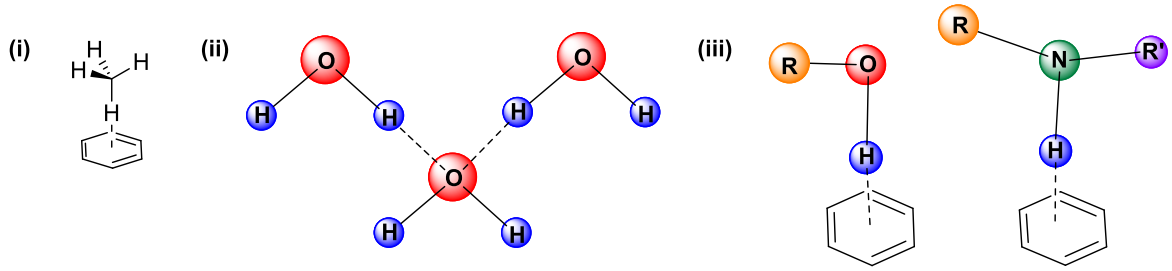

Figure 1.5 Schematic depiction of hydrogen bonding: (i) C-H···π (ii) O-H···π (iii) N-H···π.

Sol-gel phase transitions, require a negative Gibbs free energy ($\Delta G = \Delta H - T\Delta S$). Several physical and chemical methods, such as heating, sonication, modulations of ionic strength, changing pH, redox reactions, *etc.*, can trigger gelation by decreasing or increasing, respectively, the enthalpy and/ or entropy of a system (Table 1.1). As reported by Smith, in the case of physical gels, the mode of self-assembly is a rather hierarchical process, comprising certain steps.[42] Initially, non-covalent intermolecular interactions cause molecules to form aggregates, known as fibrils, which then assemble into fibres (nanoscale bundles). Finally, a higher ordered three-dimensional network emerges from the interaction and entanglement of these fibres, ultimately yielding a self-supporting gel (Figure 1.6).

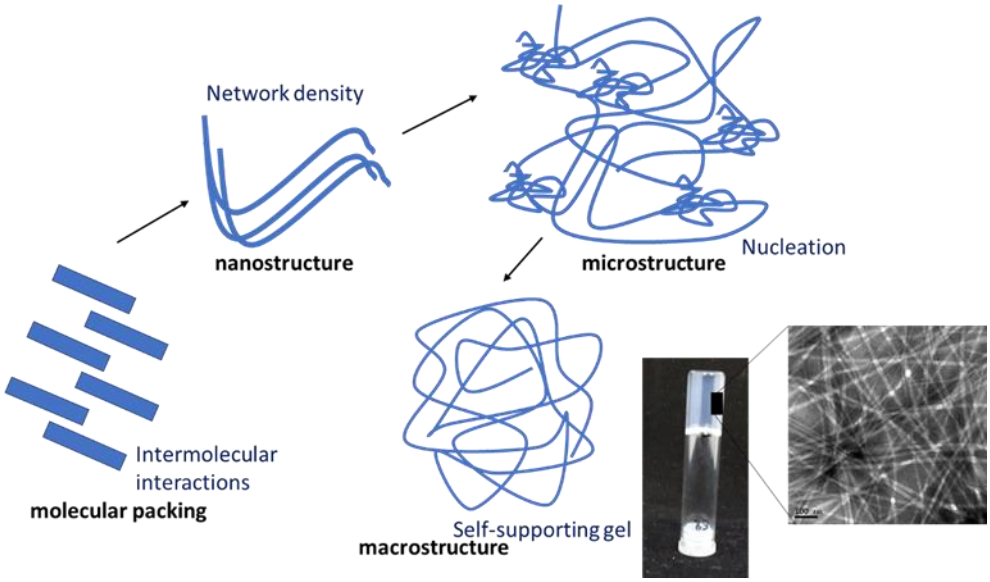

Figure 1.6 Schematic representation of self-assembly steps.

Table 1.1 Gelation triggers and outcomes.

Gelation Trigger	Outcome
Sonication	Favours dissolution and dispersion of undissolved molecules
Heating/cooling cycles	Heating induces solubilization whereas cooling promotes self-assembly
Solvent switch	An organic solvent solubilizes gelator molecules whereas addition of water promotes gelation
pH change	Promotes reversible protonation/deprotonation of certain functional groups and induces solubilization
Chemical reactions	A precursor molecule (non-gelator) converts to a gelator
Use of enzymes	Gelation process is based on biomimicry

Certain requirements regarding the structural features of the gelator molecules which can lead to the formation of aggregates need to be met. The self-assembly into nanoscale architectures is due to a balanced equilibrium between solubility and insolubility. The gelator molecules must be neither too soluble nor too insoluble. Any modification of their structural characteristics, through the incorporation of certain functional groups and chemical moieties,

shapes their amphiphilic nature which in turns controls the development and orientation of the non-covalent intermolecular interactions.

Heating and/or applying ultrasonic energy favours the solubilisation of the gelator molecules, whereas their self-assembly into aggregates occurs during the cooling/relaxation process. Furthermore, the concentration is also critical for the overall gelation mechanism since there is a certain value below which gelation is not possible (critical gelation concentration). The gelator concentration affects the crystallization process, which in turn influences the entropy of the system. An increased entropy favours the promotion of a higher ordered molecular organization, whereas heating increases the enthalpic factor, favouring the less organized or disordered molecular state. Therefore, the transition temperature (T_{gel}), the temperature at which a solution turns into a gel during cooling or the gel into solution during heating, has a direct impact on the formation of concentration-dependent gels and is one of the basic reported physical parameters.[43]

The stability of hydrophobic interactions and the extent of H-bond formation is highly dependent on temperature. Heating supports gelation, as it solubilizes the gelator molecules; however, it has a direct impact on gel stability, especially for those gels that are thermally reversible. In addition, hydrogels differ in thermodynamic terms from organogels; self-assembly in water is supported by entropy, while in organic solvents, the process is enthalpy driven.[44,45] Although a controlled heating-cooling process represents the main gelation trigger technique, increasing the temperature of an already formed gel could induce either its solubilisation or, at the other extreme, its precipitation due to syneresis, as reported by Xu *et al*.[46]

Alternatively, sonication helps the dissolution and dispersion of undissolved molecules, while in some cases it can also rearrange the supramolecular architecture. Sonication can result in the breaking of H-bonds and π-π stacking interactions observed in aggregates. This process depends on the chemical features of the gelator molecules and the solvent used. As reported by Gu *et al*., treatment with ultrasound accelerated the gelation process and induced the formation of a three-dimensional network of an L-lysine based hydrogelator.[47] Although treatment with ultrasound favours the formation of fibrils, there are cases where it has been reported to cause precipitation.[48]

Solvent plays a crucial role in the gelation trigger mechanism and the properties of the formed gels. The solvent switch technique is based on the solubilization of the gelator

molecules in an organic solvent followed by the addition of water. Adams and co-workers assessed the effects of a solvent switch technique compared to that of a pH change for a library of dipeptide based gelators.[49] Based on their findings, certain structural features (one of the amino acids is phenylalanine) were observed to govern the ability of the gelator molecules to gel through different gelation triggers. In addition, the type and amount of an organic solvent can have a profound effect on the mechanical strength of a gel as mentioned by Raeburn and co-workers for a Fmoc-protected diphenylalanine based gel prepared by the solvent switch method .[50]

Changing pH is a common chemical method for triggering gelation. The formation of peptide-based hydrogels by this method is mainly attributed to the reversible protonation-deprotonation of the *N*-terminus and *C*-terminus sites of the peptide backbone, in addition to that of any basic and/ or acidic functional groups (side chain). In most cases, the pH is initially adjusted to induce the solubilisation of the gelator molecules in water, while further changes result in their self-assembly through the development of non-covalent interactions. In general, this method is effective and easy to perform as pH can be accurately measured and controlled.

Based on acidity, hydrogels are classified into three main categories, namely those formed at (i) low[51] (ii) physiological[52–54] and (iii) high[55,56] pH. Changes in acidity can affect the strength of H-bonding and the orientation of aromatic-aromatic interactions, resulting in differences in the conformation and robustness of the formed supramolecular nanostructures. This can have a direct impact on the physicochemical and macroscopic properties of the developed materials, such as fluorescence and the shape of the fibres.[57,58] In addition, pH change via a gradual and uniform increase of the proton concentration introduces homogeneity and reproducibility to the mode of aggregation. Such a case was reported by Adams and Donald *et al.*, who managed to gradually change the pH of the gelator solution based on the hydrolysis of glucono-*δ*-lactone to gluconic acid.[59,60]

Chemical reactions are widely used for the formation of polymeric gels. Despite this, the structural modification of the reactant molecules yields novel products, bearing different chemical characteristics and physical properties from the starting materials. Therefore, gelation could be triggered by a chemical reaction of a gelator precursor that will "unmask" the actual gelator molecule. Such an approach could be considered exceptionally useful for the design and preparation of prodrugs that could be part of the higher order supramolecular

systems, from which their controlled release could be generated by a number of stimuli. Even though a plethora of synthetic routes and chemical reactions are available, this specific methodology is not widely applied for the preparation of LMW gels. A simple example of a chemical modification leading to the formation of a hydrogel, was reported by Xu *et al.*, where the hydrolysis of the carboxylic ester **58** generated the free acid **59** (Figure 1.7), with improved solubility in water, leading to a kinetically stable hydrogel over a range of pH values.[61]

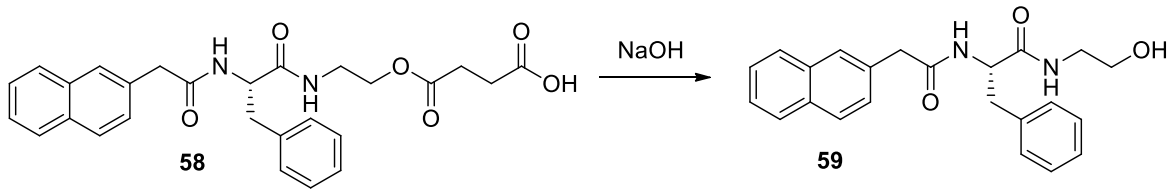

Figure 1.7 Structural modification of a phenylalanine-based ester via hydrolysis reaction.

The structural features of the gelator molecules regulate the type of chemical reactions that can be used. An example of a redox reaction was reported by Nilsson *et al.*, where the reduction of a disulfide bond controlled the self-assembly of a cyclic peptide.[62] Subsequently, photochemical reactions have been utilised for the preparation of hydrogels with potential applications in drug delivery, wound healing and tissue engineering.[63,64] Furthermore, enzymatic reactions have been also used for the formation of hydrogels. The catalytic capacity of proteins in living systems has inspired researchers to mimic nature in their efforts to initiate the self-assembly of precursor molecules when treated by enzymes. For instance, dephosphorylation of **60** by an alkaline phosphatase yielded hydrogelator **61** (Figure 1.8), while Ulijn *et al.* achieved the formation of a peptide-based hydrogel *via* reverse hydrolysis by employing thermolysin.[65,66]

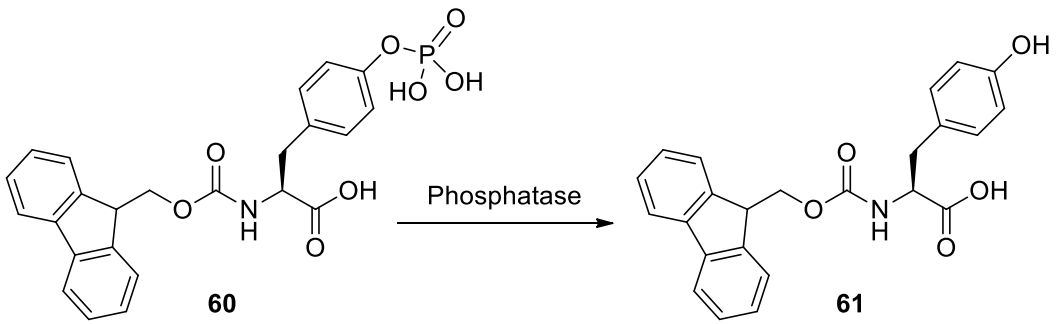

Figure 1.8 Enzymatic dephosphorylation of precursor **60** for the preparation of Fmoc-tyrosine **61**.

The advantages of using enzymes for the formation of hydrogels lies in their structural affinity for the substrates, the formation of desired supramolecular secondary structures and, finally, their accessibility.

1.3 Research overview

Even though dibenzoyl-L-cysteine **1** (Figure 1.9), the first LMW hydrogelator, was synthesized in 1929 by Hoffmann,[67] the characterization of gels by means of physical methods was reported almost 70 years later by Menger *et al*.[68] What was intriguing was the observation of aromatic-aromatic interactions of **1** which induced gelation in water. Since these interactions were present in protein supramolecular scaffolds, attempts to design analogues of such molecules resulted the introduction of biomimicry to the field of gelator synthesis.[69,46]

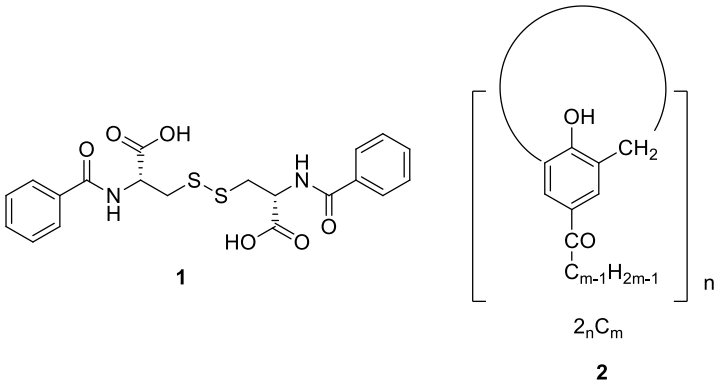

Figure 1.9 Molecular structures of the first LMW hydrogelator **1** and calixarene gelator **2**.

In most cases, the discovery of novel gelator compounds was based on serendipity as researchers working towards different goals noticed molecules forming a gel in a solvent. For instance, calix[8]arene **2** (Figure 1.9), the first macrocyclic gelator, was discovered accidentally during the development of a new synthetic route by Shinkai *et al*.[70]

The development of novel hydrogels and the control of their properties has flourished during the past two decades, as indicated by the growth in published work. Specifically, the work undertaken in this field prior to 2004 was reviewed by Hamilton[25], while Xu addressed the latest advances up to 2016.[71] Furthermore, the elucidation of the macroscopic and physical properties of gels, the studies of their self-assembly mechanisms and the investigation of their structure-functionality relationships, are some of the main aspects presented in recent reviews.[34,72–74]

1.4 Designing gelator building blocks for the preparation of hydrogels

Certain functional groups and chemical moieties are responsible for the gelation properties of the molecular building blocks. In the case of supramolecular gels, it is these structural characteristics that govern the development of non-covalent intermolecular interactions. These promote the gelators' self-assembly and dictate their spatial alignment, resulting a unique supramolecular fibrous matrix. Moreover, it is extremely difficult to accurately identify a gelator *a priori* based on its structural features, as it is hard to evaluate which certain forces between the solvent molecules and the building blocks are effective to trigger the formation of such highy ordered architectures. Despite this, gelation is defined as "a balance" between the crystallization and solubilisation process, suggesting that any hydrophilic and hydrophobic moieties present on the same molecular structure could render them suitable gelator candidates. Therefore, any attempt to design novel, soft, functional materials should be in accordance with the development of intermolecular interactions and the amphiphilic nature of their building blocks.[25,71]

Based on their structural features, LMW gelators can be classified into five main families of compounds: (i) small organic molecules, (ii) coordination complexes, (iii) nucleobase derivatives, (iv) amino acid/peptide-based gelators, and (v) carbohydrate derivatives. Each family of compounds can be further divided into subcategories. From the literature, it is evident that by combining structures from different families, more sophisticated gelators can be discovered, leading to novel materials with interesting properties.[71]

Additionally, multicomponent LMW gels have recently gained an increased prominence, due to the greater degree of information they contain compared to single gelator systems and the efforts to control the molecular alignment of their building blocks.[74] Depending on the gelation ability of each component, these materials constitute three different classes, as defined by Buerkle and Rowan.[75] Specifically, the first class consists of two components, both necessary for triggering gelation when mixed but unable to form gels on their own, the second consists of two components capable of gelation independently and the third class refers to the mixing of a gelator and a non-gelling additive.

Examples of LMW gelators that belong to different families are described briefly below, however those bearing carbohydrate and peptide moieties are discussed in greater detail in subsequent sections.

1.5 Gels based on small organic molecules

A recent example of a LMW hydrogel, originating from the family of small organic molecules, derived from bolaamphiphile **3** (Figure 1.10). As reported by Liu *et al.*, a self - assembled nano-helix is formed when **3** gels water. The hydrogel is described as metastable and shows selective responsiveness towards amino acids and nucleobases.[76] With reference to the work of Dastidar *et al.* on supramolecular hydrogels and their efforts to synthesize structurally related pyridyl urea-based hydrogelators, it is evident how structure influences gelation. Based on their findings, although the *para* urea-substituted pyridine **4** is a successful hydrogelator, the *meta* and *ortho* derivatives **5** and **6** (Figure 1.10) do not gel water.[77] Structural modifications of the building blocks can thus affect the properties of the gels. In addition, introducing certain functional groups to the original structure of the building blocks can drastically alter their properties. This is evident when the organogelator 1,3(*R*):2,4(*S*)-dibenzylidene-D-sorbitol (DBS) **7** is converted to a hydrogelator through the introduction of hydrophilic groups. *In silico* studies of **7** and its derivatives DBS-COOH **8** and DBS-$CONHNH_2$ **9** (Figure 1.10) showcased that the carboxylate analogue is the strongest hydrogelator. The simulations revealed that although intermolecular hydrogen bonds (H-bonds) are observed between **7**, **8** and **9** as pure substances, in the presence of water they are partially replaced by intramolecular ones leading to more rigid and fixed molecular conformations.[78]

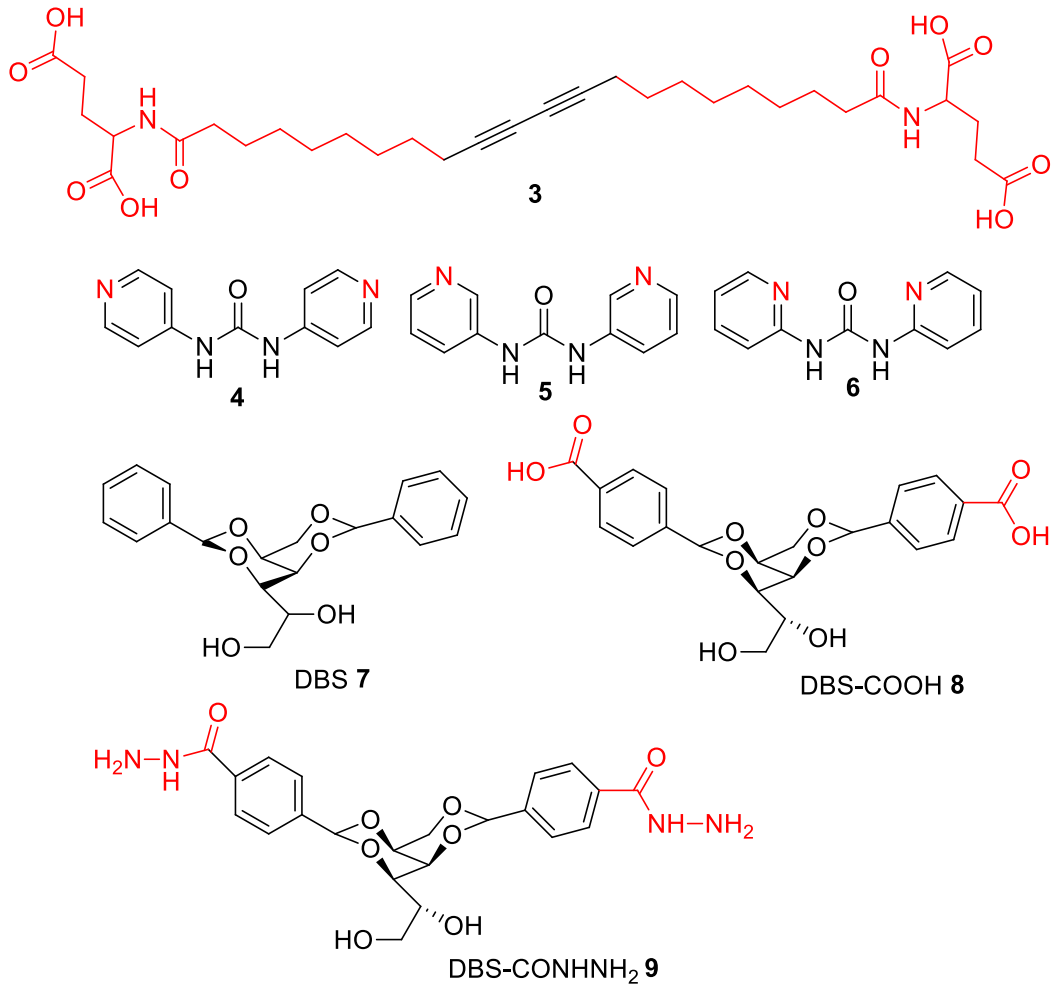

Figure 1.10 Chemical structures of small organic molecular building blocks, used for the preparation of LMW gels.

Calixarenes and their derivatives represent the third generation of supramolecular host compounds, with applications as drug delivery systems, due to their stability, sensitivity, targeting and high loading efficiency. These macrocyclic oligomers, based on the hydroxyalkylation of a phenolic moiety and an aldehyde, form hydrophobic cavities able to host small molecules (Figure 1.11). The host-guest complexes arise from reversible hydrophobic interactions which are responsible for the complexation and decomplexation processes.[79] Calixarenes belong to the family of hydrogelators bearing a cavity. Gelation is induced by the presence of certain functional groups on the calixarene scaffold and by adjusting pH values (*i.e.* deprotonable COOH and protonable NH_2). Further to this, the presence of specific ions is responsible for an observed guest-induced stimulus responsive behavior of these gels.[71]

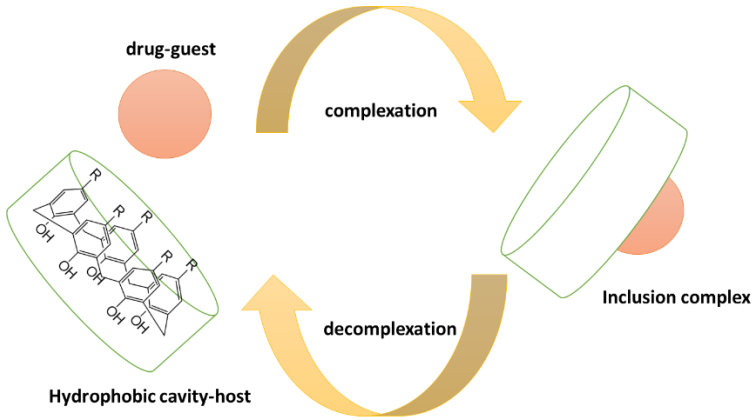

Figure 1.11 Schematic representation of an inclusion complex formation. Complexation and decomplexation are based on reversible host-guest interactions which are responsible for a guest-induced stimulus responsive behavior of the gels.

1.6 Gels based on coordination complexes

The incorporation of metals into soft materials serves a dual role. Their type (valence, size) defines the electron donor-acceptor interactions with the organic ligands and the properties of the formed metallogels. Based on the nature of the organic ligands, these gelators are further classified as compounds bearing carboxylic, thiol or phosphate groups, those consisting of nitrogen atoms as electron donors and compounds consisting of other moieties and functional groups.

Metallogels are materials with interesting properties and are useful for many applications. In a recently reported case, when the carboxamide gelator **10** (Figure 1.12) coordinates with different metals, the formed metallogels can selectively sense different anions. Specifically, copper complexes sense thiocyanate SCN^-, the zinc senses bromide Br^-, nickel can sense cyanide CN^- and di/trivalent iron senses sulfide S^{2-}. When the metallogels bind selectively with the anions, the aggregation-induced fluorescence emission is switched either on or off.[80]

In another example, the naphthalimide (NP)-based organogelator **11** (Figure 1.12) when complexed with cadmium acetate yielded a stimulus-responsive metallogel. While the NP gelator was able to gel organic solvents, it was found that it could also bind with metal ions due to its terpyridine group. The storage (G′) and loss (G″) moduli of the organogels were lower compared to that of the metallogel, suggesting that the metal salt enhanced the mechanical strength. Additionally, the metallogel exhibited multiple responsive-properties to chemical (presence of Na_2S) and physical (heat, shearing) stimuli with reversible phase changes.[81]

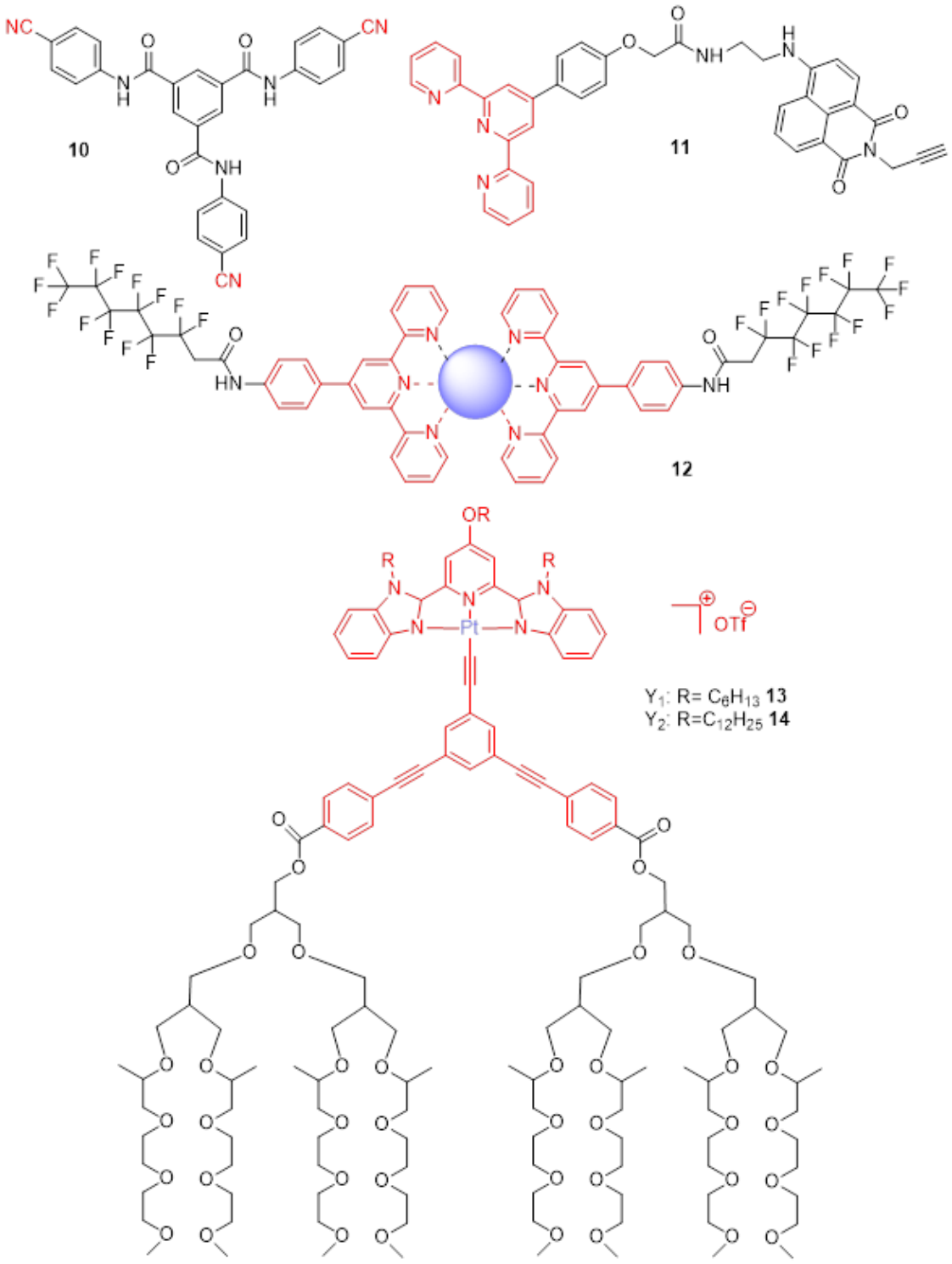

Figure 1.12 Organic ligands and coordination complexes yielding metallogels. Red indicates the binding site of the metal ions.

A similar perfluorinated terpyridine-based gelator **12** (Figure 1.12) yielded supramolecular metallogels when complexed with iron (Fe^{2+}), cobalt (Co^{2+}) and nickel (Ni^{3+}) ions. Fluorine-fluorine interactions were responsible for the lateral assembly of the fibrillar network, while

the gelation process appeared to be counter-anion selective. The formed gels had tuneable mechanical and thermal properties based on the nature of the metal cations. Furthermore, when repeated cycles of stress-strain were applied, the materials exhibited self-healing properties.[82]

Supramolecular metallogels can undergo multiple phase transitions. As reported by Jiang and Yang, the Y-shaped amphiphilic alkynyl-platinum (II) complexes **13** and **14** (Figure 1.12) showcased such transitions triggered by heat. Specifically, solution-to-metallogel-to-solid transitions were observed for **13** and metallogel (I)-to-metallogel (II)-to-solid transitions for **14**. Metallogel (I) appeared to be stable both at low and room temperature, whereas metallogel (II) was stable up to 40 °C.[83]

The controlled release and delivery of confined molecules in gels is greatly dependent on the molecules conformational changes. Such an example was reported by Sheikhi *et al.*, regarding the controlled trapping of biomacromolecules within metallogels.[84] Dextran was used as a model macromolecule, which was entrapped into a zirconium-cellulose based metallogel. According to their findings, dextran's conformation could be manipulated by the introduction of cellulose nanocrystals which competed with dextran in binding zirconium.

1.7 Gels based on nucleobase derivatives

Supramolecular gels originating from nucleobase, nucleoside and nucleotide derivatives have been reviewed recently by Peters and Davis.[85] These bioinspired materials are of particular interest due to their biocompatibility and stimuli-responsive properties. Xu *et al.* has also reported that conjugates of saccharides, amino acids and nucleobases yielded mammalian cell compatible hydrogels.[86,87] Nucleobases are heterocyclic compounds containing nitrogen atoms acting as hydrogen bond donor-acceptor sites. According to their chemical structure, they are classified as purines (adenine (A) **15**, guanine (G) **16**) and pyrimidines (uracil (U) **17**, thymine (T) **18**, cytosine (C) **19**) (Figure 1.13). Non-covalent interactions between the base pairs of DNA (base complementarity) are responsible for the formation of the double helix structure. In addition, the phosphorylated hexoses can participate in electrostatic interactions, providing multiple ways both for the spatial alignment of the building blocks and molecular recognition. These weak forces, and specifically the formation of H-bonds, represent the driving force for the self-assembly mechanism observed in this type of gels.

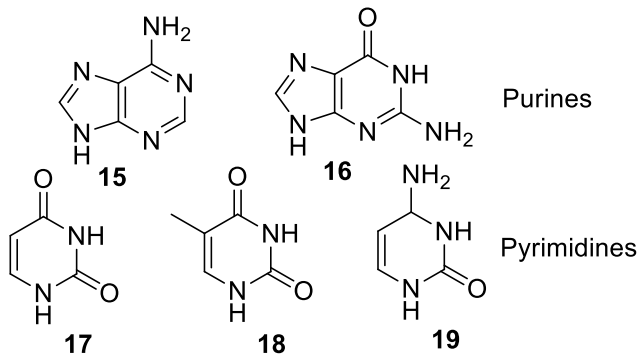

Figure 1.13 Chemical structures of purine and pyrimidine nucleobases.

As stated by Peters and Davis, some of the binding motifs observed between nucleobases are Watson-Crick, reverse Watson-Crick, Hoogsteen and the base triples (Figure 1.14)

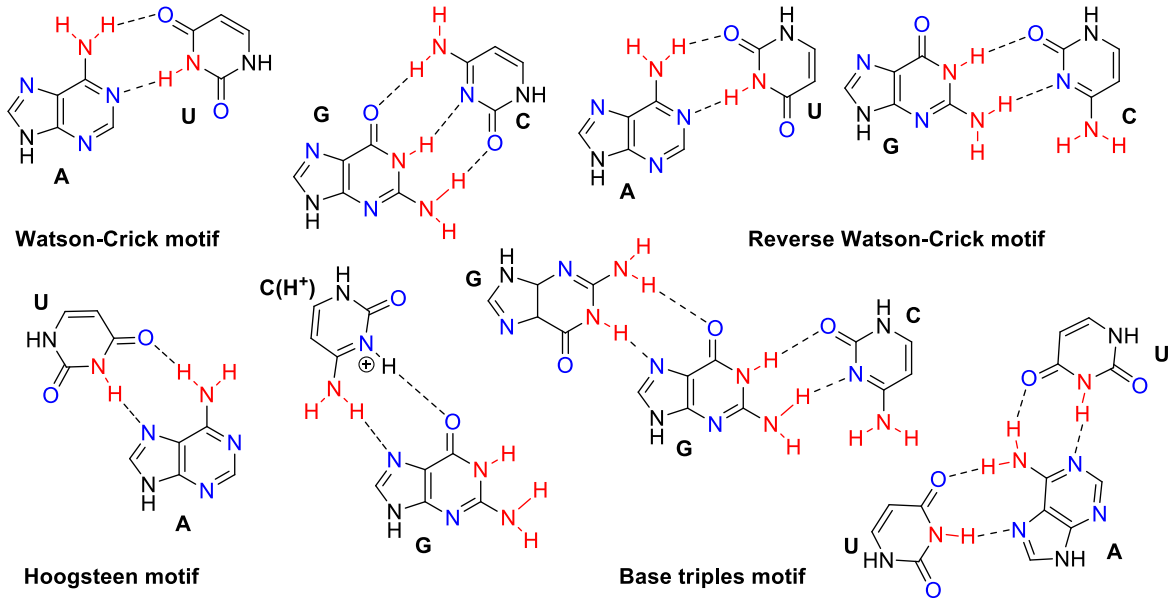

Figure 1.14 Hydrogen binding motifs of base pairs. Red indicates H-donors and blue indicates H-acceptors.

Derivatization of nucleobases, nucleosides and nucleotides by addition of lipophilic moieties introduces the necessary degree of hydrophobicity required to induce gelation. Marlow *et al.* prepared a series of novel cytosine based gelators **20a-20d** by the selective acylation of cytosine at *N*-4-position with fatty acids (Figure 1.15). These compounds gelled two binary solvent systems, namely water: DMSO and water: ethanol, at different solvent volume fractions. Fluorescein molecules were loaded within the gel matrices and release studies showcased their potential use as drug delivery vehicles.[88]

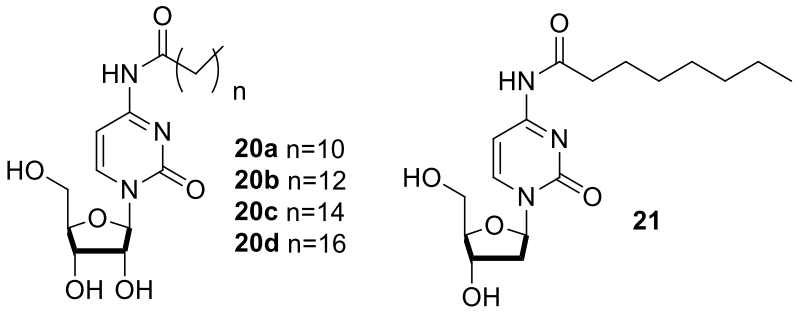

Figure 1.15 Chemical structures of LMW cytosine based gelators.

In their effort to further broaden the gel's ability for drug delivery applications, Marlow and co-workers modified the structure of cytosine based gelators **20a-20d** so as to avoid the need for ethanol. Indeed, among the 2′,3′-dideoxycytidine and 2′-deoxycytidine derivatives prepared, *N*-4-octanoyl 2′-deoxycytidine **21** (Figure 1.15) formed a self-healing hydrogel, stable under relatively high strain.[20] Further to this, gels are often in contact with surfaces of other materials. Studies on gel films prepared from **20b**, revealed that surface properties affected both the self-assembly and the mechanical properties of the gels.[89] Indeed, two surfaces with different hydrophobicity were used as substrates for gel formation while mechanical properties were measured via nanoindentation with AFM. In a recent example, surface-tunable gels were prepared by incorporating various fatty acids at the 3′-O (**23a-23e**) and 3′,5′-O (**22a-22c**) positions of the sugar moiety of thymidine (Figure 1.16).

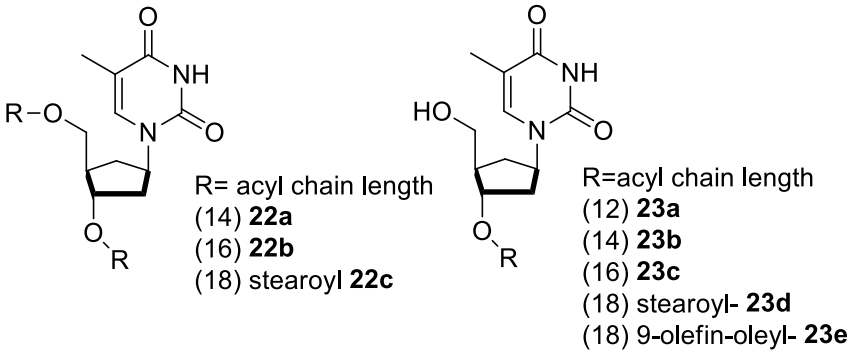

Figure 1.16 Chemical structures of thymidine derivatives.

Interestingly, the surface of the xerogels fabricated from the 3′-O monosubstituted fatty acid gelators **23a-23e** could be tuned to range from highly hydrophobic to hydrophilic depending on the solvent used. The disubstituted analogues **22a-22c**, appeared to be sensitive to the presence of Hg^{2+} ions, with T-Hg-T interactions being observed by NMR and mass analysis (MALDI-TOF).[90]

1.8 Gels based on peptides and amino acid derivatives

Peptide amphiphiles (PA) and derivatized amino acids have been widely used for the development of novel soft materials, due to their inherent biocompatibility and ease of preparation. Solid state synthesis allows the preparation and modification of peptides in a timely and effective manner and in large quantities. The formation of aggregates and their mode of self-assembly is driven by the development of non-covalent interactions, enabling the formation of higher architectures, able to encapsulate solvent molecules. Peptide-based LMW hydrogelators represent simple models for the elucidation of the self-assembly in such systems. The specific building blocks typically yield transparent gels when mixed with water and do not polymerize in the conventional sense as their fibrous network is formed *via* H-bonding, aromatic interactions and hydrophobic effects.[45] Several structural motifs have been reported regarding the nature of the building blocks, revealing how drastically structure affects their secondary organization and determines the functionality of the supramolecular systems they form.[73,91–93]

Depending on their design, three main types of peptide and protein fibrous materials are observed: those based on amyloid-like structures, α-helical assemblies and peptide amphiphiles. Amyloid-like structures arise from small peptide fragments, adopting conformations which lead to *β*-strands. These are then bound together via H-bonds, to form *β*-sheets. In *α*-helical assemblies, H-bonding is mainly observed locally on the backbone of the helical fibrils, while inter-chain interactions are determined by the primary organization of the amino acids. In the case of PAs, the secondary organization is mainly driven by the functional modification of their building blocks. Amphiphilicity leads to rod-like structures and fibrous micelles which derive from the topology of the hydrophobic and hydrophilic moieties present on each molecule.[94]

Aromatic PAs represent one of the major classes of building blocks originating from the structural modification of simple amino acids. Their self-assembly leads to stacking arrangements capable of forming supramolecular nanostructures, such as spheres, worms, sheets, fibres and tubes. Their generic structure consists of four components, namely the *N*- and *C*-terminal segments, the linker component and an aromatic moiety (Figure 1.17).[95]

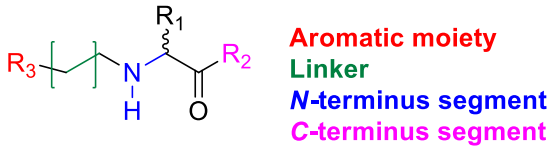

Figure 1.17 Generic structure of an aromatic peptide amphiphile.

The incorporation of different types of aromatic components has resulted a rich family of structurally sophisticated aromatic PAs. Indeed, fluorene, naphthalene, azobenzene, pyrene and phenyl derivatives have been employed for the protection of the free amine group, in an effort to introduce aromaticity. Besides these, the fluorenylmethyloxycarbonyl group (Fmoc-) has been extensively used for the preparation of this type of gelators (Figure 1.18).[96,97]

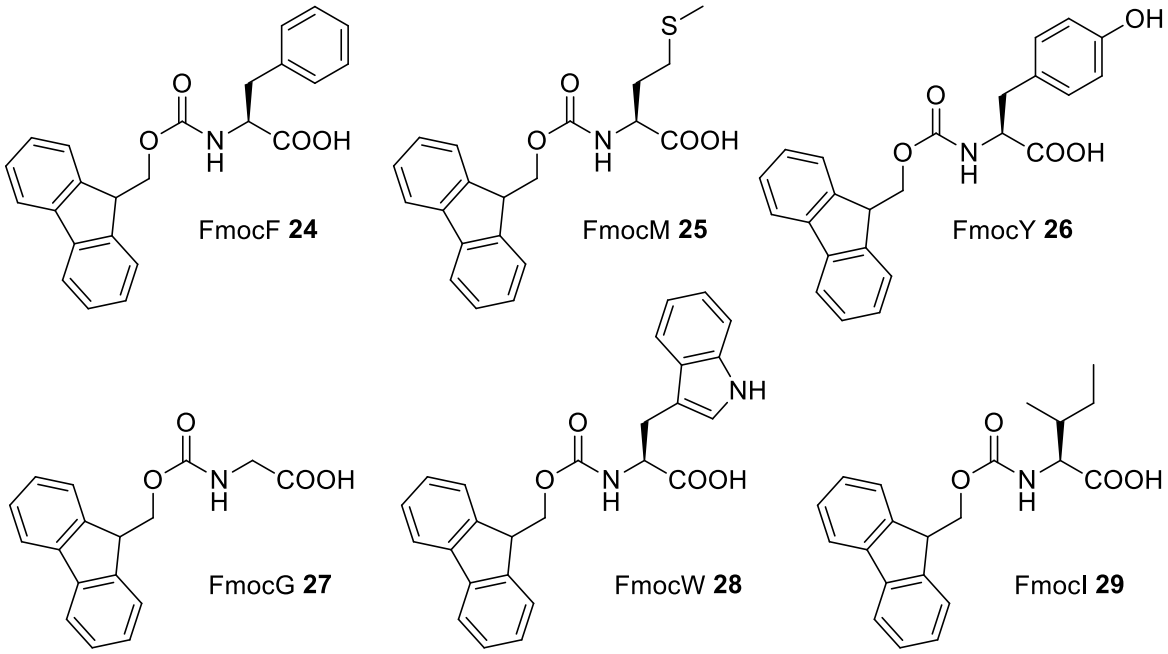

Figure 1.18 Chemical structures of Fmoc-protected amino acids.

Interestingly, each aromatic group facilitates the development of π-π stacking interactions with the assistance of the linker component. The latter contributes to the molecular alignment *via* rotation of its C-C bonds, which determines the spatial orientation of the aromatic moieties.[95] Structurally related amphiphilic phenylalanine derivatives[98] **30-35** (Figure 1.19) have been used as simple gelator models for the elucidation of aromatic interactions. Among these, the cinnamoyl analogue **35** offers an alternative pathway for the rearrangement of the formed fibres due to the reversible *cis/trans*-isomerization, triggered by UV irradiation.

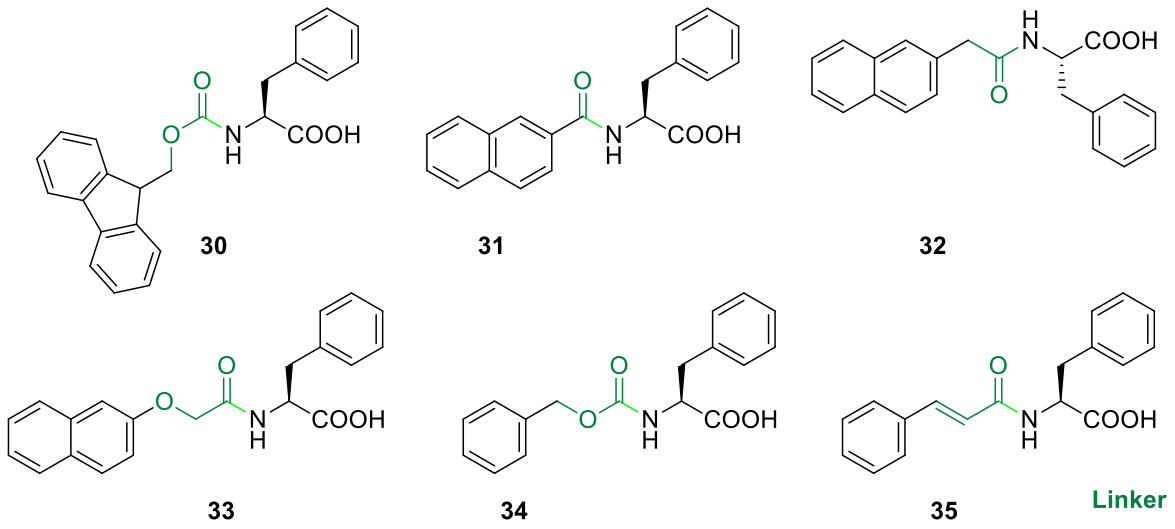

Figure 1.19 Chemical structures of the phenylalanine derivatives.

The number of amino acids in the backbone of the gelator molecules and their sequential order (primary organization) play a fundamental role in the formation of supramolecular nanostructures. They introduce weak inter-chain interactions between the entangled fibres, such as electrostatic, dipole-dipole, Van der Waals interactions and H-bonds. *In silico* studies promoted the design of successful tripeptide based gelators, originating from the enormous sequential space of the 20 natural amino acids.[49,99–101] In addition, tetra-peptide based hydrogelators confirmed the importance of primary sequence on the self-assembly process.[102]

Dipeptide and tripeptide based LMW hydrogelators have gained great attention as they are commercially available and cost-effective compounds which have already proved to be successful hydrogelators. Adams in his review,[100] describes the gelation triggers, the mechanisms of self-assembly and applications of these materials. Coupling of dipeptides and tripeptides with aromatic moieties such as fluorenylmethyloxycarbonyl (Fmoc), naphthalene, pyrene and spiropyran consist some representatives of this class of gelators, as mentioned in his review. One of the most well studied dipeptide hydrogelators is the Fmoc protected diphenylalanine **68** (Figure 1.20) which yielded biocompatible hydrogels, while gelation was triggered by adjusting the pH value of its aqueous solutions.[103] Another example of the diphenylalanine family of hydrogelators is the indole protected derivative **69** (Figure 1.20) which gave an exceptionally strong hydrogel.[104] Different amino acids have also been employed such as the naphthalene capped alanine-valine derivative **119**[105] which

gelled by adjusting the pH in a controlled manner *via* the hydrolysis of glucono-*δ*-lactone to gluconic acid .

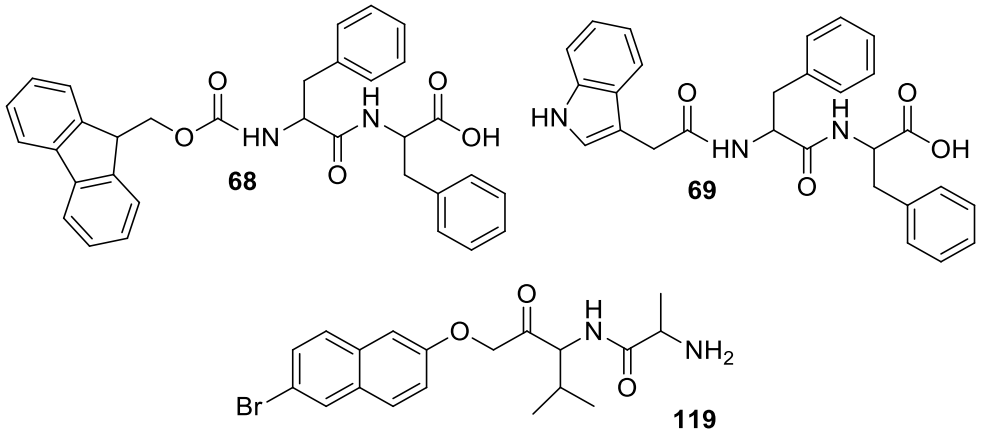

Figure 1.20 Examples of dipeptide hydrogelators

The sequential order of amino acids proved critical for the formation of hydrogels. Indeed, as stated by Tuttle and co-workers,[99] *in silico* studies of their primary organization showed that in tripeptide structures, gelation was favoured when aromatic amino acids occupied positions 2 and 3 whereas positive and hydrogen-bonding residues occupied position 1 (*N*-terminus) and negative residues position 3 (*C*-terminus). Further to this, by searching literature, Tuttle *et al.* found that the unprotected L-tripeptides Lys-Tyr-Phe, Lys-Tyr-Tyr, Lys-Phe-Phe and Lys-Tyr-Trp were efficient hydrogelators validating this way the results of their simulations.

The *C*-terminal segment of the peptide backbone directly affects the gelation mechanism.[95] When gelation is triggered by modification of the pH values the free carboxylic groups can be either deprotonated (COO^-) or not (COOH), whereas the protected ones influence the solubility of the building blocks. Further to this, coupling reactions at the free *C*-terminus active site, control not only a PA's solubility, but can also be used in the formation of lipopeptides, peptide-saccharides and other peptide derivatives.[95]

In Nature, supramolecular peptide structures have a direct impact on the existence and advancement of living systems. Such architectures have inspired the design of synthetic soft materials, capable of mimicking the properties of their natural analogues. For instance, elastin is an elastic protein responsible for the recoil of connective and flexible tissues. Despite their high insolubility in water, elastin-based peptides and various recombinant forms of its soluble precursor, tropoelastin, have been employed for the preparation of

elastin-like materials.[106] Interestingly, small peptide systems known as collagen mimetic peptides (CMPs) were adapted for the investigation of collagen's triple helix structure.[107] Polypeptides bearing the three amino acid sequence proline-hydroxyproline-lysine, a repeating unit abundant in natural collagen, were found to replicate its self-assembly.[108] Another group of these bioinspired materials are gels designed to replicate the properties of the extracellular matrix (ECM).[109,110] These supramolecular systems aim at the anchorage, entrapment, adhesion, differentiation and preservation of cells within the fibrous matrix for cell culture and tissue engineering applications.[111–115] Biomimicry has also led to smart systems capable of either mimicking enzymes or enhancing enzymatic activity when used as hydrogel matrices.[116] Such a case was reported by Bai and Ulijn, where SiO_2 nanoparticles emulsified peptide gel microparticles, providing tunable environments for both protein immobilization and bio-catalysis.[117]

Some peptide and polypeptide-based gelators can gel in response to external stimuli such as pH, heat, enzymes, metal ions and light. These smart materials have potential applications in areas such as cosmetics, drug delivery, bio-sensing and tissue engineering.[118] A case of α-helical peptides, represents the first example of heat-responsive materials, as reported by Adams *et al*.[119] In another example, a number of external stimuli (pH, ionic strength and heat) were able to cause reversible transitions from random coil to β-folded structures of antibacterial peptides, as described by Zhao and co-workers.[56] A similar case of a pH-responsive polypeptide refers to the reversible transitions from liquid-to-gel-to-insoluble states, dictated by the zeta potential values of the system.[55]

1.9 Gels based on carbohydrate derivatives

Carbohydrates are chiral, biocompatible, poly-hydroxylated and water-soluble molecules that have been successfully used for the *ad hoc* preparation of LMW gels. These materials have been extensively used, due to their inherent biocompatibility, for cell culture, drug delivery, tissue engineering and wound healing applications.[25,71]

Shinkai and *co*-workers were the first to explore the gelation properties of LMW saccharides. In 1998, three chiral analogues, that of D-glucose **36**, D-galactose **37** and D-mannose **38** (Figure 1.21) were synthesized and their gelation ability towards a broad spectrum of solvents was tested. It was demonstrated for the first time that monosaccharides were promising precursors for the design of novel gelators.[120]

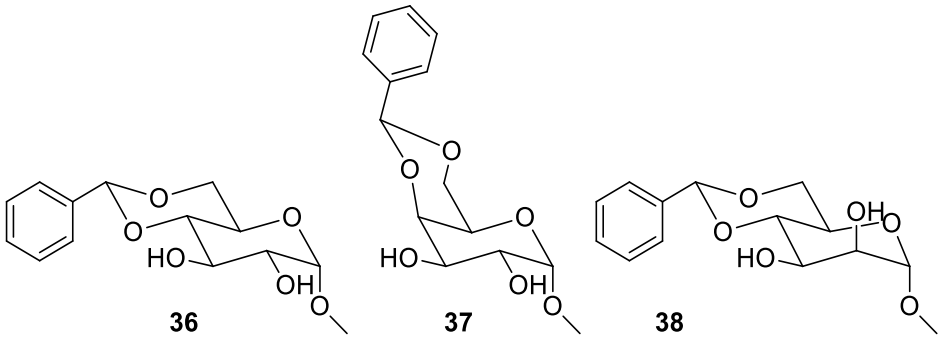

Figure 1.21 Chemical structures of D-glucose, D-galactose and D-mannose derivatives.

In the same year, the gelation ability of the *p*-nitrophenyl derivatives of D-glucose **39**, D-galactose **40** and D-mannose **41** (Figure 1.22) illustrated that gelation was profoundly related to structure. Indeed, **39** appeared to be an excellent gelator, gelling 10 solvents in total, while **40** was sparingly soluble and **41** was too soluble.[121]

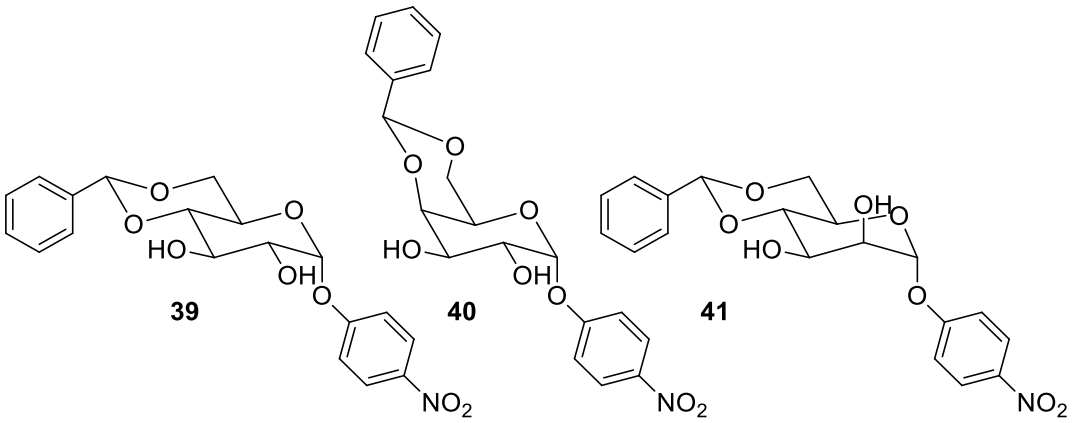

Figure 1.22 Chemical structures the p-nitrophenyl analogues of D-glucose, D-galactose and D-mannose derivatives.

A year later, the *β*-isomers **42** and **43** (Figure 1.23) were prepared and their gelation ability was compared to that of the *α*-isomers **36**, **37** and **38**. It was confirmed once more that gelation was affected by structure; substituents at the anomeric sites drastically affected the gelation outcome. The *β*-isomer **42** was described as "too cohesive" and formed a precipitate in most solvents. By contrast, the *α*-isomers **36** and **37** were "moderately cohesive" and appeared to be successful gelators, whereas compound **38** was "less cohesive" and too soluble in most solvents.[122] Furthermore, structural modifications at the benzylidene protecting group of the D-glucopyranoside gave derivatives **44a-44c** and similarly D-mannopyranoside derivative **45** (figure 1.23). It was found that only the *p*-substituted

compounds **44c** and **45** were able to gel both water and organic solvents, establishing a new bifunctional class of LMW gelators.[123]

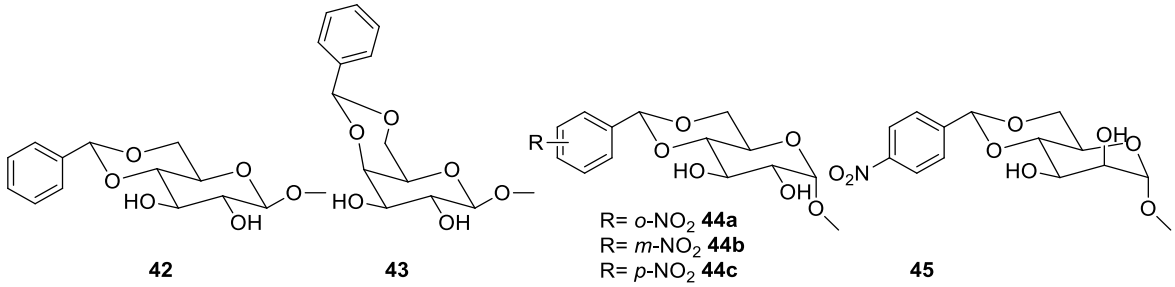

42 43 45

Figure 1.23 Chemical structures of the *β*-isomers of D-glucose and D-galactose derivatives (**42**, **43**) and those of the nitro-substituted D-gluco and D-mannopyranoside derivatives (**44a**-**44c** and **45**).

Further studies afforded two pairs of the structurally related compounds **46**-**49** (Figure 1.24), consisting of an amino-phenyl moiety and a long chain alkyl group. The amphiphilic aldopyranoside derivatives **46** and **47**, together with bolaamphiphiles **48** and **49**, exhibited similar bifunctional properties, gelling both water and organic solvents.[124,125]

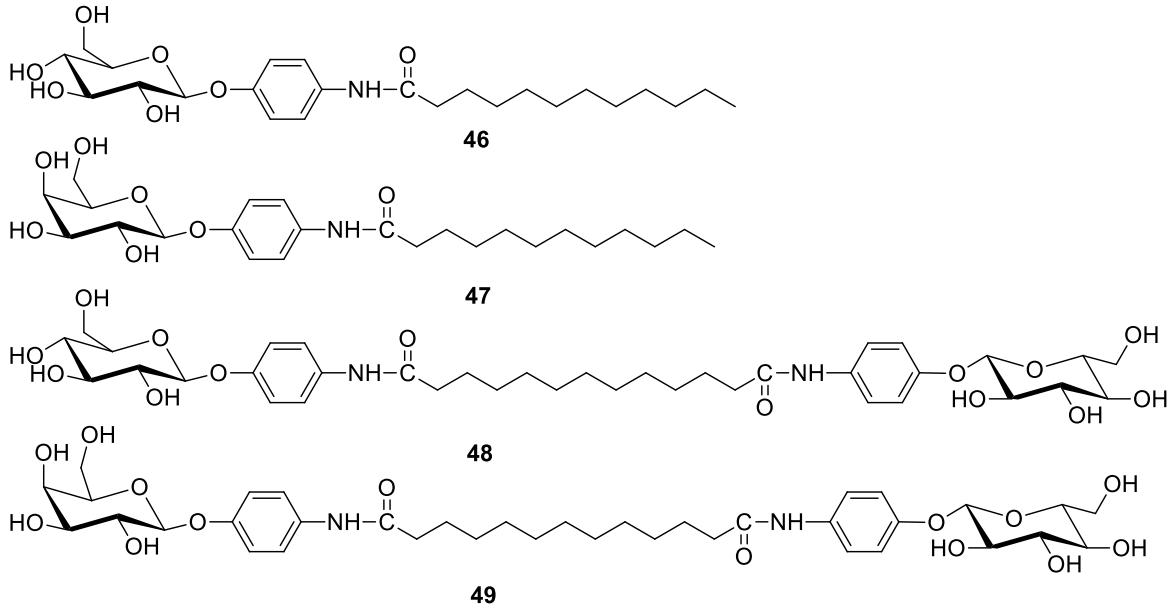

46

47

48

49

Figure 1.24 Chemical structures of aldopyranoside based amphiphilic gelators.

In addition, the *β*-D-glucopyranosyl azobenzene based analogue **50** (Figure 1.25) was found to be the first "super" hydrogelator of the carbohydrate family, able to gel water at concentrations lower than 0.1 wt. %.[126]

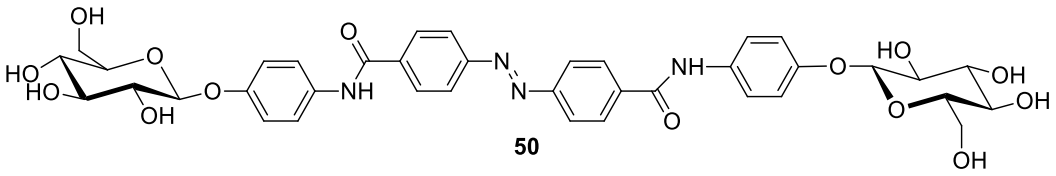

Figure 1.25 Chemical structure of a sugar based "super" hydrogelator.

Due to their structural diversity, carbohydrates are ideal synthons for the preparation of successful hydro- and organogelators. By combining sugars with other chemical moieties, it is possible to produce a rich family of building blocks. In their efforts to establish a set of structurally related gelators, Shinkai and co-workers reported in 2003 on a combinatorial library of LMW glycosylated building blocks, based on the solid phase synthesis of artificial glycolipids.[127]

Almost two decades after the first citation of LMW sugar-based gelators, researchers continue to systematically investigate the gelation abilities of this class of compounds. Some of the most recent examples are briefly described in the following paragraphs.

An example inspired by biomineralization, concerns a one-dimensional supramolecular structure that was found to induce the growth of calcite crystals along an unusual axis. This approach was based on the ordered crystallization of $CaCO_3$ onto the fibrous template of gelator **51** (Figure 1.26).[128] Another example shows how gel properties may be controlled through the structural modification of gelator building blocks. Indeed, the synthesis of novel di-acetylated and di-benzoylated L/D-arabinose derivatives (**52a,b** and **53a,b** respectively in Figure 1.26) illustrated the effects of ester protecting groups on gel mechanical strength. Rheological studies showed that the di-benzoylated derivatives yielded stiffer gels, due to the formation of thinner and more extensively cross-linked fibres, compared to the di-acetylated derivatives.[129]

A rare case in which LMW gelators can gel ionic liquids was reported by Marr *et al.* A novel sugar-based gelator, originating from isosorbide **54,** and two others derived from D-mannitol **55**, **56** (Figure 1.26), were found to gel 21 ionic liquids containing a range of different ions. This study demonstrated that the ability of the ionic liquids to induce H-bonding was the driving force of gelation. Specifically, the larger the size of the cations, the higher was the minimum gelation concentration (MGC) of the gelator molecules used.[130]

Sugars are cost effective compounds which can be used in bulk amounts in order to address practical issues in cases such as marine oil-spill recovery. Indeed, five new gelators, originating from D-glucose **57a-e** (Figure 1.26) were synthesized and their ability as phase-transfer organogelators was tested. Gelator **57a** was the most efficient, since it could be applied directly, in low amounts, as a solid on the surface of contaminated water to congeal crude oil.[131]

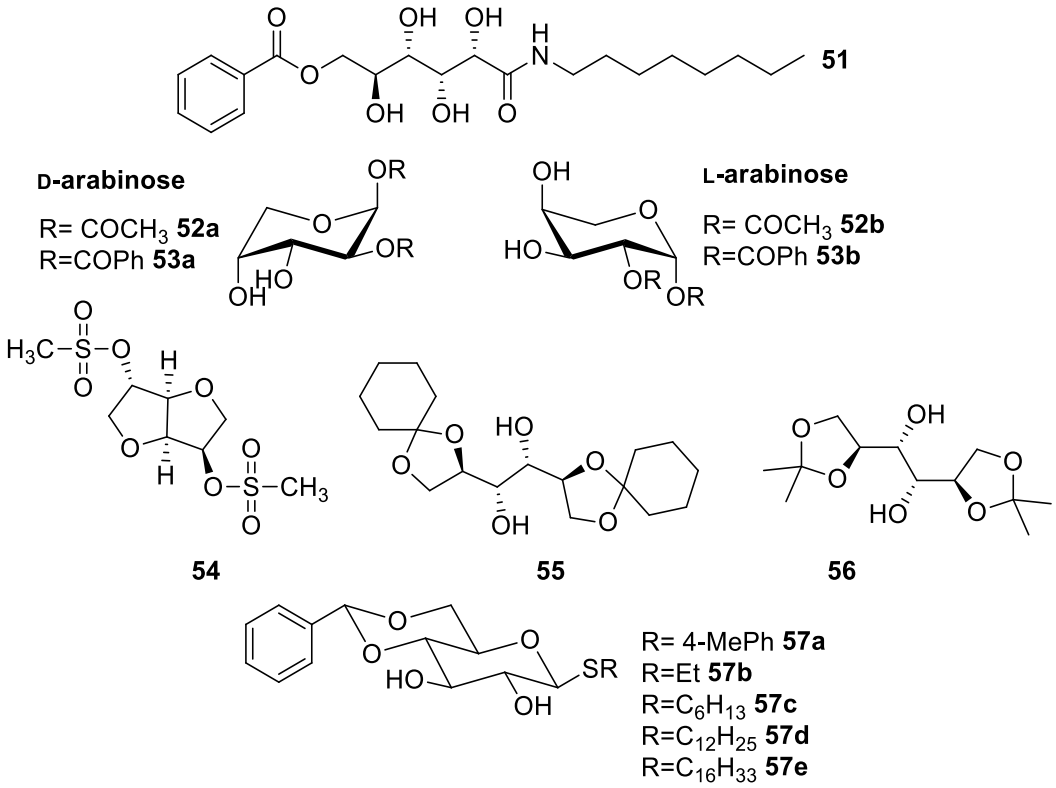

Figure 1.26 Chemical structures of sugar based gelators.

1.10 Gel characterization techniques

One of the primary questions researchers are called upon to answer is "how the molecular building blocks do arrange themselves in a highly ordered supramolecular matrix?" A wide range of techniques is available for the elucidation of the primary, secondary and tertiary structural architectures of supramolecular systems (Table 1.2).[132,71] These allow in-depth study of the self-assembly modes, both at the nanoscale and at the molecular level. Even though high-resolution techniques can provide valuable information regarding the organization of the formed fibres, sample handling and preparation are not easy tasks to perform. Any mishandling will affect the original structural characteristics of the gel sample and introduce artefacts, providing misleading information.

Table 1.2 Characterization methods of hydrogels

Characterization method	Outcomes
Visual inspection	Observation of the free gravitational flow
Phase transition temperature	Determines the temperature of the gel-sol transition
Spectroscopy methods: CD, UV-vis, IR, fluorescence, Raman, NMR	Assessment of the microenvironment of the molecular building blocks-assessment of the supramolecular arrangement
Rheology	Assessment of the mechanical properties of hydrogels
X-ray diffraction	Assessment of the spatial arrangement of a crystalline matrix. Observation of polymorphism

Initially, a visual inspection of the free gravitational flow, through the "tube inversion method", is required to characterize the formed materials either as gels or partial gels, solutions, viscous liquids or "solid like" gels.[57]

Furthermore, microscopy techniques allow the visualization of the fibres. Such techniques include atomic force microscopy (AFM) and scanning force microscopy (SFM), each with nanometer scale resolution, and electron microscopy techniques such as transmission and scanning electron microscopy (TEM/SEM) with a resolution on the order of pico-meter scale. Although fundamental information can be obtained regarding the morphology, the shape and entanglement of the fibres, the drying procedure of the samples under high vacuum conditions and sample staining to increase the electron density, may cause alterations to the original structure and introduce optical artefacts.[71]

One of the most frequently reported characteristics of hydrogels is their phase transition temperature (T_{gel}), which determines the temperature at which the fibrous network collapses on heating. Several methodologies can be used for the determination and study of T_{gel}, namely differential scanning calorimetry (DSC), the 'dropping ball' method and rheology.[133,134]

The stiffness of soft materials reflects the strength and cohesion of their fibrous network. Oscillatory rheology is used for the study of flow and can provide data regarding the tertiary architecture of the structure. These data reflect the type, number and strength of the cross-linked matrixes within the supramolecular system. Viscoelastic materials appear to have a higher value of elastic modulus (G′) with respect to the loss modulus (G″) (G′ > G″). Other key factors that can correlate to the above measured values include the applied stress, the temperature, the duration of the experiment and the concentration of the gelator molecules. Usually, a layer of gel is placed between a stationary surface (lower geometry) and a movable component (upper geometry). Depending on the nature of the material, various set-ups can be used, such as parallel plates, concentric cylinders, cone and plate, *etc*.[135,136]

Additional methodologies used for the elucidation of the structural characteristics of hydrogels, include circular dichroism (CD), UV/Vis, infrared (IR), fluorescence, Raman and NMR spectroscopies. Depending on the chemical structure of the building blocks, a combination of techniques can provide data regarding the configuration and conformation of the gel supramolecular arrangement, imposed by the chiral centers of the molecules and the type of weak interactions at play (*e.g*. aromatic-aromatic interactions, H-bonds, electrostatic forces and solvophobic effects).[71]

X-ray diffraction (XRD) experiments provide information regarding the spatial arrangement of a crystalline matrix. Xerogels, originating from "wet" gel samples, can be tested, while the obtained data can be interpreted alongside results obtained from computational studies (Molecular Dynamics, Density Functional Theory). Such an approach can provide valuable information regarding the dimensions and spatial orientation of the molecular alignment. Indeed, the d-spacing dimensions of the xerogels can be used in computational calculations. XRD can also determine the possible presence of polymorphism, which has an immediate effect on the reproducibility of the gel preparation methods, given the differences in solubility of different polymorphs.[137]

1.11 Cell culture applications of LMW hydrogels and tissue engineering

LMW hydrogels are soft materials with tuneable characteristics that have been widely used for cell culture applications. Their supramolecular architecture mimics the extracellular matrix,[110] their mechanical properties[138] may resemble those of soft tissues and can also support cell adhesion.[139] In contrast to stiff materials widely used in cell culturing (two dimensional cell cultures) such as polystyrene and glass, hydrogels can be employed for

three dimensional cell cultures mimicking the physiological conditions of the human body.[140]

Certain requirements need to be met though in order to facilitate soft hydrogels as matrices for cell culture applications.[7] Indeed, they should be biocompatible as to allow cells to adhere, migrate, function normally and proliferate. Further to this, when used as implanted materials they must not trigger any immune reactions which could lead to rejection from the human body. Since materials of this type are met to be used for tissue engineering purposes, they must be biodegradable and allow cells to develop their own extracellular matrix.[141] Additionally, the formed by-products of their degradation must be non-toxic and exit easily the human body.

The viscoelastic properties of LMW hydrogels (stiffness, elasticity) have an immediate effect on cells viability, proliferation and/or differentiation.[112] Furthermore, *in vivo* applications in the field of tissue engineering require gels to possess mechanical properties which are consistent with the anatomic site in which they will be implanted.[7] Additionally, the supramolecular matrix of the hydrogels should have adequate large pores to allow penetration and migration of the cells within the fibrous network and sufficient diffusion of nutrients towards the cells.[114]

Finally, the supramolecular fibrous scaffold should be stable under the applied cell culture conditions (temperature, cell medium, antibiotics *etc*.). An interesting case has been reported by Thordarson *et al.*[104] where cell death occurred after 24 h for all tested cell lines when they were seeded on the surface of an indole based supramolecular hydrogel. According to the authors, that resulted due to the presence of salts in the cell culture medium which increased the ionic strength of the system causing large fibres to break down to smaller proto-fibers which interacted with the cell membrane.

1.12 Aims and objectives of the PhD research project

The PhD research project aimed on the development of novel LMW hydrogels as functional biomaterials with potential for tissue culture application. Several LMW gelator molecules have been previously synthesized and partially characterized by a previous group member[142] whereas none of their corresponding hydrogels were tested as substrates for cell culture. The research project therefore aimed to:

- The full characterization of those hydrogels formed by gelator molecules that were previously synthesized.
- The optimization of sample handling as to keep hydrogels intact during the characterization process.
- The development of standard protocols for the assessment of the microscopic and macroscopic properties of the materials.
- The synthesis of novel hydrogelators and the characterization of their corresponding hydrogels.
- A preliminary biocompatibility evaluation of all gels.

Finally, it was necessary to give an answer to some fundamental questions such as:

- How do structural differences of the molecular building blocks affect their gelation ability?
- Is the supramolecular network of structurally related hydrogelators similar?
- How could we control the microscopic and macroscopic properties of hydrogels?
- Is the structure of the molecular building blocks and/or the applied gelation trigger responsible for the biocompatibility of the formed hydrogels?

1.13 References

(1) Wang, Q.; Yang, Z.; Wang, L.; Ma, M.; Xu, B. Molecular Hydrogel-Immobilized Enzymes Exhibit Superactivity and High Stability in Organic Solvents. *Chem. Commun.* **2007**, No. 10, 1032-1034.

(2) Boynuegri, T. A.; Gürü, M. Catalytic Dehydrogenation of Calcium Borohydride by Using Hydrogel Catalyst. *Int. J. Hydrogen Energy* **2017**, *42* (28), 17869-17873.

(3) Ikeda, M.; Ochi, R.; Wada, A.; Hamachi, I. Supramolecular Hydrogel Capsule Showing Prostate Specific Antigen-Responsive Function for Sensing and Targeting Prostate Cancer Cells. *Chem. Sci.* **2010**, *1* (4), 491-498.

(4) Qian, H.; Aprahamian, I. An Emissive and PH Switchable Hydrazone-Based Hydrogel. *Chem. Commun.* **2015**, *51* (56), 11158-11161.

(5) Shin, J.; Cherstvy, A. G.; Metzler, R. Sensing Viruses by Mechanical Tension of DNA in Responsive Hydrogels. *Phys. Rev. X* **2014**, *4* (2), 1-13.

(6) Dankers, P. Y. W.; Harmsen, M. C.; Brouwer, L. A.; van Luyn, M. J. A.; Meijer, E.

W. A Modular and Supramolecular Approach to Bioactive Scaffolds for Tissue Engineering. *Nat. Mater.* **2005**, *4* (7), 568-574.

(7) O'Brien, F. J. Biomaterials & Scaffolds for Tissue Engineering. *Mater. Today* **2011**, *14* (3), 88-95.

(8) Ryan, D. M.; Nilsson, B. L. Self-Assembled Amino Acids and Dipeptides as Noncovalent Hydrogels for Tissue Engineering. *Polym. Chem.* **2012**, *3* (1), 18-33.

(9) Sheehy, E. J.; Mesallati, T.; Kelly, L.; Vinardell, T.; Buckley, C. T.; Kelly, D. J. Tissue Engineering Whole Bones Through Endochondral Ossification: Regenerating the Distal Phalanx. *Biores. Open Access* **2015**, *4* (1), 229-241.

(10) Malda, J.; Visser, J.; Melchels, F. P.; Jüngst, T.; Hennink, W. E.; Dhert, W. J. A.; Groll, J.; Hutmacher, D. W. 25th Anniversary Article: Engineering Hydrogels for Biofabrication. *Adv. Mater.* **2013**, *25* (36), 5011-5028.

(11) Tam, R. Y.; Smith, L. J.; Shoichet, M. S. Engineering Cellular Microenvironments with Photo- and Enzymatically Responsive Hydrogels: Toward Biomimetic 3D Cell Culture Models. *Acc. Chem. Res.* **2017**, *50* (4), 703-713.

(12) Caliari, S. R.; Burdick, J. A. A Practical Guide to Hydrogels for Cell Culture. *Nat. Methods* **2016**, *13* (5), 405-414.

(13) Latxague, L.; Ramin, M. A.; Appavoo, A.; Berto, P.; Maisani, M.; Ehret, C.; Chassande, O.; Barthélémy, P. Control of Stem-Cell Behavior by Fine Tuning the Supramolecular Assemblies of Low-Molecular-Weight Gelators. *Angew. Chemie - Int. Ed.* **2015**, *54* (15), 4517-4521.

(14) Lee, J. M.; Seo, H. I.; Bae, J. H.; Chung, B. G. Hydrogel Microfluidic Co-Culture Device for Photothermal Therapy and Cancer Migration. *Electrophoresis* **2017**, 1-7.

(15) Agubata, C. O.; Okereke, C.; Nzekwe, I. T.; Onoja, R. I.; Obitte, N. C. Development and Evaluation of Wound Healing Hydrogels Based on a Quinolone, Hydroxypropyl Methylcellulose and Biodegradable Microfibres. *Eur. J. Pharm. Sci.* **2016**, *89*, 1-10.

(16) Short, A. R.; Koralla, D.; Deshmukh, A.; Wissel, B.; Stocker, B.; Calhoun, M.; Dean, D.; Winter, J. O. Hydrogels That Allow and Facilitate Bone Repair, Remodeling, and Regeneration. *J. Mater. Chem. B* **2015**, *3* (40), 7818-7830.

(17) Almeida, J. S.; Benvegnú, D. M.; Boufleur, N.; Reckziegel, P.; Barcelos, R. C. S.; Coradini, K.; de Carvalho, L. M.; Bürger, M. E.; Beck, R. C. R. Hydrogels Containing Rutin Intended for Cutaneous Administration: Efficacy in Wound Healing in Rats. *Drug Dev. Ind. Pharm.* **2012**, *38* (7), 792-799.

(18) Yang, Z.; Liang, G.; Ma, M.; Abbah, A. S.; Lu, W. W.; Xu, B. D-Glucosamine-Based Supramolecular Hydrogels to Improve Wound Healing. *Chem. Commun.* **2007**, 8, 843-845.

(19) Dai, L.; Liu, R.; Hu, L.-Q.; Wang, J.-H.; Si, C.-L.; Kuang, H.; He, H.; Zhang, Z.; Qi, Y.; Xie, Z.; et al. Self-Assembled PEG–carboxymethylcellulose Nanoparticles/α-Cyclodextrin Hydrogels for Injectable and Thermosensitive Drug Delivery. *RSC Adv.* **2017**, *7* (5), 2905-2912.

(20) Skilling, K. J.; Kellam, B.; Ashford, M.; Bradshaw, T. D.; Marlow, M. Developing a Self-Healing Supramolecular Nucleoside Hydrogel. *Soft Matter.* **2016**, *12* (43), 8950-8957.

(21) Eskandari, S.; Guerin, T.; Toth, I.; Stephenson, R. J. Recent Advances in Self-Assembled Peptides: Implications for Targeted Drug Delivery and Vaccine Engineering. *Adv. Drug Deliv. Rev.* **2017**, *110* (111), 169-187.

(22) Costa, D.; Valente, A. J. M.; Queiroz, J. Stimuli-Responsive Polyamine-DNA Blend Nanogels for Co-Delivery in Cancer Therapy. *Colloids Surf. B Biointerfaces* **2015**, *132*, 194-201.

(23) Vintiloiu, A.; Leroux, J.-C. Organogels and Their Use in Drug Delivery - A Review. *J. Control. Release* **2008**, *125* (3), 179-192.

(24) Sangeetha, N. M.; Maitra, U. Supramolecular Gels: Functions and Uses. *Chem. Soc. Rev.* **2005**, *34*, 821-836.

(25) Estroff, L. a; Hamilton, A. D. Water Gelation by Small Organic Molecules Water Gelation by Small Organic Molecules. **2004**, *104*, 1201-1218.

(26) Abdallah, D. J.; Weiss, R. G. Organogels and Low Molecular Mass Organic Gelators. *Adv. Mater.* **2000**, *12* (17), 1237-1247.

(27) Lv, O.; Tao, Y.; Qin, Y.; Chen, C.; Pan, Y.; Deng, L.; Liu, L.; Kong, Y. Highly Fluorescent and Morphology-Controllable Graphene Quantum Dots-Chitosan Hybrid

Xerogels for in Vivo Imaging and pH-Sensitive Drug Carrier. *Mater. Sci. Eng. C* **2016**, *67*, 478-485.

(28) Lazrag, M.; Steiner, E.; Lemaitre, C.; Mutelet, F.; Privat, R.; Rode, S.; Hannachi, A.; Barth, D. Experimental and Thermodynamic Comparison of the Separation of CO2/Toluene and CO2/Tetralin Mixtures in the Process of Organogel Supercritical Drying for Aerogels Production. *J. Sol-Gel Sci. Technol.* **2017**, *84* (3), 453-465.

(29) Du, A.; Zhou, B.; Zhang, Z.; Shen, J. A Special Material or a New State of Matter: A Review and Reconsideration of the Aerogel. *Materials (Basel).* **2013**, *6* (3), 941-968.

(30) De France, K. J.; Hoare, T.; Cranston, E. D. Review of Hydrogels and Aerogels Containing Nanocellulose. *Chem. Mater.* **2017**, *29* (11), 4609-4631.

(31) Miravet, J. F.; Escuder, B. Pyridine-Functionalised Ambidextrous Gelators: Towards Catalytic Gels. *Chem. Commun.* **2005**, *46*, 5796-5798.

(32) Awadallah-F, A.; Elkhatat, A. M.; Al-Muhtaseb, S. A. Impact of Synthesis Conditions on Meso- and Macropore Structures of Resorcinol-Formaldehyde Xerogels. *J. Mater. Sci.* **2011**, *46* (24), 7760-7769.

(33) Li, J.-L.; Yuan, B.; Liu, X.-Y.; Wang, R.-Y.; Wang, X.-G. Control of Crystallization in Supramolecular Soft Materials Engineering. *Soft Matter.* **2013**, *9* (2), 435-442.

(34) Moore, J. S. Supramolecular Materials. *MRS Bull.* **2000**, *25* (4), 26-29.

(35) Grzybowski, B. A.; Wilmer, C. E.; Kim, J.; Browne, K. P.; Bishop, K. J. M. Self-Assembly: From Crystals to Cells. *Soft Matter.* **2009**, *5* (6), 1110-1128.

(36) Mann, S. Self-Assembly and Transformation of Hybrid Nano-Objects and Nanostructures under Equilibrium and Non-Equilibrium Conditions. *Nat. Mater.* **2009**, *8* (10), 781-792.

(37) Tantakitti, F.; Boekhoven, J.; Wang, X.; Kazantsev, R. V.; Yu, T.; Li, J.; Zhuang, E.; Zandi, R.; Ortony, J. H.; Newcomb, C. J.; et al. Energy Landscapes and Functions of Supramolecular Systems. *Nat. Mater.* **2016**, *15* (4), 469-476.

(38) Raeburn, J.; Zamith Cardoso, A.; Adams, D. J. The Importance of the Self-Assembly Process to Control Mechanical Properties of Low Molecular Weight Hydrogels. *Chem. Soc. Rev.* **2013**, *42* (12), 5143-5156.

(39) Ramos Sasselli, I.; Halling, P. J.; Ulijn, R. V.; Tuttle, T. Supramolecular Fibers in Gels Can Be at Thermodynamic Equilibrium: A Simple Packing Model Reveals Preferential Fibril Formation versus Crystallization. *ACS Nano* **2016**, *10* (2), 2661-2668.

(40) Salonen, L. M.; Ellermann, M.; Diederich, F. Aromatic Rings in Chemical and Biological Recognition: Energetics and Structures. *Angew. Chemie - Int. Ed.* **2011**, *50* (21), 4808-4842.

(41) Carrillo, R.; López-Rodríguez, M.; Martín, V. S.; Martín, T. Quantification of a CH-π Interaction Responsible for Chiral Discrimination and Evaluation of Its Contribution to Enantioselectivity. *Angew. Chem. Int. Ed.* **2009**, *48* (42), 7803-7808.

(42) Smith, D. K. Lost in Translation? Chirality Effects in the Self-Assembly of Nanostructured Gel-Phase Materials. *Chem. Soc. Rev.* **2009**, *38* (3), 684-694.

(43) Terech, P.; Rossat, C.; Volino, F. On the Measurement of Phase Transition Temperatures in Physical Molecular Organogels. *J. Colloid Interface Sci.* **2000**, *227*, 363-370.

(44) De Loos, M.; Feringa, B. L.; Van Esch, J. H. Design and Application of Self-Assembled Low Molecular Weight Hydrogels. *European J. Org. Chem.* **2005**, 17, 3615-3631.

(45) Johnson, E. K.; Adams, D. J.; Cameron, P. J. Peptide Based Low Molecular Weight Gelators. *J. Mater. Chem.* **2011**, *21* (7), 2024-2027.

(46) Zhang, Y.; Gu, H.; Yang, Z.; Xu, B. Supramolecular Hydrogels Respond to Ligand-Receptor Interaction. *J. Am. Chem. Soc.* **2003**, *125* (45), 13680-13681.

(47) Garvin, K. A.; VanderBurgh, J.; Hocking, D. C.; Dalecki, D. Controlling Collagen Fiber Microstructure in Three-Dimensional Hydrogels Using Ultrasound. *J. Acoust. Soc. Am.* **2013**, *134* (2), 1491-1502.

(48) Roy, B.; Bairi, P.; Nandi, A. K. Metastability in a Bi-Component Hydrogel of Thymine and 6-Methyl-1,3,5-Triazine-2,4-Diamine: Ultrasound Induced vs. Thermo Gelation. *Soft Matter.* **2012**, *8* (8), 2366-2369.

(49) Awhida, S.; Draper, E. R.; McDonald, T. O.; Adams, D. J. Probing Gelation Ability for a Library of Dipeptide Gelators. *J. Colloid Interface Sci.* **2015**, *455*, 24-31.

(50) Raeburn, J.; Mendoza-Cuenca, C.; Cattoz, B. N.; Little, M. A.; Terry, A. E.; Zamith Cardoso, A.; Griffiths, P. C.; Adams, D. J. The Effect of Solvent Choice on the Gelation and Final Hydrogel Properties of Fmoc–diphenylalanine. *Soft Matter.* **2015**, *11* (5), 927-935.

(51) Grigoriou, S.; Johnson, E. K.; Chen, L.; Adams, D. J.; James, T. D.; Cameron, P. J. Dipeptide Hydrogel Formation Triggered by Boronic Acid-Sugar Recognition. *Soft Matter.* **2012**, *8* (25), 6788-6791.

(52) Marchesan, S.; Waddington, L.; Easton, C. D.; Winkler, D. A.; Goodall, L.; Forsythe, J.; Hartley, P. G. Unzipping the Role of Chirality in Nanoscale Self-Assembly of Tripeptide Hydrogels. *Nanoscale* **2012**, *4* (21), 6752-6760.

(53) Nanda, J.; Banerjee, A. B-Amino Acid Containing Proteolitically Stable Dipeptide Based Hydrogels: Encapsulation and Sustained Release of Some Important Biomolecules at Physiological PH and Temperature. *Soft Matter.* **2012**, *8* (12), 3380-3386.

(54) Nonoyama, T.; Ogasawara, H.; Tanaka, M.; Higuchi, M.; Kinoshita, T. Calcium Phosphate Biomineralization in Peptide Hydrogels for Injectable Bone-Filling Materials. *Soft Matter.* **2012**, *8* (45), 11531-11536.

(55) Fletcher, N. L.; Lockett, C. V.; Dexter, A. F.; Garbern, J. C.; Minami, E.; Stayton, P. S.; Murry, C. E.; Guziewicz, N.; Best, A.; Perez-Ramirez, B.; et al. A pH-Responsive Coiled-Coil Peptide Hydrogel. *Soft Matter.* **2011**, *7* (21), 10210-10218.

(56) Liu, Y.; Yang, Y.; Wang, C.; Zhao, X. Stimuli-Responsive Self-Assembling Peptides Made from Antibacterial Peptides. *Nanoscale* **2013**, *5* (14), 6413-6421.

(57) Pal, A.; Dey, J. Rheology and Thermal Stability of PH-Dependent Hydrogels of N-Acyl-L-Carnosine Amphiphiles: Effect of the Alkoxy Tail Length. *Soft Matter.* **2011**, *7* (21), 10369-10376.

(58) Bernet, A.; Albuquerque, R. Q.; Behr, M.; Hoffmann, S. T.; Schmidt, H.-W. Formation of a Supramolecular Chromophore: A Spectroscopic and Theoretical Study. *Soft Matter.* **2012**, *8*, 66-69.

(59) Aufderhorst-Roberts, A.; Frith, W. J.; Kirkland, M.; Donald, A. M. Microrheology and Microstructure of Fmoc-Derivative Hydrogels. *Langmuir* **2014**, *30* (15), 4483-

4492.

(60) Chen, L.; Revel, S.; Morris, K.; Adams, D. J. Energy Transfer in Self-Assembled Dipeptide Hydrogels. *Chem. Commun.* **2010**, *46* (24), 4267-4269.

(61) Zhao, F.; Gao, Y.; Shi, J.; Browdy, H. M.; Xu, B. Novel Anisotropic Supramolecular Hydrogel with High Stability over a Wide PH Range. *Langmuir* **2011**, *27* (4), 1510-1512.

(62) Bowerman, C. J.; Nilsson, B. L. A Reductive Trigger for Peptide Self-Assembly and Hydrogelation. *J. Am. Chem. Soc.* **2010**, *132* (28), 9526-9527.

(63) Hill-West, J. L.; Dunn, R. C.; Hubbell, J. a. Local Release of Fibrinolytic Agents for Adhesion Prevention. *J. Surg. Res.* 1995, 759-763.

(64) Anseth, K. Photoencapsulation of Chondrocytes in Poly (Ether Oxide) -Based Semi-Interpenetrating Networks Photoencapsulation of Chondrocytes in Poly (Ethylene Oxide) -Based Semi-Interpenetrating Networks. *J. Biomed. Mater. Res.* **2000**, 464-171.

(65) Yang, Z.; Gu, H.; Fu, D.; Gao, P.; Lam, J. K.; Xu, B. Enzymatic Formation of Supramolecular Hydrogels. *Adv. Mater.* **2004**, *16* (16), 1440-1444.

(66) Toledano, S.; Williams, R. J.; Jayawarna, V.; Ulijn, R. V. Enzyme-Triggered Self-Assembly of Peptide Hydrogels via Reversed Hydrolysis. *J. Am. Chem. Soc.* **2006**, *128* (4), 1070-1071.

(67) Gortner, R. A.; Hoffman, W. F. An Interesting Colloid Gel. *J. Am. Chem. Soc.* **1921**, *43* (263), 2199-2202.

(68) Menger, F. M.; Caran, K. L. Anatomy of a Gel. Amino Acid Derivatives That Rigidify Water at Submillimolar Concentrations. *J. Am. Chem. Soc.* **2000**, *122* (47), 11679-11691.

(69) Nlung, M.; Kuang, Y.; Gao, Y.; Zhang, Y.; Gao, P.; Xu, B. Aromatic-Aromatic Interactions Induce the Self-Assembly of Pentapeptidic Derivatives in Water to Form Nanofibers and Supramolecular Hydrogels. *J. Am. Chem. Soc.* **2010**, *132* (8), 2719-2728.

(70) Aoki, M.; Murata, K.; Shinkai, S. Calixarene-Based Gelators of Organic Fluids.

Chem. Lett. **1991**, *20* (10), 1715-1718.

(71) Du, X.; Zhou, J.; Shi, J.; Xu, B. Supramolecular Hydrogelators and Hydrogels: From Soft Matter to Molecular Biomaterials. *Chem. Rev.* **2015**, *115* (24), 13165-13307.

(72) Qiu, Y.; Park, K. Environment-Sensitive Hydrogels for Drug Delivery. *Adv. Drug Deliv. Rev.* **2001**, *53*, 321–339.

(73) Zelzer, M.; Ulijn, R. V. Next-Generation Peptide Nanomaterials: Molecular Networks, Interfaces and Supramolecular Functionality. *Chem. Soc. Rev.* **2010**, *39* (9), 3351-3357.

(74) Draper, E. R.; Adams, D. J. Low-Molecular-Weight Gels : The State of the Art. **2017**, 390-410.

(75) Buerkle, L. E.; Rowan, S. J. Supramolecular Gels Formed from Multi-Component Low Molecular Weight Species. *Chem. Soc. Rev.* **2012**, *41* (18), 6089-6102.

(76) Meng, Y.; Jiang, J.; Liu, M. Self-Assembled Nanohelix from a Bolaamphiphilic Diacetylene via Hydrogelation and Selective Responsiveness towards Amino Acids and Nucleobases. *Nanoscale* **2017**, *9* (21), 7199-7206.

(77) Kumar, D. K.; Jose, D. A.; Das, A.; Dastidar, P. First Snapshot of a Nonpolymeric Hydrogelator Interacting with Its Gelling Solvents. *Chem. Commun.* **2005**, 4059-4061.

(78) Knani, D.; Alperstein, D. Simulation of DBS, DBS-COOH, and DBS-$CONHNH_2$ as Hydrogelators. *J. Phys. Chem. A* **2017**, *121* (5), 1113-1120.

(79) Zhou, Y.; Li, H.; Yang, Y.-W. Controlled Drug Delivery Systems Based on Calixarenes. *Chinese Chem. Lett.* **2015**, *26* (7), 825-828.

(80) Malviya, N.; Das, M.; Mandal, P.; Mukhopadhyay, S. A Smart Organic Gel Template as Metal Cation and Inorganic Anion Sensor. *Soft Matter.* **2017**, *13* (36), 6243-6249.

(81) Zhang, A.; Zhang, Y.; Xu, Z.; Li, Y.; Yu, X.; Geng, L. Naphthalimide-Based Fluorescent Gelator for Construction of Both Organogels and Stimuli-Responsive Metallogels. *RSC Adv.* **2017**, *7* (41), 25673-25677.

(82) Arnedo-Sánchez, L.; Nonappa, N.; Bhowmik, S.; Hietala, S.; Puttreddy, R.; Lahtinen, M.; De Cola, L.; Rissanen, K. Rapid Self-Healing and Anion Selectivity in

Metallosupramolecular Gels Assisted by Fluorine–fluorine Interactions. *Dalt. Trans.* **2017**, *46* (22), 7309-7316.

(83) Jiang, B.; Chen, L.-J.; Yin, G.-Q.; Wang, Y.-X.; Zheng, W.; Xu, L.; Yang, H.-B. Multiphase Transition of Supramolecular Metallogels Triggered by Temperature. *Chem. Commun.* **2017**, *53* (1), 172-175.

(84) Sheikhi, A.; van de Ven, T. G. M. Squishy Nanotraps: Hybrid Cellulose Nanocrystal-Zirconium Metallogels for Controlled Trapping of Biomacromolecules. *Chem. Commun.* **2017**, *53* (62), 8747-8750.

(85) Peters, G. M.; Davis, J. T. Supramolecular Gels Made from Nucleobase, Nucleoside and Nucleotide Analogs. *Chem. Soc. Rev.* **2016**, *45* (11), 3188-3206.

(86) Li, X.; Kuang, Y.; Xu, B. "Molecular Trinity" for Soft Nanomaterials: Integrating Nucleobases, Amino Acids, and Glycosides to Construct Multifunctional Hydrogelators. *Soft Matter.* **2012**, *8* (10), 2801-2806.

(87) Yuan, D.; Du, X.; Shi, J.; Zhou, N.; Baoum, A. A.; Xu, B. Synthesis of Novel Conjugates of a Saccharide, Amino Acids,Nucleobase and the Evaluation of Their Cell Compatibility. *Beilstein J. Org. Chem.* **2014**, *10*, 2406-2413.

(88) Skilling, K. J.; Ndungu, A.; Kellam, B.; Ashford, M.; Bradshaw, T. D.; Marlow, M. Gelation Properties of Self-Assembling N-Acyl Modified Cytidine Derivatives. *J. Mater. Chem. B* **2014**, *2*, 8412-8417.

(89) Angelerou, M. G. F.; Sabri, A.; Creasey, R.; Angelerou, P.; Marlow, M.; Zelzer, M. Surface-Directed Modulation of Supramolecular Gel Properties. *Chem. Commun.* **2016**, *52* (23), 4298-4300.

(90) Nuthanakanti, A.; Srivatsan, S. G. Surface-Tuned and Metal-Ion-Responsive Supramolecular Gels Based on Nucleolipids. *ACS Appl. Mater. Interfaces* **2017**, *9*, 2284-2287.

(91) Zhao, X.; Pan, F.; Xu, H.; Yaseen, M.; Shan, H.; Hauser, C. a E.; Zhang, S.; Lu, J. R. Molecular Self-Assembly and Applications of Designer Peptide Amphiphiles. *Chem. Soc. Rev.* **2010**, *39* (9), 3480-3498.

(92) Cavalli, S.; Albericio, F.; Kros, A. Amphiphilic Peptides and Their Cross-Disciplinary Role as Building Blocks for Nanoscience. *Chem. Soc. Rev.* **2010**, *39* (1),

241-263.

(93) Mitra, R. N.; Das, D.; Roy, S.; Das, P. K. Structure and Properties of Low Molecular Weight Amphiphilic Peptide Hydrogelators. *J. Phys. Chem. B* **2007**, *111*, 14107-14113.

(94) Woolfson, D. N.; Mahmoud, Z. N. More than Just Bare Scaffolds: Towards Multi-Component and Decorated Fibrous Biomaterials. *Chem. Soc. Rev.* **2010**, *39* (9), 3464-3479.

(95) Fleming, S.; Ulijn, R. V. Design of Nanostructures Based on Aromatic Peptide Amphiphiles. *Chem. Soc. Rev.* **2014**, *43* (23), 8150-8177.

(96) Jayawarna, V.; Richardson, S. M.; Hirst, A. R.; Hodson, N. W.; Saiani, A.; Gough, J. E.; Ulijn, R. V. Introducing Chemical Functionality in Fmoc-Peptide Gels for Cell Culture. *Acta Biomater.* **2009**, *5* (3), 934-943.

(97) Draper, E. R.; Morris, K. L.; Little, M. A.; Raeburn, J.; Colquhoun, C.; Cross, E. R.; McDonald, T. O.; Serpell, L. C.; Adams, D. J. Hydrogels Formed from Fmoc Amino Acids. *CrystEngComm* **2015**, *17* (42), 8047-8057.

(98) Shi, J.; Gao, Y.; Yang, Z.; Xu, B. Exceptionally Small Supramolecular Hydrogelators Based on Aromatic-Aromatic Interactions. *Beilstein J. Org. Chem.* **2011**, *7*, 167-172.

(99) Frederix, P. W. J. M.; Scott, G. G.; Abul-Haija, Y. M.; Kalafatovic, D.; Pappas, C. G.; Javid, N.; Hunt, N. T.; Ulijn, R. V; Tuttle, T. Exploring the Sequence Space for (Tri-)Peptide Self-Assembly to Design and Discover New Hydrogels. *Nat. Chem.* **2014**, *7* (1), 30-37.

(100) Adams, D. J. Dipeptide and Tripeptide Conjugates as Low-Molecular-Weight Hydrogelators. *Macromol. Biosci.* **2011**, *11* (2), 160-173.

(101) Reddy, S. M. M.; Shanmugam, G.; Duraipandy, N.; Kiran, M. S.; Mandal, A. B. An Additional Fluorenylmethoxycarbonyl (Fmoc) Moiety in di-Fmoc-Functionalized L -Lysine Induces pH-Controlled Ambidextrous Gelation with Significant Advantages. *Soft Matter.* **2015**, *11*, 8126-8140.

(102) Tena-Solsona, M.; Miravet, J. F.; Escuder, B. Tetrapeptidic Molecular Hydrogels: Self-Assembly and Co-Aggregation with Amyloid Fragment Aβ1-40. *Chem. Eur. J.* **2014**, *20* (4), 1023-1031.

(103) Jayawarna, V.; Ali, M.; Jowitt, T. A.; Miller, A. F.; Saiani, A.; Gough, J. E.; Ulijn, R. V. Nanostructured Hydrogels for Three-Dimensional Cell Culture through Self-Assembly of Fluorenylmethoxycarbonyl-Dipeptides. *Adv. Mater.* **2006**, *18* (5), 611-614.

(104) Martin, A. D.; Robinson, A. B.; Mason, A. F.; Wojciechowski, J. P.; Thordarson, P. Exceptionally Strong Hydrogels through Self-Assembly of an Indole-Capped Dipeptide. *Chem. Commun.* **2014**, *50* (98), 15541-15544.

(105) Chen, L.; Morris, K.; Laybourn, A.; Elias, D.; Hicks, M. R.; Rodger, A.; Serpell, L.; Adams, D. J. Self-Assembly Mechanism for a Naphthalene-Dipeptide Leading to Hydrogelation. *Langmuir* **2010**, *26* (7), 5232-5242.

(106) Almine, J. F.; Bax, D. V.; Mithieux, S. M.; Nivison-Smith, L.; Rnjak, J.; Waterhouse, A.; Wise, S. G.; Weiss, A. S. Elastin-Based Materials. *Chem. Soc. Rev.* **2010**, *39* (9), 3371-3379.

(107) Fallas, J. A.; O'Leary, L. E. R.; Hartgerink, J. D. Synthetic Collagen Mimics: Self-Assembly of Homotrimers, Heterotrimers and Higher Order Structures. *Chem. Soc. Rev.* **2010**, *39* (9), 3510-3527.

(108) O'Leary, L. E. R.; Fallas, J. A.; Bakota, E. L.; Kang, M. K.; Hartgerink, J. D. Multi-Hierarchical Self-Assembly of a Collagen Mimetic Peptide from Triple Helix to Nanofibre and Hydrogel. *Nat. Chem.* **2011**, *3* (10), 821-828.

(109) Collier, J. H.; Rudra, J. S.; Gasiorowski, J. Z.; Jung, J. P. Multi-Component Extracellular Matrices Based on Peptide Self-Assembly. *Chem. Soc. Rev.* **2010**, *39* (9), 3413-3424.

(110) Liyanage, W.; Vats, K.; Rajbhandary, A.; Benoit, D. S. W.; Nilsson, B. L. Multicomponent Dipeptide Hydrogels as Extracellular Matrix-Mimetic Scaffolds for Cell Culture Applications. *Chem. Commun.* **2015**, *51*, 11260-11263.

(111) Liu, J.; Sun, Z.; Yuan, Y.; Tian, X.; Liu, X.; Duan, G.; Yang, Y.; Yuan, L.; Lin, H. C.; Li, X. Peptide Glycosylation Generates Supramolecular Assemblies from Glycopeptides as Biomimetic Scaffolds for Cell Adhesion and Proliferation. *ACS Appl. Mater. Interfaces* **2016**, *8* (11), 6917-6924.

(112) Das, R. K.; Gocheva, V.; Hammink, R.; Zouani, O. F.; Rowan, A. E. Stress-

Stiffening-Mediated Stem-Cell Commitment Switch in Soft Responsive Hydrogels. *Nat. Mater.* **2016**, *15* (3), 318-325.

(113) Zhou, M.; Smith, A. M.; Das, A. K.; Hodson, N. W.; Collins, R. F.; Ulijn, R. V.; Gough, J. E. Self-Assembled Peptide-Based Hydrogels as Scaffolds for Anchorage-Dependent Cells. *Biomaterials* **2009**, *30* (13), 2523-2530.

(114) Beniash, E.; Hartgerink, J. D.; Storrie, H.; Stendahl, J. C.; Stupp, S. I. Self-Assembling Peptide Amphiphile Nanofiber Matrices for Cell Entrapment. *Acta Biomater.* **2005**, *1* (4), 387-397.

(115) Sur, S.; Newcomb, C. J.; Webber, M. J.; Stupp, S. I. Tuning Supramolecular Mechanics to Guide Neuron Development. *Biomaterials* **2013**, *34* (20), 4749-4757.

(116) Gao, Y.; Zhao, F.; Wang, Q.; Zhang, Y.; Xu, B. Small Peptide Nanofibers as the Matrices of Molecular Hydrogels for Mimicking Enzymes and Enhancing the Activity of Enzymes. *Chem. Soc. Rev.* **2010**, *39* (9), 3425-3433.

(117) Scott, G.; Roy, S.; Abul-Haija, Y. M.; Fleming, S.; Bai, S.; Ulijn, R. V. Pickering Stabilized Peptide Gel Particles as Tunable Microenvironments for Biocatalysis. *Langmuir* **2013**, *29* (46), 14321-14327.

(118) Lowik, D. W. P. M.; Leunissen, E. H. P.; van den Heuvel, M.; Hansen, M. B.; van Hest, J. C. M. Stimulus Responsive Peptide Based Materials. *Chem. Soc. Rev.* **2010**, *39* (9), 3394-3412.

(119) Banwell, E. F.; Abelardo, E. S.; Adams, D. J.; Birchall, M. a; Corrigan, A.; Donald, A. M.; Kirkland, M.; Serpell, L. C.; Butler, M. F.; Woolfson, D. N. Rational Design and Application of Responsive Alpha-Helical Peptide Hydrogels. *Nat. Mater.* **2009**, *8* (7), 596-600.

(120) Yoza, K.; Ono, Y.; Yoshihara, K.; Akao, T.; Shinmori, H.; Takeuchi, M.; Shinkai, S.; Reinhoudt, D. N. Sugar-Integrated Gelators of Organic Fluids: On Their Versatility as Building-Blocks and Diversity in Superstructures. *Chem. Commun.* **1998**, *8*, 907-908.

(121) Amanokura, N.; Yoza, K.; Shinmori, H.; Shinkai, S.; Reinhoudt, D. N. New Sugar-Based Gelators Bearing a p-Nitrophenyl Chromophore: Remarkably Large Influence of a Sugar Structure on the Gelation Ability. *J. Chem. Soc. Perkin Trans. 2* **1998**, *0*

(12), 2585-2592.

(122) Yoza, K.; Amanokura, N.; Ono, Y.; Akao, T.; Shinmori, H.; Takeuchi, M.; Shinkai, S.; Reinhoudt, D. N. Sugar-Integrated Gelators of Organic Solvents-Their Remarkable Diversity in Gelation Ability and Aggregate Structure. *Chem. Eur. J.* **1999**, *5* (9), 2722-2729.

(123) Gronwald, O.; Shinkai, S. 'Bifunctional' Sugar-Integrated Gelators for Organic Solvents and Water—on the Role of Nitro-Substituents in 1-O-Methyl-4,6-O-(Nitrobenzylidene)-Monosaccharides for the Improvement of Gelation Ability. *J. Chem. Soc. Perkin Trans. 2* **2001**, *10*, 1933-1937.

(124) Jung, J. H.; John, G.; Masuda, M.; Yoshida, K.; Shinkai, S.; Shimizu, T. Self-Assembly of a Sugar-Based Gelator in Water: Its Remarkable Diversity in Gelation Ability and Aggregate Structure. *Langmuir* **2001**, *17* (23), 7229-7232.

(125) Jung, J. H.; Shinkai, S.; Shimizu, T. Spectral Characterization of Self-Assemblies of Aldopyranoside Amphiphilic Gelators: What Is the Essential Structural Difference between Simple Amphiphiles and Bolaamphiphiles? *Chem. Eur. J.* **2002**, *8* (12), 2684-2690.

(126) Kobayashi, H.; Friggeri, A.; Koumoto, K.; Amaike, M.; Shinkai, S.; Reinhoudt, D. N. Molecular Design of "Super" Hydrogelators: Understanding the Gelation Process of Azobenzene-Based Sugar Derivatives in Water. *Org. Lett.* **2002**, *4* (9), 1423-1426.

(127) Kiyonaka, S.; Shinkai, S.; Hamachi, I. Combinatorial Library of Low Molecular-Weight Organo- and Hydrogelators. **2003**, *4*, 976-983.

(128) Sukegawa, H.; Nishimura, T.; Yoshio, M.; Kajiyama, S.; Kato, T. One-Dimensional Supramolecular Hybrids: Self-Assembled Nanofibrous Materials Based on a Sugar Gelator and Calcite Developed along an Unusual Axis. *Cryst. Eng. Comm* **2017**, *19* (12), 1580-1584.

(129) Rajkamal; Pathak, N. P.; Halder, T.; Dhara, S.; Yadav, S. Partially Acetylated or Benzoylated Arabinose Derivatives as Structurally Simple Organogelators: Effect of the Ester Protecting Group on Gel Properties. *Chem. Eur. J.* **2017**, *23* (47), 11323-11329.

(130) McNeice, P.; Zhao, Y.; Wang, J.; Donnelly, G. F.; Marr, P. C. Low Molecular Weight

Gelators (LMWGs) for Ionic Liquids: The Role of Hydrogen Bonding and Sterics in the Formation of Stable Low Molecular Weight Ionic Liquid Gels. *Green Chem.* **2017**, *19* (19), 4690-4697.

(131) Vibhute, A. M.; Muvvala, V.; Sureshan, K. M. A Sugar-Based Gelator for Marine Oil-Spill Recovery. *Angew. Chem. Int. Ed.* **2016**, *55* (27), 7782-7785.

(132) Yu, G.; Yan, X.; Han, C.; Huang, F. Characterization of Supramolecular Gels. *Chem. Soc. Rev.* **2013**, *42* (16), 6697-6722.

(133) Carré, A.; Le Grel, P.; Baudy-Floc'h, M. Hydrazinoazadipeptides as Aromatic Solvent Gelators. *Tetrahedron Lett.* **2001**, *42* (10), 1887-1889.

(134) Takahashi, A.; Sakai, M.; Kato, T. Melting Temperature of Thermally Reversible Gel. VI. Effect of Branching on the Sol–Gel Transition of Polyethylene Gels. *Polymer Journal*. **1980**, 335-341.

(135) Zuidema, J. M.; Rivet, C. J.; Gilbert, R. J.; Morrison, F. A. A Protocol for Rheological Characterization of Hydrogels for Tissue Engineering Strategies. *J. Biomed. Mater. Res. - Part B Appl. Biomater.* **2014**, *102* (5), 1063-1073.

(136) Yan, C.; Pochan, D. J. Rheological Properties of Peptide-Based Hydrogels for Biomedical and Other Applications. *Chem. Soc. Rev.* **2010**, *39* (9), 3528-3540.

(137) Lee, A. Y.; Erdemir, D.; Myerson, A. S. Crystal Polymorphism in Chemical Process Development. *Annu. Rev. Chem. Biomol. Eng* **2011**, *2*, 259-280.

(138) Pashuck, E. T.; Cui, H.; Stupp, S. I. Tuning Supramolecular Rigidity of Peptide Fibers through Molecular Structure. *J. Am. Chem. Soc.* **2010**, *132* (17), 6041-6046.

(139) Storrie, H.; Guler, M. O.; Abu-Amara, S. N.; Volberg, T.; Rao, M.; Geiger, B.; Stupp, S. I. Supramolecular Crafting of Cell Adhesion. *Biomaterials* **2007**, *28* (31), 4608-4618.

(140) Tibbitt, M W., Anseth, K. S. Hydrogel as Extracellular Matrix Mimics for 3D Cell Culture. *NIH Public Access* **2010**, *103* (4), 655-663.

(141) Babensee, J.; Babensee, J. E.; Anderson, J.; McIntire, L.; Anderson, J. M.; Mikos, A.; Mcintire, L. V; Mikos, A. G. Host Response to Tissue Engineered Devices, Adv. *Drug Del. Rev* **1998**, *33*, 111-139.

(142) Piras, C. C. Low molecular weight gelators : synthesis and self - assembly of sugar amphiphiles. Medway School of Pharmacy, Universities of Greenwich and Kent, PhD Thesis, **2016**, 1-266.

2. SYNTHESIS OF LMW HYDROGELATORS

2.1 Introduction

Evaluating the structure-function relationships and gelation behavior of the gelator molecules (building blocks of the hydrogels) was an essential part of the current project. Indeed, any structural modifications of the molecular building blocks were expected to have an immediate effect upon molecular packing and therefore upon the macroscopic and microscopic properties of the formed hydrogels. Further to this, it was important to assess the impact of the supramolecular conformation of the fibrous matrix on mammalian cells viability. Based on the obtained results it would be possible to propose certain structural motifs that could induce cell proliferation. Therefore, in an attempt to enrich the set of known LMW hydrogelators, several novel, structurally-related compounds were prepared and their gelation properties tested (see chapter 3). Based on their structural features, the three sets of potential hydrogelators reported herein are classified as fluorenylmethyloxycarbonyl (Fmoc), biotinylated and diphenylalanine analogues, respectively (Figure 2.1). The synthetic approach followed to obtain the desired compounds is described below.

Along with the known Fmoc-protected galactosamine (GalNHFmoc) **62** and glucosamine (GlcNHFmoc) **63** hydrogelators,[1] the galactopyranosylamine **64** and glucopyranosylamine **65** derivatives were also prepared. This set of compounds was synthesized with the intention to evaluate how structural differences might affect the gelation properties. For example, the inverted stereochemistry of the hydroxyl group at position C-4 could affect H-bonding, whereas the effect of aromatic-aromatic interactions on self-assembly can be explored by changing the position of the Fmoc-protected amine group on the carbohydrate scaffold. More specifically, this is attachment of the Fmoc moiety at C-2 for gelators **62** and **63** and C-1 for compounds **64** and **65 (**Figure 2.1). Subsequently, to assess the self-assembly of gelator molecules lacking an aromatic moiety, two new compounds were synthesized by incorporation of biotin at the amine group at the C-2 position of the carbohydrate scaffold (instead of the Fmoc-moiety) to yield compounds **66** and **67**.

Biotin was chosen due to its biological activity. Specifically, it consists a cofactor of several carboxylase enzymes responsible for transferring CO_2. Furthermore, biotin is involved to the metabolism of fats and carbohydrates, to the protein synthesis process and influences cell growth. Finally, it has a high affinity for protein binding (biotinylation) such as streptavidin

and avidin. Biotinylation therefore, consists an important biochemical technique to evaluate the localization of proteins and their interactions.

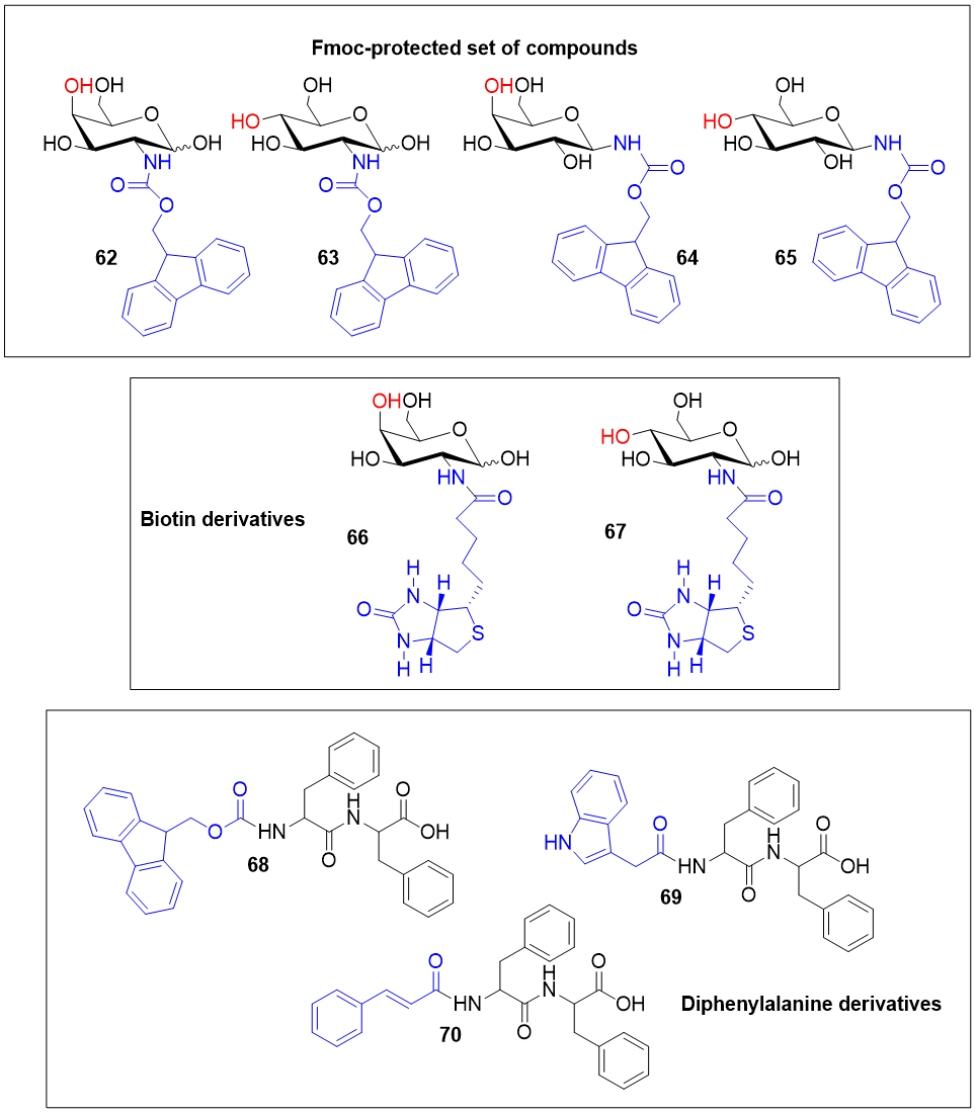

Figure 2.1 Chemical structures of the three sets of targeted hydrogelators.

In addition to the known aromatic dipeptides Fmoc-F-F[2–5] **68** and Ind-F-F[6] **69**, the cinnamoyl-capped diphenylalanine derivative Cin-F-F **70** was synthesized (L-phenylalanine unless stated otherwise). The preparation of Ind-F-F **69** was repeated, following a solution phase synthesis, instead of a solid phase protocol which has been described previously.[6] Gelation studies of these three dipeptide amphiphiles would illustrate the structural effects of three different aromatic moieties (Fmoc-, indole- and cinnamoyl-groups) on self-assembly and thus gelation.

Based on the known hydrogelators **62**, **63** and **68**, **69** it was necessary to proceed with the synthesis of novel analogues as to answer the following questions:

- In which extent any stereochemical differences upon structural related compounds could affect their gelation efficiency?
- Which structural effects could alter the configuration of the formed supramolecular network?
- Could we tune the properties of the formed hydrogels by incorporating certain functional moieties on the scaffold of the molecular building blocks?
- Could novel compounds affect cell viability and proliferation differently compared to the known ones?

2.2 Results and discussion

2.2.1 Preparation of the Fmoc-protected glycopyranosylamine derivatives 64 and 65

2.2.1.1 Retrosynthetic schemes

For the preparation of the Fmoc-protected glycopyranosylamine derivatives **64** and **65**, three different retrosynthetic schemes were designed overall since the first two synthetic attempts were found to be problematic. The first retrosynthetic scheme was designed to ease purification by performing flash column chromatography instead of multiple washings but issues occurred (Scheme 2.1- retrosynthesis I). This was addressed by the design of retrosynthesis II, where the deacetylation step of the hydroxyl groups (compounds **75**/**76**) would precede that of the Fmoc-amine coupling, in order to avoid the potential cleavage of the formed carbamate linkage (compounds **79**/**80**) under basic conditions. Unfortunately, after several attempts, no optimum basic conditions were found to achieve the synthesis of **64** and **65**.

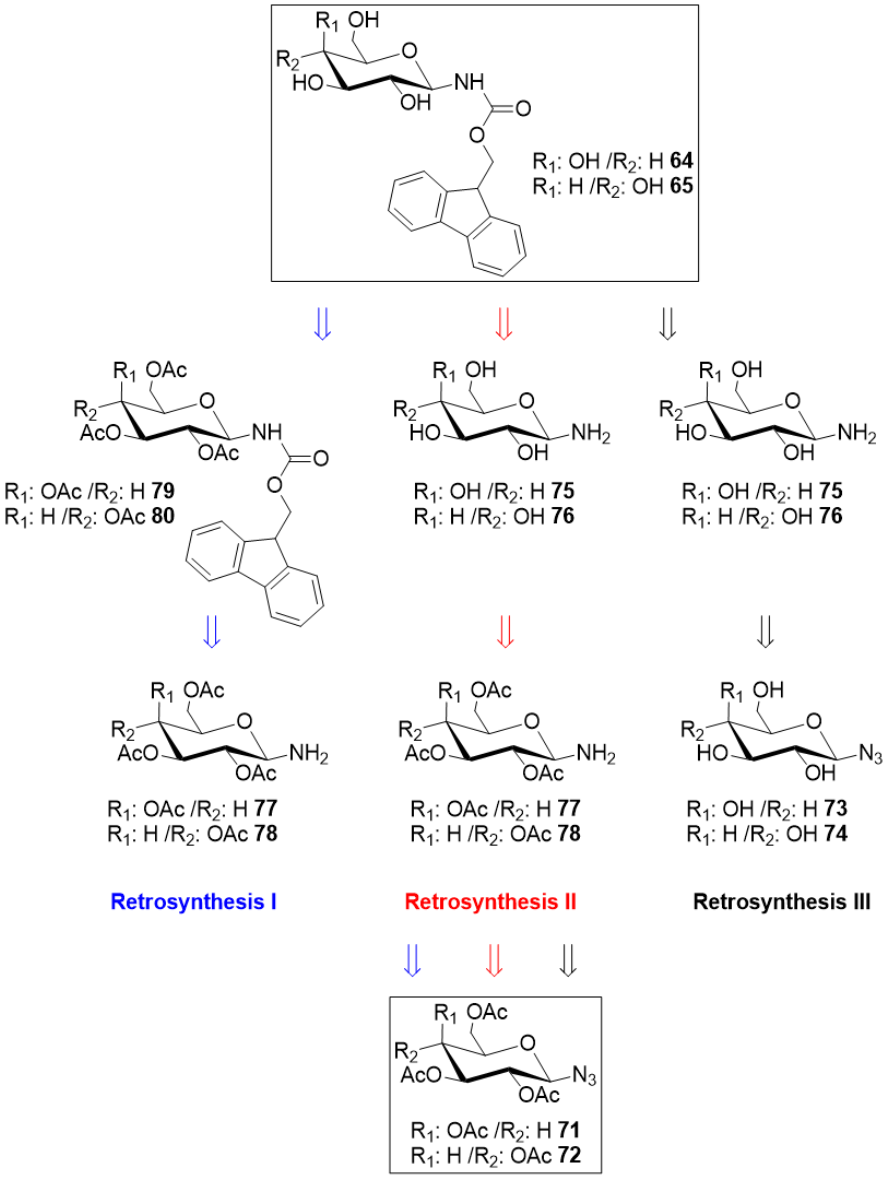

Scheme 2.1 The three retrosynthetic approaches attempted for the preparation of the Fmoc-protected glycopyranosylamine derivatives **64** and **65**.

The third retrosynthetic scheme, which led to the successful synthesis of the desired compounds **64** and **65**, was based on the published work of Hague *et al.* in which the Fmoc-protected glycopyranosylamines **64** and **65** were prepared as intermediate synthons for the synthesis of Fmoc-protected glycopyranosylamine uronic acids (Scheme 2.1-Retrosynthesis III).[7] Based on their protocol, compounds **64** and **65** could be obtained by protecting the amino group of glycopyranosylamines **75/76**. These could be synthesized by the reduction of the corresponding azides **73/74**, which themselves could be derived by deprotection of their peracetylated precursors **71/72** under basic conditions.

2.2.1.2 Synthetic routes

The first synthetic attempt failed to yield the desired product **64** and the Fmoc-protected compound **79** was obtained instead (Scheme 2.2). During the first step, the reduction of the peracetylated galactopyranosylazide **71** afforded the peracetylated amine **77** in stoichiometric yield. The amine was then used without further purification and coupled with Fmoc-Cl to afford a mixture of **79** and unreacted Fmoc-Cl, which was separated easily by flash column chromatography. The final deacetylation step under basic conditions was unsuccessful and led to the removal of the Fmoc moiety. Alternative reaction conditions for the selective deprotection of the acetyl groups were not explored and it was decided to evaluate compound **79** (50% overall yield over two steps) for its potential as an organogelator.

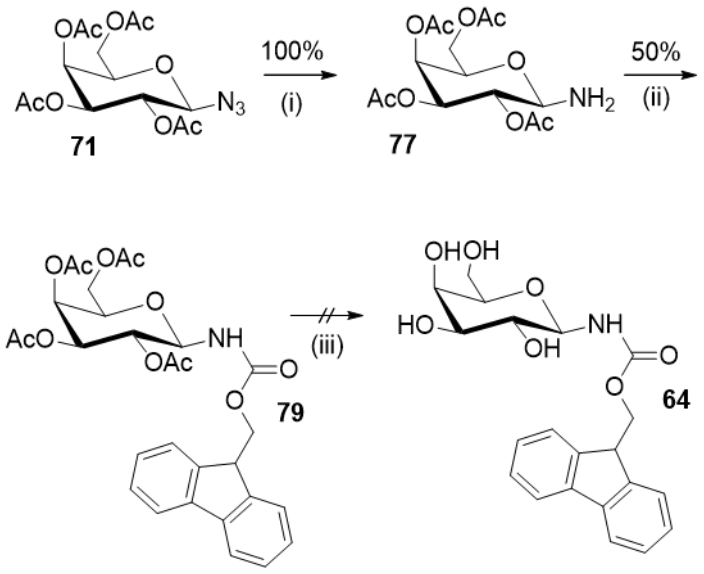

Scheme 2.2 Synthesis of the Fmoc-protected galactopyranosylamine **79**. Reagents and conditions: (i) anh. MeOH, Pd/C (0.2 eq), H_2, rt ; (ii) Fmoc-Cl (2.0 eq), $NaHCO_3$ (2.6 eq.), dioxane:water (2:1), rt ; (iii) anhyd. MeOH, NaOMe (0.1 eq), rt.

During the second synthetic approach, hydrogenation of the glycopyranosylamine **72** afforded the peracetylated amine **78** in stoichiometric amount (Scheme 2.3). The subsequent deprotection of **78** was performed under basic conditions, following the protocol of Zamyatina *et al*.[8] Therefore, **78** was dissolved in a methanol : water : triethylamine solvent mixture (7:3:1) and was left to stir at room temperature until thin layer chromatography (TLC) confirmed the consumption of the starting material after 3 hours. IR analysis of the residue however revealed the presence of a C=O peak at 1736 cm^{-1}, indicating either a partial

deacetylation reaction or the migration of an acetyl protective group to yield the acetylated amine **81** (Scheme 2.3 and Figure 2.2).

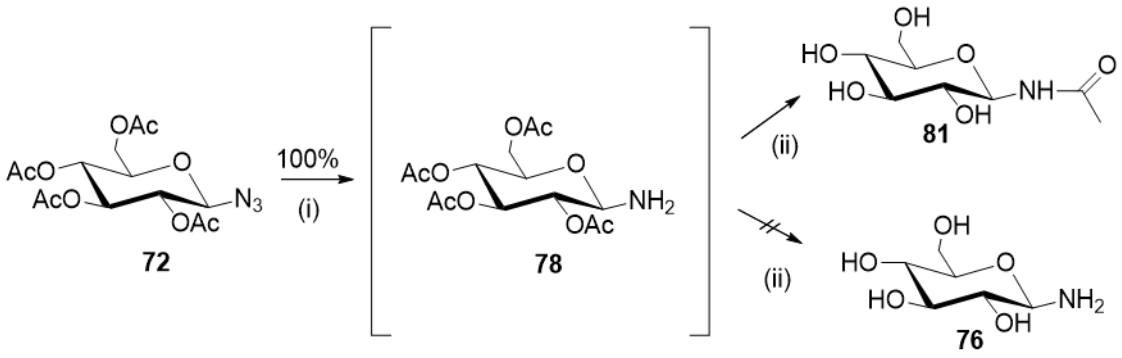

Scheme 2.3 Synthesis of the acetylated amine **81**. Reagents and conditions: (i) anh. MeOH, Pd/C (0.2 eq), H_2, rt; (ii) MeOH: water : Et_3N (7:3:1), rt.

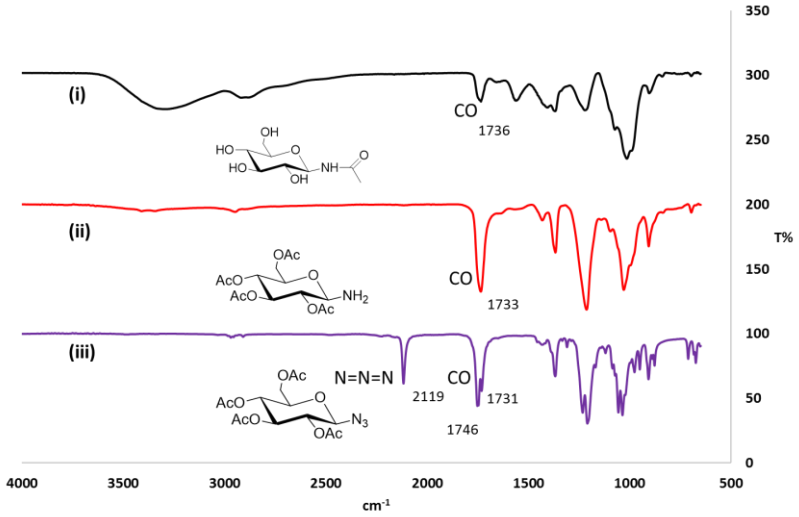

Figure 2.2 IR spectra (neat) of (i) the obtained compound **81** compared to (ii) the intermediate amine **78** and (iii) the starting material **72**.

A similar neighbouring group effect has been reported previously by Leino and co-workers in their studies on the migration of acetyl, pivaloyl, and benzoyl protective groups in a series of *β*-D-galactopyranoses and their relative stabilities under a range of pH conditions.[9] For this reason, trial reactions of **78** were performed by using K_2CO_3 as a base, following the protocol of Furstner *et al.*, as used in the total synthesis of Enigmazole A.[10] However, the desired product **76** could neither be isolated nor further purified, since K_2CO_3 was only partial soluble in methanol.

The last synthetic attempt was based on the published protocol of Hague *et al.* and was used for the preparation of both glycopyranosylamine derivatives **64** and **65** (Scheme 2.4).[7] During the first step, a suspension of the peracetylated azides **71/72** in anhydrous methanol, was treated with sodium methoxide, giving the glycosyl azides **73/74** in stoichiometric yield. Following hydrogenation in the presence of a catalytic amount of Pd/C, the glycosylamines **75/76** were formed. During the final step, a coupling reaction of **75/76** with Fmoc *N*-hydroxy-succinimide ester, yielded the desired products **64** (26% yield over 3 steps from **71**) and **65** (19% yield over 3 steps from **72**).

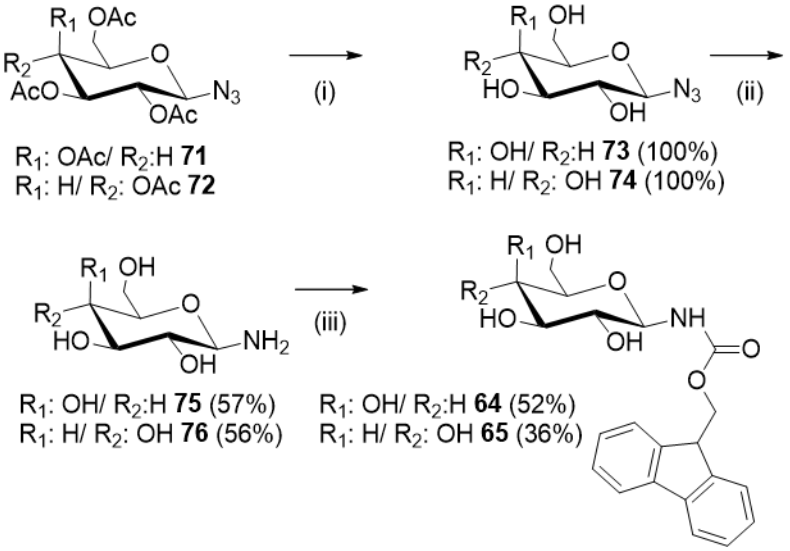

Scheme 2.4 Synthesis of the Fmoc-protected glycopyranosylamine analogues **64** and **65**. Reagents and conditions: (i) anh. MeOH, NaOMe (0.1 eq), rt; (ii) anh. MeOH, Pd/C (0.2 eq), H_2, rt; (iii) anh. Pyridine, Fmoc-OSu (1.04 eq) rt.

Although the same reaction conditions were applied for the synthesis of both glycopyranosylamine analogues **64** and **65**, the isolation and purification processes during the final step were different. For compound **65**, evaporation to dryness followed by washing of the residue with dichloromethane (DCM) yielded a precipitate which was further purified by recrystallization from methanol (MeOH), as described in the published protocol.[7] However, for compound **64**, washing of the residue with DCM did not afford a precipitate. Instead, addition of 1M aqueous HCl yielded a precipitate, which was washed further with water and DCM prior to the final recrystallization process with methanol. The acidic conditions led to the formation of the pyridine hydrochloric salt which was removed from the precipitate by washing with water. For both compounds, the intermediate products **73/74**

and **75/76** were isolated and characterized by IR (Figure 2.3, A and B) and NMR spectroscopy and then used without any further purification.

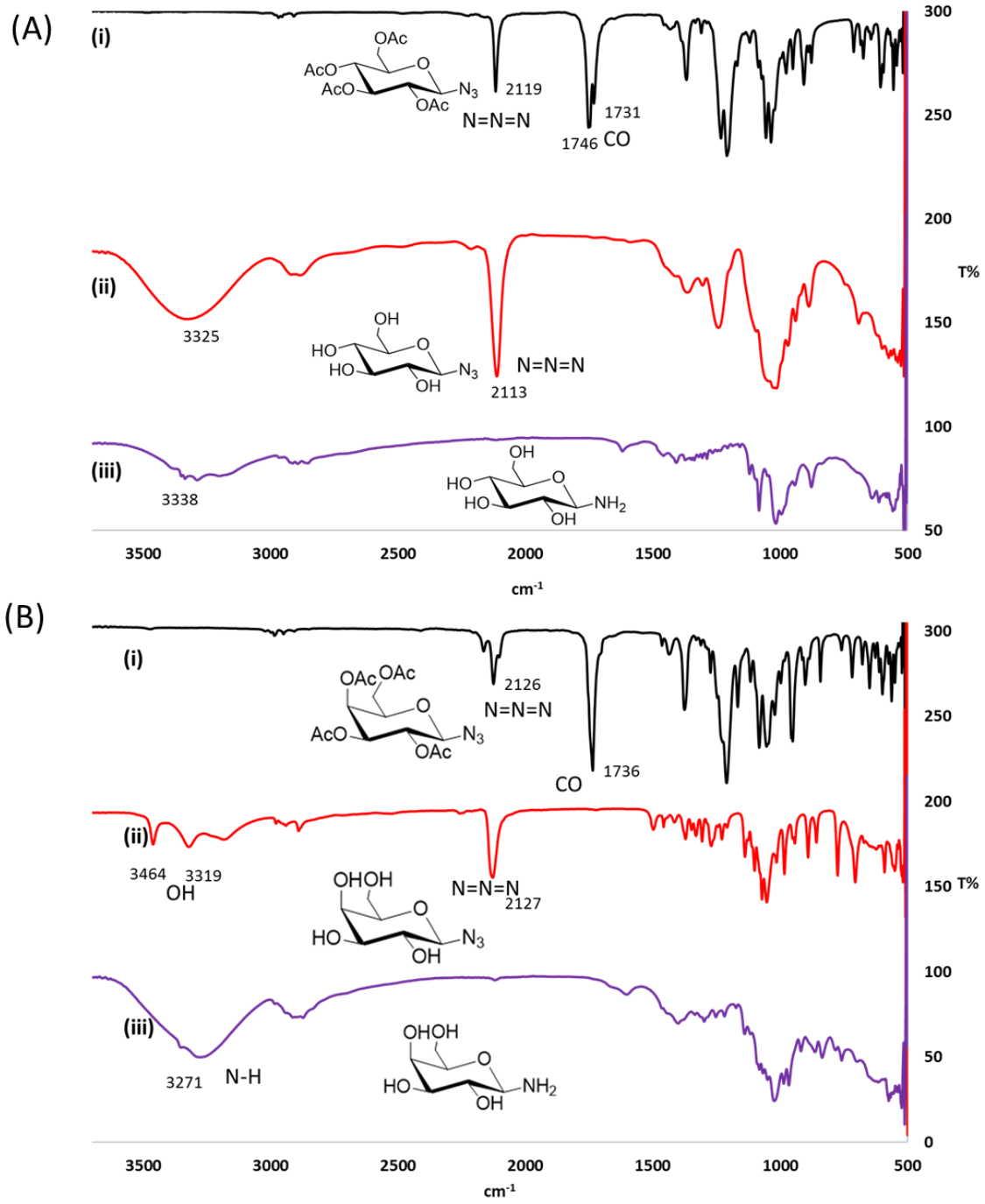

Figure 2.3 IR spectra (neat) of (i) starting material **71/72** and intermediate compounds **73/74** and **75/76** (ii-iii) isolated during the synthesis of the Fmoc-protected glucopyranosylamine **65** (A) and of the Fmoc-protected galactopyranosylamine **64** (B).

2.2.2 Synthesis of biotin-D-galactosamine 66 and biotin-D-glucosamine 67

Biotin derivatives **66** and **67** could be synthesized *via* a coupling reaction between biotin **82** and the corresponding amino sugars, galactosamine **117** and glucosamine **118**. Therefore, to form a new amide bond two retrosynthetic schemes were designed, either by activation of biotin **82** using a coupling agent[11] (retrosynthetic approach I) or by converting it to its more reactive acyl chloride analogue **83** (retrosynthetic approach II) (Scheme 2.5). In both cases, the synthesis is a single step followed by a facile purification protocol and a predicted high yield of the desired product. The ability for scale up and reproducibility of the reaction were two important aspects to consider.

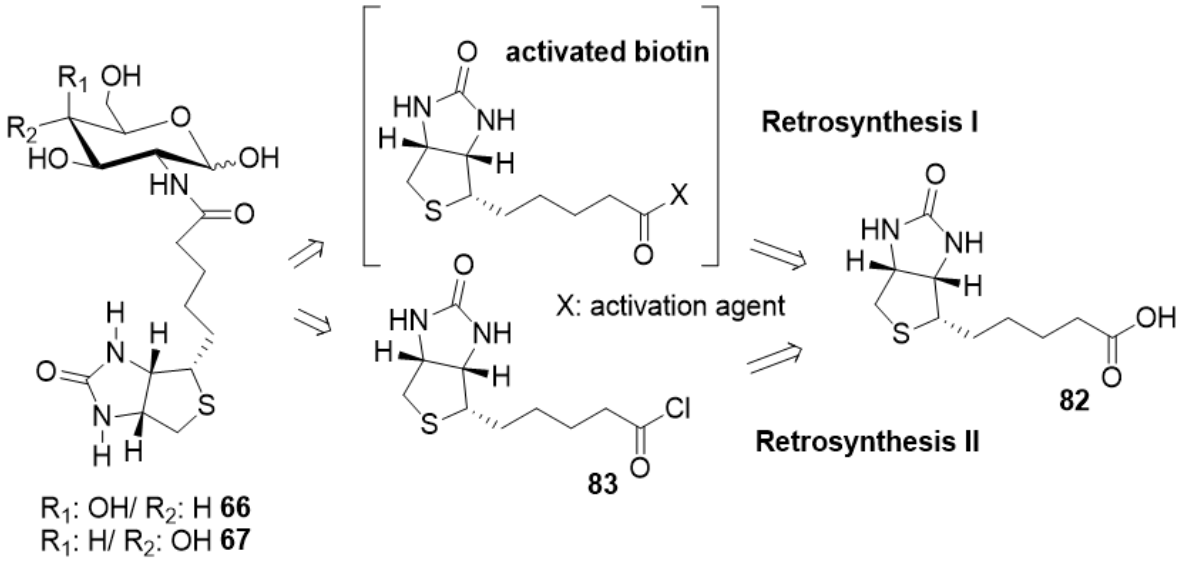

Scheme 2.5 Retrosynthetic schemes for the preparation of compounds **66** and **67**. (I) Biotinylation based on the activation of biotin using coupling agents and (II) biotinylation based on the conversion of biotin to its acyl chloride.

A series of trial reactions, aimed at the synthesis of biotinylated glucosamine **67**, were undertaken to test the effectiveness of each proposed synthetic method. Following the first approach, biotin **82** was activated, under basic conditions, with a coupling agent either *in situ* or separately (Table 2.1). *O*-(Benzotriazol-1-yl)-*N*,*N*,*N*′,*N*′-tetramethyluronium tetrafluoroborate (TBTU) and *N*-(3-Dimethylaminopropyl)-*N*′-ethylcarbodiimide hydrochloride/*N*-Hydroxysuccinimide (EDC/NHS) were used as coupling agents, while either flash column chromatography or washing of the obtained residues were performed for the isolation and purification of the desired product, depending on the TLC profile of each reaction mixture.

Table 2.1 Reaction conditions based on the first retrosynthetic scheme to form **67**. All equivalents (mmol) were calculated based on the amount of glucosamine used.
^ could not purify product, * could not isolate product

Trial reaction	Base	Base equivalents	Coupling agent(s)	Coupling agent(s) equivalents	*In situ* activation	Yield
1	DIPEA	2.5	TBTU	1.5	Yes	^
2	$NaHCO_3$	1.3	EDC-NHS	1.5	No	*
3	$NaHCO_3$	2.5	TBTU	1.5	Yes	88%
4	$NaHCO_3$	2.0	TBTU	1.0	No	90%

For all trial reactions anhydrous dimethylformamide (DMF) was used as a solvent, while the hydrochloric salt of glucosamine was converted to the corresponding amine by suspending the salt in DMF under basic conditions. After 30 minutes, the initial suspension became a transparent solution, indicating conversion of the salt to the free base.

In the first trial reaction, glucosamine was formed by reacting the salt with *N,N*-diisopropylethylamine (DIPEA) while biotin **82** was activated *in situ* in the presence of TBTU.

The second trial was based on the protocol followed by Pitcovski *et al.*, during their work on the synthesis and study of haptens on protein-carrier immunogenicity.[12] The glucosamine salt was reacted with $NaHCO_3$, but biotin **82** was reacted separately with EDC/NHS. After 30 minutes, the amino sugar solution was added to that of the activated biotin and the reaction was left to stir overnight at room temperature.

In the third trial reaction, biotin **82** was coupled *in situ* using TBTU, with glucosamine being formed by addition of $NaHCO_3$.

For the final trial reaction, activation of biotin **82** was performed separately using TBTU before addition to the glucosamine solution.

In all trial reactions, the solvent was evaporated to dryness before initiating the work-up process. Purification of the obtained residue originating from the second trial was performed *via* flash column chromatography, as indicated by the published protocol.[12] However, the eluent solvent system of MeOH : DCM (5%:95%) failed to yield the desired product; only

impurities were present in all obtained aliquots. In trials 1, 3 and 4, when the residue was suspended in DCM: ethyl acetate (EA) (1:1), a precipitate was formed and isolated. TLC of the precipitate in EA: MeOH: H_2O (7:2:1) showed three different spots with R_f values of 0.55 (impurity), 0.45 (product) and 0.25 (impurity) (Figure 2.4). The upper spot was successfully removed by washing with EA and the lower spot by washing with cold methanol. It should be noted that the product was partially soluble in methanol and continuous washing resulted in lowered yields. However, when DIPEA was used as a base (trial 1), methanol washing did not remove the lower spot. The use of $NaHCO_3$ and addition of fewer equivalents of TBTU (trial 4) reduced the formation of this impurity. That suggested that the lower spot referred to a biotin-intermediate, formed during the activation process, whereas the upper spot had the same R_f as biotin **82**. The impurities were neither isolated nor characterized.

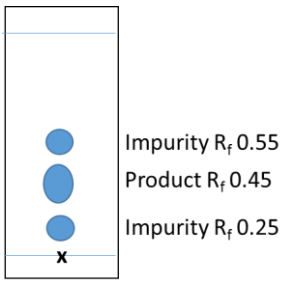

Figure 2.4 TLC of the obtained precipitate from trials 1, 3 and 4 for the synthesis of biotinylated glucosamine **67**. The solvent system used was EA: MeOH: H_2O (7:2:1), Hanessian's stain.

Depending on the work-up process employed (type of solvent and number of washings), different ratios of the α and β anomers of the product were obtained for trials 1, 3 and 4 (proton peaks around 4.95 ppm, Figure 2.6), as shown in the NMR spectra below (Figures 2.5 and 2.6). In addition, the NMR spectra of the product isolated by trial 1 contained impurities compared to those of trials 3 and 4. Due to the complexity of the spectra and the overlap of the proton peaks it wasn't possible to determine the exact α: β anomeric ratio in each trial. It appears though that the performed treatment affected the α: β ratio of anomers and presumably the crystallization process of the biotinylated sugar. Indeed, the obtained solids were clearly different in texture and colour indicating differences in their crystal structure (possible polymorphism). Unfortunately, there was no reproducibility regarding the anomeric ratio obtained, since a different number of washings was required in each trial. It would be interesting to explore the gelation ability of the obtained products of each trial and evaluate how different anomeric ratios might affect gelation using various triggers.

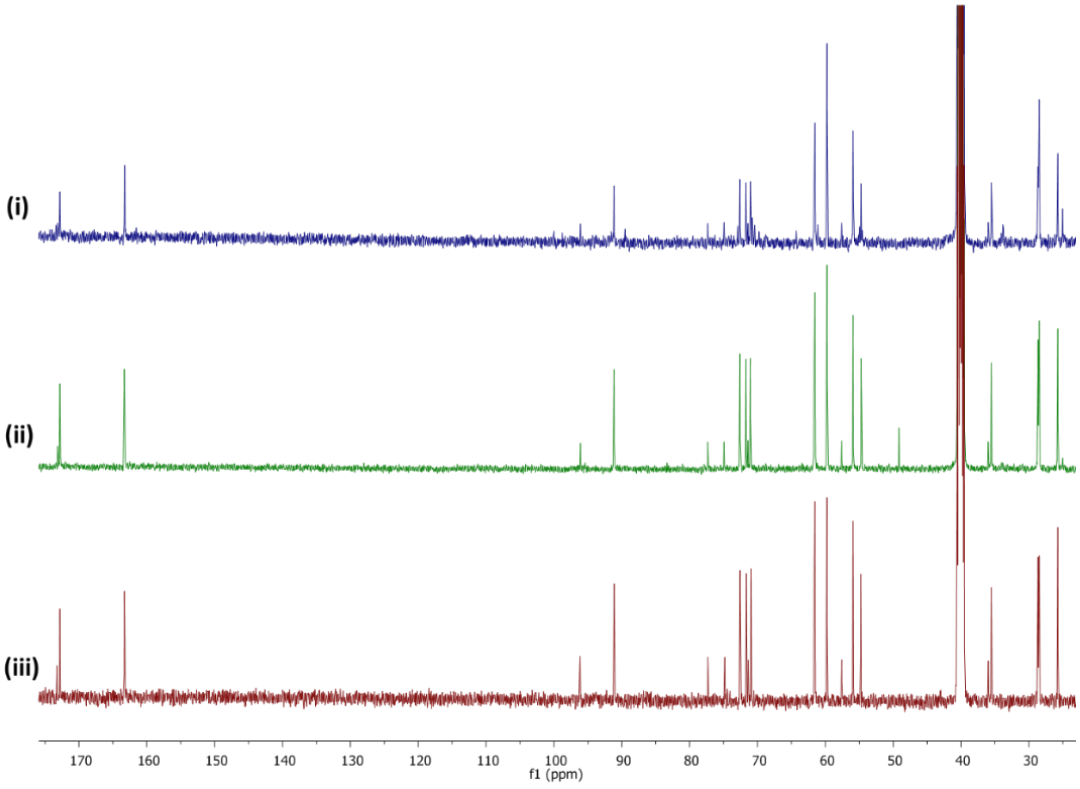

Figure 2.5 ^{13}C NMR (500 MHz, dmso-d_6) of **67** obtained from trials (i) 1, (ii) 3 and (iii) 4.

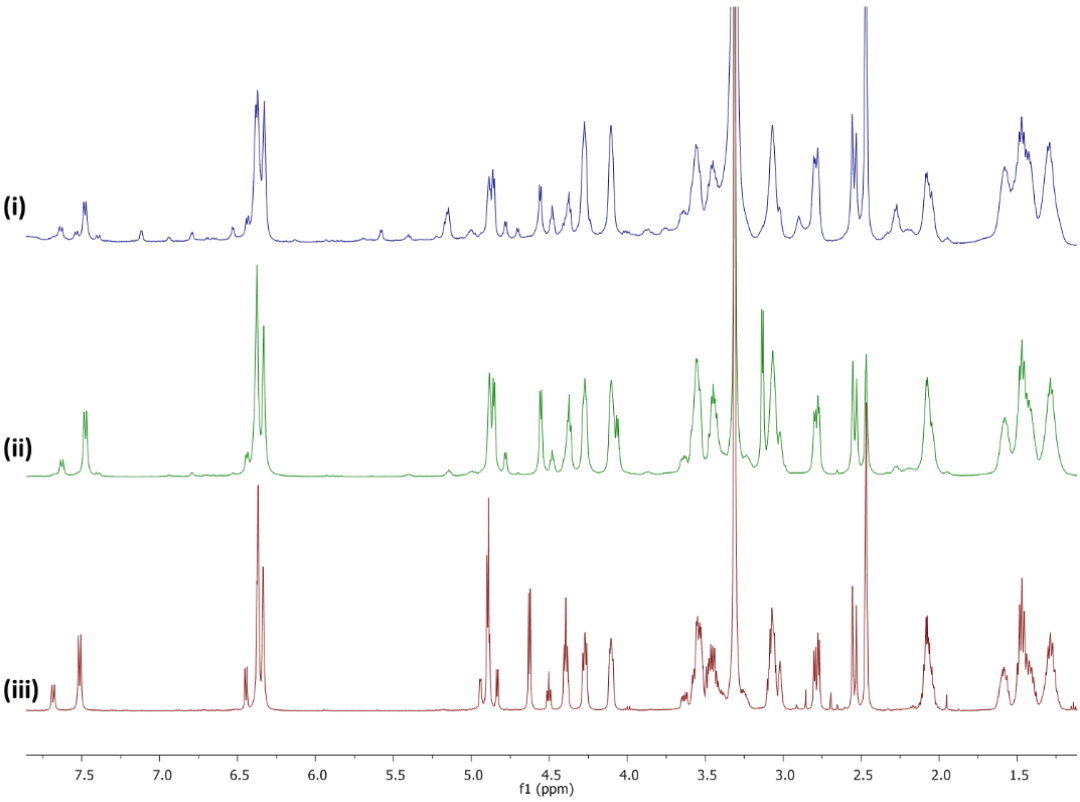

Figure 2.6 ^{1}H NMR (500 MHz, dmso-d_6) of **67** obtained by trials (i) 1, (ii) 3 and (iii) 4.

In the second synthetic approach, biotin **82** was converted to its corresponding acyl chloride derivative **83** by treatment with thionyl chloride.[13,14] A number of trial reactions were performed, differing in the type of base used, the amount of thionyl chloride employed and the number of steps followed *i.e. in situ* preparation of **83** or multiple step synthesis (Table 2.2). In all cases, the amino sugar glucosamine **118** was used as starting material for the evaluation of the effectiveness of each trial.

Table 2.2 Reaction conditions based on the second retrosynthetic scheme to prepare the biotinylated glucosamine **67**. All equivalents (mmol) were calculated based on the amount of glucosamine **118** used.

Trial reaction	Base	Base equivalents	$SOCl_2$ equivalents	*In situ* acylation
5	K_2PO_4	1.0	1.0	Yes
6	NaOH	1.0	3.0	No
7	$NaHCO_3$	1.0	4.0	No
8	$NaHCO_3$	3.0	4.0	No
9	DIPEA	3.0	4.0	No

Trial 5 was designed with the aim of *in situ* conversion of biotin **82** to the analogue **83**. The hydrochloric salt of glucosamine **118** was suspended in DMF in the presence of K_2PO_4 and left to stir for 30 minutes before the addition of biotin **82** and $SOCl_2$. The progress of the reaction was monitored by TLC; however the presence of the desired product was not observed during the 12 hours reaction time.

Following a different approach, trial 6 was performed in three steps. Biotin **82** was initially suspended in DCM with $SOCl_2$, but the reaction did not start until the addition of DMF, due to biotin's poor solubility in DCM. The solvent mixture of DCM: DMF (1:1) proved to be ideal. Under these conditions, the initial white suspension in DCM turned into a transparent yellow solution and an increase of the reaction's temperature was also observed, indicating the exothermic nature of the acyl chloride **83** formation (confirmed by TLC). The reaction mixture was flushed several times with N_2 and then left to stir overnight at room temperature. The next day, TLC verified the total consumption of the starting material. The formation of glucosamine **118** was achieved by suspending the hydrochloric salt in DMF under basic

conditions (NaOH). The two solutions were then mixed at 0°C and the reaction mixture was left to stir for a day at room temperature. After TLC confirmed the formation of a product, the solvent was evaporated, and the obtained residue was dissolved in MeOH, filtered (to remove NaCl), and finally evaporated to yield a thick black oil. Unfortunately, NMR analysis did not confirm the presence of **67**.

A different approach, based on the work of Hashimoto and co-workers, was followed for trial reaction 7.[15] For the formation of acyl chloride **83**, biotin **82** was dissolved in $SOCl_2$ and stirred for one hour at room temperature. The solution was then evaporated, and the residue dissolved in DMF. Glucosamine was prepared by reacting the hydrochloric salt with $NaHCO_3$ (solid) in DMF. Finally, the two solutions were mixed, and the reaction mixture was left to stir overnight. However, once again, TLC did not confirm the formation of the desired biotinylated product **67**.

Analysis of the general mechanism for acyl chloride formation revealed that HCl is formed and, for that reason, two equivalents of the amine should be used (Scheme 2.6). One equivalent reacts with the acyl chloride and the other with HCl to form an ammonium salt. In all trials, only one equivalent of the hydrochloric salt of glucosamine **118** was used and this could explain why the couplings failed. By increasing the equivalents of the base for the conversion of glucosamine hydrochloride to the free base, it was possible to address this (removal of HCl in the form of a salt) and proceed with the coupling. Therefore, trial 8 was performed in the same manner as 7 but this time 3.0 equivalents of $NaHCO_3$ were used instead of 1.0. Unfortunately, TLC still did not show the formation of the product. The same outcome was attained when the base was changed to DIPEA (trial 9).

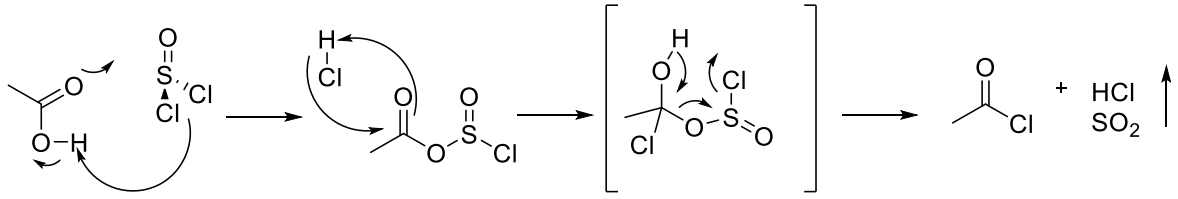

Scheme 2.6 General mechanism of acyl chloride formation.

Even though, all solvents used were anhydrous and the reactions were performed under dry conditions, the possible formation of water during the conversion of glucosamine hydrochloride to the free amine **118**, could cause the hydrolysis of the acyl chloride **83** to

the biotin acid form **82**. Due to restricted time, and since the desired product was formed using the coupling reagent strategy, further trial reactions were suspended.

2.2.3 Preparation of cinnamoyl-protected diphenylalanine 70

For the synthesis of Cin-F-F **70**, two different approaches were attempted since the first one was unsuccessful. For first retrosynthetic scheme I, the desired product **70** could be obtained by deprotection of the intermediate **84** (Scheme 2.7). A coupling reaction between cinnamoyl-phenylalanine **85** (Cin-F) and the protected phenylalanine **86** should yield ester **84**. The free acid **85** could be prepared by deprotection of the cinnamoyl-phenylalanine derivative **87**, originating from the coupling of cinnamic acid **88** with the phenylalanine ester **86**.

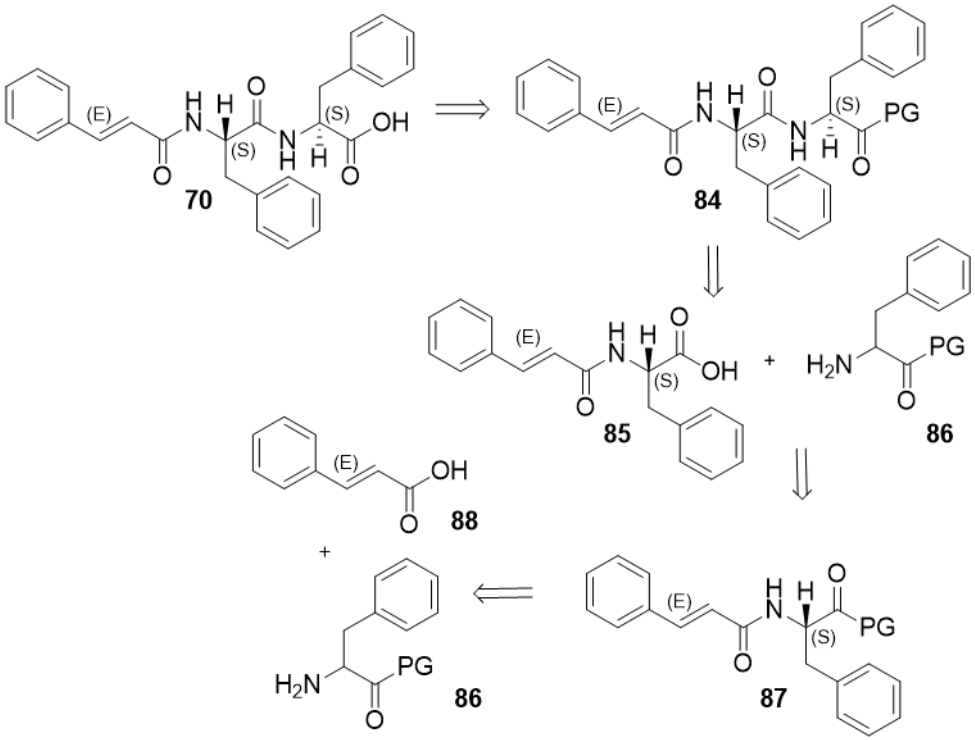

Scheme 2.7 Retrosynthetic scheme I for Cin-L-F-L-F **70**.

The first step of the synthesis involved the formation of an amide bond between cinnamic acid **88** and the *tert*-butyl ester of phenylalanine **89**, giving the enantiopure intermediate **90** (Cin-FO*t*Bu) in 90% yield (Scheme 2.8). Deprotection of ester **90** under acidic conditions provided the free acid **85** (Cin-F) in quantitative yield; which was used without further purification. The second coupling reaction was performed under an inert N_2 atmosphere using TBTU as a coupling agent and $NaHCO_3$ as the base for the deprotonation of acid **85**.

However, after isolation of the resulting products, NMR spectroscopy confirmed the formation of an epimeric mixture containing compounds **91** (Cin-L-F-L-FO*t*Bu) and **92** (Cin-D-F-L-FO*t*Bu) in a 2:1 ratio (Scheme 2.8). The presence of six carbonyl signals instead of three, in addition to the double doublet peaks of the vinyl protons (6.70 ppm) and that of the NH group (8.60- 8.20 ppm) verified the presence of epimers **91** and **92** (Figures 2.7 and 2.8). These could not be separated by flash column chromatography or filtration as they showed the same R_f value and appeared as a single spot on the TLC plate. The epimeric mixture of **91** and **92** was then deprotected under acidic conditions to yield quantitatively the corresponding mixture of free acids **70** and **93**, in a 2:1 ratio (Cin-L-F-L-F: Cin-D-F-L-F) and 43% total yield over four steps.

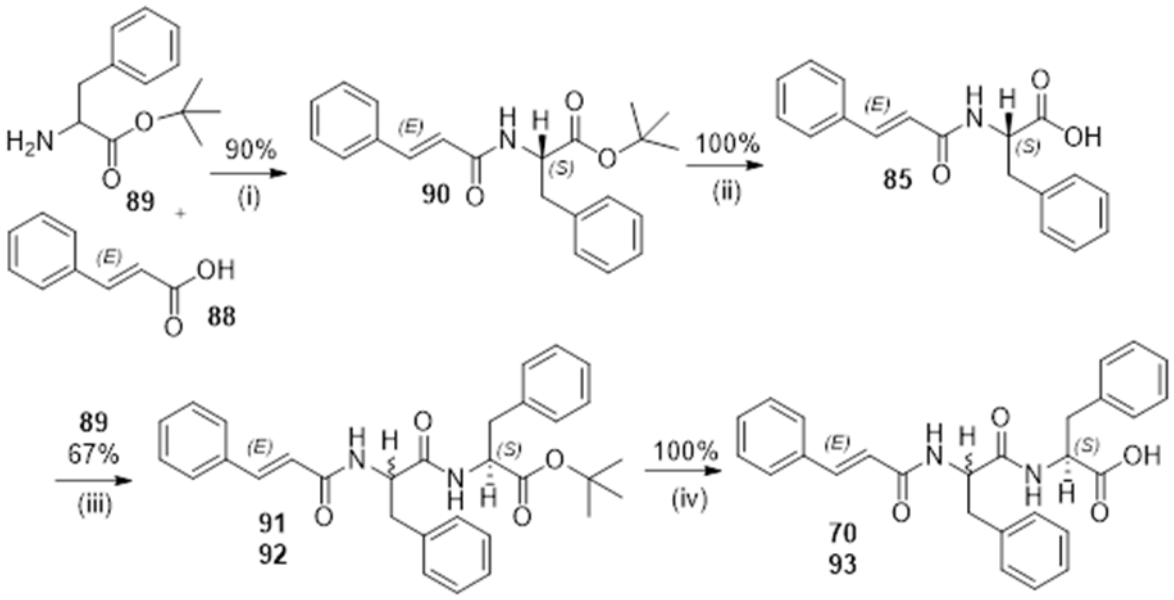

Scheme 2.8 Synthesis based on retrosynthetic scheme I. Reagents and conditions: (i) anh. DMF, TBTU (1.5 eq), $NaHCO_3$ (2.5 eq), rt; (ii) DCM, TFA (10 eq); (iii) anhydrous DMF, TBTU (1.5 eq), $NaHCO_3$ (2.5 eq), rt; (iv) DCM, TFA (10 eq), rt.

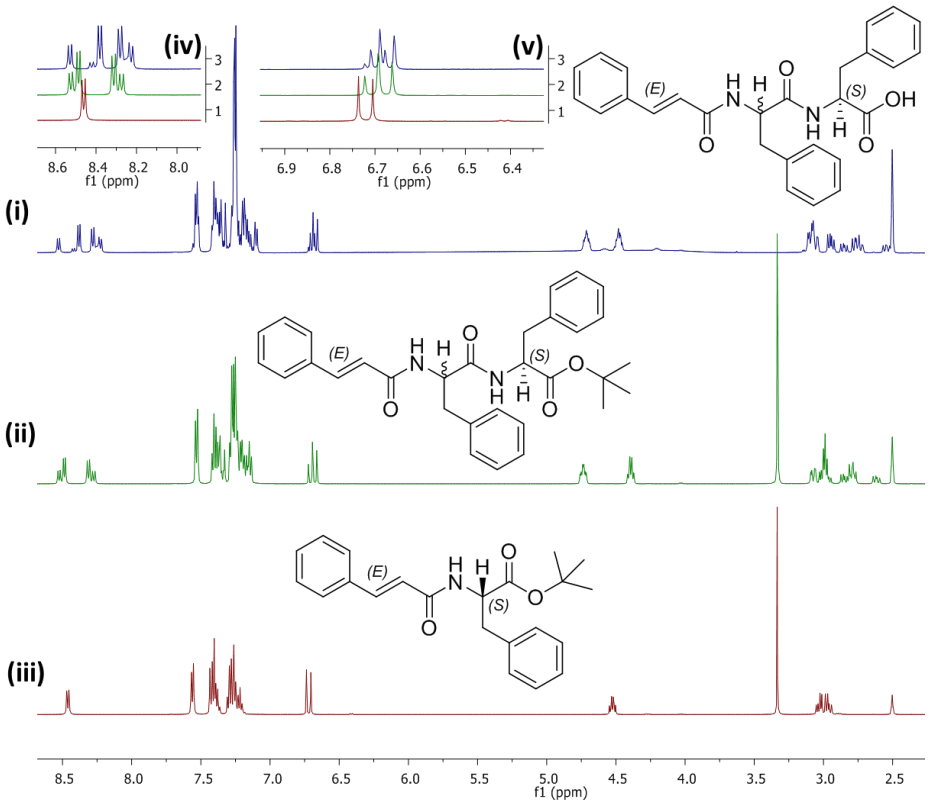

Figure 2.7, ^{1}H NMR (500 MHz, dmso-d_6) spectra of (i) Cin-D/L-F-L-F **70/93**, (ii) Cin-D/L-F-L-FO*t*Bu **91/92** and (iii) Cin-L-FO*t*Bu **90** with (iv) and (v) enlarged areas.

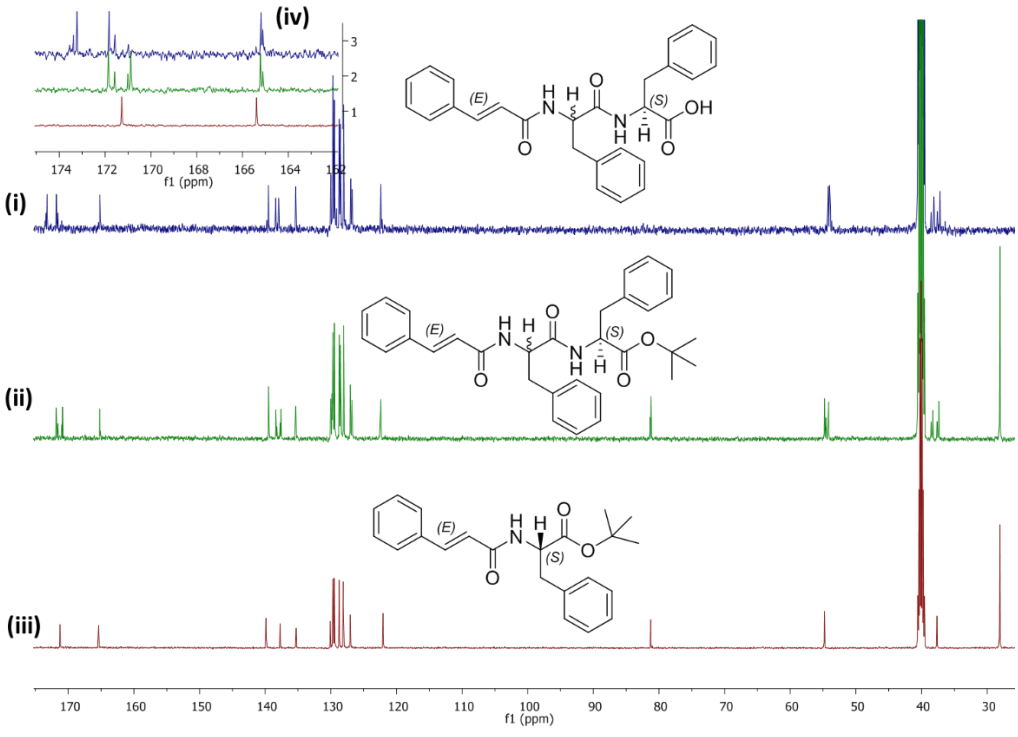

Figure 2.8 ^{13}C NMR (126 MHz, dmso-d_6) spectra of (i) Cin-D/L-F-L-F **70/93**, (ii) Cin-D/L-F-L-FO*t*Bu **91/92**, (iii) Cin-L-FO*t*Bu **90** and (iv) enlarged area.

The epimerization of diphenylalanine derivatives **91** and **92** was investigated further by repeating the second coupling reaction under the same conditions (Scheme 2.8), but with different coupling agents. TBTU was replaced by 1-hydroxy-7-azabenzotriazole (HOAT) (1.1 eq) and *N, N'*-diisopropylcarbodiimide (DIC) (1.0 eq), while a stoichiometric amount of the same base ($NaHCO_3$, 1.1 eq) was used for the deprotonation of acid **85**. Interestingly, the same ratio of epimers **91** and **92** was obtained. Based on the findings, it was suggested that the nature of the coupling agent and the amount of base used were not responsible for the inversion of stereochemistry. This therefore implied it was the structure of the reactants that could have affected the stereochemical outcome of the reaction.

This led to the following epimerization mechanism being proposed in an attempt to explain the formation of the second epimer **92** (Cin-D-F-L-FO*t*Bu) (Scheme 2.9, A).

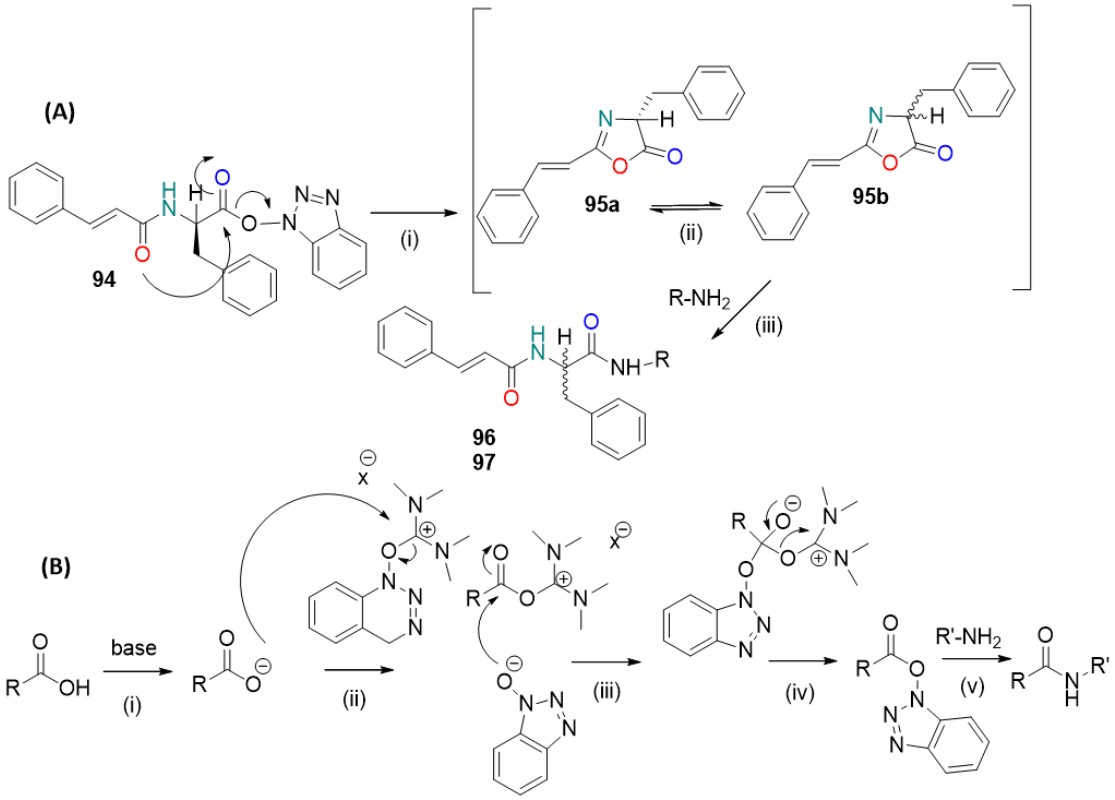

Scheme 2.9 Proposed epimerization mechanism (A) and the amide bond formation mechanism (B) where activation is achieved by the use of TBTU, an uronium type coupling agents.[16]

The presence of two adjacent carbonyl groups on the same activated reactant **94** (A-i) could trigger an intramolecular nucleophilic attack, as the oxygen of the first group can react with the electrophilic carbon of the second carbonyl group. This would lead to the formation of the intermediate oxazolone **95a** which can be epimerized **95b** (A-ii). Finally, the opening of

the ring yields the epimers **96** and **97** respectively. The epimerization mechanism (A) refers to steps (B-iii) and (B-iv) of the general amide bond formation mechanism (Scheme 2.9, B). Indeed, deprotonation of the acid (B-i) follows a nucleophilic attack on the electrophilic carbon of TBTU (B-ii) leading to an intramolecular rearrangement (B-iii) and the formation of the activated acid (B-iv). During the final step (B-v) a nucleophilic attack of the amine to the activated carbon leads to the formation of a new amide bond (Scheme 2.9, B).

As the first synthetic approach failed to yield the enantiopure product **70**, a second retrosynthesis was proposed (Scheme 2.10). Cin-F-F **70** could be obtained by deprotection of intermediate **84** under acidic conditions. The protected diphenylalanine cinnamoyl derivative **84** could be obtained by coupling cinnamic acid **88** with dipeptide **98**. Selective deprotection of the amine group of **99** could afford the intermediate **98**. By this retrosynthetic scheme, the desired stereochemistry of **70** is introduced during the first step of the synthesis by coupling the protected amino acids **86** and **100**.

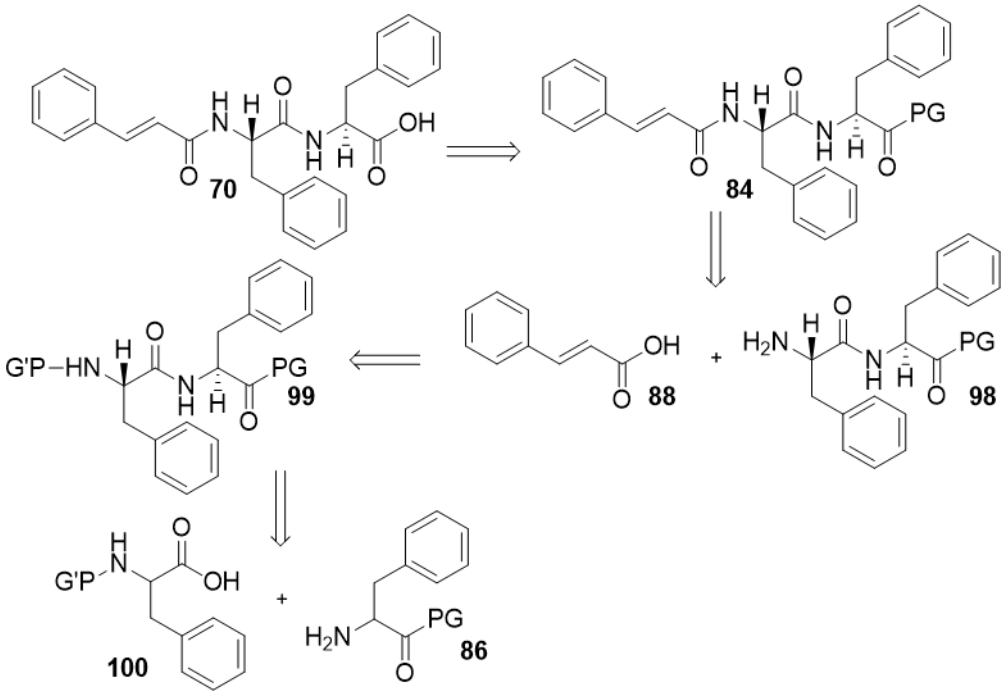

Scheme 2.10 Retrosynthetic scheme II for the synthesis of Cin-L-F-L-F **70**.

Amino acids **89** and **101** were coupled by dissolving the hydrochloride salt of **89** in anhydrous DMF, under basic conditions ($NaHCO_3$), followed by the addition of TBTU and the free acid **101** (Scheme 2.11).

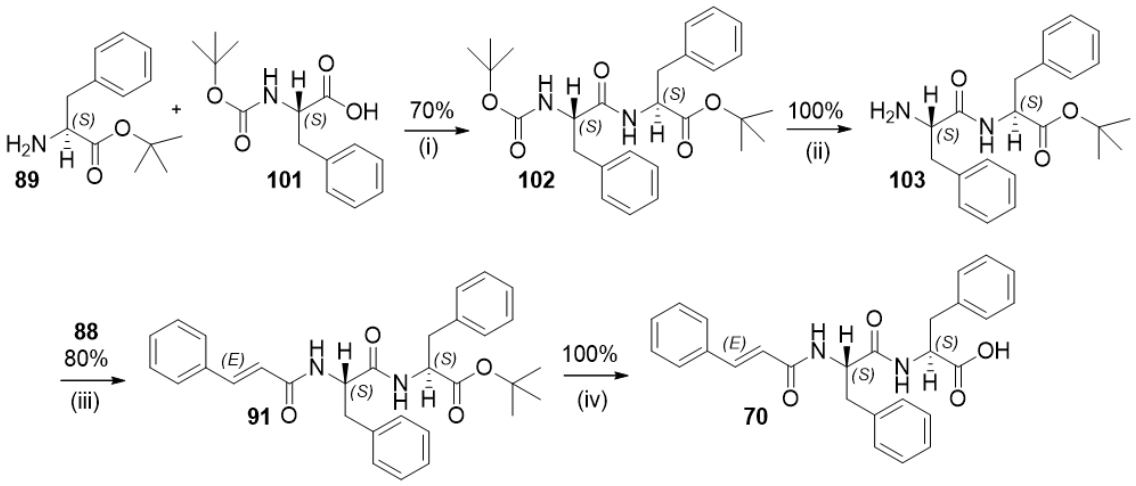

Scheme 2.11 Synthesis based on retrosynthetic scheme II. Reagents and conditions: (i) anh. DMF, TBTU (1 eq.), $NaHCO_3$ (2.1 eq), rt; (ii) *tert*-Butyl acetate, con. H_2SO_4 (3 eq), rt; (iii) anh. DMF, TBTU (1.5 eq), $NaHCO_3$ (2.5 eq) rt; (iv) DCM, TFA (20 eq), rt.

TLC confirmed the consumption of the starting materials after 12 hours, at which point the solution was evaporated to dryness. The remaining residue was dissolved in EA and washed with water. Finally, the desired product **102** was purified by flash column chromatography, using an eluent system of hexane (Hex: EA, 3:1) to obtain **102** as an off-white, glassy solid in 97% yield.

Several attempts of the above coupling reaction under the same conditions failed to reproduce this initial result. Instead of the di-protected dipeptide **102**, a mixture of two compounds (same spot on the TLC), in an almost 1:1 ratio, was obtained every time, as confirmed by NMR spectroscopy (Figure 2.9). Due to the hindered C-N bond rotation of the *Boc*-group adjacent to the phenyl moiety present in **101**, it was proposed that the amino acid **101** could exist in the form of two distinct rotamers. Indeed, a ^{1}H NMR spectrum of **101** acquired at 25 °C verified the presence of the two rotamers (Figure 2.10). Such a hypothesis could explain a presumably equal reaction of the two *Boc*-protected **101** rotamers which could potentially lead to the formation of two conformers of dipeptide **102**.

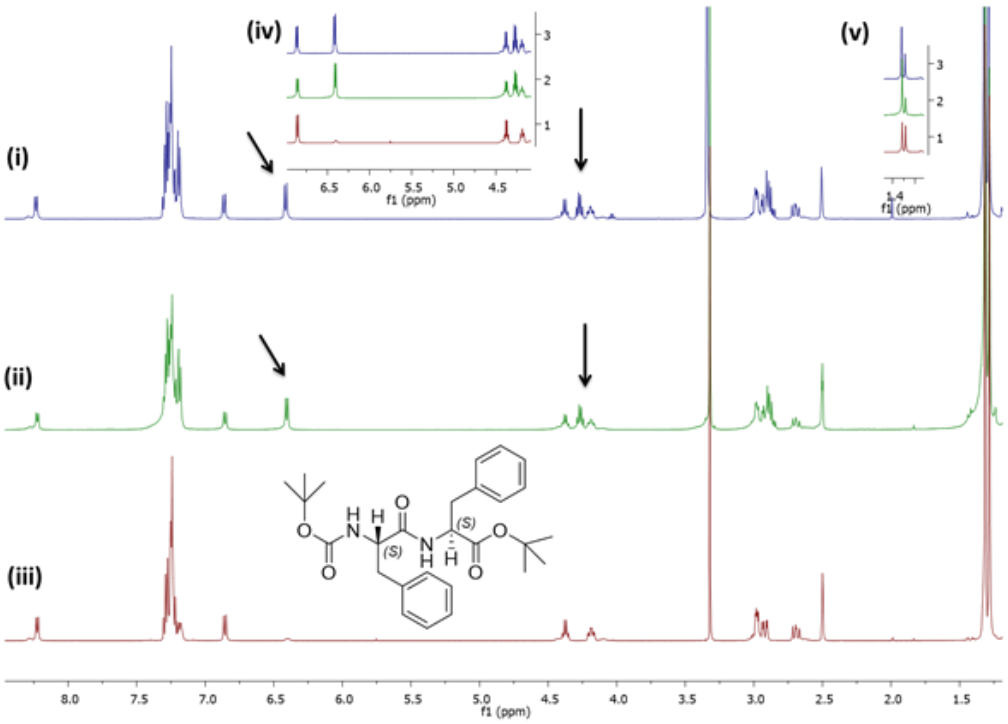

Figure 2.9 ^{1}H NMR (400 MHz, dmso-d_6) spectra at 25 °C of the mixture of the two possible conformers of **102** isolated over (i) first attempt and (ii) second attempt and (iii) dipeptide **102** which was obtained during the first reaction which couldn't be reproduced. Enlarged areas are (iv) and (v). Arrows indicate NH (left) and CH (right) proton signals which distinguish the two conformers.

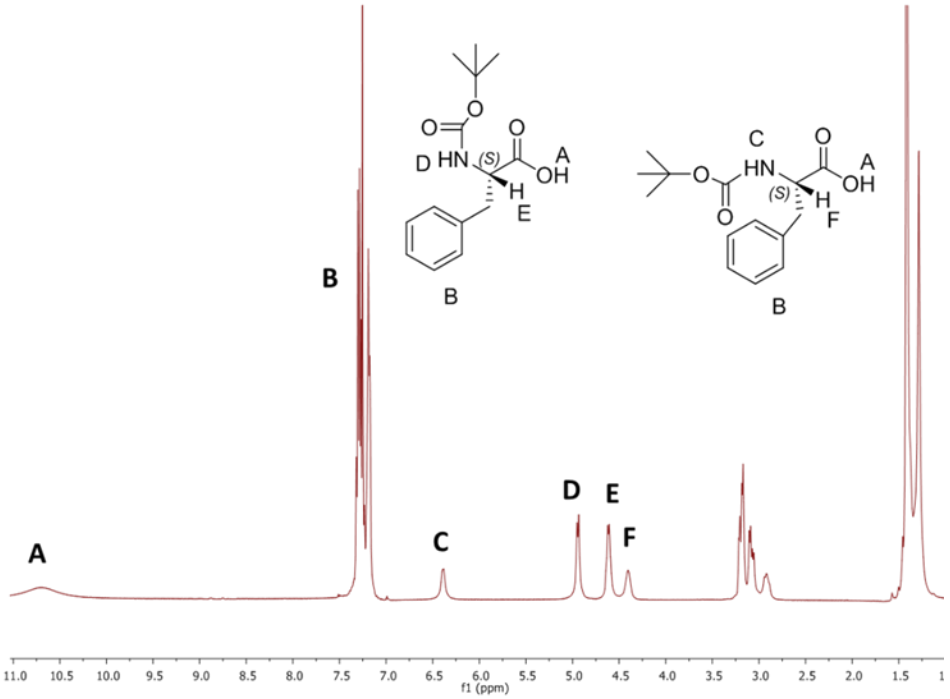

Figure 2.10 ^{1}H NMR (400 MHz, $CDCl_3$) spectrum of the *Boc*-protected amino acid **101** at 25 °C. The indicated proton peaks C-F suggest two rotamers.

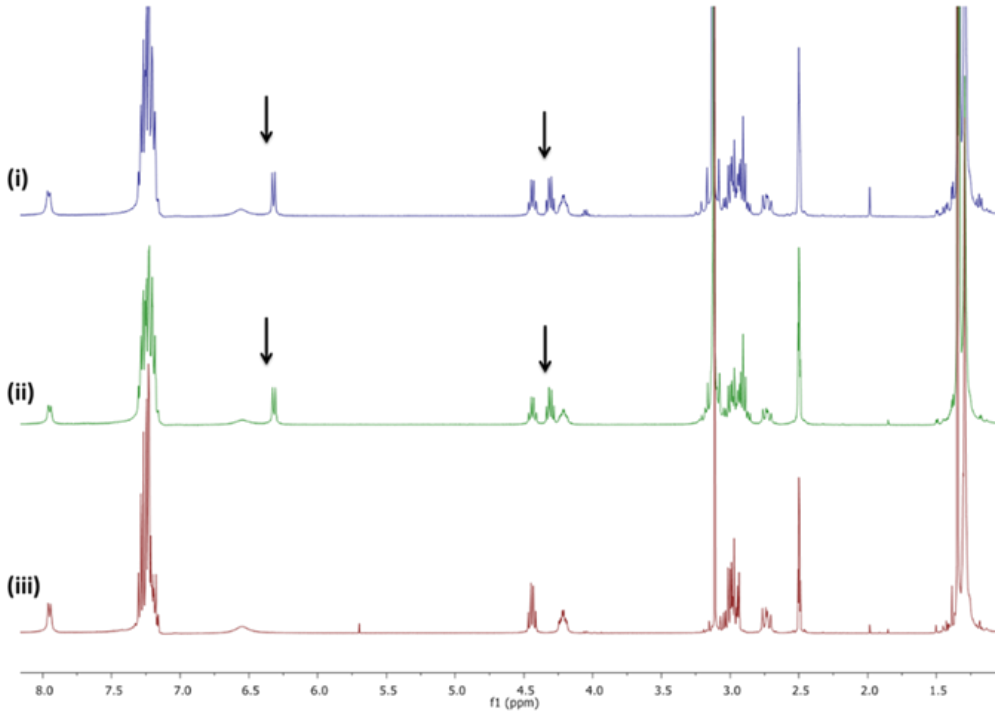

Figure 2.11 ^{1}H NMR (400 MHz, dmso-d_6) spectra at 70 °C of the mixture of the two possible conformers of **102** isolated over the (i) first attempt and (ii) second attempt and (iii) dipeptide **102** obtained during the first reaction which couldn't be reproduced. Arrows indicate the extra NH (left) and CH (right) proton signals.

In order to verify the presence of the two conformers of **102**, variable-temperature NMR studies of the obtained mixtures were performed at 70 °C and 25 °C where it was expected that at a higher temperature the extra proton signals (6.41 ppm and 4.27 ppm observed at 25 °C) would disappear. However, this was shown not to be the case, indicating that the mixture was not a pair of conformers, but instead consisted of the desired product **102** and an unknown compound (Figures 2.9 and 2.11).

Since NMR studies confirmed the presence of the two rotamers for the *Boc*-protected amino acid **101**, therefore, repeating the coupling reaction at higher temperatures (Table 2.3) could possibly shift the thermodynamic equilibrium between the two rotamers by lowering the energy barrier for their interconversion.

Table 2.3 Coupling reaction outcome performed at different temperatures.

Temperature (°C)	Outcome
r.t.	Mixture of two compounds (**102** and **89**)
35	Mixture of two compounds (**102** and **89**)
60	*tert*-butyl ester of phenylalanine **89**

The obtained data revealed that, at 60 °C, the reaction failed to yield the desired product **102**, instead the starting material **89** was recovered by flash column chromatography. Based on NMR analysis, the next two attempts at room temperature and at 35 °C confirmed the mixture of **102** and **89**, but in different ratios of the individual components. Clearly one rotamer favors synthesis of dipeptide **102** and the other does not. It seems that the rotamer formed at elevated temperature (60 °C) is not the one that forms **102** due to hindrance. This explains why heating did not give the product. Lowering the temperature would possibly favor the reaction of the more reactive rotamer *i.e.* the one not visible in the final compound. Due to time constrains no trial reactions were attempted at reduced temperatures. Therefore, hindrance due to the presence of rotamers should be assessed further in the future. From the above studies, it was apparent that the coupling reaction of the two protected amino acids **89** and **101** was not reproducible. In addition, raising the temperature to 35 °C failed to provide the desired product, yielding instead mixtures with different ratios of **102** and of the starting material **89**. The amino acid **89** and the product **102** could not be separated by flash column chromatography, as both compounds appeared on the TLC plate as a single spot. Filtration and recrystallization trials were also performed but were unsuccessful. Regardless of the completion of the coupling reaction there would be continued issues of purification if the reaction did not go to completion.

After consideration of alternative reaction conditions, dipeptide **102** was synthesized successfully following a different experimental protocol. The hydrochloride salt of *tert*-butyl phenylalanine ester **89** was dissolved in anhydrous DMF with $NaHCO_3$, while the activation of the free acid **101** by TBTU was performed separately. The two solutions were then mixed, and the reaction was monitored by TLC. After 3 hours, the starting materials were absent, and the solvent was evaporated under vacuum. Based on the work-up process reported by Carpino and co-workers,[17] the obtained residue was dissolved in DCM and washed with water. The organic phase was further washed with water, 1M aqueous HCl and, finally, with

saturated aqueous $NaHCO_3$, to yield the enantiopure compound **102** in 70% yield without the need for further purification. The above protocol was repeated several times and the outcome was reproducible.

The second synthetic step was based on Coudert's *et al* selective deprotection protocol under mild conditions.[18] The dipeptide **102** was dissolved in tetrahydrofuran (THF) and reacted with tetrabutylammonium fluoride (TBAF) at room temperature. However, the reaction did not progress even when heated at 60 °C. In a second attempt, the substrate **102** was dissolved in *tert*-butyl acetate and reacted with concentrated sulfuric acid, yielding the mono-protected derivative **103** in quantitative yield (Scheme 2.11). As reported by Lin *et al.*,[19] the selective deprotection of the *Boc*-group in the presence of *tert*-butyl esters is an irreversible process due to the protonation of the amine product and the release of CO_2 (Scheme 2.12).

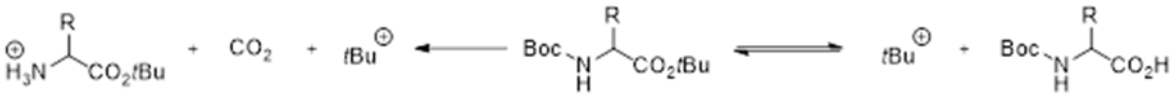

Scheme 2.12 Selective deprotection mechanism of the *N-tert*-butoxycarbonyl group in the presence of *tert*-butyl esters.[19]

The synthesis proceeded with the coupling reaction between the deprotected derivative **103** and cinnamic acid **88** using TBTU as a coupling agent in a basic environment, yielding intermediate **91** (Cin-F-FO*t*Bu) with the desired stereochemistry (Scheme 2.11). Finally, by deprotection of the ester **91** under acidic conditions, the final product **70** (Cin-F-F) was obtained in quantitative yield. The overall yield of Cin-F-F **70** was 29% over four steps (Scheme 2.11).

2.2.4 Solution phase synthesis of indole-protected diphenylalanine 69

The second member of the synthesized diphenylalanine set of compounds was the indole capped derivative **69** (Ind-F-F). Even though a solid phase experimental protocol has been reported,[6] its preparation was attempted by a linear, solution phase synthetic approach based on the following retrosynthetic scheme (Scheme 2.13).

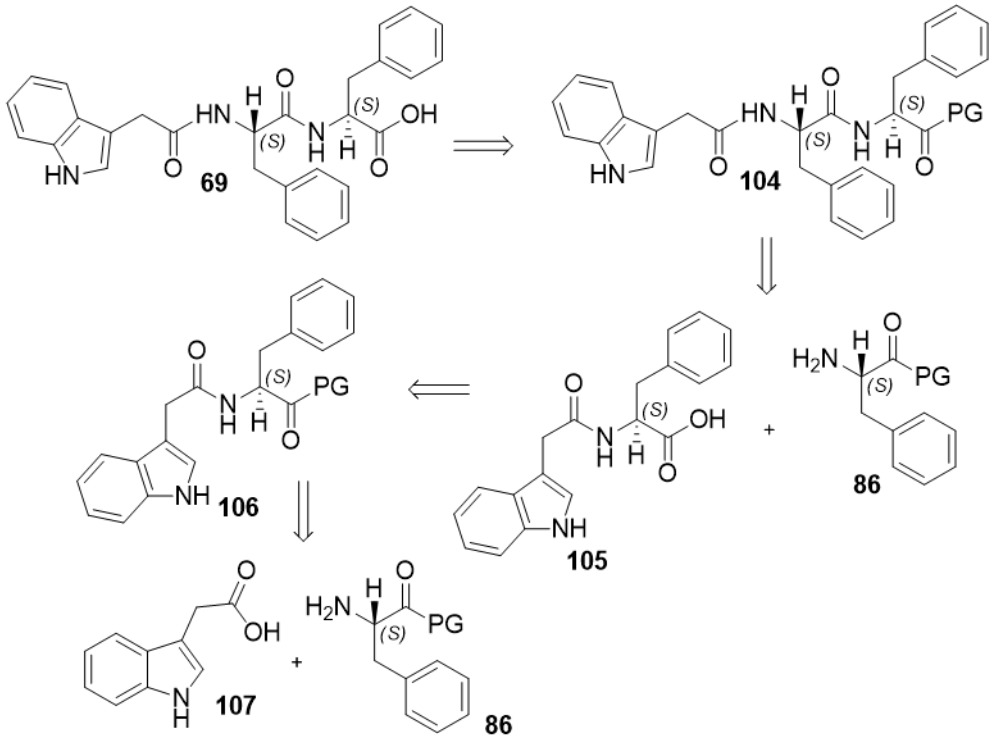

Scheme 2.13 Proposed retrosynthetic scheme for the synthesis of indole-capped diphenylalanine **69**.

The desired indole-capped diphenylalanine derivative **69** can be obtained from the deprotection of intermediate **104**. A coupling reaction between the protected amino acid **86** and the indole derivative **105** was expected to yield dipeptide **104** as a pure enantiomer. Deprotection of **106** would afford the free acid **105**, while the initial coupling reaction between indole acetic acid **107** and the protected phenylalanine **86** would yield the desired precursor **106**.

The indole bearing precursor **108** was obtained from the coupling of indole acetic acid **107** with the hydrochloride salt of *tert*-butyl phenylalanine ester **89** in 73% yield, following the amide bond formation protocol used previously (Scheme 2.14). During the second step of the synthesis, the ester derivative **108** was dissolved in DCM and reacted with trifluoroacetic acid (TFA), yielding the free acid **109** in quantitative yield. Without further purification, **109** was coupled with the protected phenylalanine **89**. The second coupling reaction proved problematic, with five different by-products being obtained (couldn't be identified by NMR). Although the desired intermediate **110** was obtained in 37% yield, its purification by flash column chromatography was not efficient and traces of impurities were still detectable by NMR. However, the synthesis was continued with the deprotection of the *tert*-butyl group of **110** under acidic conditions and the final product **69** was obtained as a dark green gum.

Due to the small amount of the impure compound **69** isolated, further purification trials were not performed.

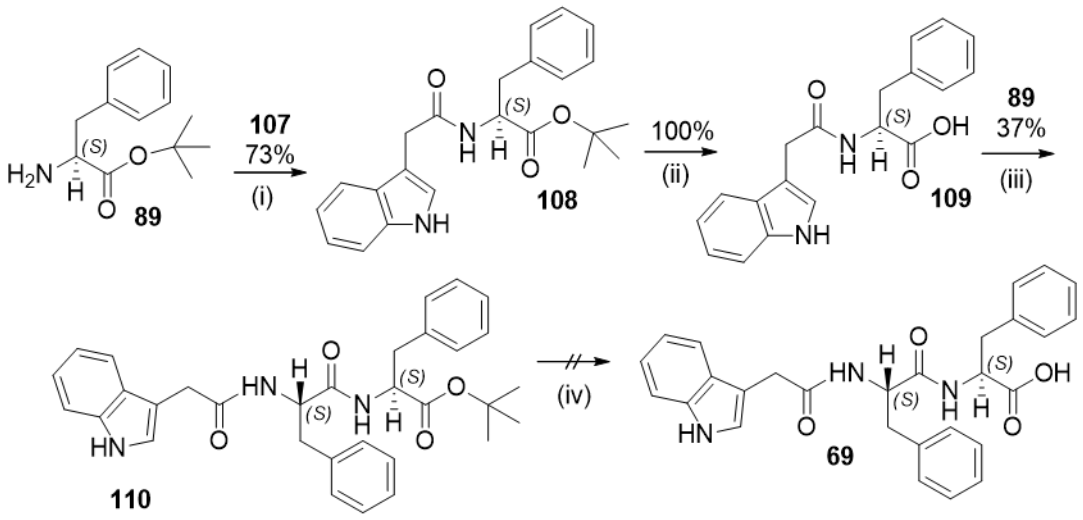

Scheme 2.14 Attempted synthesis of indole-protected diphenylalanine **69**. Reagents and conditions: **(**i) anh. DMF, TBTU (1.5 eq), $NaHCO_3$ (2.5 eq), rt; (ii) DCM, TFA (10 eq), rt; (iii) anh. DMF, TBTU (1.5 eq), $NaHCO_3$ (2.5 eq), rt; (iv) DCM, TFA (10 eq), rt.

The overall synthetic approach was not successful since the desired product **69** could not be purified. Further to this, the introduction of the second phenylalanine moiety was problematic as the diphenylalanine derivative **110** was obtained in only 37% yield and its purification proved inefficient. Presumably, a different activation agent could give a better yield by minimizing the formed impurities (possible unreacted intermediates). An alternative approach would be the retrosynthesis used for the Cin-F-F **70** derivative (Scheme 2.10). Indeed, the di-protected diphenylalanine synthon could be synthesized first followed by the addition of the indole moiety. However, due to time constrains this second synthetic approach for **69** was not performed.

2.3 Conclusions

A number of structurally related compounds was synthesized to assess their gelation properties (Table 2.4). Based on their structural features, the three sets of potential hydrogelators were classified as fluorenylmethyloxycarbonyl (Fmoc-), biotinylated and diphenylalanine analogues, respectively.

Table 2.4 Synthesis overview and research goals

Compound	Results	Research goals
N-Fmoc-D-galactopyranosylamine **64**	19% yield over 3 steps	Assess gelation compared to analogue *N*-Fmoc-D galactosamine **62**
N-Fmoc-D-glucopyranosylamine **65**	26% yield over 3 steps	Assess gelation compared to analogue *N*-Fmoc-D glucosamine **63**
Biotin-D-galactosamine **66**	36% over 1 step	Assess gelation and characterize potential hydrogel
Biotin-D-glucosamine **67**	90% over 1 step	Assess gelation and characterize potential hydrogel
Cin-F-F **70**	29% over 4 steps	Assess gelation compared to analogue Fmoc-F-F **68**
Ind-F-F **69**	Unsuccessful	Compare solution phase to solid phase synthesis. Assess gelation compared to analogue Fmoc-F-F **68**

For the preparation of the Fmoc-protected glycopyranosylamine derivatives **64** and **65** three synthetic attempts were followed. The first two were unsuccessful, since the deprotection of the acetyl groups in the presence of the Fmoc moiety proved problematic. However, changing the deprotection sequence allowed the removal of the acetyl groups leaving the Fmoc moiety intact. Although the synthesis was performed under the same conditions for both compounds their purification was different. Indeed, **65** (26% yield over 3 steps) was obtained by recrystallization from methanol whereas the reaction residue of **64** (19% yield over 3 steps) had to be acidified first with aqueous HCl (1.0 M) before recrystallization from methanol.

The biotinylated derivatives of galactosamine **66** and glucosamine **67** were synthesized over one step by coupling biotin with the corresponding amino sugars. To form a new amide bond two approaches were followed, that of activating biotin using a coupling agent and conversion of biotin to the corresponding acyl chloride derivative. The first synthetic route showed that the type and amount of base and coupling agent used affected the purification

process. In addition, although the desired product was obtained, a different ratio of anomers was present after each reaction trial (confirmed by NMR spectroscopy). The second approach failed to yield biotinylated derivatives **66** and **67**. Several trial reactions were undertaken, differing in the type of base used, the amount of thionyl chloride employed and the number of steps followed. Unfortunately, in most cases the products were not formed as indicated by TLC or it was impossible to be isolated and purified.

The cinnamoyl and indole protected diphenylalanine derivatives **70** and **69** were the last two dipeptide-based compounds to be synthesized. The preparation of **70** started with coupling of cinnamic acid with phenylalanine, followed by a second coupling reaction for the incorporation of the second phenylalanine moiety. The synthesis though resulted in a pair of epimers Cin-L-F-L-F: Cin-D-F-L-F **70/93** (43% yield over 4 steps) being formed in a reproducible 2:1 ratio which couldn't be separated. To obtain derivative **70**, a different approach was undertaken based on the initial formation of the diphenylalanine scaffold followed by the incorporation of the cinnamoyl moiety. Indeed, no stereochemical inversion was observed while optimization of the reaction conditions over four steps established a facile method for the synthesis and purification of Cin-L-F-L-F **70** (29% yield over 4 steps).

Finally, the synthesis of indole protected diphenylalanine product **69** was based on the formation of the Ind-F derivative **109** followed by its coupling with a second phenylalanine moiety. In contrast to the cinnamic analogues **70/93**, no inversion of stereochemistry was observed however the intermediate products were obtained either as thick oils or gums which resulted in insufficient purification due to solubility issues. Time constrains didn't allow further synthetic attempts to be undertaken.

2.4 Experimental

Materials

All commercial reagents and solvents (analytical and HPLC grade) were purchased from Aldrich (Dorset, UK), VWR (Lutterworth, UK), Fisher (Loughborough, UK), Goss Scientific (Crewe, UK), Merck (Darmstadt, Germany), Alfa Aesar (Heysham, UK), Bachem (Bubendorf, Switzerland) and Carbosynth (Compton, UK) and were used as supplied. All reactions were performed under a nitrogen atmosphere unless stated otherwise. Reactions were monitored by TLC, which was performed on aluminum sheets coated with 60 F254 silica (Merck). TLC sheets were checked for any UV activity (254/325 nm) prior to staining

and visualized using either Hanessian's stain or ninhydrin, as stated in the description. Flash column chromatography was performed on silica gel (100-200 mesh, Merk).

Instruments

Low resolution mass spectra (*m/z*) were recorded using an electrospray ionization (ESI) technique in the positive and/or negative mode (as stated). ESI mass spectra were measured on a Waters Ultima mass spectrometer using direct injection (1 μL). All IR spectra were recorded in the range of 4000-650 cm^{-1} by ATR on a Perkin Elmer Spectrum One FT-IR Spectrometer (given abbreviations for peak characterization: strong (s), weak (w), very weak (vw), shoulder (sh)). ^{1}H and ^{13}C nuclear magnetic resonance spectra (NMR) were recorded in the deuterated solvent stated on a Jeol ECP 400 MHz FT NMR spectrometer, incorporating a tuneable H (5) 400 probe (^{1}H:400 MHz and ^{13}C:101 MHz) or on a Jeol ECA, 500 MHz FT NMR Spectrometer, incorporating a NM-50TH5AT/FG2 probe, (^{1}H:500 MHz and ^{13}C:126 MHz).

All chemical shifts (δ) are quoted in ppm and coupling constants (*J*) are averaged values (in Hz). Residual signals from the solvents or TMS signal were used as an internal reference. ^{1}H resonances were assigned with the aid of 2D techniques such as COSY and HSQC. ^{13}C resonances were assigned using a DEPT 135 sequence and HSQC. To interpret the spectra, anomers are quoted using Greek letters α and β while different species (mixture of compounds) with capital letters. Carbon atoms are quoted with a number (*i.e.* C-3, carbon at position 3) while hydrogen atoms are quoted with lowercase letters (*i.e.* CH-f, 1H A, refers to one hydrogen atom, at position f that belongs to species A). For all compounds, an image of the chemical structure with numerical and letter quotations is given for clarity.

All ^{1}H, ^{13}C NMR, IR and MS data are supplied in appendix.

Synthetic protocols

Synthesis of *N*-Fmoc-D-galactopyranosylamine **64**

The peracetylated galactopyranosyl azide **71** (1870 mg, 5.0 mmol) was suspended in anhydrous MeOH (20 mL) followed by addition of a methanolic $NaOCH_3$ solution (0.5 M, 1.0 mL). After 30 minutes, TLC (Hex: EA, 1:1) confirmed the consumption of the starting material. The solution was neutralized with Dowex-50 (H^+) resin, filtered and concentrated to dryness. The galactopyranosyl azide **73** (1011 mg, 4.928 mmol) was dissolved in

anhydrous MeOH (20 mL) and 10% Pd/C (105 mg, 0.1 mmol) was added. The reaction mixture was then left under a hydrogen atmosphere which was maintained by balloon for 12 h. Upon completion of the reaction, as indicated by TLC (EA: MeOH: H_2O, 7:2:1, R_f of **75** 0.03), Pd/C was removed by filtration (under vacuum, celite was used) and the solution was concentrated to dryness. The galactopyranosylamine **75** (502 mg, 2.801 mmol) was suspended in anhydrous pyridine and Fmoc-OSu (983 mg, 2.913 mmol) was added. The reaction mixture was left to stir overnight at rt and, the next day, pyridine was evaporated under vacuum. The obtained residue was washed with DCM (150 mL) and aqueous HCl (1.0 M, 150 mL). The obtained precipitate was recrystallized from MeOH, yielding the desired product **64** as a white solid in 52% yield (582 mg, 22% yield over four steps).

m.p. 210.2-211.1 °C, **$[\alpha]_D^{20}$** (not measured)*, **HR-MS (ESI-TOF)**: *m/z* for $C_{21}H_{24}NO_7^+$ $[M+H]^+$ calculated 401.1553, found 402.1554, **IR** (neat): 3470 (s), 3342 (s), 3040 (vw), 2951 (vw), 2919 (vw), 2827 (vw), 2848 (vw), 1700 (s), 1533 (w), 1450 (s), 1407 (s), 1330 (s), 1278 (s), 1256 (s), 1229 (s), 1110 (sh), 1084 (s), 1055 (s), 1026 (s), 987 (sh), 759 (s), 745 (s), 735 (s) cm^{-1}.

*Compound **64** was partially soluble in water, methanol, ethyl acetate, dimethylsulfoxide, pyridine, pryperidine, 2,2,2-trifluoroethanol, therefore no optical rotation measurements were undertaken.

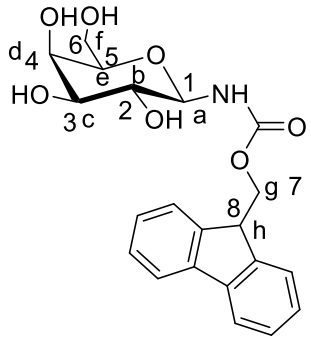

^{1}H NMR (400 MHz, methanol-d_3) δ 7.79 (d, *J* = 7.5 Hz, **Ar**, **2H**), 7.67 (d, *J* = 7.4 Hz, **Ar**, **2H**), 7.38 (t, *J* = 7.4 Hz, **Ar**, **2H**), 7.30 (t, *J* = 7.3 Hz, **Ar**, **2H**), 4.65 (d, *J* = 8.0 Hz, **H-a**, **1H**), 4.39 (d, *J* = 6.9 Hz, **H-g**, **2H**), 4.22 (t, *J* = 6.7 Hz, **H-h**, **1H**), 3.87 (s, **H-d**, **1H**), 3.74 – 3.64 (m, **H-f**, **2H**), 3.59 – 3.47 (m, **H-b**, **H-c**, **H-e**, **3H**).

^{13}C NMR (101 MHz, methanol-d_3) δ 157.78, 156.65, 143.90, 141.27, 127.46, 126.85, 124.86, 119.58, 82.95 (**C-1**), 76.72 (**C-5**), 74.46 (**C-2**), 69.85 (**C-3**), 69.10 (**C-4**), 66.71 (**C-7**), 61.17 (**C-6**), 46.8 (**C-8**).

Synthesis of *N*-Fmoc-D-glucopyranosylamine **65**

The peracetylated glucopyranosyl azide **72** (1870 mg, 5.0 mmol) was suspended in anhydrous MeOH (20 mL) followed by addition of $NaOCH_3$ solution in MeOH (0.5 M, 1.0 mL). After 30 minutes, TLC (Hex: EA, 1:1) confirmed the consumption of the starting material. The solution was neutralized by Dowex-50 (H^+) resin, filtered and concentrated to dryness. The glucopyranosyl azide **74** (1025 mg, 4.995 mmol) was dissolved in anhydrous MeOH (20mL) and 10% Pd/C (106 mg, 0.1 mmol) was added. The reaction mixture was then left under a hydrogen atmosphere which was maintained by balloon for 12 h. Upon completion of the reaction, as indicated by TLC (EA: MeOH: H_2O, 7:2:1, R_f of **76** 0.03) Pd/C was removed by filtration (under vacuum, celite was used) and the solution was concentrated to dryness. The glucopyranosylamine **76** (500 mg, 2.790 mmol) was suspended in anhydrous pyridine and Fmoc-OSu (979 mg, 2.910 mmol) was added. The reaction mixture was left to stir overnight at rt and then pyridine was evaporated under vacuum. The resulting residue was washed with DCM (150 mL) and the obtained solid was recrystallized from MeOH, yielding the desired product **65** as a white solid in 35 % yield (389 mg, 19% yield over four steps).

m.p. 206.4-208.2 °C, **$[\alpha]_D^{20}$** +1.4° (1% w/v in DMSO), **HR-MS (ESI-TOF)**: *m/z* for $C_{21}H_{24}NO_7^+$ $[M+H]^+$ calculated 401.1553, found 402.1559, **IR** (neat): 3313 (s), 2933 (w), 2860 (vw), 1694 (s), 1691 (s), 1672 (s), 1651 (sh), 1549 (s), 1455 (w), 1304 (w), 1277 (w), 1241 (w), 1110 (sh), 1084 (sh), 1062 (sh), 1039 (s), 1023 (s), 1000 (sh), 892 (vw), 865 (vw), 760 (w), 738 (s) cm^{-1}.

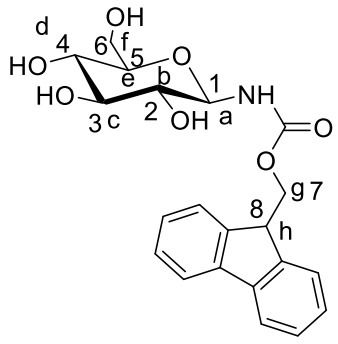

^{1}H NMR (400 MHz, dmso-d_6) δ 7.97 (d, *J* = 9.2 Hz, **NH**, **1H**), 7.90 (d, *J* = 7.4 Hz, **Ar**, **2H**), 7.74 (dd, *J* = 8.9, 8.3 Hz, **Ar**, **2H**), 7.42 (td, *J* = 7.5, 0.9 Hz, **Ar**, **2H**), 7.34 (t, *J* = 7.4 Hz, **Ar**, **2H**), 4.97 (d, *J* = 4.5 Hz, **OH**, **1H**), 4.88 (dd, *J* = 9.5, 5.3 Hz, **OH**, **2H**), 4.49 (dd, *J* = 11.1, 7.1 Hz, **H-a**, **2H**), 4.35 (dd, *J* = 9.9, 6.4 Hz, **H-g**, **1H**), 4.25 (dt, *J* = 15.9, 6.8 Hz, **H-g´**, **H-h**,

2H), 3.63 (dd, *J* = 10.3, 5.7 Hz, **H-f**, **1H**), 3.44 – 3.37 (m, **H-f′**,1H), 3.17 (d, *J* = 5.2 Hz, **H-c**, **OH**, 2H), 3.08 (m, **H-b**, **H-d**, **H-e**, 3H).

^{13}C NMR (101 MHz, dmso-d_6) δ 156.54, 144.50, 144.31, 141.30, 128.21, 127.66, 125.91, 125.78, 120.69, 83.02 (**C-1**), 78.95, 78.16 (**C-3**), 72.56 (**C-2**), 70.50, 66.22 (**C-7**), 61.49 (**C-6**), 47.10 (**C-8**).

Synthesis of Biotin-D-glucosamine **67**

Glucosamine hydrochloride **118** (441 mg, 2.046 mmol) and $NaHCO_3$ (172 mg, 2.046 mmol) were suspended in anhydrous DMF (10 mL) under a N_2 atmosphere and left to stir at rt for 30 minutes. A second solution of biotin (500 mg, 2.046 mmol), TBTU (657 mg, 2.046 mmol) and $NaHCO_3$ (172 mg, 2.046 mmol) was prepared under the same conditions. After 30 minutes, the two solutions were mixed, and the reaction was left to stir overnight at rt. DMF was then removed and the residue was suspended in DCM (30 mL) and EA (30 mL). The obtained precipitate was collected and washed with EA (30 mL) until TLC (EA: MeOH: H_2O, 7:2:1, Hanessian's stain, R_f of **67** 0.19) confirmed no impurities were present. The desired product **67** was collected by filtration as an off-white solid in 90% yield (749 mg).

m.p. 204.0-207.1 °C, **$[\alpha]_D^{20}$** +64.2° (1% w/v in DMSO), **HR-MS (ESI-TOF)**: *m/z* for $C_{16}H_{28}N_3O_7S^+$ $[M+H]^+$ calculated 406.1648, found 406.1637, **IR** (neat): 3290 (s), 2932 (s), 2863 (w), 1683 (s), 1627 (s), 1550 (s), 1464 (s), 1426 (w), 1324 (w), 1267 (w), 1141 (sh), 1060 (s), 1025 (s), 969 (sh) cm^{-1}.

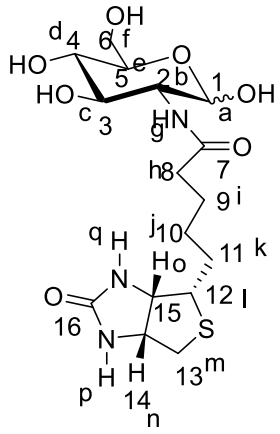

Two species were present, one minor (A) and one major (B), in a 0.22:0.68 ratio, however it was not possible to assign which anomer corresponded to the minor and major species. The *α*: *β* assignment of the anomeric ratio could not be determined as the anomeric proton

peaks at C-1 position overlapped with sugar ring OH peaks (appendix, Figures A 2.10 and 2.11). In addition, there was not an equal number of signals for the anomers α and β whereas some peaks could not be assigned due to signal overlap.

^{1}H NMR (500 MHz, dmso-d_6) δ 7.72 (d, *J* = 8.3 Hz, **NH-g**, **1H-A**), 7.55 (d, *J* = 7.9 Hz, **NH-g**, **1H-B**), 6.48 (d, *J* = 6.4 Hz, **NH-p**, **1H-A**), 6.39 (t, *J* = 9.8 Hz, **NH-p**, **NH-q**, **2H**), 4.98 – 4.96 (m, **OH**, **1H-A**), 4.92 (t, *J* = 4.4 Hz, **H-a**, **1H-B**), 4.87 (d, *J* = 5.1 Hz, **OH**, **1H-A**), 4.66 (d, *J* = 5.3 Hz, **OH**, **1H-B**), 4.54 (t, *J* = 5.8 Hz, **CH**, **1H-A**), 4.42 (dd, *J* = 10.0, 4.5 Hz, **OH**, **1H-B**), 4.34 – 4.28 (m, **CH**, **1H-B**), 4.16 – 4.10 (m, **CH**, **1H-B**), 3.67 (dd, *J* = 11.1, 5.5 Hz, **CH**, **1H**), 3.63 – 3.54 (m, **CH$_2$**, **CH**, **2H**), 3.53 – 3.44 (m, **CH$_2$**, **2H**), 3.14 – 3.07 (m, **CH**, **2H**), 3.05 (s, **CH**, **1H**), 2.82 (dd, *J* = 12.4, 5.0 Hz, **CH$_2$**, **1H**), 2.58 (d, *J* = 12.4 Hz, **CH$_2$**, **1H**), 2.15 – 2.05 (m, **CH$_2$**, **2H**), 1.62 (td, *J* = 12.9, 9.3, 6.3 Hz, **CH$_2$**, **1H**), 1.55 – 1.40 (m, **CH$_2$**, **3H**), 1.37 – 1.26 (m, **CH$_2$**, **2H**).

^{13}C NMR (126 MHz, dmso-d_6) δ 173.27 (**CO-A**), 172.82 (**CO-B**), 163.31 (**CO**), 96.16 (**C-1 A**), 91.13 (**C-1 B**), 77.31 (**CH-A**), 74.84 (**CH-A**), 72.58 (**CH-B**), 71.64 (**CH-B**), 71.38 (**CH-A**), 70.95 (**CH-B**), 61.64 (**CH**), 61.52 (**CH$_2$**), 59.76 (**CH-B**), 57.59 (**CH-A**), 55.93 (**CH-B**), 54.78 (**CH-B**), 40.38 (**CH$_2$**), 35.98 (**CH$_2$ -A**), 35.53 (**CH$_2$ -B**), 28.66 (**CH$_2$**), 28.59 (**CH$_2$**), 28.50 (**CH$_2$**), 25.75 (**CH$_2$ -B**).

Synthesis of Biotin-D-galactosamine **66**

This compound was prepared using the protocol described for compound **67** using the hydrochloric salt of galactosamine **117** instead of glucosamine **118**. The desired product was collected as an off-white solid in 36% yield (293 mg).

m.p. 178.4-180.1 °C, **$[\alpha]_D^{20}$** +58.0° (1% w/v in dmso), **HR-MS (ESI-TOF)**: *m/z* for $C_{16}H_{28}N_3O_7S^+$ $[M+H]^+$ calculated 406.1648, found 406.1653, **IR** (neat): 3268 (s), 2929 (s) 2858 (w), 1667 (sh), 1674 (s), 1649 (sh), 1631 (sh), 1550 (s), 1462 (s), 1426 (w), 1323 (s), 1267 (s), 1146 (sh), 1104 (sh), 1076 (sh), 1025 (sh), 1022 (s), 969 (sh), 864 (vw), 762 (vw), 689 (vw) cm^{-1}.

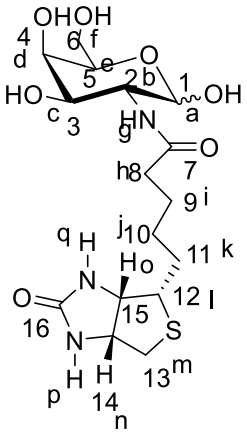

There are two species present, one minor (A) and one major (B), in a 0.23:0.59 ratio, however it was not possible to assign which anomer corresponded to the minor and major species. The assignment of the α: β anomeric ratio couldn't be determined as one anomeric proton peak at C-1 position is given as a singlet and its coupling constant with the adjacent proton at C-2 position couldn't be calculated. The second anomeric proton overlapped with OH signals (appendix Figures A 2.13 and 2.14). The major species (B) is fully assigned whereas only a partial assignment is possible for minor (A).

^{1}H NMR (500 MHz, dmso-d_6) δ 7.67 (d, *J* = 7.5 Hz, **NH-g**, **1H-B**), 7.40 (t, *J* = 26.7 Hz, **NH-g**, **1H-A**), 6.37 (dd, *J* = 23.1, 7.6 Hz, **NH-p**, **NH-q**, **H-a**, **3H-B**), 4.92 (s, **CH**, **1H-A**), 4.60 (s, **OH**, **1H-B**), 4.50 (d, *J* = 5.9 Hz, **OH**, **1H-B**), 4.45 (s, **OH**, **1H-B**), 4.38 (t, *J* = 7.4, 6.8 Hz, **CH**, **1H-B**), 4.31 (s, **CH**, **1H-B**), 4.13 (s, **CH**, **2H-B**), 3.97 (s, **OH**, **1H-A**), 3.77 (d, *J* = 23.8 Hz, **CH**, **1H-A**), 3.70 (d, *J* = 17.1 Hz, **CH**, **1H-A**), 3.62 (d, *J* = 11.8 Hz, **CH**, **2H-B**), 3.53 (d, *J* = 4.9 Hz, **CH**, **1H**), 3.47 (d, *J* =4.5 Hz, **CH**, **1H-B**), 3.29 (d, *J* = 6.1 Hz, **CH**, **1H-B**), 3.17 (d, *J* = 5.1 Hz, **CH**, **1H-B**), 3.10 (s, **CH**, **1H-B**), 2.82 (dd, *J* = 12.2, 4.6 Hz, **CH$_2$**, **1H-B**), 2.57 (d, *J* = 12.4 Hz, **CH$_2$**, **1H-B**), 2.09 (s, **CH2** , **2H-B**), 1.61 (s, **CH$_2$**, **1H-B**), 1.56 – 1.40 (m, **CH$_2$, 3H-B**), 1.33 (d, *J* = 6.6 Hz, **CH$_2$, 2H-B**).

^{13}C NMR (126 MHz, dmso-d_6) δ 173.83 (**CO-B**), 173.09 (**CO-A**), 163.28 (**CO-B**), 96.56 (**CH-B**), 91.55 (**CH-A**), 75.56 (**CH-B**), 72.22 (**CH-B**), 70.93 (**CH-A**), 68.82 (**CH-A**), 68.02 (**CH-B**), 67.94 (**CH-A**), 61.53 (**CH-B**), 61.17 (**CH$_2$-A**), 61.06 (**CH$_2$-B**), 59.75 (**CH-B**), 55.95 (**CH-B**), 54.51 (**CH-B**), 50.71 (**CH-A**), 49.13 (**CH-A**), 40.38 (**CH$_2$-B**), 35.96 (**CH$_2$-B**), 35.60 (**CH$_2$-A**), 28.60 (**CH$_2$-B**), 28.53 (**CH$_2$-B**), 25.80 (**CH$_2$-B**).

Synthesis of Cin-F-O*t*Bu ester **90**

The hydrochloride salt of phenylalanine *tert*-butyl ester **89** (871 mg, 3.377 mmol) was dissolved in anhydrous DMF (15 mL) with $NaHCO_3$ (710 mg, 8.443 mmol) and the solution was stirred at rt under N_2 atmosphere for 30 minutes. Cinnamic acid **88** (500 mg, 3.377 mmol) and TBTU (1627 mg, 5.066 mmol) were then added and the reaction mixture was monitored by TLC. After 24 hours, all the cinnamic acid had been consumed and a new spot appeared (Hex: EA 2:3, Hanessian's stain, R_f of **90** 0.69). The solvent was evaporated to dryness and the obtained residue was dissolved in EA (50 mL). The solution was washed with water (3 x 50 mL) and the aqueous layer was back-extracted with EA (50 mL). The combined organic phases were dried ($MgSO_4$), then evaporated under vacuum to give a residue that was purified by flash column chromatography (Hex: EA, 3:1) to yield **90** as a white powder (1069 mg, 90%).

m.p. 120.1-121.2 °C, **$[\alpha]_D^{20}$** -23.4° (1% w/v in MeOH), **MS (ES^+)**: not found,* **IR** (neat): 3354 (s), 3036 (vw), 3000 (vw), 2977 (w), 2933 (w), 1718 (s), 1665 (s), 1621 (s), 1534 (s), 1474 (vw), 1457 (w), 1449 (vw), 1366 (m), 1347 (m), 1313 (m), 1284 (m), 1265 (m), 1218 (s), 1150 (s), 1114 (sh), 999 (m), 975 (s), 874 (w), 850 (m), 771 (m), 741 (m), 718 (m), 701 (s) cm^{-1}.

* Low resolution mass spectroscopy (LRMS) was run for **90** (concentration of the sample was 1.0 mg/mL in methanol), however mass was not found. That was presumably due to low solubility of **90** in methanol (appendix, Figure A 2.17).

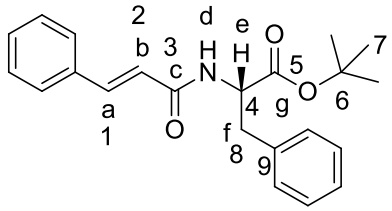

^{1}H NMR (500 MHz, dmso-d_6) δ 8.47 (d, J = 7.8 Hz, **NH-d**, **1H**), 7.58 – 7.54 (m, **Ar**, **2H**), 7.45 – 7.36 (m, **Ar**, **CH-a**, **4H**), 7.32 – 7.20 (m, **Ar**, **5H**), 6.72 (d, J = 15.8 Hz, **CH-b**, **1H**), 4.53 (dt, J = 8.1, 6.5 Hz, **CH-e**, **1H**), 3.00 (td, J = 22.3, 13.8, 7.4 Hz, **CH_2-f**, **2H**), 1.34 (s, **CH_3**, **9H**).

^{13}C NMR (126 MHz, dmso-d_6) δ 171.27 (**C-5**), 165.39 (**C-3**), 139.87, 137.74, 135.29, 130.10, 129.69, 129.48, 128.73, 128.11, 127.05 (**Ar**, **C-1**), 122.05 (**C-2**), 81.27 (**C-6**), 54.80 (**C-4**), 37.65 (**C-8**), 28.08 (**C-7**).

Synthesis of Cin-F **85**

A solution of **90** (840 mg, 2.390 mmol) in DCM (2 mL) was prepared and TFA (1.8 mL, 23.9 mmol) was added dropwise at 0 °C. The reaction was left to stir at rt and monitored by TLC (Hex: EA 2:3). After 22 hours, all the starting material had been consumed and the reaction mixture was then evaporated under vacuum. TFA was removed by co-evaporation (x 5) of the dissolved residue with DCM and by drying under vacuum overnight. The desired product **85** was obtained as a transparent oil and was used without further purification.

Synthesis of Cin-L-F-L-FO*t*Bu **91** and Cin-D-F-L-FO*t*Bu **92** mixture

The hydrochloride salt of phenylalanine *tert*-butyl ester **89** (611 mg, 2.369 mmol) was dissolved in anhydrous DMF (12 mL) and $NaHCO_3$ (498 mg, 5.923 mmol) added and stirred at rt under an N_2 atmosphere for 30 minutes. Cin-F **85** (706 mg, 2.369 mmol) and TBTU (1141 mg, 3.554 mmol) were then added and the reaction mixture was further stirred at rt while being monitored by TLC (Hex: EA, 1:1). After 24 hours the free acid had been consumed and a new spot had appeared (Hex: EA, 1:1, R_f of **91/92** mixture as a single spot 0.74). The solvent was evaporated under vacuum and the obtained residue was dissolved in EA (50 mL). The solution was washed with water (3x50 mL) and the aqueous layer was back extracted with EA (50 mL). The combined organic phases were dried ($MgSO_4$) and evaporated under vacuum. The residue was purified by flash column chromatography (Hex: EA, 3:1) to yield the epimeric mixture of **91** and **92** in a 2:1 ratio as a white powder (794 mg, 67%).

m.p. 86.5-88.6 °C, **$[\alpha]_D^{20}$** -20.3° (1% w/v in MeOH), **MS (ES^+)**: *m/z* 499 $[M+H]^+$, **IR** (neat): 3268 (br), 3063 (vw), 3030 (vw), 2979 (vw), 2931 (vw), 1733 (m), 1650 (s), 1617 (s), 1541 (s), 1497 (sh), 1452 (w), 1368 (w), 1343 (w), 1220 (s), 1151 (s), 980 (w), 846 (w), 740 (w), 698 (s) cm^{-1}.

The reaction yielded a mixture of Cin-L-F-L-FO*t*Bu **91** and Cin-D-F-L-FO*t*Bu **92** in a 2:1 ratio as seen in Figure 2.7 (ii) (section 2.2.3) and Figure A 2.22 in appendix. For clarity reasons, the NMR interpretation of Cin-D-F-L-FO*t*Bu **92** and Cin-L-F-L-FO*t*Bu **91** are

reported separately. It is of note that several peaks overlap since the structures of **92** and **91** are almost identical.

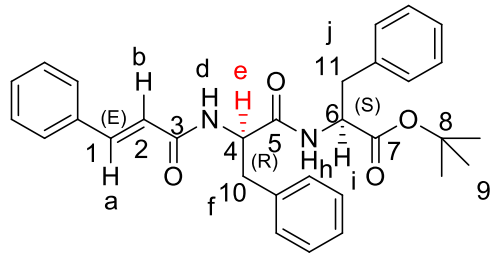

Cin-D-F-L-FO*t*Bu **92**

^{1}H NMR (500 MHz, dmso-d_6) δ 8.52 (d, J = 8.0 Hz, **NH-h**, **1H**), 8.27 (d, J = 8.7 Hz, **NH-d**, **1H**), 7.53 (d, J = 7.2 Hz, **Ar**, **2H**), 7.42 – 7.31 (m, **Ar**, **3H**), 7.30 – 7.12 (m, **Ar**, **CH-a**, **11H**), 6.69 (dd, J = 15.2, 14.7 Hz, **CH-b**, **1H**), 4.73 (td, J = 9.4, 4.1 Hz, **CH-e**, **1H**), 4.39 (q, J = 7.2 Hz, **CH-i**, **1H**), 3.07 (dd, J = 13.9, 3.9 Hz, **CH_2-f**, **2H**), 2.87 – 2.81 (m, **CH_2-j**, **1H**), 2.61 (dd, J = 13.7, 9.8 Hz, **CH_2-j**, **1H**), 1.35 (s, **CH_3**, **9H**).

^{13}C NMR (126 MHz, dmso-d_6) δ 171.58 (**C-5**), 171.00 (**C-7**), 165.11 (**C-3**), 139.50 (**C-1**), 138.37, 137.62, 135.34, 130.01, 129.75, 129.70, 129.47, 128.71, 128.56, 128.04, 127.03, 126.74 (**Ar**), 122.40 (**C-2**), 81.37 (**C-8**), 54.55 (**C-6**), 54.26 (**C-4**), 38.54 (**C-10**), 37.63 (**C-11**), 28.07 (**C-9**).

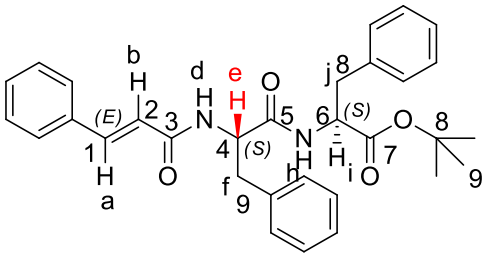

Cin-L-F-L-FO*t*Bu **91**

^{1}H NMR (500 MHz, dmso-d_6) δ 8.48 (d, *J* = 7.4 Hz, **NH-h**, **1H**), 8.31 (d, *J* = 8.6 Hz, **NH-d**, **1H**), 7.53 (d, J = 7.2 Hz, **Ar**, **2H**), 7.42 – 7.31 (m, **Ar**, **3H**), 7.30 – 7.12 (m, **Ar**, **CH-a**, **11H**), 6.69 (dd, J = 15.2, 14.7 Hz, **CH-b**, **1H**), 4.73 (td, J = 9.4, 4.1 Hz, **CH-e**, **1H**), 4.39 (q, J = 7.2 Hz, **CH-i**, **1H**), 3.07 (dd, J = 13.9, 3.9 Hz, **CH_2-f**, **2H**), 2.87 – 2.81 (m, **CH_2-j**, **1H**), 2.61 (dd, J = 13.7, 9.8 Hz, **CH_2-j**, **1H**), 1.32 (s, CH_3, **9H**).

^{13}C NMR (126 MHz, dmso-d_6) δ 171.86 (**C-5**), 170.88 (**C-7**), 165.22 (**C-3**), 139.50 (**C-1**), 138.37, 137.62, 135.34, 130.01, 129.75, 129.70, 129.47, 128.71, 128.56, 128.04, 127.03,

126.80 (**Ar**), 122.40 (**C-2**), 81.21 (**C-8**), 54.79 (**C-6**), 54.16 (**C-4**), 38.25 (**C-9**), 37.35 (**C-8**), 28.05 (**C-9**).

Synthesis of Cin-D-F-L-F **93** and Cin-L-F-L-F **70** mixture

A solution of the **91**/**92** mixture in 2:1 ratio (727 mg, 1.458 mmol) in DCM (2 mL) was prepared and cooled to 0 °C, after which TFA (1.1 mL, 1.458 mmol) was added dropwise. The reaction was left to stir at rt for 24 hours until TLC (Hex: EA 1:1, Hanessian's stain, R_f = 0.23) confirmed the consumption of the starting materials and the formation of a new spot. After evaporation of the solvent, TFA was removed by additional co-evaporation (x5) with DCM. The obtained residue was dried under vacuum overnight and afforded a mixture of the organic acids **70** and **93** in a 2:1 ratio as an off-yellow solid in quantitative yield (645 mg, 100%).

m.p. 53.8-56.1 °C, **$[\alpha]_D^{20}$** -13.8° (1% w/v in DMF), **HR-MS (ESI-TOF)**: *m/z* for $C_{27}H_{27}N_2O_4^+$ $[M+H]^+$ calculated 443.1971, found 443.1973. **HR-MS (ESI-TOF**): *m/z* for $C_{27}H_{26}N_2O_4$ Na [M+Na] calculated 465.1790, found 465.1794. **IR** (neat): 3277 (br), 3064 (vw), 3029 (vm), 1724 (w), 1650 (m), 1606 (m), 1534 (m), 1346 (m), 1206 (sh), 1168 (s), 975 (w), 735 (w), 695 (s) cm^{-1}.

The reaction yielded a mixture of Cin-L-F-L-F **70** and Cin-D-F-L-F **93** in a 2:1 ratio as seen in Figure 2.7 (i) (section 2.2.3) and Figure A 2.27 in appendix. For clarity reasons, the NMR interpretation of Cin-D-F-L-F **93** and Cin-L-F-L-F **70** is reported separately. It is of note that several peaks overlap since the structures of **70** and **93** are almost identical.

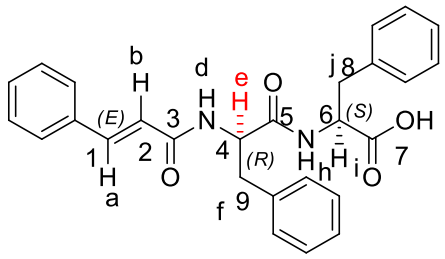

Cin-D-F-L-F **93**:

^{1}H NMR (500 MHz, dmso-d_6) δ 8.52 (d, J = 8.3 Hz, **NH-h**, **1H**), 8.22 (d, J = 8.7 Hz, **NH-d**, **1H**), 7.52 (dt, J = 8.6, 2.9 Hz, **Ar**, **2H**), 7.44 – 7.07 (m, **Ar**, **CH-a**, **14H**), 6.68 (dd, J = 15.8, 10.2 Hz, **CH-b**, **1H**), 4.74 – 4.67 (m, **CH-e**, **1H**), 4.51 – 4.43 (m, **CH-i**, **1H**), 3.12 – 3.02 (m, **CH_2-f**, **2H**), 2.84 (dd, J = 13.6, 9.9 Hz, **CH_2-j**, **1H**), 2.54 (dd, J = 13.7, 9.9 Hz, **CH_2-j**, **1H**).

^{13}C NMR (126 MHz, DMSO- d_6) δ 173.38 (**C-7**), 171.58 (**C-5**), 165.12 (**C-3**), 139.51 (**C-1**), 138.29, 138.00, 135.36, 130.01, 129.70, 129.69, 129.47, 128.73, 128.55, 128.05, 126.96, 126.76 (**Ar**), 122.18 (**C-2**), 54.29 (**CH**), 53.88 (**CH**), 38.56 (**CH_2**), 37.59(**CH_2**).

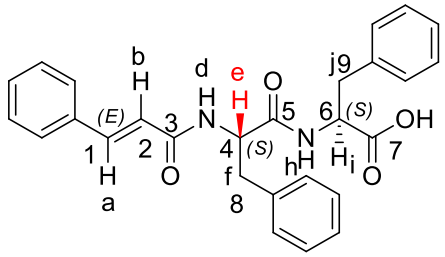

Cin-L-F-L-F **70**:

^{1}H NMR (500 MHz, DMSO- d_6) δ 8.38 (d, *J* = 7.8 Hz, **NH-h**, **1H**), 8.22 (d, *J* = 8.5 Hz, **NH-d**, **1H**), 7.52 (dt, J = 8.6, 2.9 Hz, **Ar**, **2H**), 7.44 – 7.07 (m, **Ar**, **CH-a**, **14H**), 6.68 (dd, J = 15.8, 10.2 Hz, **CH-b**, **1H**), 4.74 – 4.67 (m, **CH-e**, **1H**), 4.51 – 4.43 (m, **CH-i**, **1H**), 3.12 – 3.02 (m, **CH_2-f**, **2H**), 2.84 (dd, J = 13.6, 9.9 Hz, **CH_2-j**, **1H**), 2.54 (dd, J = 13.7, 9.9 Hz, **CH_2-j**, **1H**).

^{13}C NMR (126 MHz, DMSO- d_6) δ 173.23 (**C-7**), 171.83 (**C-5**), 165.19 (**C-3**), 139.51 (**C-1**), 138.40, 137.94, 135.36, 130.01, 129.70, 129.69, 129.47, 128.73, 128.55, 128.05, 126.96, 126.76 (**Ar**), 122.41 (**C-2**), 54.20 (**CH**), 54.01 (**CH**), 38.11 (**CH_2**), 37.17 (**CH_2**).

Synthesis of *Boc*-F-FO*t*Bu **102**

$NaHCO_3$ (63 mg, 0.754 mmol) and TBTU (242 mg, 0.754 mmol) were added to a DMF (2 mL) solution of *Boc*-protected phenylalanine **101** (200 mg, 0.754 mmol) under an N_2 atmosphere. The reaction mixture was left to stir for 1 hour at rt. A solution of *tert*-butyl phenylalanine **89** (214 mg, 0.829 mmol) and $NaHCO_3$ (70 mg, 0.829 mmol) in anhydrous DMF (2 mL) was prepared under the same conditions. The two solutions were mixed and, after 3 hours, as indicated by TLC, all starting materials had been consumed and a new spot had formed (Hex: EA 2:1, Hanessian's stain, R_f = 0.5). The solvent was evaporated under vacuum and the residue was dissolved in DCM (10 mL) and washed with water (50 mL). The aqueous phase was back extracted twice with DCM (10 mL), then the organic phases were combined and washed sequentially with water (2 x 50 mL), 1M aqueous HCl (10 mL), water (50 mL, pH of organic phase 5-6) and, finally, with saturated aqueous solution of

$NaHCO_3$ (20 mL, pH of organic phase 6-7).The organic phase was dried with $MgSO_4$, filtered and, after evaporation under vacuum, afforded the product **102** as an off-white glassy solid (247 mg, 70%).

m.p. 134.7-135.7 °C, **$[\alpha]_D^{20}$** +6.8° (1% w/v in DMSO), **HR-MS (ESI-TOF)**: *m/z* for $C_{27}H_{37}N_2O_5$ $[M+H]^+$ calculated 469.2702, found 469.270 , **IR** (neat): 3299 (br), 2978 (vw), 2932 (vw), 1733 (sh), 1677 (sh), 1654 (s), 1523 (w), 1497 (m), 1456 (w), 1393 (w), 1366 (s), 1252 (m), 1223 (sh), 1152 (s), 1115 (sh), 1081 (sh), 1048 (w), 1024(w), 847 (w), 740 (w), 698 (s) cm^{-1} .

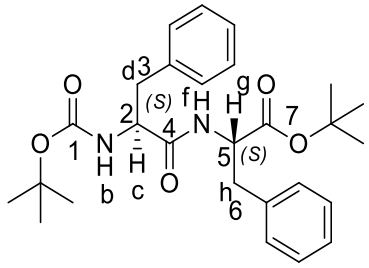

^{1}H NMR (500 MHz, dmso-d_6) δ 8.23 (d, *J* = 7.5 Hz, **NH-f**, **1H**,), 7.30 – 7.20 (m, **Ar**, **10H**), 6.86 (d, *J* = 8.8 Hz, **NH-b**, **1H**), 4.37 (q, *J* = 7.4 Hz, **CH-g**, **1H**), 4.19 (td, *J* = 10.5, 3.9 Hz, **CH-c**, **1H**), 3.00 – 2.94 (m, **CH_2-h**, **2H**), 2.92 (dd, *J* = 13.9, 3.9 Hz, **CH_2-d**, **1H**), 2.69 (dd, *J* = 13.7, 10.7 Hz, **CH_2 -d**, **1H**), 1.31 (s, **CH_3**, **9H**), 1.28 (s, **CH_3**, **9H**).

^{13}C NMR (126 MHz, dmso-d_6) δ 172.26 (**C-4),** 170.93 (**C-7**), 155.68 (**C-1**), 138.66, 137.62, 129.80, 129.69, 128.69, 128.50, 127.04, 126.69 (**Ar**), 81.23 (**C**(CH_3)), 78.50 (**C**(CH_3)), 56.04 (**C-2**), 54.62 (**C-5**), 37.97 (**C-3**), 37.43 (**C-6**), 28.65 (**CH_3**), 28.03 (**CH_3**).

Synthesis of F-FO*t*Bu **103**

The di-protected dipeptide **102** (1.0 g, 2.13 mmol) was suspended in *tert*-butyl acetate (11 mL) to give a final concentration of 0.2 M. Concentrated H_2SO_4 (0.34 mL, 6.402 mmol) was then added dropwise at rt. The pH of the reaction mixture (1-2) was measured by Fisher brand pH indicator test sticks. After 1 h, TLC (Hex: EA, 3:1, Hanessian's stain) confirmed the formation of a new spot (R_f = 0.57). The reaction mixture was then neutralized (pH 6-7) using saturated aqueous $NaHCO_3$ and extracted with EA (100 mL). The organic phase was dried with $MgSO_4$ and evaporated to dryness, yielding the mono- protected dipeptide **103** as a gummy off-white solid (786 mg, 100%). **103** was used without further purification or

characterization other than NMR spectroscopy which confirmed the structure of the desired product and its purity.

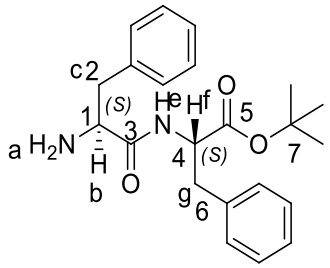

^{1}H NMR (500 MHz, dmso-d_6) δ 8.16 (d, *J* = 8.0 Hz, **NH-e**, **1H**), 7.29 – 7.13 (m, **Ar**, **NH-a**,**11H**), 4.44 (q, *J* = 7.0 Hz, **CH-f**, **1H**), 3.40 (dt, *J* = 19.7, 9.9 Hz, **CH-b**, **1H**), 2.94 (d, *J* = 7.0 Hz, **CH_2-g**, **2H**), 2.93 – 2.89 (m, **CH_2-c**, **1H**), 2.56 (dd, *J* = 13.5, 8.4 Hz, **CH_2-c**, **1H**), 1.33 (s, **CH_3**).

^{13}C NMR (126 MHz, dmso-d_6) δ 174.61 (**C-3**), 170.96 (**C-5**), 139.09, 137.44, 129.91, 129.80, 128.68, 128.61, 127.07, 126.65 (**Ar**), 81.40 (**C-7**), 56.32 (**C-1**), 53.98 (**C-4**), 41.26 (**C-2**), 37.77 (**C-6**), 28.07 (**CH_3**).

Synthesis of Cin-F-FO*t*Bu **91**

Cinnamic acid **88** (248 mg, 1.68 mmol), $NaHCO_3$ (294 mg, 3.49 mmol) and TBTU (673 mg, 2.09 mmol) were suspended in anhydrous DMF (4 mL) under an N_2 atmosphere. The solution was stirred at rt for 30 minutes, then dipeptide **103** (515 mg, 1.40 mmol) was added and the reaction was left to stir overnight under the same conditions. The following day, TLC (Hex: EA 1:1, Hanessian's stain) confirmed the absence of the dipeptide (R_f = 0.10) and the appearance of a new spot (R_f = 0.66). The solvent was then removed under vacuum. The residue was dissolved in EA (10 mL) and the organic solution was extracted with water (3x20 mL). The organic phases were combined, dried with $MgSO_4$ and evaporated to dryness. The obtained residue was purified by flash column chromatography (Hex: EA 3:1) to give a mixture of a white solid and a transparent oil (undissolved urea derivative). When the mixture was dissolved in a minimum amount of methanol, a white precipitate was formed which was isolated by filtration under vacuum. The reaction yielded the desired product **91** as an off white glassy solid (559 mg, 80%).

m.p. 90.8-92.7 °C, **$[\alpha]_D^{20}$** -12.7° (1% w/v in DMSO), **MS (ES^+)**: *m/z* 499 ([M+H+]+, **(ES^-)**: *m/z* 543 ([M+2Na^+-H^+]$^-$, **IR** (neat): 3275 (br), 3061 (vw), 3030 (vw), 2976 (vw), 2926 (w),

1733 (m), 1649 (s), 1616 (s), 1541 (s), 1497 (sh), 1455 (w), 1367 (m), 1344 (m), 1221 (m), 1150 (s), 977(m), 847 (m), 740 (m), 698 (s) cm^{-1}.

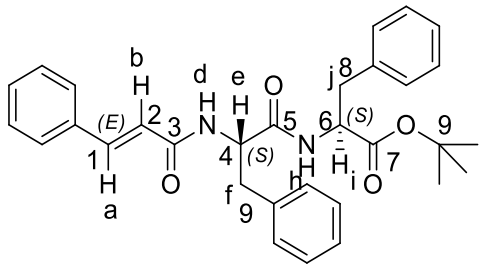

^{1}H NMR (500 MHz, dmso-d_6) δ 8.48 (d, *J* = 7.4 Hz, **NH-h**, **1H**), 8.31 (d, *J* = 8.6 Hz, **NH-d**, **1H**), 7.53 (dd, *J* = 5.2, 3.3 Hz, **Ar**, **2H**), 7.43 – 7.36 (m, **Ar**, **3H**), 7.34 (d, *J* = 15.8 Hz, **CH-a**, **1H**), 7.30 – 7.15 (m, **Ar**, **10H**), 6.67 (d, *J* = 15.8 Hz, **CH-b**, **1H**), 4.73 (td, *J* = 10.1, 8.8, 4.1 Hz, **CH-e**, **1H**), 4.39 (dd, *J* = 14.6, 7.5 Hz, **CH-i**, **1H**), 3.07 (dd, *J* = 13.9, 4.0 Hz, **CH_2 -f**, **1H**), 3.03 – 2.94 (m, **CH_2-j**, **2H**), 2.78 (dd, *J* = 13.9, 10.2 Hz, **CH_2-f**, **1H**), 1.32 (s, CH_3, **9H**).

^{13}C NMR (126 MHz, DMSO- d_6) δ 171.86 (**C-5**), 170.88 (**C-7**), 165.22 (**C-3**), 139.50 (**C-1**), 138.37, 137.62, 135.34, 130.01, 129.75, 129.70, 129.47, 128.71, 128.56, 128.04, 127.03, 126.80 (**Ar**), 122.40 (**C-2**), 81.21 (**C-9**), 54.79 (**C-6**), 54.16 (**C-4**), 38.25 (**C-9**), 37.35 (**C-8**), 28.05 (**CH_3**).

Synthesis of Cin-F-F **70**

The protected dipeptide **91** (150 mg, 0.3 mmol) was dissolved in DCM (0.3 mL) followed by addition of TFA (0.46 mL, 6.0 mmol) dropwise at 0 °C. The reaction mixture was left to stir at rt overnight and next day, TLC (Hex: EA 1:1, Hanessian's stain) confirmed the consumption of the starting material while a new spot appeared (R_f = 0.24). The solvent was then evaporated, and the obtained residue was left to dry overnight under vacuum. The residue was washed three times with DCM (1.0 mL) to afford the organic acid **70** as a white solid in quantitative yield (133 mg, 100%).

m.p. 210.5-212.2 °C, **$[\alpha]_D^{20}$** -14.8° (1% w/v in DMSO), **HR-MS (ESI-TOF)**: *m/z* for $C_{27}H_{27}N_2O_4^+$ $[M+H]^+$ calculated 443.1971, found 443.1970, **IR** (neat): 3350 (s), 3262 (s), 1707 (s), 1662 (s), 1646 (sh), 1587 (s), 1533 (s), 1496 (w, sh), 1350 (w), 1331 (w), 1307 (w), 1271 (s), 1224 (sh), 1212 (s), 1182 (s), 1116 (w), 1054 (vw), 990 (s), 794 (w), 771 (w), 734 (s), 696 (s) cm^{-1}.

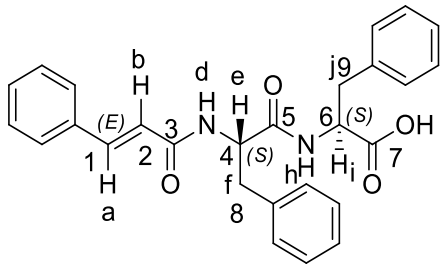

^{1}H NMR (500 MHz, dmso-d_6) δ 12.76 (s, **OH**, **1H**), 8.38 (d, *J* = 7.8 Hz, **NH-h**, **1H**), 8.27 (d, *J* = 8.5 Hz, **NH-d**, **1H**), 7.53 (d, *J* = 7.1 Hz, **Ar**, **2H**), 7.43 – 7.36 (m, **Ar**, **3H**), 7.34 (d, *J* = 15.8 Hz, **CH-a**, **1H**), 7.28 – 7.14 (m, **Ar**, **10H**), 6.67 (d, *J* = 15.8 Hz, **CH-b**, **1H**), 4.71 (td, *J* = 9.7, 4.0 Hz, **CH-e**, **1H**), 4.47 (dd, *J* = 13.3, 8.2 Hz, **CH-i**, **1H**), 3.12 – 3.02 (m, **CH_2-f**, **2H**), 2.94 (dd, *J* = 13.8, 8.8 Hz, **CH_2-j**, **1H**), 2.76 (dd, *J* = 13.8, 10.2 Hz, **CH_2-j**, **1H**).

^{13}C NMR (126 MHz, DMSO- d_6) δ 173.23 (**C-7**), 171.83 (**C-5**), 165.19 (**C-3**), 139.51 (**C-1**), 138.40, 137.94, 135.36, 130.01, 129.70, 129.69, 129.47, 128.73, 128.55, 128.05, 126.96, 126.76 (**Ar**), 122.41 (**C-2**), 54.20 (**CH**), 54.01 (**CH**), 38.11 (**CH_2**), 37.17 (**CH_2**).

Synthesis of Ind-FO*t*Bu **108**

The hydrochloride salt of phenylalanine *tert*-butyl ester **89** (736 mg, 2.854 mmol) was dissolved in anhydrous DMF (15 mL) with $NaHCO_3$ (600 mg, 7.135 mmol) and stirred at rt under a N_2 atmosphere for 30 minutes. Indole-3-acetic acid **107** (500 mg, 2.854 mmol) and TBTU (1375 mg, 4.281 mmol) were then added and the reaction mixture was monitored by TLC. After 24 hours, all the indole acetic acid had been consumed and a new spot had appeared (Hex: EA, 2:3, Hanessian's stain, R_f = 0.48). The solvent was evaporated under vacuum and the obtained residue was dissolved in EA (50 mL). The solution was washed with water (3x50 mL) and the aqueous layer was back extracted with EA (50 mL). The combined organic phases were dried ($MgSO_4$) and evaporated under vacuum to give a residue that was purified by flash column chromatography (Hex: EA, 2:1) to yield the desired product **108** as a red oil (791 mg, 73%).

$[\alpha]_D^{20}$ -1.57° (1% w/v in DMF), **MS (ES^+)**: *m/z* 379 $[M+H]^+$, *m/z* 401 $[M+Na]^+$, **IR** (neat): 3394(sh), 3276 (br), 2977 (vw), 2931 (vw), 1731 (m), 1651 (s), 1415 (m), 1457 (m), 1368 (m), 1340 (sh), 1280 (sh), 1251 (sh), 1230 (m), 1152 (s), 1010 (w), 843 (w), 738 (s), 700 (s) cm^{-1}.

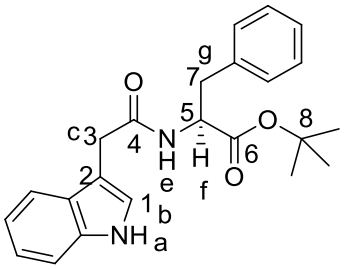

^{1}H NMR (500 MHz, dmso-d_6) δ 10.84 (s, **NH-a**, **1H**), 8.18 (d, J = 7.9 Hz, **NH-e**, **1H**), 7.44 (d, J = 7.9 Hz, **Ar**, **1H**), 7.32 (d, J = 8.1 Hz, **Ar**, **1H**), 7.25 – 7.19 (m, **Ar**, **3H**), 7.17 (dd, J = 7.8, 1.5 Hz, **Ar**, **2H**), 7.11 (d, J = 2.3 Hz, **CH-b**, **1H**), 7.05 (td, J = 8.1, 7.1, 1.1 Hz, **Ar**, **1H**), 6.93 (td, J = 7.9, 7.1, 0.9 Hz, **Ar**, **1H**), 4.39 (td, J = 8.2, 6.2 Hz, **CH-f**, **1H**), 3.52 (s, **CH-c**, **2H**), 2.97 (dd, J = 13.7, 6.1 Hz, **CH-g**, **1H**), 2.90 (dd, J = 13.7, 8.5 Hz, **CH-g**, **1H**), 1.30 (s, **CH_3**, **9H**).

^{13}C NMR (126 MHz, DMSO- d_6) δ 171.23 (**CO**), 171.11 (**CO**), 137.71, 136.60, 129.71, 128.64, 127.71, 126.97 (**Ar**), 124.30 (**C-1**), 121.43, 119.21, 118.78, 111.74, 109.10 (**Ar**), 81.15 (**C-8**), 54.59 (**C-5**), 37.51 (**C-7**), 32.78 (**C-3**), 28.04 (**CH_3**).

Synthesis of Ind-F **109**

Ind-FO*t*Bu **108** (656 mg, 1.733 mmol) was dissolved in DCM (1.5 mL) followed by addition of TFA (1.3 mL, 17.333 mmol) dropwise at 0 °C. The reaction mixture was left to stir at rt and monitored by TLC. Next day, the starting material was consumed, and the solvent was evaporated under vacuum. TFA was removed by co-evaporation (x5) with DCM and by drying the obtained residue under vacuum overnight. The free acid **109** was obtained quantitatively as a purple glassy solid which was used without further purification or characterization.

Synthesis of Ind-F-FO*t*Bu **110**

The hydrochloride salt of phenylalanine *tert*-butyl ester **89** (447 mg, 1.734 mmol) was dissolved in anhydrous DMF (9 mL) with $NaHCO_3$ (364 mg, 4.355 mmol) and stirred at rt under a N_2 atmosphere for 30 minutes. The free acid **109** (559 mg, 1.734 mmol) and TBTU (835 mg, 2.601 mmol) were then added and the reaction was monitored by TLC. After 2 days, the phenylalanine *tert*-butyl ester **89** was consumed and two new spots appeared (Hex: EA, 2:3, Hanessian's stain, R_f = 0.58 (impurity) and 0.53 (product **110**)). The solvent was evaporated under vacuum and the obtained residue was dissolved in EA (20 mL). The

solution was washed with water (6x20 mL) and the aqueous layer was back extracted with EA (20 mL). The combined organic phases were dried ($MgSO_4$) and evaporated to dryness to give a residue that was purified by flash column chromatography (Hex: EA, 1:1) to yield the desired product **110** as a dark golden gum (339 mg, 37%).

The obtained gum was only partially soluble in a range of solvents, therefore due to practical issues (sticky gum) no optical rotation and melting point were acquired.

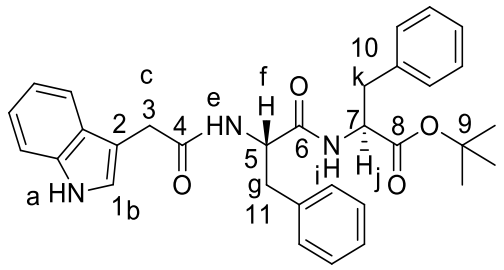

MS (ES$^+$): m/z 526 $[M+H]^+$ **(ES$^-$)**: m/z 524 $[M-H^+]^-$ **IR** (neat): 3292 (br), 3061 (vw), 2931 (vw), 1733 (m), 1644 (s), 1510 (sh), 1497 (m), 1455 (m), 1439 (sh), 1368 (m), 1339 (sh), 1281 (sh), 1249 (sh), 1224 (m), 1152 (s), 844 (s), 740 (s), 699 (s) cm^{-1}.

^{1}H NMR (500 MHz, dmso-d_6) δ 10.79 (s, **NH-a**, **1H**), 8.39 (d, J = 7.4 Hz, **NH-e**, **1H**), 7.99 (d, J = 8.5 Hz, **NH-i**, **1H**), 7.35 – 7.15 (m, **Ar**, **CH-b**, **12H**), 7.05 – 7.00 (m, **Ar**, **2H**), 6.92 – 6.87 (m, **Ar**, **1H**), 4.58 (td, J = 9.6, 4.1 Hz, **CH-f**, **1H**), 4.35 (q, J = 7.4 Hz, **CH-j**, **1H**), 3.46 (d, J = 5.0 Hz, **CH_2-c**, **2H**), 2.99 (dd, J = 13.7, 4.0 Hz, **CH_2-k**, **1H**), 2.96 – 2.91 (m, **CH_2-g**, **2H**), 2.74 (dd, J = 13.7, 9.8 Hz, **CH_2-k**, **1H**), 1.30 (s,**CH_3**, **9H**).

The ^{13}C NMR shows clearly 6 carbon atoms with no substituents (Figure A 2.50, appendix) while instead of the 18 aromatic carbons only 16 signals are present. That is probably due to the overlap of the phenyl carbons.

^{13}C NMR (126 MHz, dmso-d_6) δ 171.42 (**C-4**), 170.52 (**C-6**), 170.49 (**C-8**), 137.80 , 137.14, 136.14, 129.36, 129.31, 128.28, 128.02, 127.28, 126.63, 126.30, 123.86, 120.94, 118.77, 118.34, 111.26, 108.69 (**Ar**,**C-1**), 80.77 (**C-9**), 54.31 (**C-7**), 53.51 (**C-5**), 37.76 (**C-11**), 36.98 (**C-10**), 32.44 (**C-3**), 27.62 (**CH_3**).

Synthesis of Ind-F-F **69**

The *tert*-butyl ester **110** (225 mg, 0.428 mmol) was dissolved in DCM (0.4 mL) followed by addition of TFA (0.15 mL, 4.280 mmol) dropwise at 0 °C. The reaction mixture was left to

stir at rt for 31 hours before extra TFA (0.15 mL, 4.280 mmol) and DCM (0.4 mL) were added. After 35 hours, TLC (Hex: EA, 1:1, Hanessian's stain) confirmed the conversion of the starting material and the presence of a new spot (R_f= 0.09). The reaction mixture was evaporated to dryness and the residue was dried overnight under vacuum. The free organic acid **69** was obtained as a dark green gum (200 mg, 100%) and was only partially characterized. It is of note that there were impurities present in the NMR spectra (Figure A 2.51, appendix), therefore due to the small amount of **69** and practical issues (sticky gum) no further purification was attempted, and the synthesis was considered not successful.

The obtained gum was only partially soluble in a range of solvents, therefore due to practical issues (sticky gum) no optical rotation and melting point were acquired.

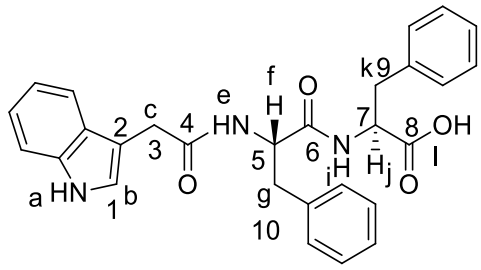

HR-MS (ESI-TOF): *m/z* for $C_{28}H_{27}N_3O_4$ $[M+H]^+$ calculated 470.2080, found 470.2081, **IR** (neat): 3358 (br), 3064 (vw), 3031 (vw), 2926 (br), 1780 (sh), 1722 (m), 1633 (s), 1525 (m), 1497 (sh), 1456 (m), 1441 (sh), 1414 (sh), 1341 (vw), 1208 (sh), 812 (vw), 741 (s), 698 (s) cm^{-1}.

^{1}H NMR (500 MHz, dmso-d_6) δ 10.78 (s, **NH-a**, **1H**), 8.29 (d, J = 7.8 Hz, **NH-e**, **1H**), 7.95 (d, J = 8.5 Hz, **NH-i**, **1H**), 7.33 – 7.28 (m, **Ar**, **2H**), 7.26 – 7.12 (m, **Ar**, **CH-b**, **10H**), 7.02 (ddd, J = 12.2, 9.7, 1.7 Hz, **Ar**, **2H**), 6.89 (td, J = 7.8, 4.0 Hz, **Ar**, **1H**), 4.55 (td, J = 9.5, 4.2 Hz, **CH-f**, **1H**), 4.47 – 4.40 (m, **CH-j**, **2H**), 3.44 (d, J = 8.3 Hz, **CH_2-c**, **2H**), 3.04 (dd, J = 13.9, 5.4 Hz, **CH_2-g**, **1H**), 2.97 (dd, J = 13.8, 4.1 Hz, **CH_2-k**, **1H**), 2.90 (dd, J = 13.9, 8.6 Hz, **CH_2-g**, **1H**), 2.72 (dd, J = 13.8, 9.7 Hz, **CH_2-k**, **1H**).

^{13}C NMR (126 MHz, dmso-d_6) δ 173.23 (**C-6**), 171.82 (**C-4**), 170.91 (**C-8**), 138.23, 137.87, 136.55, 129.78, 129.65, 128.72, 128.43, 127.70, 126.98, 126.67, 124.27, 121.36, 119.17, 118.77, 111.67, 109.08 (**Ar**), 54.00 (**C-5**), 53.95 (**C-7**), 38.03 (**C-9**), 37.20 (**C-10**), 32.83 (**C-3**).

2.5 References

(1) Birchall, L. S.; Roy, S.; Jayawarna, V.; Hughes, M.; Irvine, E.; Okorogheye, G. T.; Saudi, N.; De Santis, E.; Tuttle, T.; Edwards, A. A.; et al. Exploiting CH-π Interactions in Supramolecular Hydrogels of Aromatic Carbohydrate Amphiphiles. *Chem. Sci.* **2011**, *2* (7), 1349-1355.

(2) Raeburn, J.; Pont, G.; Chen, L.; Cesbron, Y.; Lévy, R.; Adams, D. J. Fmoc-Diphenylalanine Hydrogels: Understanding the Variability in Reported Mechanical Properties. *Soft Matter* **2012**, *8* (4), 1168-1174.

(3) Smith, A. M.; Williams, R. J.; Tang, C.; Coppo, P.; Collins, R. F.; Turner, M. L.; Saiani, A.; Ulijn, R. V. Fmoc-Diphenylalanine Self Assembles to a Hydrogel via a Novel Architecture Based on π-π Interlocked β-Sheets. *Adv. Mater.* **2008**, *20* (1), 37-41.

(4) Jayawarna, V.; Richardson, S. M.; Hirst, A. R.; Hodson, N. W.; Saiani, A.; Gough, J. E.; Ulijn, R. V. Introducing Chemical Functionality in Fmoc-Peptide Gels for Cell Culture. *Acta Biomater.* **2009**, *5* (3), 934-943.

(5) Draper, E. R.; Morris, K. L.; Little, M. A.; Raeburn, J.; Colquhoun, C.; Cross, E. R.; McDonald, T. O.; Serpell, L. C.; Adams, D. J. Hydrogels Formed from Fmoc Amino Acids. *CrystEngComm* **2015**, *17* (42), 8047-8057.

(6) Martin, A. D.; Robinson, A. B.; Mason, A. F.; Wojciechowski, J. P.; Thordarson, P. Exceptionally Strong Hydrogels through Self-Assembly of an Indole-Capped Dipeptide. *Chem. Commun.* **2014**, *50* (98), 15541-15544.

(7) Ying, L.; Gervay-Hague, J. Synthesis of N-(Fluoren-9-Ylmethoxycarbonyl)Glycopyranosylamine Uronic Acids. *Carbohydr. Res.* **2004**, *339* (2), 367-375.

(8) Baum, D.; Kosma, P.; Zamyatina, A. Synthesis of Zwitterionic 1,1′-Glycosylphosphodiester: A Partial Structure of Galactosamine-Modified Francisella Lipid A. *Org. Lett.* **2014**, *16* (14), 3772-3775.

(9) Roslund, M. U.; Aitio, O.; Wärna, J.; Maaheimo, H.; Murzin, D. Y.; Leino, R. Acyl Group Migration and Cleavage in Selectively Protected β-D-Galactopyranosides as

Studied by NMR Spectroscopy and Kinetic Calculations. *J. Am. Chem. Soc.* **2008**, *130* (27), 8769-8772.

(10) Ahlers, A.; De Haro, T.; Gabor, B.; Fürstner, A. Concise Total Synthesis of Enigmazole A. *Angew. Chemie - Int. Ed.* **2016**, *55* (4), 1406-1411.

(11) Valeur, E.; Bradley, M. Amide Bond Formation: Beyond the Myth of Coupling Reagents. *Chem Soc Rev* **2009**, *38* (2), 606-631.

(12) Gefen, T.; Vaya, J.; Khatib, S.; Rapoport, I.; Lupo, M.; Barnea, E.; Admon, A.; Heller, E. D.; Aizenshtein, E.; Pitcovski, J. The Effect of Haptens on Protein-Carrier Immunogenicity. *Immunology* **2015**, *144* (1), 116-126.

(13) Zhang, L.; Wang, X. jun; Wang, J.; Grinberg, N.; Krishnamurthy, D. K.; Senanayake, C. H. An Improved Method of Amide Synthesis Using Acyl Chlorides. *Tetrahedron Lett.* **2009**, *50* (24), 2964-2966.

(14) Leggio, A.; Belsito, E. L.; De Luca, G.; Di Gioia, M. L.; Leotta, V.; Romio, E.; Siciliano, C.; Liguori, A. One-Pot Synthesis of Amides from Carboxylic Acids Activated Using Thionyl Chloride. *RSC Adv.* **2016**, *6* (41), 34468-34475.

(15) Muto, Y.; Murai, Y.; Sakihama, Y.; Hashidoko, Y.; Hashimoto, M. Effective Friedel-Crafts Acylation of Biotin Acid Chloride in Trifluoromethanesulfonic Acid. *Biosci. Biotechnol. Biochem.* **2012**, *76* (11), 2162-2164.

(16) Valeur, E.; Bradley, M. Amide Bond Formation : Beyond the Myth of Coupling Reagents. *Chem.Soc.Rev.* **2009**, *38*, 606-631.

(17) Carpino, L. 1-Hydroxy-7-Azabenzotriazole. An Efficient Peptide Coupling Additive. *J. Am. Chem. Soc.* **1993**, *115* (13), 4397-4398.

(18) Lefoix, M.; Routier, S.; Me, J.; Jacquemard, U. Mild and Selective Deprotection of Carbamates with Bu_4NF. *Tertahedron* **2004**, *60*, 10039-10047.

(19) Lin, L. S.; Jr, T. L.; Laszlo, S. E. De; Truong, Q.; Kamenecka, T.; Hagmann, W. K. Deprotection of N - Tert -Butoxycarbonyl (Boc) Groups in the Presence of Tert - Butyl Esters. *Tetrahedron Lett.* **2000**, *41*, 7013-7016.

3. CHARACTERIZATION OF LMW HYDROGELS

3.1 Introduction

In order to develop novel LMW hydrogels as functional biomaterials suitable for tissue culture applications, an interdisciplinary approach was required. Working at the border of organic, physical and supramolecular chemistry, a set of structurally related hydrogelators was synthesized followed by the preparation of their corresponding hydrogels and evaluation of their properties. A range of techniques employed for their characterization [1–3] and an overview of the findings are presented in this chapter.

As the title of the thesis denotes, *"controlling the interfaces of supramolecular hydrogels"* was assessed by combining two different approaches, *i.e.* by incorporating certain functional groups on the gelator scaffold and by using different gelation conditions. Indeed, due to their amphiphilic nature, the synthesized compounds were expected to engage in non-covalent interactions, promote molecular packing and show different tolerances towards gelation triggers.[4–8] Further to this, different gelation protocols were expected to affect the self-assembly process, the topology of the formed supramolecular matrix, thermodynamics, *etc.* and hence the properties of the corresponding gels.

Hydrogel preparation and handling were tested under different gelation conditions, both in water and phosphate-buffered saline (PBS) solution, followed by a visual inspection of the treated samples. This process was based on the vial inversion method, which allowed the observation of the gravitational free flow of the samples and, thus, their characterization either as hydrogels, viscous solutions (partial gelation), suspensions or precipitates.[9] This initial screening allowed identification of those compounds which were successful as hydrogelators.

Stability tests then provided important information regarding the effects of ionic strength and concentration on the gels' stiffness. Thermal studies were employed for measuring the hydrogels' transition temperatures ($T_{gel\text{-}sol}$) and for exploring the dynamic nature of the self-assembly process. Transmission (TEM) and scanning electron microscopy (SEM) were used for the visualization of the shape, size and entanglement of the formed fibres, while X-ray diffraction (XRD) measurements revealed the presence of polymorphism.

The chirality of the supramolecular gels was evaluated by exploring the conformational alignment and spatial orientation of the formed fibres (topology of the supramolecular

network) by circular dichroism (CD) spectroscopy. Further to this, the identification of certain intermolecular interactions and the formation of J- or H-aggregates was assessed by UV/Vis, infrared (IR), NMR and fluorescence spectroscopies. It is of note that a new methodology was developed for the study of LMW hydrogels which was based on synchrotron radiation circular dichroism (SRCD) spectroscopy and is described in Chapter 4.[10]

Finally, optimization of known rheological techniques resulted in minimal handling of the gel specimens during data acquisition. This allowed the assessment of the materials' mechanical strengths by avoiding any alterations of the initial supramolecular matrix.[11–13] Comparing the values of the measured gross (G*), elastic (G′) and loss (G″) moduli, both elasticity and stiffness were assessed while the obtained graphs confirmed the viscoelastic nature of the tested hydrogels.

3.2 Experiments and methods

3.2.1 Materials

All hydrogels were prepared using either high purity water (Romil, Super Purity, Cambridge, UK) or phosphate-buffered saline (PBS) solution. PBS solution was prepared by dissolving one PBS tablet (Sigma Aldrich, Dorset, UK) in 100 mL of high purity water. Fmoc-F-F **68** was purchased from Biogelx (Newhouse, UK) while the rest of hydrogelators were prepared as reported in chapter 2. Brine was prepared by adding sodium chloride (Sigma Aldrich, Dorset, UK) in high purity water until a saturated solution was obtained. Additionally, a fully supplemented cell medium (Dulbecco's Modified Eagle Medium, DMEM) was used which contained 10% fetal bovine serum (FBS), 1% antibiotic (antimicotic) and 1% sodium pyruvate. The DMEM medium, antibiotic (antimicotic) and FBS were purchased from Gibco by Life Technologies. Sodium pyruvate was purchased from Sigma Aldrich, Dorset, UK.

3.2.2 Preparation of hydrogels and obtaining minimum gelation concentration (MGC)

Set of compounds

Several sets of structurally related compounds (Figure 3.1) were available to evaluate their ability to gel water and/or PBS solution by applying different gelation triggers such as sonication and heating as summarized in Table 3.1. Among these, compounds **64**, **65**, **66**, **67**, **69** and **70** were synthesized during the current project whereas the rest were prepared by

a previous group member.[14] In addition to the novel compounds, a full characterization was attempted for those partially characterized previously (Table 3.1).

Table 3.1 Applied gelation conditions for the preparation of self-supporting hydrogels. Based on the gelation results further characterization techniques were employed or not.
* Half gel-half viscous solution, ** Viscous suspension (white aggregates were present), # compounds partially characterized previously.

Compound	**Used Protocol**	**Used Solvent**	**Used conc. for testing hydrogels (mg/mL)**	**Minimum gelation conc. (wt.%)**
#GalNHFmoc **62**	**A, B, C**	Water and PBS	2.0	0.2
#GlcNHFmoc **63**	**A, B, C**	Water and PBS	3.0	0.2
N-Fmoc-D-galactopyranosylamine **64**	**A, B, C**	Water and PBS	Unsuccessful gelation	Unsuccessful gelation
N-Fmoc-D-glucopyranosylamine **65**	**A, B, C**	Water and PBS	Unsuccessful gelation	Unsuccessful gelation
#Biotin-D-galactosamine **66**	**A, B, C**	Water and PBS	Unsuccessful gelation	Unsuccessful gelation
#Biotin-D-glucosamine **67**	**A, B, C**	Water and PBS	Unsuccessful gelation	Unsuccessful gelation
#GalNH-F-Fmoc **111**	**A, C**	Water and PBS	2.0	0.2
#GlcNH-F-Fmoc **112***	**A**	Water and PBS	3.0	0.3

#GalNH-Diclofenac **113****	**D**	Water	3.0	0.3
#GlcNH-Diclofenac **114**	**D**	Water	3.0	0.3
#GalNH-Indomethacin **115**	**D**	Water	3.0	0.3
#GlcNH-Indomethacin **116**	**D**	Water	3.0	0.3
Fmoc-F-F **68**	**B**	PBS	2.0	0.2
Cin-F-F **70**	**D**	PBS	2.0	0.15
Cin-L/D-F-L-F **70/93**	**D**	PBS	2.0	0.15

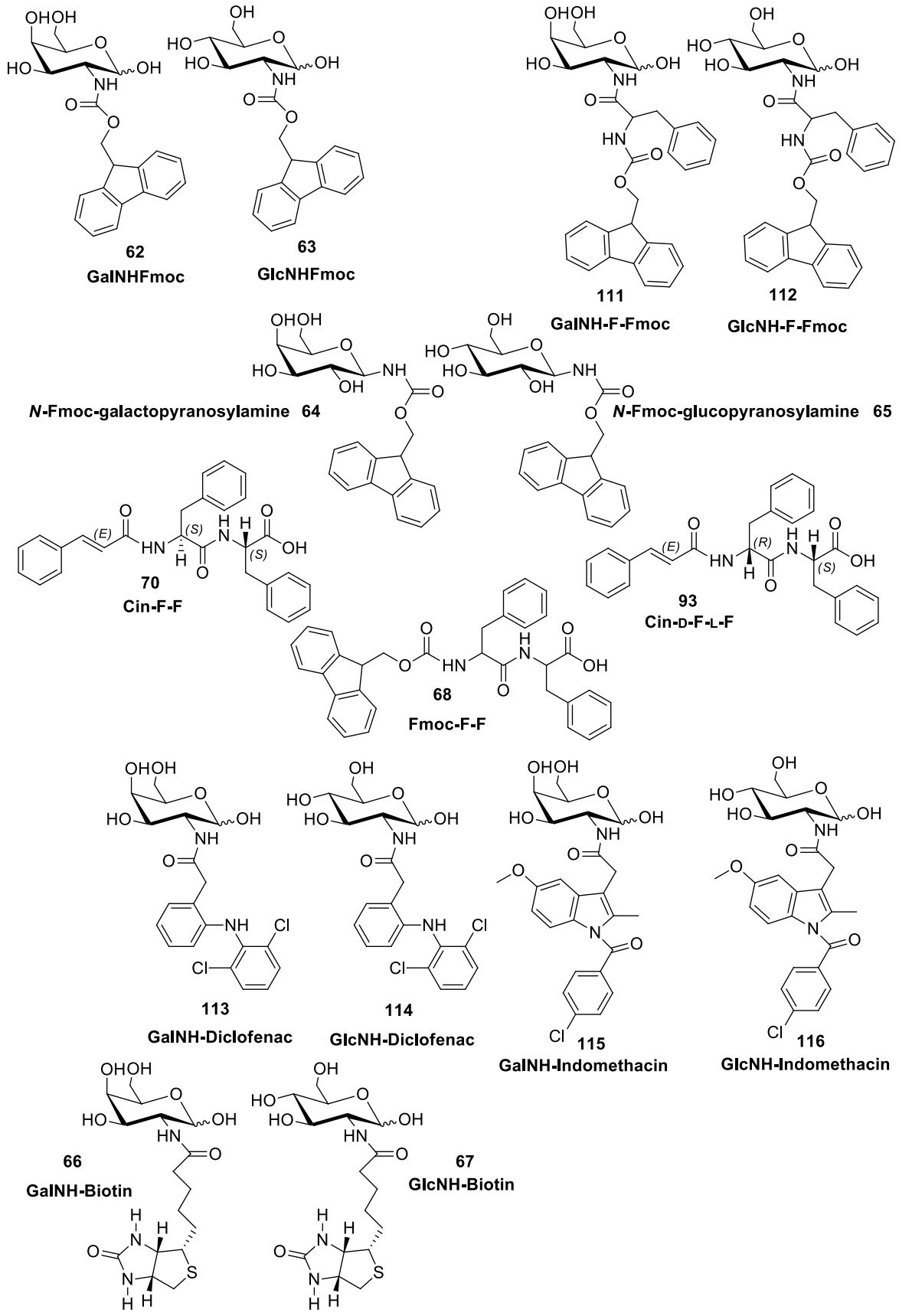

Figure 3.1 Chemical structures of compounds that were tested as potential hydrogelators.

Previous gelation experiments (sonication only, controlled heating/cooling and heating/rapid cooling) for compounds **62**, **63**, **111**, **112**, **113**, **114**, **115** and **116** indicated the minimum amount necessary to gel water or PBS solution.[14] The minimum gelation concentration (MGC) is expressed as wt.% (grams of hydrogelator in 100 mL of stated liquid or solution). For practical reasons, all concentrations applied herein are expressed as mg of the hydrogelator in 1.0 mL of water or PBS solution. It is of note that in some cases, a concentration of the hydrogelator higher than its MGC was used since the formed hydrogel was stiffer and therefore easier to handle during its characterization.

Extensive optimization experiments were performed to determine the MGC for the novel compounds using a range of concentrations (1.0-10 mg in 1.0 mL of water and PBS) under different conditions. Only the successful protocols are reported herein (see gelation protocols below and Table 3.1 for MGC and other concentrations used).

General protocols

Hydrogels were prepared in glass vials (Fisherbrand type III soda lime glass vials; diameter: 10 mm, volume: 3.0 mL) purchased by Fisher Scientific, Loughborough, UK. For heating the vials, a QBD2 Grant block heater was used. An amount of each gelator (see Table 3.1) was mixed with 1.0 mL of water or PBS solution, followed by vortexing (1 minute) and sonication (5 minutes) until a fine suspension was formed. The resulting suspension was then treated accordingly, based on one the following four gelation protocols (as summarized in Table 3.1):

Protocol (A) *(sonication-controlled heating/cooling cycles)*:[14] The suspension was heated in a controlled manner using a block heater. The temperature was gradually increased (55-95 °C) by 10 °C in 10-minute intervals. The cooling cycle was achieved by reducing the temperature by 20 °C every hour until it reached room temperature. The sample was then left undisturbed for at least 12 hours.

Protocol (B) *(sonication only)*:[14] The suspension was left undisturbed at room temperature for at least 12 hours.

Protocol (C) *(sonication-heating)*:[8] The suspension was heated in a block heater at 95 °C (1 hour) until a clear solution was obtained. The sample was then left undisturbed at room temperature at least for 12 hours.

Protocol (D) *(sonication-heating-sonication)*: The suspension was heated in a block heater at 95 °C (1 hour) until a clear solution was obtained. The solution was then sonicated for 1 minute immediately after heating for a second time and the sample was left undisturbed for at least 12 hours at room temperature.

Regardless of the protocol employed, gelation was evaluated the next day by visual inspection of the hydrogels using the vial inversion method. Gel specimens were prepared in triplicate and the results were reproducible in all cases.

3.2.3 Stability tests

Stability tests focused on the macroscopic evaluation of the hydrogels' stiffness and swelling in response to an increased ionic strength and dilution of the samples. For each hydrogelator, hydrogel specimens were prepared in triplicate following the standard gelation protocol (**A**, **B**, **C** or **D** accordingly) to create an approximately 1.0 mL volume of the hydrogel sample in a vial. The height of the formed hydrogels was indicated using a marker pen on the vial. Then 1.0 mL of either purified water, PBS solution, cell medium (DMEM) or brine was added to the vial on top of the hydrogel surface. The samples were left to rest at room temperature overnight. The following day, both swelling and stiffness were visually assessed by vial inversion.

3.2.4 Measurement of phase-transition temperature ($T_{gel\text{-}sol}$)

The temperature at which a gel breaks (observed free flow) during heating is defined as the phase-transition temperature ($T_{gel\text{-}sol}$). Self-supporting hydrogels were heated in a controlled manner (in triplicate) using a block heater. The temperature was gradually increased from 35 °C to 85 °C in 5 °C steps in 10-minute intervals. Gel specimens were visually inspected by inversion of the vials at each temperature increment to identify the $T_{gel\text{-}sol}$. Reformation of the disturbed hydrogels was then evaluated after 12 hours resting at room temperature by the vial inversion method.

3.2.5 TEM and SEM microscopy

Extensive optimization of sample preparation was undertaken to improve the visibility of the formed supramolecular network. It was found that, to give the best results, disturbed and diluted hydrogels had to be used instead of the initial intact self-supporting gels. Further to this, micrographs appeared blurred when samples were stained by a 2% methylamine

vanadate aqueous solution (Nanovan). Therefore, a gel specimen for TEM and SEM observation was prepared in a vial based on the standard protocol for each compound (Table 3.1). The obtained self-supporting gel was then shaken by use of a vortex mixer and diluted with purified water in a 1:5 (gel: water) ratio. 5 μL of the diluted hydrogel was then pipetted onto carbon films (400 mesh Cu, Agar Scientific) and left to dry in a fume hood. To protect the sample from being contaminated (*e.g.* dust particles), carbon films were kept in a Petri dish with its cover semi-open.

In addition to the samples from hydrogels, xerogels were also used. To prepare xerogels, self-supporting hydrogels were freeze dried for 24 hours using a Scan Vac Coolsafe Freeze Drier instrument. A small amount (0.5-1.0 mg) of the xerogel was then transferred onto stubs coated with carbon cement.

Micrographs were obtained by a Hitachi SU8030 microscope, switching between TEM and SEM modes accordingly, at magnifications of x120, x500 and x1000. All photographs were processed using ImageJ software.

3.2.6 X-ray diffraction

Diffractograms were acquired for both xerogels and the corresponding gelators which were obtained as glassy solids or thin powders.

A D8 Advance X-ray Diffractometer (Bruker, Germany) in theta-theta geometry in reflection mode was used for XRD measurements. Cu $_{K(\alpha)}$ radiation was at 40 kV and 40 mA. A primary Göbel mirror was used for parallel beam X-rays and removal of Cu $_{K(\beta)}$ radiation; a primary 4º Soller slit; a 0.2 mm exit slit; knife edge; sample rotation at 15 rpm; a LynxEye silicon strip position sensitive detector set with an opening of 3º, the LynxIris set at 6.5mm and a secondary 2.5º Soller slit. Data collection was between 2-55º 2θ, step size of 0.02º and a counting time of 0.3 seconds per step. With 176 active channels in the detector, this is equivalent to a total counting time of 52.8 seconds per step. Data was collected using DIFFRAC plus XRD Commander version 2.6.1 software (Bruker-AXS). Qualitative assessment was achieved with the aid of EVA version 16.0 (Bruker-AXS) and the PDF-2 database (ICDD, 2008).

3.2.7 Circular dichroism (CD)

Optimization of sample preparation and handling of hydrogel samples for conventional CD analysis established that the hydrogel sample was best formed within non-demountable cells (*in situ*). This allowed CD measurements to be recorded in a manner that avoided any possible alteration of their supramolecular structure by handling, such as with the use of demountable cells (see the results and discussion section). All gel specimens were prepared the day before spectral acquisition to allow for maximum gelation.

Each gelator was weighted into a vial (see Table 3.1) and mixed with 1.0 mL of purified water or PBS solution. The samples were then sonicated and vortexed until a fine suspension was formed. Based on the gelation protocols mentioned above the suspensions were treated accordingly:

Protocol (A) *(sonication-controlled heating/cooling cycles)*: The suspension was pipetted into a non-demountable cell and treated as per protocol **A**. Heating was performed using a block heater from which the blocks were removed. The cells were placed upright, attached to the internal wall of the heater and covered by foil paper to achieve homogeneous heating.

Protocol (B) *(sonication only)*: The sonicated suspension was pipetted into a non-demountable cell and left undisturbed at room temperature for a day.

Protocol (C) *(sonication-heating)*: The suspension was pipetted into a non-demountable cell and heated at 95 °C in a block heater at least for one hour. The cell was then left undisturbed at room temperature for a day.

Protocol (D) *(sonication-heating-sonication)*: The suspension was heated at 95 °C in a vial using a block heater until a clear solution was obtained. The sample was then sonicated immediately after heating for a second time (1-2 minutes) before it was pipetted into a non-demountable cell. The sample was then left undisturbed at room temperature for a day.

To avoid signal saturation, several path lengths were used (0.5, 0.2 and 0.1 mm) since dilution of the gels would reduce the concentration below the minimum gelation concentration. Identification of the most appropriate path length was achieved by measuring the absorbance of each sample prior to any CD measurement. Once the pathlength was optimized, the obtained CD spectra were truncated where the corresponding absorbance value exceeded 1.0 AU. All conventional CD measurements were performed using a

Chirascan spectrophotometer. Prior to any CD measurements of the samples, an empty cell spectrum was acquired followed by the appropriate solvent baseline.

All spectra (CD and absorbance) were acquired at a wavelength range of 180-360 nm, by setting a wavelength step value of 1, time per point of 0.5 s and with 4 acquisitions. The resulting data was then processed using Microsoft Excel software. All spectra were corrected for the solvent baseline and generated as the average of the 4 acquisitions. The differential absorbance of left and right circularly polarized light, *i.e.* CD, is shown as ellipticity θ which was expressed in mdeg and not as molar ellipticity due to the nature of the samples. The temperature was also controlled, depending on the type of the performed experiment.

3.2.8 UV-vis and fluorescence spectroscopy

A Tecan Infinite 200 PRO multifunctional microplate reader was used for both UV-Vis and fluorescence measurements. Hydrogels were prepared in vials as per the standard protocol for each compound described above (Table 3.1) and allowed to rest for a day before being pipetted (75 μL) into the wells of a quartz 96-well flat bottom microplate in triplicate. An absorbance scan (UV-Vis, 230-600 nm) was performed to measure the λ_{max} (abs) to be used as the λ excitation value for the measurement of fluorescence intensity. The parameters used were: number of flashes 25, wavelength step size 1, gain 50, Z position 20000. The same experimental setup was used for a fluorescence scan to measure the λ_{max} of emission. The parameters used were the same as those for the absorbance scan except for the wavelength range (280-600 nm, as the instrument's software cannot measure below 280 nm in fluorescence mode). Finally, using the excitation and emission values, the fluorescence intensity was acquired. All spectra were baseline corrected while measurements of the gelators methanolic solutions were also performed using the same concentration as the hydrogels and under the same conditions.

3.2.9 Infrared spectroscopy (IR)

IR spectra were recorded in attenuated total reflectance (ATR) mode on a Perkin Elmer Spectrum One FT-IR spectrometer. All spectra were recorded in the range of 4000-500 cm^{-1} using 124 scans. Gel specimens were prepared in water (H_2O), PBS solution and deuterated water (D_2O). The IR of xerogels were also recorded. Hydrogels were prepared in vials using the standard gelation protocol for each compound (Table 3.1) and rested for a day prior to any IR recordings. 75 μL of the gel was then pipetted on the sample compartment and left

undisturbed for 30 minutes before commencing any measurements. All IR spectra were baseline corrected and processed using Microsoft Excel software.

3.2.10 Nuclear magnetic resonance (NMR)

Hydrogel specimens of gelators **62** and **63** were prepared for NMR analysis as per protocol **C** (*sonication-heating*) in deuterated water. Suspensions were (1.0 mL) initially heated in vials using a block heater before being transferred by pipette into NMR tubes. These samples were then heated for a further hour at 95 °C using a water bath and then left undisturbed at room temperature for a day before proceeding with spectral acquisition.

Solutions of hydrogelators **62** and **63** were also prepared in vials, in mixtures of deuterated dimethyl sulfoxide and deuterated water, in different ratios (9:1, 8:2, 7:3 of d_6-dmso: D_2O). The compounds were suspended in 1.0 mL of the solvent mixture, using the concentration used for preparation of their corresponding hydrogels and sonicated (at least for 5 minutes) until a clear solution was obtained. The resulting solutions (1.0 mL) were then transferred by pipette into an NMR tube and left for a day at room temperature prior to any spectra acquisition.

For the NMR thermal studies, the ^{1}H NMR spectra were recorded at a range of temperatures (35, 45, 55, 65, 75 °C) using 128 scans and setting relaxation delay of 1s. Before switching to a different temperature, a thermal equilibration had to be set up. For that reason, the desired temperature was selected, and a ^{1}H NMR spectrum was recorded running 1 scan and setting relaxation delay of 900 s. For equilibration purposes, an increase of the relaxation delay achieved the desired temperature in the probe. When this was done then the NMR spectrum of the sample was recorded. It takes almost 20 mins for the temperature to equilibrate and 5 minutes to acquire the ^{1}H NMR spectrum.

^{1}H NMR spectra of the solution and hydrogel samples were recorded using a Jeol ECP 400 MHz FT NMR spectrometer, incorporating a tuneable H (5) 400 probe (1H: 400 MHz and 13C: 100 MHz) and a Jeol ECA 500 MHz FT NMR Spectrometer, incorporating a NM-50TH5AT/FG2 probe. All chemical shifts (δ) are quoted in ppm and coupling constants (*J*, Hz) averaged. Residual signals from the solvents or TMS signal were used as an internal reference. All spectra were processed using MestReNova software. NMR tubes (Standard series tubes 400 MHz and 500 MHz, 7″, 5mm) were purchased by GPE Scientific Limited, Bedfordshire, UK

3.2.11 Rheological studies of hydrogels

Rheology measurements were performed using an Anton Paar MRC 302 modular compact rheometer with an upper geometry cylinder (cylinder-relative ST10-4V-8.8/97.5). Gel specimens were prepared in glass vials (Fisherbarnd type III lime glass specimen vials, diameter: 19 mm, volume: 8.0 mL) purchased from Fisher Scientific, Loughborough, UK.

Gel specimens (1.0 mL volume) were prepared in triplicate following the standard gelation protocol for each compound and rested for a day prior to any data acquisition. Only self-supporting hydrogels were tested, *i.e.* the viscoelastic properties of soft dynamic materials were not assessed. The samples were prepared in glass vials which were then fixed on the lower geometry of the instrument and screwed until secure. The upper geometry was inserted into the vial, adjusting the gap accordingly so as to be completely covered by the hydrogel. A waiting time period of 30 minutes was used before any measurement.

Strain amplitude measurements were performed within the linear viscoelastic region (LVR) where the elastic G′ and loss G″ moduli are independent of the strain amplitude. The G′ and G″ were measured at a frequency of 1 Hz. Frequency scans were performed from 0.1 rad/s to 100 rad/s under a certain strain γ% different for each specimen. All measurements were taken at a temperature of 25 °C.

3.3 Results and discussion

A key aim of this project was the assessment of hydrogels properties. As part of this, previous preliminary and partial characterization of a number of hydrogels were considered.[14] Initially, a range of techniques was optimized, which involved the development of new methodologies to allow the gels to be handled in a manner that did not disrupt their self-assembly during the experimental work.

The hydrogels were categorized as four groups based on the structural features of their constituent building blocks: (i) the Fmoc set of compounds, (ii) the indomethacin and diclofenac derivatives, (iii) the biotin-based compounds and (iv) the diphenylalanine analogues (Figure 3.1). A brief description of the optimization work and the results of the obtained characterization are given below. The materials of the first three groups have already been partially characterized[14] (Table 3.2) therefore only the new characterization data is reported herein.

Table 3.2 Partial characterization of compounds that were previously prepared. Experiments performed (green), not performed (red).

*IR spectra were recorded for specimens prepared in water or PBS solution only *i.e.* no deuterated water was used and the IR of xerogels were not recorded. Microscopy was applied for hydrogels but not for xerogels. Preliminary CD work was employed using demountable cells (gel specimens were not prepared *in situ*). Rheology measurements were undertaken on hydrogels transferred onto the lower geometry of the instrument. An upper geometry of a parallel plate was used which did not allow *in situ* preparation of the samples either.

Compound	**62**	**63**	**66**	**67**	**111**	**112**	**113**	**114**	**115**	**116**
Gelation tests										
Stability tests										
$T_{gel/sol}$										
***IR**										
***CD**										
UV-vis										
Fluorescence										
XRD										
***Rheology**										
***Microscopy**										
Biological tests										

3.3.1 Characterization of the Fmoc-based hydrogels

This set of materials consists of hydrogels prepared from two pairs of epimeric hydrogelators; GalNHFmoc **62** and GlcNHFmoc **63**, GalNH-F-Fmoc **111** and GlcNH-F-Fmoc **112** (Figure 3.1). Based on previous findings, the stiffest and most stable self-supporting gel was that formed from GalNHFmoc **62**;[14] therefore, it was used as the model gel for the optimization work. In addition, a complete characterization study of the gels prepared from **62** and **63** has been reported by Birchall *et al.* in 2011.[8] This indicated that the molecular self-assembly was due to a combination of CH-π and T-stacking interactions. Since the four hydrogelators (**62**, **63**, **111** and **112**) are structurally related, Birchall's paper was used to guide the design of the characterization work undertaken. The findings for **62** and **63** reported herein were qualitatively similar to that reported by Birchall *et al.*, despite different gelation conditions being employed in this work.

Gelation tests

Gelation was achieved following protocols **A-C** (see Table 3.1) and the materials were assessed using the tube inversion method. A description of the formed hydrogels after visual inspection is given below (Table 3.2).

White aggregates were observed for the hydrogels of GlcNHFmoc **63** in PBS solution and those prepared using GalNH-F-Fmoc **111** in PBS and water. When gelation was inspected at later time points (a few hours and after one week) partial disruption of the hydrogel structure was noticed suggesting syneresis had occurred, *i.e.* shrinking of gels and ejection of solvent.[15,9] White aggregates presumably resulted from partial solubilization of the hydrogelator during heating and/or sonication. Therefore, the presence of white aggregates (the concentration of gelator molecules possibly dissolved in entrapped water within the matrix is smaller to that used for the preparation of the hydrogel), in addition to the increased ionic strength due to the presence of salts in PBS solution, could explain syneresis. Overall, the Fmoc-set of hydrogelators yielded stiff, self-supporting hydrogels with the exception of GlcNH-F-Fmoc **112** which formed a partial gel.

Table 3.3 Description of formed hydrogels. Different protocols used for a single compound gave the same outcome in the stated solvent.

*****A (sonication-controlled heating/cooling cycles), B (sonication only), C (sonication/heating). The MGC was used for each compound.
****** Samples were visually evaluated after 24 of rest at r.t.
^ Gelation for compounds 64 and 65 was tested using a range of concentrations.

Compound	**Protocol***	**MGC (mg/ mL)**	**Visual evaluation****	
			PBS	**Water**
GalNHFmoc **62**	**A, B, C**	2.0	Self-supporting semi-transparent gel	
GlcNHFmoc **63**	**A, B, C**	2.0	Self-supporting semi-transparent gel with visible white aggregates	Self-supporting semi-transparent gel
GalNH-F-Fmoc **111**	**A, C**	2.0	Self-supporting semi-transparent gel with visible white aggregates	
GlcNH-F-Fmoc **112**	**A**	3.0	Half gel-half viscous solution	
N-Fmoc-D-galactopyranosylamine **64**	**A, B, C**	1.0-10^	A precipitate was formed	
N-Fmoc-D-glucopyranosylamine **65**	**A, B, C**	1.0-10^	A precipitate was formed	

Stability tests

Stability tests were performed on GalNHFmoc **62** based hydrogels in PBS solution by addition of brine and water onto the surface of the samples. Other hydrogels of this set of hydrogelators weren't tested. Firstly, gelation was triggered by sonication and heating (protocol **C**) to yield self-supporting gels (Figure 3.2-i). All observations reported herein were after 24 hours. Brine was found to penetrate the gel (Figure 3.2-ii), while the hydrogel remained intact (even after a month), although white aggregates did appear within 24 hours. By contrast, water caused partial disruption of the hydrogel almost immediately after addition to give a viscous, free-flowing solution (Figure 3.2-iii). Therefore, increasing the ionic strength was found to support the self-assembly rather than disrupt it which occurred when the ionic strength was lowered.

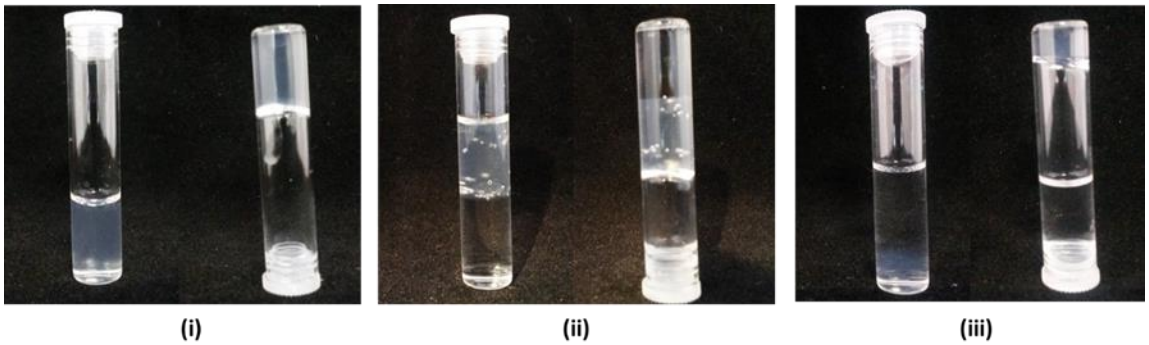

Figure 3.2 Stability tests of GalNHFmoc **62** based hydrogels prepared in PBS: (i) initial gel; (ii) addition of brine; (iii) addition of water. Gels were prepared following protocol **C** at a concentration of 2.0 mg/mL. Samples were tested in triplicates at r.t. and their stability was assessed after 24 h of addition of water and brine.

Hydrogels are dynamic systems therefore they behave differently under different conditions. Penetration of brine through the gel clearly suggested that water molecules moved through the gel. In addition, no swelling or shrinkage of the gel was observed which suggested presumably a dynamic equilibrium in the movement of water molecules from brine to gel and *vice versa*. It is of note that in the case of brine, water molecules interact strongly with the sodium and chloride ions. Although it was expected the driving force of brine movement through the hydrogel to be water diffusion from the isotonic environment within the supramolecular network to a hypertonic environment (brine on the surface of the gel), this was not the case as no shrinkage of the gel was apparent. Therefore, an exchange of water molecules through the interface that separated the gel from brine was more likely. Such a movement could potentially trigger crystallization and/or an increase of local concentration of the hydrogelator **62**, thus potentially explaining the appearance of white aggregates. The hydrophobic moieties of the gelator molecules could also interact in a greater extent and enhance the gel's stiffness since shaking of the vial didn't cause any disruption of the gel. Alternatively, white aggregates could also be attributed to salt entrapped within the gel.

By contrast, addition of water increased the degree of dissolution of hydrogel, leading to the cleavage of intermolecular interactions of the hydrogelators and finally dilution of the gel. In fact, the amphiphilic nature of GalNHFmoc **62** could explain the solvation, since the added water molecules could possibly act as antagonists for H-bonding (with the OH groups of the sugar moiety) by the development of intermolecular H-bonds.

Phase transition temperature ($T_{gel\text{-}sol}$) measurements

The phase transition temperature ($T_{gel\text{-}sol}$) was measured for GalNHFmoc **62**, GlcNHFmoc **63** and GalNH-F-Fmoc **111** hydrogels (Table 3.3). The reported temperature range in which phase transition occurred was assessed visually by vial inversion while heating the samples in a controlled manner by increasing their temperature by 5 °C in 10-minute intervals.

Table 3.4 Gelation conditions and obtained results of phase transition temperature measurements. Protocol **B** *(sonication only)* and protocol **C** *(sonication/heating)* were used. The concentration was 2.0 mg/ mL for all samples.

Compound	**Solvent**	**Gelation protocol**	**Measured temperature range of phase transition (°C)**
GalNHFmoc **62**	water	**B**	50-55
	PBS	**B**	50-55
GlcNHFmoc **63**	water	**B**	35-40
	PBS	**B**	35-40
GalNH-F-Fmoc **111**	water	**C**	55-60

The highest recorded $T_{gel\text{-}sol}$ value corresponded to the GalNH-F-Fmoc **111** hydrogel, whereas the lowest was seen for GlcNHFmoc **63**. From these findings, it was clear that a change of solvent did not affect $T_{gel\text{-}sol}$ of **62** and **63**. Indeed, both GalNHFmoc **62** gels in PBS solution and water resulted identical values. The same outcome was also observed for the GlcNHFmoc **63** hydrogels. Although the hydrogelators GalNHFmoc **62** and GlcNHFmoc **63** only differ at one stereogenic center (position C4), this had a marked difference upon the phase transition temperature of the corresponding hydrogels. It is of note that they may have a similar type of self-assembly, but it is possible that a different mutarotation equilibrium may also affect their properties. Finally, possible reformation of gel state in the heated samples was evaluated 12 hours after heating. The hydrogels from GalNHFmoc **62** in PBS and water reformed, yielding stiff, self-supporting gels, while the sols of GlcNHFmoc **63**, in both water and PBS solution, remained in the sol state. This suggested a greater gel-sol reversibility and a potential annealing cycle for gel **62** compared to **63**.

FT-IR measurements

FT-IR spectra of the hydrogelators (solid powders), xerogels (lyophilized hydrogels) and hydrogels in D_2O (hydrogel with solvent subtraction) were recorded for GalNHFmoc **62**, GlcNHFmoc **63** and GalNH-F-Fmoc **111** (Figure 3.3). For practical reasons, gelation protocol **A** (*sonication only*) was applied for the Fmoc-protected carbohydrates **62** and **63** while protocol **C** (*sonication/heating*) was applied for GalNH-F-Fmoc **111**. Xerogels were prepared by lyophilization of the corresponding materials prepared in water. Based on the data obtained, characteristic absorption bands were observed for the carbamate (-NH-(CO)-O-) and amide -NH-(CO)- functional groups (1650-1850 cm^{-1}).[16] In addition, a close structural similarity is suggested between the solid state and that of xerogels, since the spectra of the xerogels appeared almost identical to those of the corresponding powders.[17]

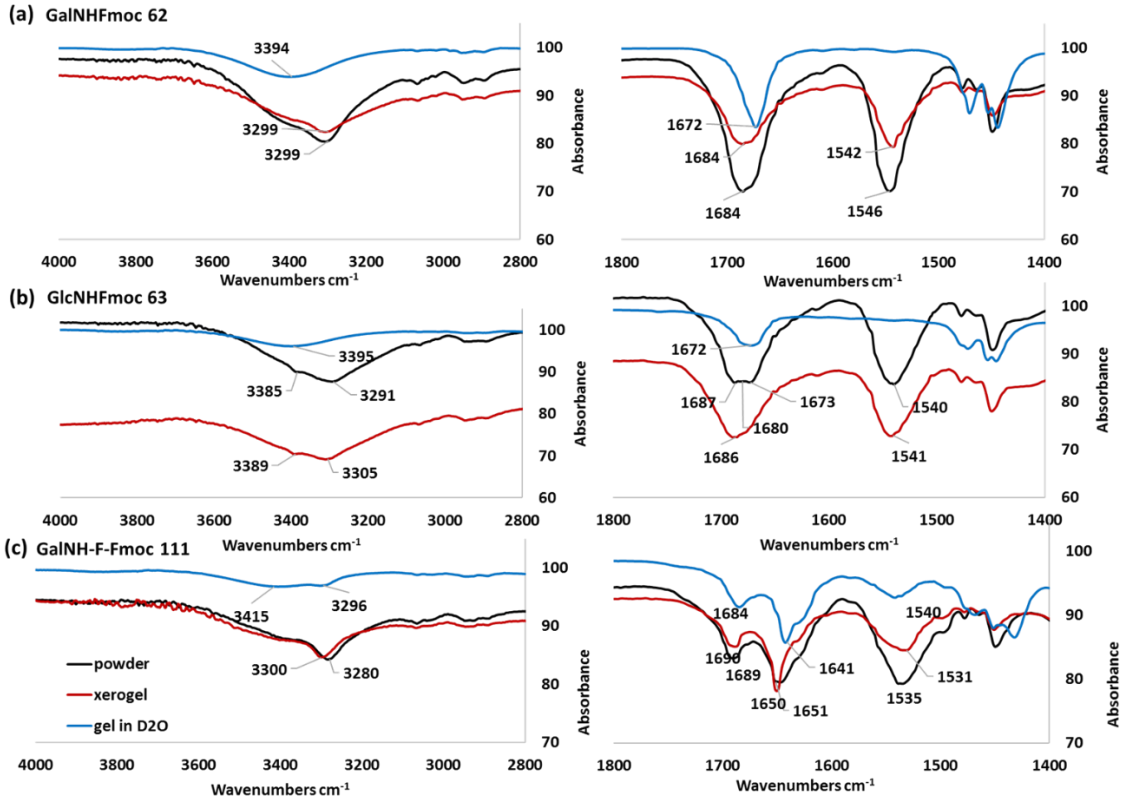

Figure 3.3 FT-IR spectra of the **powders** (black), xerogels (red) and hydrogels in D_2O (blue) of compounds (a) GalNHFmoc **62**, (b) GlcNHFmoc **63** and (c) GalNH-F-Fmoc **111**. N-H and O-H stretching wavelength region (4000-2800 cm^{-1}); N-C=O stretching and N-H bending wavelength region (1800-1400 cm^{-1})

Hydrogen bonding between a functional group of the type X-H and Y (X-H$\cdots$Y), where X is more electronegative than H and Y has a lone pair of electrons or π electrons, results in

elongation of the X-H bond which is related to a red shift and increased intensity in IR spectroscopy. The lengthening of X-H bond is therefore attributed to electrostatic interactions since the more electronegative Y attracts H to its side. The weakened X-H bond will be associated to a red shift. In contrast, when X-H is less polar as in the case of C-H and the Y is a weak hydrogen acceptor a lesser red shift or even a blue shift is observed.[18]

When comparing the powder and hydrogel spectra, a red shift of the N-**C=O** stretching peak was observed in all three cases, suggesting that it was H-bonded in the gel state. Indeed, for GalNHFmoc **62** there was a significant shift of 12 cm^{-1} (1684 to 1672 cm^{-1}), for GlcNHFmoc **63** an 8 cm^{-1} shift (1680 to 1672 cm^{-1}) and for GalNH-F-Fmoc **111** both peaks shifted 5 and 10 cm^{-1} (Fmoc >C=O 1689 to 1684 cm^{-1}, phenylalanine >C=O 1651 to 1641 cm^{-1}).

In contrast to the hydrogels of GalNHFmoc **62** and GlcNHFmoc **63**, only the hydrogel spectrum of GalNH-F-Fmoc **111** showed a weak N-H bending peak at 1540 cm^{-1} which was slightly red shifted compared to the powder. In fact, this signal was detectable only in the spectra of powders and xerogels for all three samples, suggesting a possible disruption of H-bonding for hydrogels in D_2O of **62** and **63**. Finally, a significant blue shifted and highly broadened peak at the N-H and O-H stretching band region of the wet hydrogels compared to powders and xerogels, suggested the overlap of NH and OH peaks. In fact, as stated by Gronwald and co-workers, the absence of a peak at 3600 cm^{-1} suggests the lack of free OH groups whereas the broadened signals between 3400-3280 cm^{-1} are due to intermolecular and intramolecular H-bonding interactions.[19]

NMR measurements

Variable temperature ^1H NMR studies of the GalNHFmoc **62** and GlcNHFmoc **63** hydrogels in D_2O clearly showed a downfield chemical shift of the aromatic protons as a function of increased temperature (Figure 3.4). In other spectral regions however, signals were broadened thus potential shifting was unclear to observe. Indeed, the Fmoc proton signals a, b, c and d for GalNHFmoc **62** hydrogel and the corresponding e, f, g, h for GlcNHFmoc **63** shifted almost 0.30 ppm towards lower fields. Such a shift is significant compared to what is reported in literature and may indicate disturbances in the molecular self-assembly as the temperature increased (Figure 3.4).[20–24] Although NMR characterization was limited to gels prepared in water only, as the project focused on hydrogels, it is of note that a control spectrum was needed to ascertain how significant the observed shifts were. Due to low solubility of the compounds in D_2O the majority of the peaks were broad at lower

temperatures over the spectral range. A concentration increase of the samples was not helpful either. Further to this, to better facilitate future studies, in order to assess thermal effects on chemical shifts a number of solvents should be evaluated (and should preferably promote organogelation) to generate a reliable control spectrum.

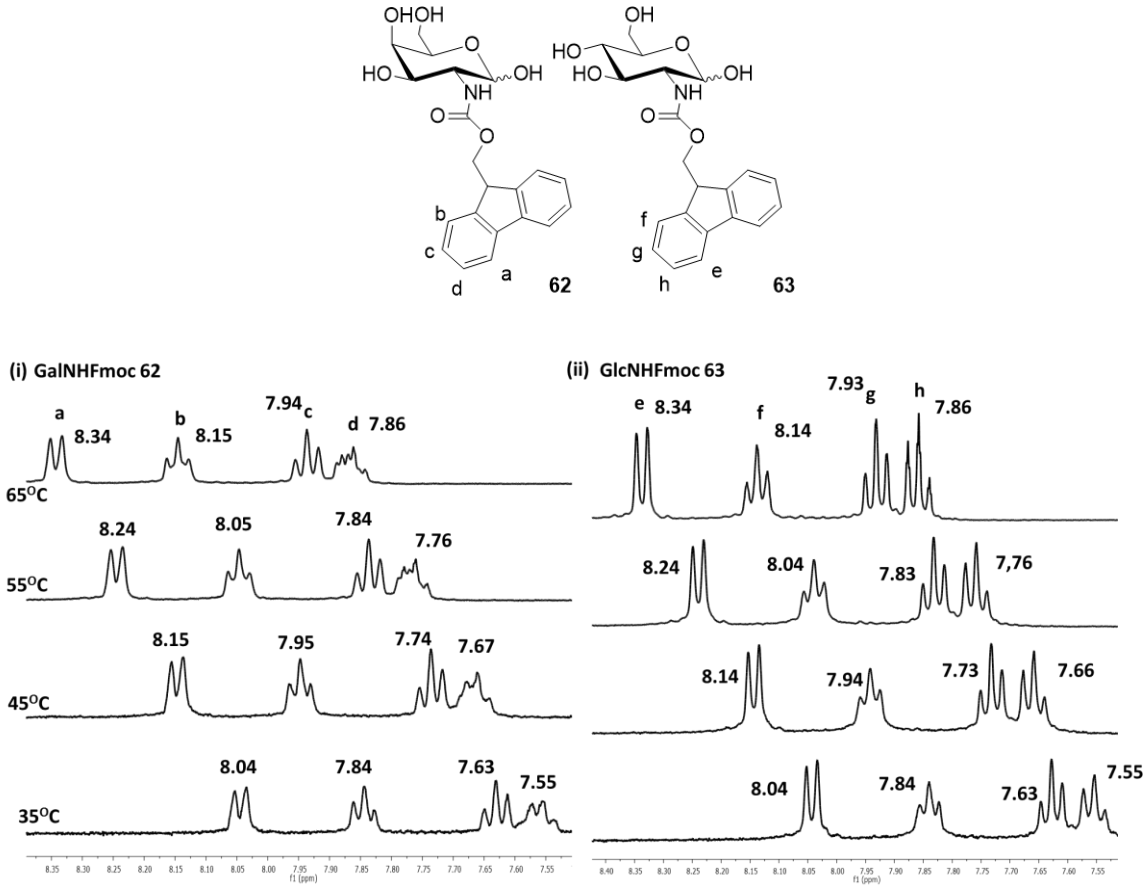

Figure 3.4 Variable temperature ^{1}H NMR (400 MHz) studies of the (i) GalNHFmoc **62** and (ii) GlcNHFmoc **63** hydrogels in D_2O. The aromatic region 8.35-7.55 ppm is depicted.

^{1}H NMR studies to explore potential gelation of GalNHFmoc **62** and GlcNHFmoc **63** in different solutions were also undertaken. Therefore, mixtures of deuterated dimethyl sulfoxide and deuterated water were used at different ratios (9:1, 8:2, 7:3 for dmso-d_6: D_2O). From the ^{1}H NMR spectra (in dmso-d_6) it was evident that two anomers were present, a major (A) and a minor (B) at a ratio of 1(A): 0.13(B) for GalNHFmoc **62** and 1(A):0.73(B) for GlcNHFmoc **63**. The aromatic protons are depicted between 7.90-7.25 ppm while $NH_{A,B}$ signals appeared between 7.15-6.15 ppm (Figure 3.5).

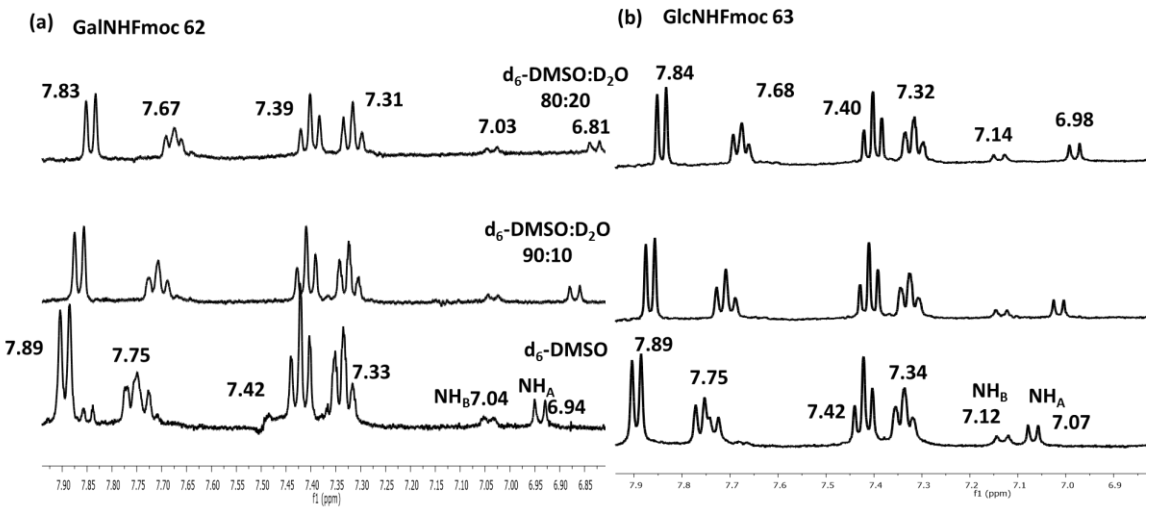

Figure 3.5 ^{1}H NMR studies of GalNHFmoc **62** and GlcNHFmoc **63** solutions in 9:1, 8:2, 7:3 dmso-d_6: D_2O. All spectra were recorded at 25 °C.

An upfield chemical shift was observed for the aromatic protons of the Fmoc moiety on addition of D_2O. The increase of electronic shielding by increasing the percentage of D_2O indicated that the hydrogelators may have adopted certain conformational and configurational spatial orientations, leading to the development of possible aromatic (π-π stacking) or other types of intermolecular interactions. Both hydrogels **62** and **63** were previously reported by Birchall *et al.* where it was proposed that self-assembly was driven by a combination of CH-π and T-stacking interactions.[8] Additionally, a similar upfield shift was also observed for the NH signals suggesting they were H-bonded.[23,22] However, a solvent effect should also be considered. To further discuss this, a control spectrum in D_2O would be needed however, due to the low solubility of hydrogelators **62** and **63** in D_2O, proton peaks appeared broadened. Further trials need to be undertaken in future to identify the optimum organic solvent to assess potential solvent effects on chemical shift. Considering the amphiphilic nature of the gelator molecules, any changes of the solvent system could possibly trigger self-assembly as signal broadening was observed by increasing the percentage ratio of D_2O.

Fluorescence studies

To observe the development of intermolecular interactions (sol-gel process) and explore the microenvironment of the fluorophores, gelation of GalNHFmoc **62** in PBS solution was monitored by fluorescence spectroscopy. A hydrogel from **62** was prepared based on protocol **C** (*sonication/heating*) and 75 μL of the hot solution were immediately pipetted

into each of three wells of a quartz 96-well flat bottom microplate. To evaluate gelation, fluorescence scan and fluorescence intensity measurements were acquired in 30-minute intervals over a period of 7 hours as the sample cooled (temperature could not be controlled by the instrument) (Figure 3.6).

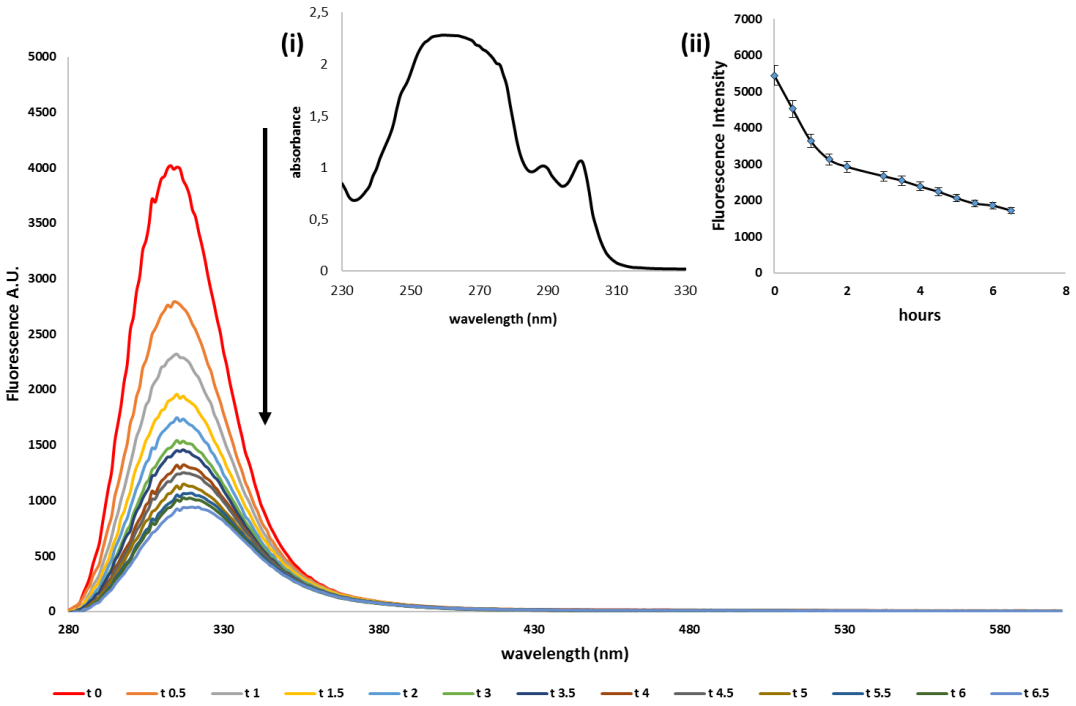

Figure 3.6 Monitoring gelation by time dependent fluorescence scan. Inserts: absorbance of hydrogel (i), fluorescence intensity (ii) of GalNHFmoc **62** in PBS. Excitation was set at 260 nm and emission at 312 nm. Fluorescence scan was run over 280-600 nm wavelength range at a constant temperature of 25 °C. All spectra were baseline corrected and averaged.

During the sol-gel transition, a decrease in fluorescence intensity was observed over time. This is in stark contrast to the findings of Yan *et al.* in their work on supramolecular gels prepared from glucose-based fluorescent low-molecular mass compounds (glucose-based naphthalene derivatives) .[25] The reverse process (gel-sol) reported by Wang *et al.* revealed also that the fluorescence intensity decreased at high temperatures which contradicts the depicted spectra.[26] As the hot solution was getting cooler and self-assembly was progressing, an increase in intensity was expected. The opposite results could be explained by the fact that during gelation the formation of aggregates increased the local concentration of the fluorophores which gave unfavourable fluorescence emission due to inner-filtering effects. In fact, a primary inner filter effect (PIFE) can justify an emission decrease by the re-absorption of emitted radiation by the Fmoc moiety. In addition, a secondary inner filter

effect (SIFE) takes place when the chromophore absorbs in the emission region. A concentration dependent fluorescence spectroscopy study for GalNHFmoc **62** and GlcNHFmoc **63**, as reported by Birchall *et al*., showed an emission decrease by increasing the concentration.[8] Since the GalNHFmoc **62** hydrogelator is amphiphilic and not soluble in either water or PBS solution, a potential fine suspension is formed by sonication and heating rather than a clear solution. It is of note though, that even when free in solution, a fluorophore can be either temperature-dependent or not. In the former case, a variation in temperature can affect both the lifetime and the intensity, whereas in the latter case these parameters are not affected. Subsequently, the reported CH-π interactions could trigger a collisional quenching mechanism explaining the emission decrease during gelation. Indeed, certain conformations during molecular packing could orientate the excited Fmoc moiety adjacent to atoms that can facilitate non-radiative transitions to the ground state. A slight red shift of roughly 3 nm was observed during gel formation. In contrast to the more substantial red shifts given by Fmoc-peptide based systems, smaller ones could be attributed to insufficient π-π stacking, *i.e.* instead of face-to-face, an edge-to face stacking could have occurred. In fact, the above findings were akin to those reported by Birchall *et al.*, which suggested that self-assembly was driven by CH-π interactions.[8] This is perhaps unsurprising given the hydrogelators are the same although, notably, the gelation protocol differs.

To explore intermolecular interactions further, additional experiments were performed. The methanolic solutions of compounds **62**, **63** and **111** were prepared to compare their fluorescence spectra versus their corresponding hydrogels (Table 3.4 and Figure 3.7). In true solutions, solvated gelator molecules engage in few or no intermolecular interactions, certainly when compared to the gel state. Gel specimens were prepared by protocol **C** (*sonication/heating*) for practical reasons and had final concentrations of 5.0 mM for **62** and **63** and 3.6 mM for **111** (2.0 mg/ mL for each hydrogelator were used). The same concentrations were also used for the methanolic solutions. An absorbance scan was measured to determine λ excitation prior any fluorescence measurements. For **62**, λ excitation values were 260 nm for the gel in PBS, 255 nm for the gel in water and 264 nm for the methanol solution. The corresponding λ excitation values for **63** were 257, 253, 263 nm and for **111** 265, 263, 264 nm.

Table 3.5 Comparison of the λ_{max} emission of hydrogels compared to the corresponding methanolic solutions of hydrogelators **62**, **63** and **111**.

	Fluorescence λ_{max} (nm)		
	Gel in PBS	**Gel in water**	**Methanolic solution**
GalNHFmoc **62**	312	315	307
GlcNHFmoc **63**	312	312	312
GalNH-F-Fmoc **111**	312	323	311

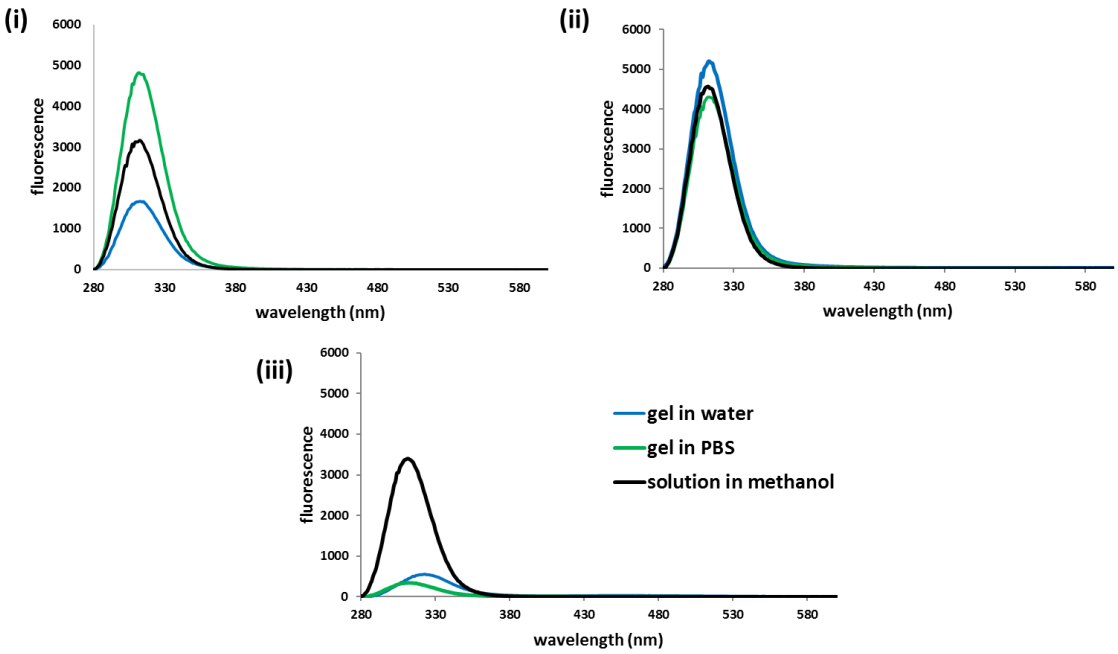

Figure 3.7 Fluorescence spectra of hydrogels versus the methanolic solutions of (i) GalNHFmoc **62**, (ii) GlcNHFmoc **63** and (iii) GalNH-F-Fmoc **111**. All fluorescence measurements were taken over 280-600 nm wavelength range at a constant temperature of 25 °C. All spectra were baseline corrected and averaged.

Comparing the obtained λ_{max} of emission, a small red shift was observed for the galactosamine derivatives **62** and **111**, whereas no shift was detected for the glucosamine **63** gels (Table 3.4) possibly due to disruption of self-assembly during handling (**63** hydrogels were softer than those prepared by **62**). The observed red shifts suggested the formation of J-aggregates, whereas their small value confirmed the development of insufficient aromatic-aromatic interactions (that is not face-to-face but rather edge-to-face stacking), such as

observed for CH-π stacking. Finally, gelation in water yielded larger shifts compared to PBS gels possibly due to the different microenvironment surrounding the chromophores *i.e.* different type of packing or different equilibrium of anomers resulting in different electronic effects.

Circular dichroism

The chirality of the formed hydrogels was explored by circular dichroism (CD) spectroscopy. A preliminary study by conventional CD was undertaken using benchtop instruments, the results of which are reported herein. These findings subsequently led to the development of a new methodology for an in-depth analysis of soft materials by synchrotron radiation (SR) CD spectroscopy, a discussion of which is presented in chapter 4.

The hydrogels were studied under a variety of conditions and all CD spectra were acquired using a Chirascan spectrophotometer. Extensive optimization trials of sample preparation and handling established that hydrogels were best formed in cells (*in situ*) to avoid any alteration of their supramolecular structure by handling, such as with the use of demountable cells. Therefore, several different cell types were initially tested such as demountable rectangular and non-demountable cylindrical with a variety of path lengths (Figure 3.8). In all cases, when gels were prepared in vials or a Petri dish and thereafter transferred (by pipette or spatula) into the cells, their supramolecular networks were broken, resulting in irreproducible CD spectra.

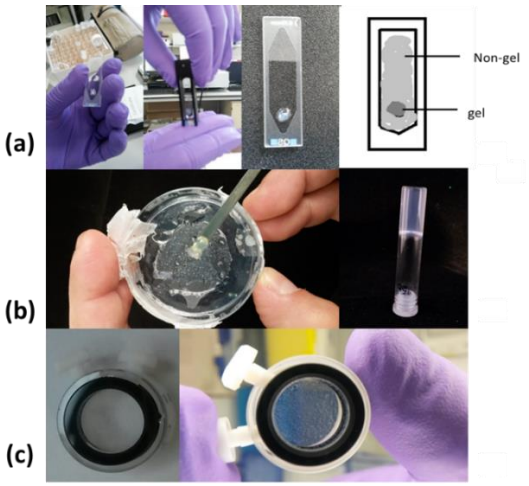

Figure 3.8 Different hydrogel preparation approaches for CD samples: (a) loading a demountable rectangular cell with samples from (b) a petri dish or a vial and (c) the *in situ* preparation within a non-demountable cylindrical cell. Gels were prepared based on the given protocols **A**, **B**, **C**, and **D**. The concentration of each hydrogelator is given at table 3.1.

For each sample, the absorbance had to be evaluated prior to acquisition of any CD spectrum. To avoid signal saturation, the CD spectrum was truncated where absorbance values were greater than 1.0 A.U. It was established that the intensity of an absorption spectrum was best regulated by changing the path length of the cell and not by diluting the samples. This was because dilution alters the original supramolecular architecture formed, especially if diluted below the MGC. For that reason, the MGC for each sample (Table 3.1) was used unless stated otherwise. All CD spectra were baseline corrected, averaged and truncated based on the corresponding absorbance profiles.

This preliminary study aimed to evaluate CD spectral features related to the self-assembly of the hydrogelators tested. To achieve this, different experimental approaches were developed, such as monitoring gel formation, comparing the CD profiles of different hydrogels, recording the CD spectra of hydrogelators as true solutions, thermally destroying the gels and evaluating their reformation.

Gelation of GalNHFmoc **62** was monitored following the controlled heating and cooling methodology (protocol **A**). CD and absorbance spectra were acquired at 50 °C, 65 °C and 85 °C (during heating) and then at 65 °C, 50 °C and 20 °C (cooling) (Figure 3.9).

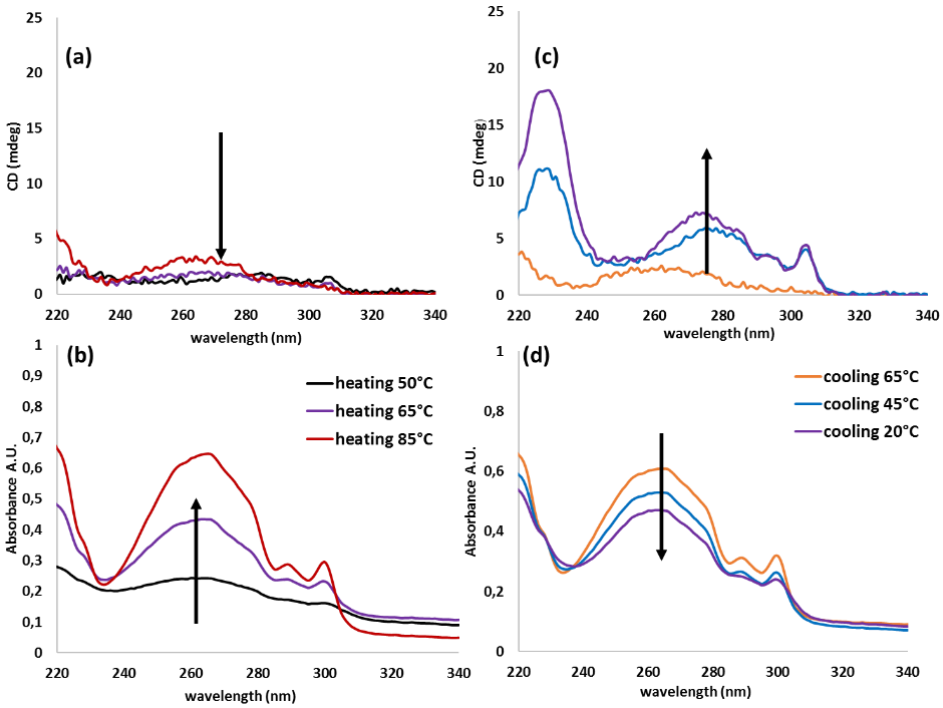

Figure 3.9 Monitoring gelation of GalNHFmoc **62** in water (2.0 mg/mL) using protocol **A** during the heating by (a) CD and (b) absorbance and during the cooling by (c) CD and (d) absorbance spectra. A rectangular demountable cell with a path length of 0.1 mm was used.

As the sol-gel process progressed, the absorbance intensity increased at higher temperatures (Figure 3.9-b) but decreased during the cooling cycle (Figure 3.9-d). In contrast, the corresponding CD spectra showed the reverse trend in intensity, where no signal was present at higher temperatures, suggesting that the sample was in the sol state (Figure 3.9-a). Well-defined peaks were observed on cooling, indicating the self-assembly of the gelator molecules and the formation of a gel (Figure 3.9-c). In general, the CD signal of a true solution of the hydrogelator is negligible compared to both the absorbance and the CD of the self-assembled hydrogelator (*i.e.* the gel). This is because the exciton coupling between the chromophores in the sol state is significantly weaker than that of the gel state.

Each hydrogel has a characteristic CD profile due to the chirality of the building blocks and the induced chirality of the formed supramolecular network. To assess any differences and/or similarities in the CD profiles of structurally related hydrogelators, the CD spectra of GalNHFmoc **62**, GlcNHFmoc **63** and GalNH-F-Fmoc **111** based hydrogels were recorded (Figure 3.10).

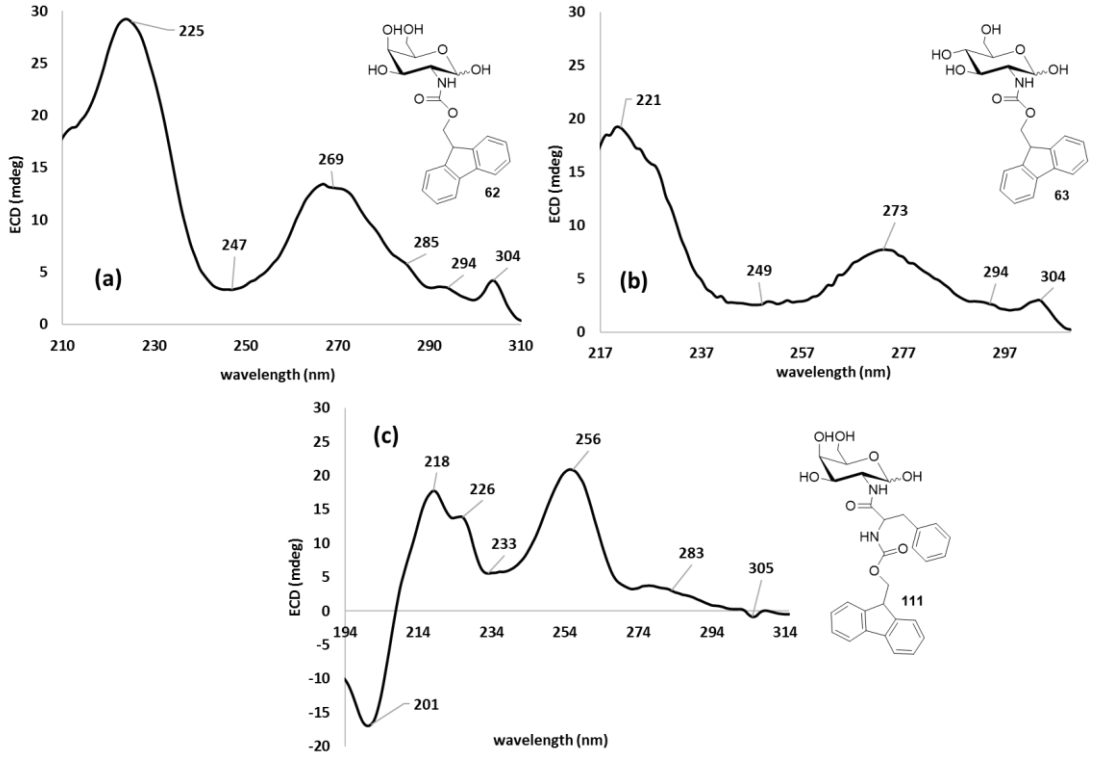

Figure 3.10 CD spectra of (a) GalNHFmoc **62** (PL 0.1 mm), (b) GlcNHFmoc **63** (PL 0.2 mm), (c) GalNH-F-Fmoc **111** (PL 0.5 mm). All compounds gelled in water within a cylindrical non-demountable cell, using the same concentration (2.0 mg/mL) and gelation protocol **A** (heating/cooling cycles).

Although the GalNHFmoc **62** hydrogel spectrum was slightly blue shifted compared to that of GlcNHFmoc **63**, both spectra appeared qualitatively and quantitatively similar to the published data.[8] The maxima at 304 and ~270 nm were attributed to the Fmoc moiety while that around 220 nm to the carbonyl group. The similar CD spectra (Figure 3.10-a and b), FT-IR spectra (Figure 3.3-a and b) and NMR spectra (Figure 3.4-i and ii) imply similar molecular packing for **62** and **63** hydrogelators. However, the lower CD intensity of the GlcNHFmoc **63** hydrogel suggests a lesser extent of organization and a softer material. That was also confirmed by the measured elastic moduli G′ values of the two samples (*vide infra*).

The CD spectrum of GalNH-F-Fmoc **111** hydrogel was different to that of the protected carbohydrates **62** and **63** gels due to the presence of the extra phenylalanine moiety. A significant blue shift was observed for the signal around 270 nm attributed to the Fmoc group. In addition, the peak centered at 305 nm was negative compared to the previous spectra. It is noted that the corresponding signal around 307 nm was also reported by Ulijn *et al.* and was attributed to the fluorenyl group.[27]

The same paper compared the CD spectra of Fmoc-F solution and Fmoc-F-F hydrogel. As reported by Ulijn *et al.* a shift of the positive peak at 305 nm present at the CD spectrum of Fmoc-F solution to a negative peak at the Fmoc-F-F hydrogel spectrum implied an opposite orientation of the fluorenyl group in the gel state compared to the solution. In addition, they suggested that the molecules were predominantly in a β-sheet conformation. This was also verified by FT-IR experiments with the presence of two distinct peaks at 1630 and 1685 cm^{-1}. Therefore, for the GalNH-F-Fmoc **111** hydrogel, the negative CD peak at 305 nm (Figure 3.10-c) and the two signals obtained by FT-IR at 1684 and 1641 cm^{-1} (Figure 3.3-c) suggest a potential β-sheet conformation of the molecules.

The lack of CD signal in solutions of the corresponding hydrogelators **62**, **63** and **111** (Figure 3.11) strongly suggested that observed CD intensity is a direct result of the handedness of the formed supramolecular networks.

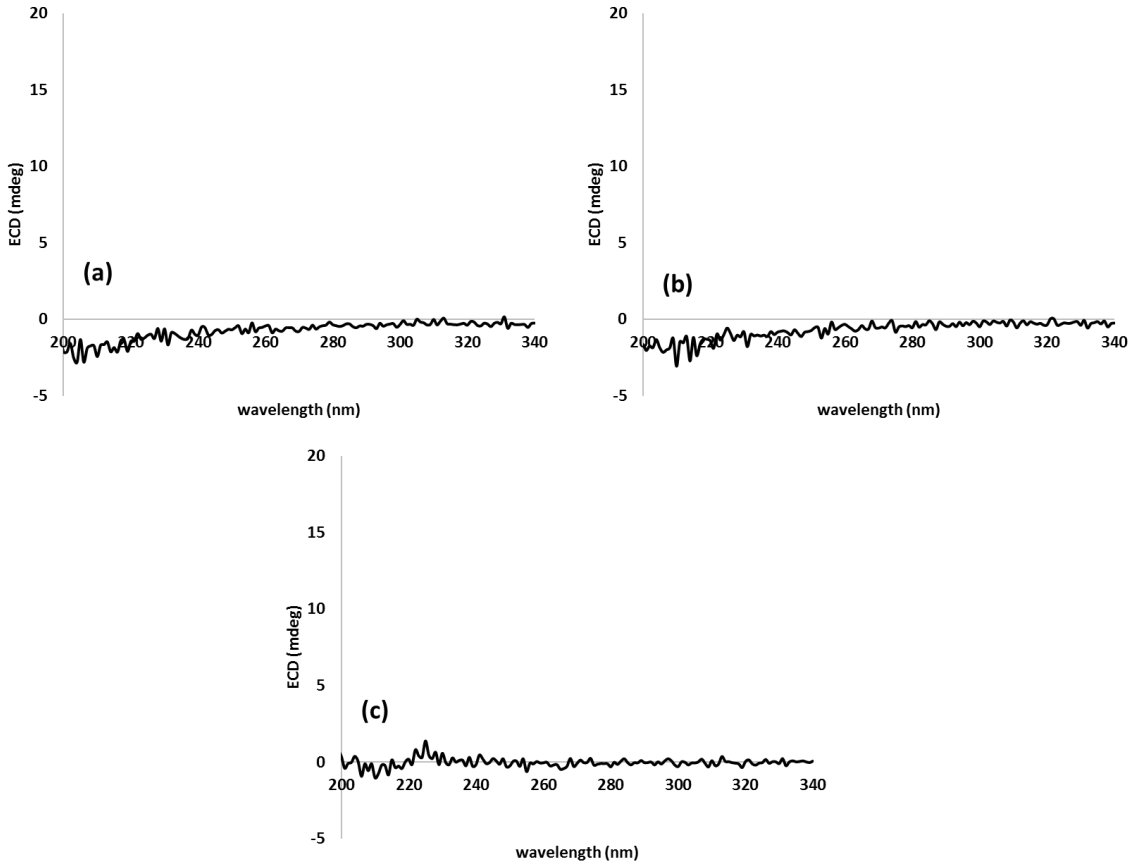

Figure 3.11 CD profiles of methanolic solutions (a) GalNHFmoc **62**, (b) GlcNHFmoc **63** and (c) GalNH-F-Fmoc **111**. All samples were recorded in a cylindrical non-demountable cell of the path length 0.1 mm at a concentration of 0.2 mg/mL at 25 °C.

Thermal studies were undertaken to assess the reversibility of the self-assembly process by thermally disrupting the formed hydrogels and then allowing gelation to recur. To achieve this, CD spectra were acquired before, during and after the heating of the gels.

The CD spectra and corresponding absorbance for the thermal study of the GalNHFmoc **62** hydrogel are depicted below (Figure 3.12). The CD spectrum of the initial gel was obtained and then the sample was heated at 85 °C for 30 minutes after which the CD signal disappeared, verifying a successful gel-sol transition. To evaluate the reformation of the gel, the sample was left at room temperature for at least 5 hours to cool and gelation to recur.

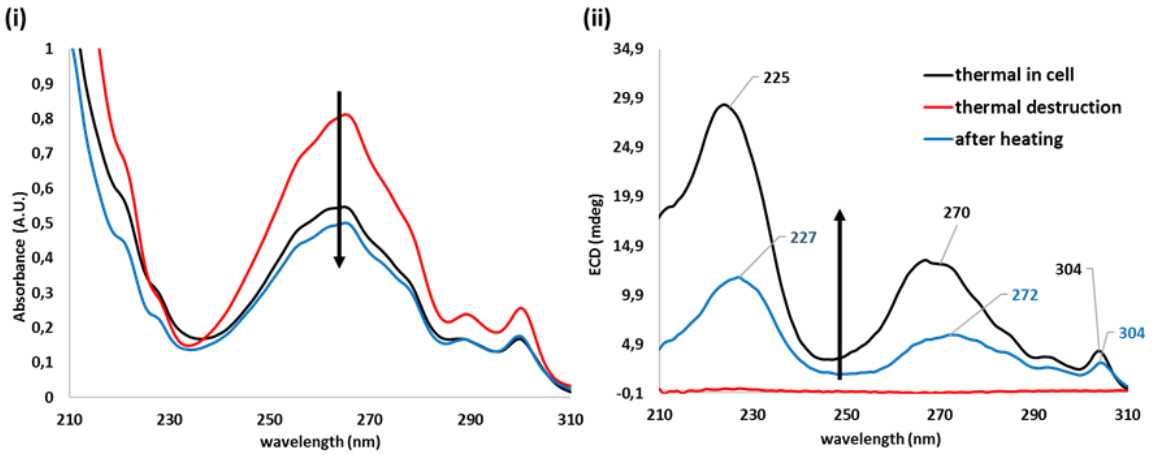

Figure 3.12 Thermal studies of GalNHFmoc **62** hydrogel. Absorbance (i) and CD (ii) spectra were recorded before, during and after heating of the gel (5 hours). The initial hydrogel was prepared following standard gelation protocol **A** (*sonication-controlled heating/cooling cycles*). Hydrogelator **62** gelled water *in situ* using a cylindrical non-demountable cell with a path length of 0.1 mm.

An increased CD signal and an analogous decrease in absorbance confirmed the reformation of the gel and the reversibility of the self-assembly process (gel-sol-gel). Indeed, the increased CD signal of the sample after heating, was due to the handedness of the ongoing formation of the supramolecular architecture during the cooling cycle. In general, the relative orientation of the hydrogelators transition moments allows the formed dipoles to acquire either a parallel or an antiparallel orientation in the gel state. This results in the initial energy of the individual molecules being split into new energetic states. In other words, gelator molecules with similar exciton energies, when in close spatial proximity, become excitons as their excited state is delocalized within the conjugated system (see section 4.2 of chapter 4). 5 hours after heating and as the gel was becoming stiffer (Figure 3.12-ii, blue CD spectrum) a small red shift in CD spectrum was observed, indicating low energy states of the gelator molecules. Also, the intensity of the CD spectrum was low compared to that of the unheated gel (Figure 3.12-ii, black CD spectrum). This was expected since the exciton coupling was still weak (ongoing transition from the sol to the gel state).

Thermal studies were also undertaken for the GalNH-F-Fmoc **111** hydrogel. The acquired CD spectra and the corresponding absorbance are featured below (Figure 3.13). The results were qualitatively similar to the GalNHFmoc **62** hydrogel, verifying the reversibility of the gel-sol-gel process.

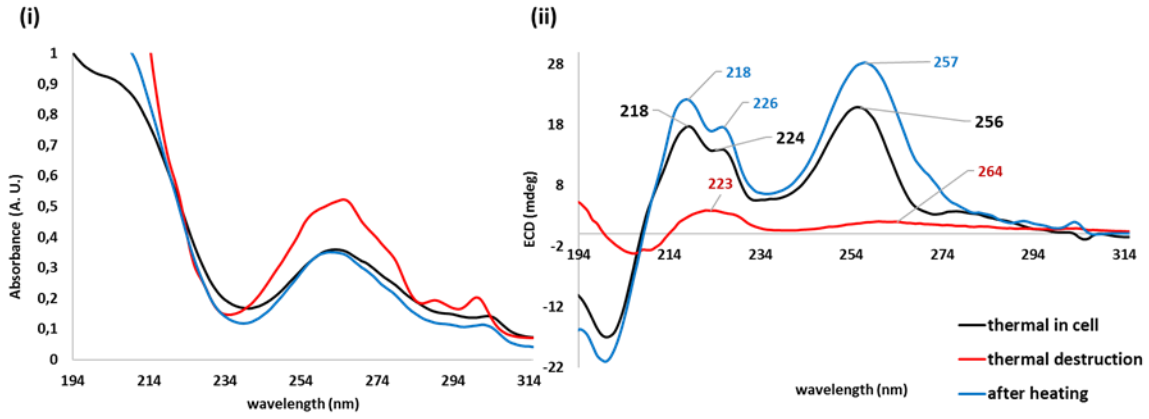

Figure 3.13 Thermal studies of GalNH-F-Fmoc **111** hydrogel. Absorbance (i) and CD (ii) spectra were recorded before, during and after heating of the gel (5 hours). The initial hydrogel was prepared following standard gelation protocol **A** (*sonication-controlled heating/cooling cycles*). Hydrogelator **111** gelled water *in situ* using a cylindrical non-demountable cell with a path length of 0.5 mm.

In this case, the self-assembly appeared to partly resist heating, since two weak broadened CD signals centered at 223 and 264 nm were observed at 85 °C. The same results were observed after extended heating. As mentioned previously, although the phase transition temperature of GalNH-F-Fmoc **111** was lower than 85 °C, heating caused the collapse of the gel, but a part of the supramolecular molecular organization was still present. Further to this, the CD intensity of the reformed gel was higher than that of the initial gel. A possible explanation would be that during the first heating cycle (protocol **A**) the cell might have not been adequately heated and the gelator molecules might have been partially solvated. A second heating cycle presumably triggered self-assembly to a greater extent, justifying the increased CD signal.

Rheology measurements

Sample preparation and handling proved fundamental for the evaluation of the viscoelastic properties of the formed hydrogels by rheology. From review of the literature, depending on the nature of the samples, supramolecular gels are either transferred[28,29] or prepared directly[9,11] on the lower geometry of the rheometer. The type of upper geometry depends on the size and volume of the tested sample, the type of experiment and conditions used, and the technical characteristics of the instrument. For the study of soft materials, either a parallel plate[30] or a cup and vane set up[31] is usually used.

Initial optimization was undertaken to prepare and transfer intact hydrogels onto the lower geometry of the instrument. Based on the applied gelation protocols, vials had to be used for

the sonication and heating process while the obtained solutions/suspensions had to be transferred into other vessels to gel. Unfortunately, the breakage of gels was inevitable whilst being transferred. This caused alterations of their supramolecular network leading to false viscoelastic data. This was also confirmed by the lack of reproducibility for measurements undertaken for the same type of gel.

To improve sample handling, gelation was therefore performed in inserts of cell cultivation plates (Nunc, polycarbonate cell culture inserts with 0.4-micron pore size in 6-well plate) (Figure 3.14). A semi permeable membrane at the bottom of the insert was peeled away and the gel was removed almost intact. That meant that the inserts could not be reused and, as each measurement had to be in triplicate, the cost of this approach was deemed too high. Furthermore, the upper surface of the gel was not smooth and did not attach properly to the upper geometry (parallel plate of 20 mm diameter) and the volume of the bulk material was not high enough to fill the space between the lower and upper geometries. A meniscus was observed on the top of the gel when in contact to the upper geometry. The bulk material needs to fill the space between the lower and upper geometries.

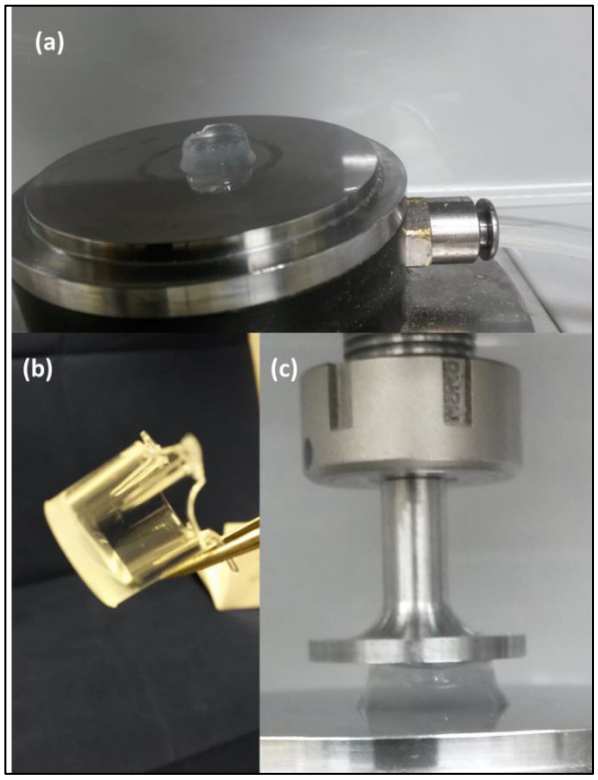

Figure 3.14 Sample preparation approach using an insert and gel transfer for rheology of hydrogels. The gel sample transferred on the (a) lower geometry from (b) an insert. (c) A meniscus was observed on the top of the gel when in contact to the upper geometry.

Another attempt to generate intact gels and transfer them successfully onto the rheometer involved the use of glass chamber slides (Nunc™ Lab-Tek™ II Chamber Slide™ System, ThermoFischer Sciendific, UK) (Figure 3.15-a). Although stiff hydrogels, such as the gel from GalNHFmoc **62**, yielded a self-supporting block of gel (Figure 3.15-b and c), this was not the case for softer materials, such as the gel from GlcNHFmoc **63** (Figure 3.15-d). Finally, even for the stiffer materials, extraction of water during transfer was inevitable (Figure 3.15-e).

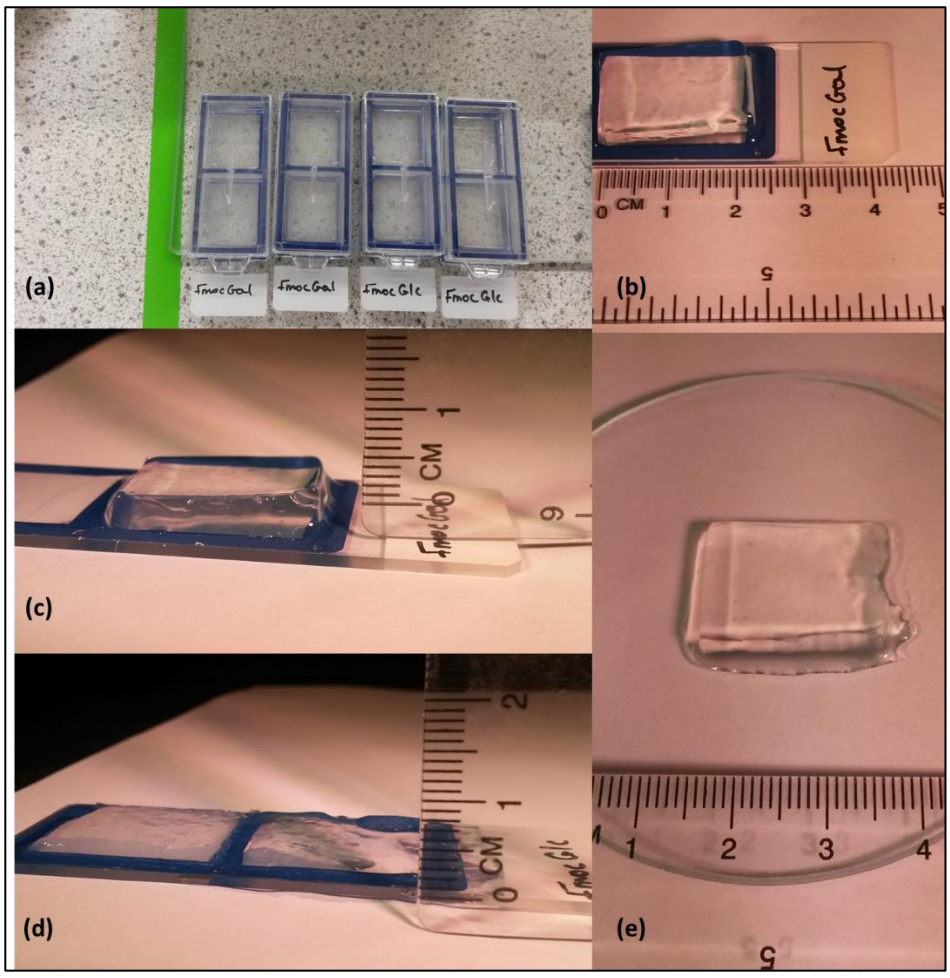

Figure 3.15 Sample preparation approach using a glass chamber slide and gel transfer for rheology of hydrogels. Gel formation in glass chamber slides for GalNHFmoc **62** hydrogel (a, b, c and e) and GlcNHFmoc **63** hydrogel (a and d).

The final approach involved the preparation of samples in glass vials which were then fixed directly onto the lower geometry of the instrument and screwed until secure (Figure 3.16). The upper geometry was then inserted into the bulk material, while its height was adjusted

accordingly as to be completely covered by the gel. Prior to any measurements, a waiting time of 30 minutes was used to allow samples to settle.

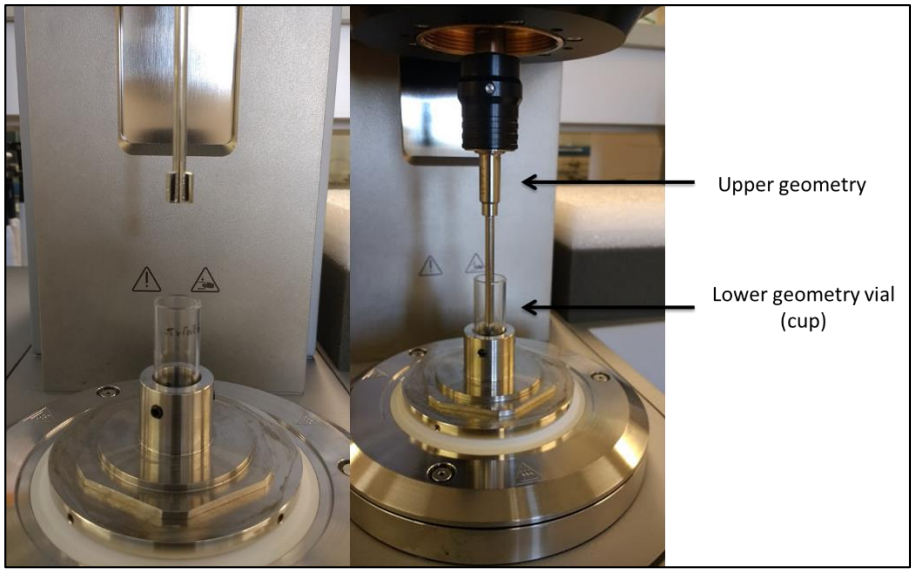

Figure 3.16 Sample preparation approach using a glass vial without transfer for rheology of hydrogels. Gels prepared in vials and tested using an Anton Paar MRC 302 modular compact rheometer with an upper geometry cylinder.

Of the above experimental attempts, the latter was used to assess the viscoelastic properties of the formed hydrogels. Indeed, *in situ* preparation of gel specimens using glass vials allowed rheology studies to be performed with minimum handling of the tested samples. Therefore, all three hydrogelators **62**, **63** and **111** were used to form their respective gels in glass vials, using PBS solution and following gelation protocol **C** (*sonication-heating*). For gelators **62** and **111**, a concentration of 2.0 mg/mL was used, whilst a concentration of 3.0 mg/mL was used for **63**. The linear viscoelastic region of each material was first determined by performing oscillatory amplitude sweep experiments at a fixed frequency of 1 rad/s. The linear viscoelastic region, where the storage modulus (G′) and loss modulus (G″) are independent of the strain amplitude, corresponded to 0.05% shear strain (γ%) for the GalNHFmoc **62** hydrogel, 0.99% for the GlcNHFmoc **63** and 0.03% for the GalNH-F-Fmoc **111** samples (Figure 3.17).

According to Figure 3.18 (iii) the obtained data for **111** hydrogel, show significant differences in the error bars. That could be possibly attributed to bubbles of air trapped within the hydrogel during its preparation. Additionally, the G″ curve of Figure 3.17 (iii) did not appear linear either.

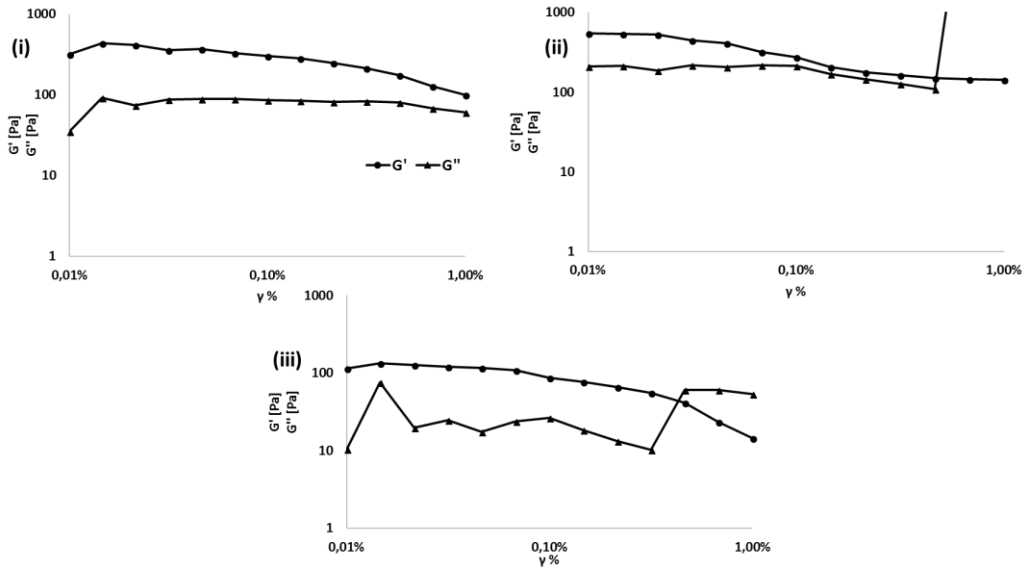

Figure 3.17 Amplitude sweep experiments at a fixed frequency of 1 Hz. Evaluation of the linear viscoelastic region of the hydrogels of (i) GalNHFmoc **62**, (ii) GlcNHFmoc **63** and (iii) GalNH-F-Fmoc **111**. All measurements were taken at a temperature of 25 °C.

Having measured the shear strain γ%, frequency sweep experiments were undertaken within the linear viscoelastic region for each material. All measurements were performed in triplicate to acquire the storage G′ and loss G″ moduli (Figure 3.18).

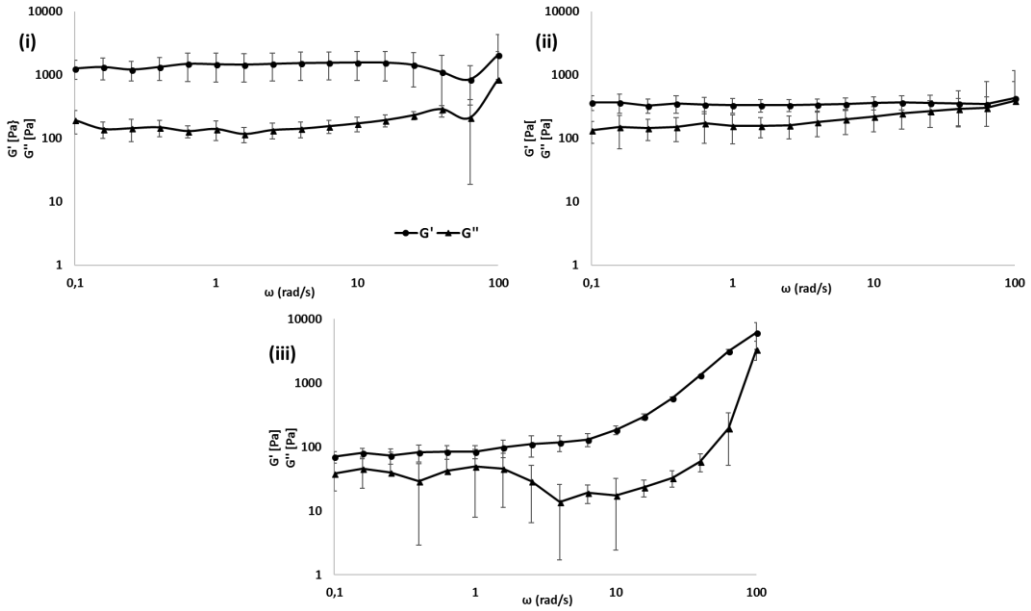

Figure 3.18 Frequency sweep experiments for the hydrogels of (i) GalNHFmoc **62** (ii) GlcNHFmoc **63** and (iii) GalNH-F-Fmoc **111** were performed from 0.1 rad/s to 100 rad/s under a 0.05% strain for **62**, 0.99% for **63** and 0.03% for **111**. All measurements were taken at a temperature of 25 °C.

For all tested samples the storage G′ modulus had a greater value compared to loss G″ modulus, confirming the viscoelastic nature of the materials (gel state). The point at which the G′ and G″ curves intersect (implies gel-sol transition and describes elasticity) is defined as the strain value in the amplitude sweep curves and was (γ%) 0.68% for the GlcNHFmoc **63** sample, (γ%) 0.46% for the GalNH-F-Fmoc **111**; no crossover point was observed for the GalNHFmoc **62** hydrogel. Therefore, based on the obtained γ% values, GalNHFmoc **62** was shown to be the most elastic material, followed by GlcNHFmoc **63** and then GalNH-F-Fmoc **111** (Figure 3.17). Finally, in terms of stiffness, GalNHFmoc **62** gel was stiffest (G′ ~1587 Pa) followed by GlcNHFmoc **63** (G′ ~341 Pa) and GalNH-F-Fmoc **111** (G′ ~85 Pa) (Figure 3.19).

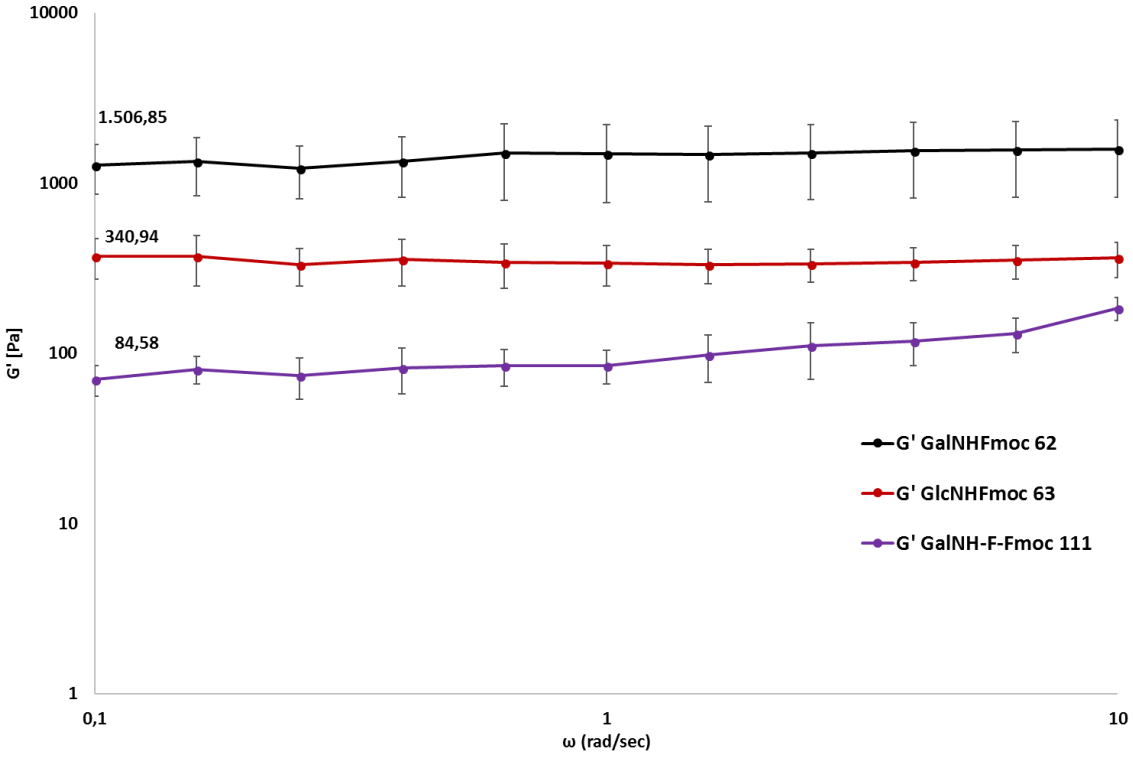

Figure 3.19 G′ curves and values for GalNHFmoc **62** (**black**), GlcNHFmoc **63** (**red**) and GalNH-F-Fmoc **111** (**purple**) hydrogels.

Summary

The Fmoc set of materials have been partially characterized previously[14] and only the additional data are reported herein. GalNHFmoc **62** was used as the model gelator for the optimization work regarding the preparation and handling of the gel specimens. In all cases, it was attempted to keep the supramolecular structures intact and to avoid potential

alterations of the self-assembly by handling of the samples as this would result in misleading and irreproducible data.

Since GlcNH-F-Fmoc **112** failed to yield a self-supporting hydrogel no characterization work was undertaken of the partial gel. Further to this, small changes of the structural features of the hydrogelators resulted in materials with different properties. Indeed, the epimers GalNHFmoc **62** and GlcNHFmoc **63** exemplify this. Although differing only at one stereogenic center at the C4 position, **62** yielded a stiff self-supporting hydrogel whereas that of **63** was softer. This was confirmed by the obtained storage moduli G′ values, the differences in $T_{gel\text{-}sol}$ and the intensity of their corresponding CD spectra. **62** and **63** showed a similar but no identical mode and extent of self-assembly since the obtained CD, FT-IR and fluorescence spectra although appeared qualitatively similar for both hydrogels had clear differences.

In contrast to GlcNH-F-Fmoc **112,** the epimer GalNH-F-Fmoc **111** yielded a self-supporting hydrogel. As the storage moduli values indicated, addition of the phenylalanine moiety resulted in a softer gel compared to the Fmoc-protected carbohydrate gels of **62** and **63**. The amino acid moiety was also responsible for the different CD, FT-IR and fluorescence profiles. These, compared to the published data for the structurally related Fmoc-F-F hydrogel,[27] suggested that **111** might adopt a similar β-sheet conformation in the gel state.

3.3.2 Characterization of the indomethacin, diclofenac and biotin-based hydrogels

Indomethacin and diclofenac based hydrogels

Previous characterization studies for this set of hydrogelators showed that gelation was induced by a heating and rapid cooling method.[14] Specifically, gelators **113**, **114**, **115** and **116** were suspended in water and sonicated (no gels were formed in PBS). The obtained suspensions and/or solutions (0.3% wt.%) were then heated at 95 °C for an hour and placed thereafter in dry ice for 10 seconds. After resting at room temperature for 20 minutes, gelation was confirmed by visually inspecting the inverted vials.

The above method failed to give reproducible results. Indeed, repeated trials for a single compound did not induce gelation to the same extent, randomly yielding either self-supporting hydrogels or viscous free-flowing solutions. This was presumably due to the lack of any precise control in the cooling process. The rapid cooling procedure possibly led the

gelator molecules to adapt variable intermediate and metastable thermodynamic states, causing different extents and/or modes of self-assembly.

To achieve reproducibility, several gelation protocols were tested; only protocol **D** (*sonication-heating-sonication*) succeeded in yielding self-supporting hydrogels for three of the four compounds. A description of the formed materials after visual inspection is summarized below (Table 3.5).

Table 3.6 Visual inspection of the formed hydrogels in water. All gel specimens were prepared following protocol **D**. The concentration was 3.0 mg/ mL for all hydrogelators.

Gelator	**Visual evaluation**
GalNH-Diclofenac **113**	White viscous suspension
GlcNH-Diclofenac **114**	Self-supporting white opaque gel
GalNH-Indomethacin **115**	Self-supporting white opaque gel
GlcNH-Indomethacin **116**	Self-supporting white opaque gel

From the findings, only GalNH-Diclofenac **113** failed to yield a gel, while the rest of the tested compounds provided self-supporting hydrogels. Gelation was tested only in water due to shortage of materials and time constraints. For that reason, no further characterization studies of the materials were undertaken except that of a preliminary biocompatibility evaluation, as described in chapter 5.

Biotin based hydrogels

According to previous gelation experiments,[14] the epimeric pair of GalNH-Biotin **66** and GlcNH-Biotin **67** yielded self-supporting gels in water and PBS solution at concentrations of 0.40, 0.80 and 1.40% wt.%. Gelation was successful when protocols **A** (*sonication-controlled heating/cooling cycles*), **B** (*sonication only*) and the heating-rapid cooling method were employed.

Lack of materials resulted in the new synthesis of **66** and **67**. However, gelation experiments of the obtained compounds, under the same conditions as employed previously, failed to yield self-supporting gels (a precipitate was formed in all cases). In fact, as described in

chapter 2 (section 2.2.2, Figures 2.5 and 2.6) compounds **66** and **67** obtained from the second synthetic batch were purer to those previously synthesized. Additionally, further trials to optimize their synthesis showed that there was no reproducibility regarding the anomeric ratio obtained, since a different number of washings was required in each trial. Therefore, the purity of **66** and **67** and differences in the anomeric ratio affected directly their gelation behavior. Since no hydrogels were obtained, both biotinylated derivatives were characterized as non-gelators.

3.3.3 Characterization of the diphenylalanine-based hydrogels

For almost two decades, peptide amphiphiles have been extensively used for the preparation of novel materials with tunable characteristics and a wide range of applications.[13,32–34] In particular, aromatic peptide amphiphiles have attracted much attention as they combine the simplicity of small molecules,[16] the enormous sequence space of the 20 amino acids[35] and the versatility of aromatic structures.[30,36-37]

Of this set of hydrogelators, Fmoc-F-F **68** is one of the most well studied aromatic peptide amphiphiles.[37,27] To explore how different gelation triggers affect molecular packing, **68** was used as a gelator model. Ulijn *et al.* reported that **68** gelled water following a sequential pH change.[37] A complete characterization study of the obtained hydrogel revealed that self-assembly was driven by a combination of H-bonds and π-π interactions between the fluorenyl groups. This resulted in supramolecular helical assemblies and a *β*-sheet structure of the molecular packing.[37,27]

The cinnamoyl-protected diphenylalanine analogue Cin-F-F **70** was prepared to explore how a different aromatic moiety would affect gelation in comparison to **68**. However, for the synthesis of **70**, two different synthetic routes were followed. The first led to an inseparable mixture of the epimers **70** and **93** in a reproducible 2:1 ratio (Cin-L-F-L-F: Cin-D-F-L-F), while the second synthetic route successfully yielded the pure epimer **70** (section 2.2.3). Further to this, it was decided to proceed with gelation trials of the epimeric mixture **70-93** to assess potential stereochemical effects on the gelation process.

This subsection therefore focuses on three key aspects regarding the self-assembly of aromatic peptide amphiphiles. The effects of (i) different gelation triggers, (ii) structural differences and (iii) stereochemical differences on molecular packing.

Gelation tests

In contrast to the published methodology,[27,37] the gelation ability of Fmoc-F-F **68** was tested in both purified water and PBS solution following protocols **A** (*sonication-controlled heating/cooling cycles*), **B** (*sonication only*), **C** (*sonication/heating*) and **D** (*sonication-heating-sonication*). Protocol **B** (*sonication only*) yielded a self-supporting, semi-transparent hydrogel in PBS solution for gelator **68** whereas all other conditions gave a precipitate (Table 3.6). The final concentration of hydrogelator **68** was 3.7 mM (2.0 mg/mL of **68** in 1.0 mL of PBS solution) or 0.2 wt.%, which is in the range of given concentrations that yielded self-supporting gels according to published data.[37] It is of note that the initial milky suspension became more transparent over time.[27] Gelation success by the vial inversion method was verified after 12 hours of rest at room temperature. Furthermore, extended sonication (over 1 minute) failed to aid gelation of the dipeptide **68** by protocols **A**, **C** and **D**.

Gelation trials, under the same conditions as above were also undertaken for Cin-F-F **70**. A self-supporting, semi-transparent hydrogel was formed in PBS solution following protocol **D** (*sonication-heating-sonication*) whereas a precipitate formed in water (Table 3.6). Interestingly, heating alone was not adequate to generate a gel, although the gelator was completely solubilized. In fact, protocol **C** (*sonication/heating*) produced a viscous, transparent free flowing solution that gelled only after sonication. Further tests showed that storage of this "pre-gel solution" (*i.e.* after sonication-heating) in the fridge (4 °C) and/or room temperature for 24 hours did not result in gelation. Only after the sample was again sonicated did it form a self-supporting hydrogel. The minimum gelation concentration of hydrogelator **70** was 3.4 mM (1.5 mg/mL in PBS solution) or 1.5% wt.%. However, to characterize the hydrogel of **70**, a concentration of 2.0 mg/mL (4.5 mM or 0.2% wt. %) was used since the prepared samples appeared stiffer and more stable.

Gelation trials of the enantiomeric mixture **70-93** resulted in a hydrogel in PBS solution under identical conditions (protocol **D**) to those used for **70** (Table 3.6). Interestingly, a similar "pre-gel" solution was also obtained when protocol **C** was followed. Other protocols (**A**, **B**,) didn't result in gelation of the epimeric mixture.

Table 3.7 Gelation tests of the hydrogelators Cin-F-F **70**, the epimeric mixture Cin-D/L-F-L-F **70-93** and Fmoc-F-F **68**. G: self-supporting hydrogel; P: precipitate. The concentration was 2.0 mg/ mL for all trials.

gelator	Gelation protocol	PBS solution	Water
Cin-F-F **70**	**D**	**G**	P
	C	P	P
	B	P	P
Cin-D/L-F-L-F **70-93**	**D**	**G**	P
	C	P	P
	B	P	P
Fmoc-F-F **68**	**D**	P	P
	C	P	P
	B	**G**	P

Polymorphism

During the synthesis and purification of the cinnamoyl derivative **70** it was observed that different reaction batches yielded products that differed in colour and texture (fine powders or glassy solids). The same outcome was observed for the epimeric mixture **70-93**. These findings may be attributed to polymorphism, this is typically defined as the ability of a solid to exist in more than one crystal structure form. Polymorphs are common in pharmacopoeia and have a direct impact on the functionality of the synthesized pharmacophores.[38,39] In the case of Cin-F-F **70**, a variety of possible conformational modes (conformational polymorphism) in the solid state or different packing arrangements (packing polymorphism) could lead to polymorphism. The presence of impurities and the inclusion of solvent molecules within the formed solids (solvatomorphs) could also yield different polymorphs.

Further to this, during the final synthetic step, Cin-F-F **70** was obtained as a thick oil that was then dissolved in dichloromethane. The solution was then evaporated and dried under vacuum leading to the formation of a glassy solid or a fine powder. Since no solvent or other

impurity peaks were present in the ^{1}H and ^{13}C NMR spectra, it was assumed that different conformational modes led to conformational polymorphs. In addition, for the epimeric mixture **70-93**, any small variations in the ratio of the two epimers within the mixture (possibly difficult to observe by ^{1}H NMR spectroscopy) could also explain differences of the formed solids.

To assess if polymorphism was present, XRD diffractograms were acquired of the obtained hydrogelators (Figure 3.20). Two synthetic bathes yielded Cin-F-F **70** as a fine powder (**70-batch 1**) and as a glassy solid (**70-batch 2**). Similarly, the epimeric mixture **70-93** was obtained by two synthetic batches as a powder (**70/93-batch 1**) and glassy solid (**70/93-batch 2**).

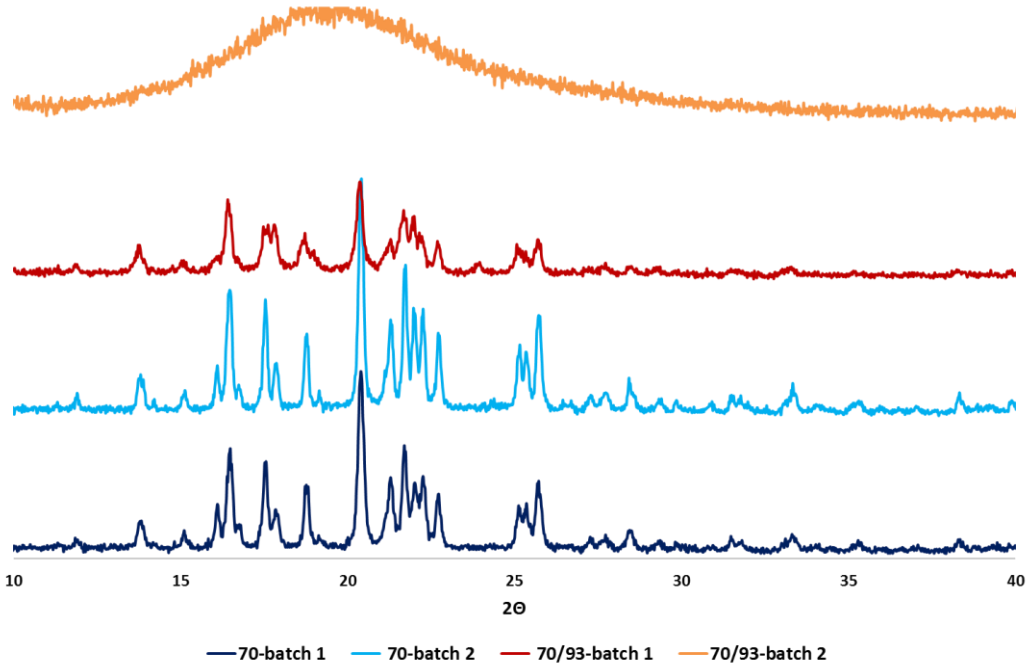

Figure 3.20 XRD diffractograms obtained from the enantiomeric mixture **70-93** (top-orange, red) and the pure enantiomer **70** (bottom-light and dark blue).

The obtained XRD diffractograms of batch 1 for the epimeric mixture showed an amorphous material (orange XRD) while batch-2 showed a crystalline solid (red XRD), confirming the presence of polymorphism. In contrast to the epimeric mixture, no polymorphs were detected for Cin-F-F **70** since the two batches showed identical diffractograms (light and dark blue XRDs). The decreased intensity of the red plot (compared to the two blue plots) is consistent with it being a mixture.

Using the above hydrogelators obtained from different reaction batches, the corresponding two xerogels of Cin-F-F (**70-xerogel 1** and **70-xerogel 2**) and those of the epimeric mixture (**70/93-xerogel 1** and **70/93-xerogel 2**) were prepared and XRD diffractograms were obtained (Figure 3.21).

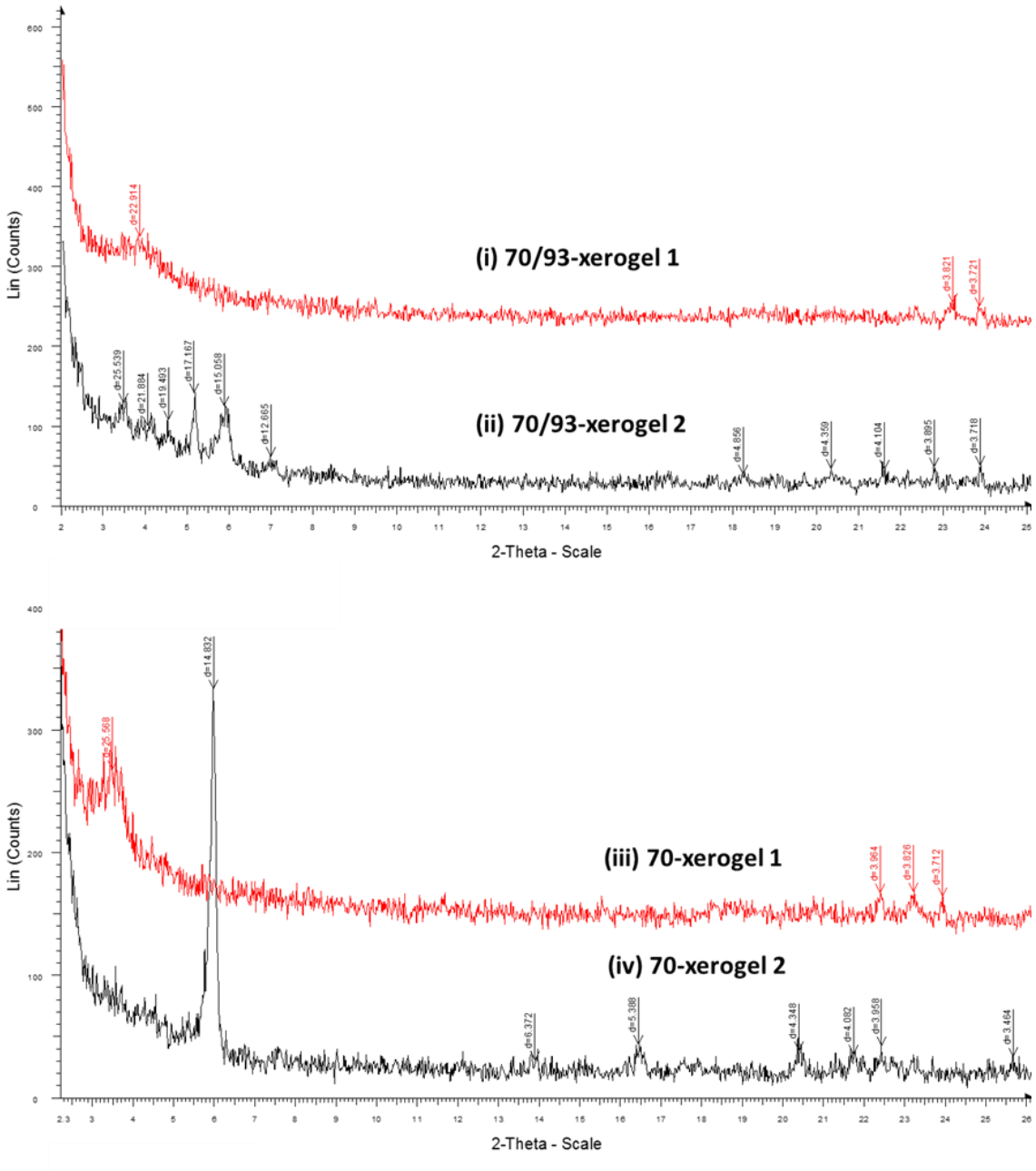

Figure 3.21 XRD diffractograms of the xerogels obtained from the epimeric mixture **70-93** (top) and the pure isomer **70** (bottom). Each color represents a different reaction batch. The hydrogelators used to form the xerogels were obtained from the synthesis as a fine powder (i and iii) and glassy solids (ii and iv).

The red diffractograms differ from black in top/bottom pairs. Further to this, the signal to noise ratio is high for both red plots. During the sublimation of water for the preparation of xerogels (lyophilization procedure via freeze drying) the gelator molecules may have adopted different conformations which led to different polymorphs. This could explain the differences in diffractograms obtained from the xerogels. Alternatively, it is more likely that conformational changes didn't occur during lyophilization of the hydrogels but rather a partial collapse of the larger self-assembled structure by the effect of removal of water. It is of note that during the gelation process though *i.e*. before the xerogels formed, the hydrogelators were completely soluble therefore polymorphism was irrelevant. In fact, the corresponding hydrogels did not show any differences when using other characterization techniques, such as CD spectroscopy and TEM microscopy (*vide infra*). This would suggest that, in the hydrated gel state, there was little or no effect on the macroscopic molecular-self-assembly, *i.e.* the hydrogel produced was not affected by polymorphism. Indeed, gelation trials were reproducible when gelators **70** and **70-93** from different reaction batches were used.

Since gelation was induced by heating of the samples at 95 °C, which dissolved the gelator molecules into true solutions (protocol **D**, *sonication-heating-sonication*), the obtained gels from gelators **70** and **70-93** (obtained from different reaction batches) were found to be identical based on the CD, FT-IR, $T_{gel\text{-}sol}$, rheology and microscopy data (*vide infra*). Presumably, different gelation triggers, such as changing the pH values or solvent exchange, could lead to materials with different properties. Similar results might be also observed for organogels. That needs to be further investigated, as polymorphism could affect solubility and hence the self-assembly, resulting in different hydrogels. Indeed, different polymorphs have different solubility but once they have dissolved, *i.e*. a true solution has been obtained, the fact of polymorphism becomes irrelevant.

Circular dichroism studies

To explore the self-assembly of Cin-F-F **70** gel and of the "pre-gel" solution, their CD spectra were compared (Figure 3.22). As anticipated, the decreased CD intensity of the "pre-gel" solution suggests a lesser extent of self-assembly relative to the gel. The observed blue shift of the CD spectral features of the gel compared to the "pre-gel" solution was presumably due to the greater exciton coupling due to closer proximity of chromophores in the assembly which has higher extent of ordering. The spectral profiles are markedly

different suggesting a difference in the packing of the dipeptide unit (as indicated in the far UV, *i.e.* below 260 nm). It is clear that the aromatic component contributes significantly to the far UV (since it is far away from baseline at 260 nm). However, is clear that the "pre-gel" solution does not equal the solution spectrum *i.e.* has some assembly but that assembly (type and/or extent of assembly) differs to that of the gel. Indeed, a tighter molecular packing leads the electronic and magnetic transition moments of the building blocks to higher energetic states (smaller wavelength values-blue shift).

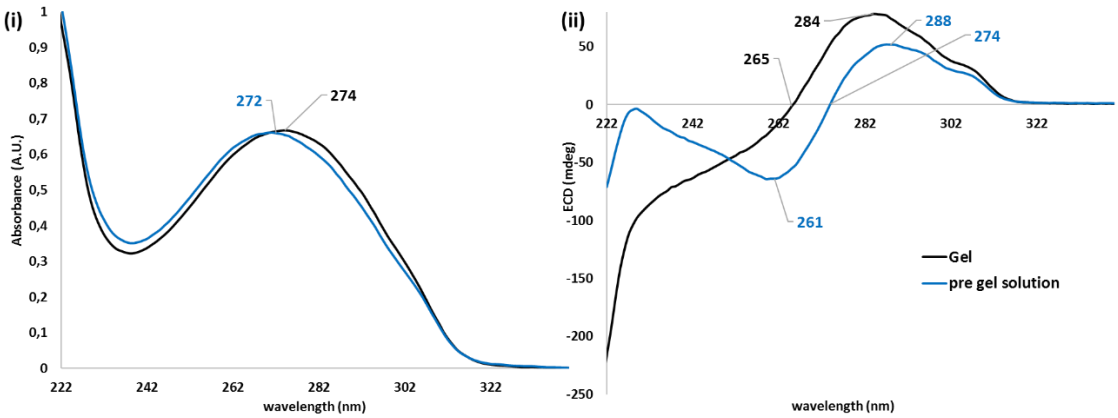

Figure 3.22 The absorbance (i) and CD spectra (ii) of the hydrogel and the "pre-gel" solution. A cylindrical non-demountable cell with a path length of 0.1 mm was used and the concentration was 2.0 mg/mL for both samples. Spectra were acquired at 25 °C.

The self-assembly of Cin-F-F **70** and epimeric mixture **70-93** was also evaluated by CD spectroscopy and compared with that of Fmoc-F-F **68** (Figure 3.23). The CD profile of **68** gel was qualitatively similar to that previously reported by Ulijn *et al.*,[27] suggesting a similar self-assembly of the supramolecular matrix, where the negative peak around 248 nm was consistent with a *β*-sheet structure for the molecular assembly, as verified by FT-IR and *in silico* studies.[27,37] The negative maxima at 243 nm for Cin-F-F **70** gel may also be attributed to a similar conformation as that of gel of Fmoc-F-F **68**. The absence of peaks at 308 and 298 nm was expected due to the absence of the Fmoc moiety, which is clearly evident from the absorbance spectra. Interestingly, the almost featureless CD spectrum of Cin-D/L-F-F gel **70-93** can be directly attributed to cancelation effects although (i) **70-93** is an epimeric and not an enantiomeric mixture and (ii) **70** and **93** were not in equal amount but in a 2:1 ratio. Further to this, TEM micrographs of Cin-F-F **70** and Cin-D/L-F-F **70-93** gels showed rather different than mirror-image related supramolecular structures (see below). Comparing their absorbance (Figure 3.23-ii) with that of their corresponding solutions (Figure 3.24-iv), a blue

shift is observed for Cin-F-F **70** in the gel state (278→254 nm) while a red shift for **70-93** mixture (278→280). This suggests the formation of H-aggregates for **70** and J-aggregates for the epimeric mixture **70-93** in the gel state.

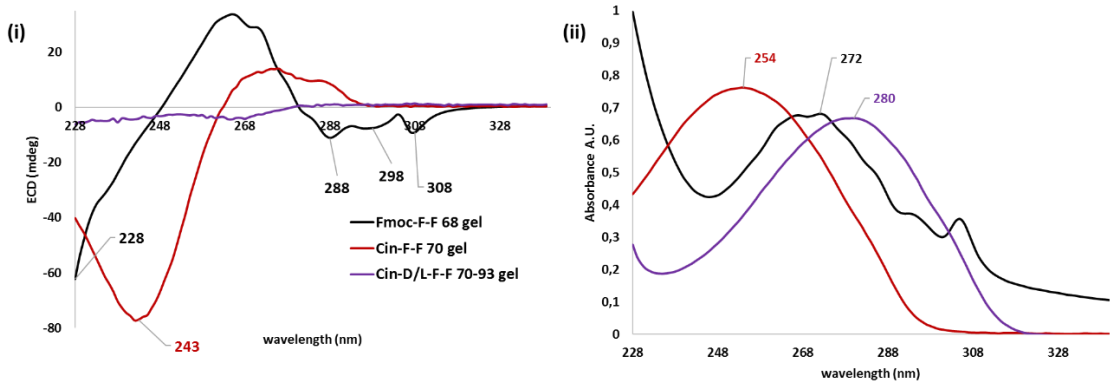

Figure 3.23 CD (i) and absorbance (ii) spectra of the **68**, **70** and **70-93** gels. A cylindrical non-demountable cell with a pathlength of 0.1 mm was used and the concentration was 2.0 mg/mL for all samples. Spectra were acquired at 25 °C.

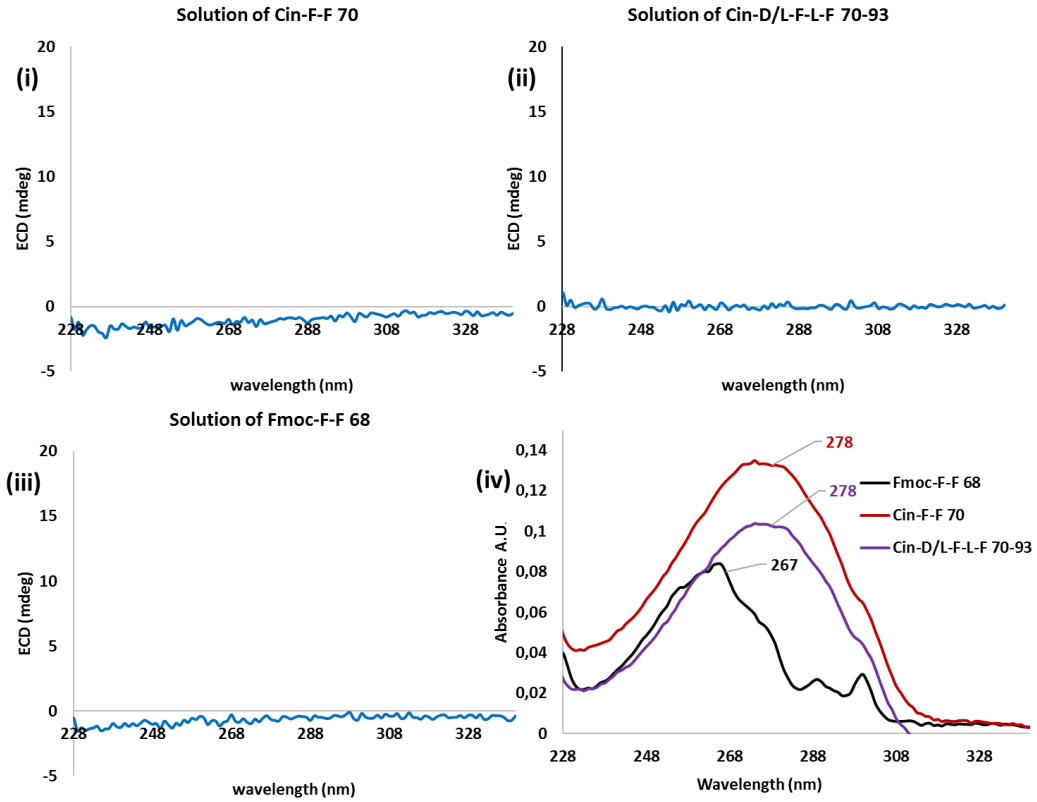

Figure 3.24 CD spectra of the methanolic solutions of Cin-F-F **70** (i), Cin-D/L-F-L-F **70-93** (ii) and Fmoc-F-F **70** (iii) and the corresponding absorbance (iv). A cylindrical non-demountable cell with a

path length of 0.1 mm was used. The concentration was 0.2 mg/mL in methanol for all samples. All measurements were performed at 25 °C.

For the gel samples of **68**, **70** and **70-93**, the observed CD signals originates from the self-assembly process, since in true solution they lack any CD signal (Figure 3.24). This was further exemplified by the differences observed between the gel and "pre-gel" solution of **70**.

To assess the reversibility of the self-assembly process, thermal studies of Fmoc-F-F **68** hydrogel and that of Cin-F-F **70** were undertaken. The initial hydrogels were formed *in situ* as described above, then heated at 85 °C for 30 minutes before resting at room temperature for at least for 5 hours to allow gelation to recur. CD spectra were acquired before, during and after heating of the gels (Figure 3.25).

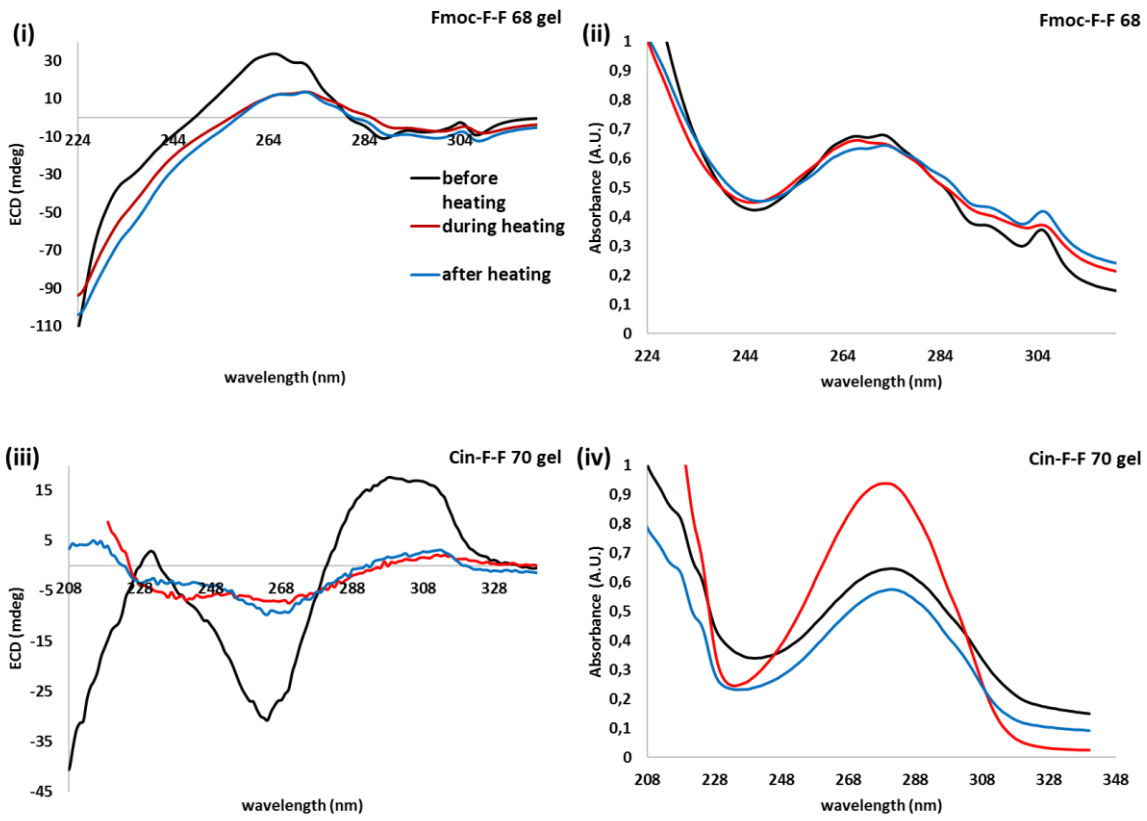

Figure 3.25 Thermal studies by circular dichroism of hydrogels **68** and **70**. (i) CD and (ii) absorbance of hydrogel **68**. (iii) CD and (iv) absorbance of hydrogel **70**. A cylindrical non-demountable cell with a path length of 0.1 mm was used. The concentration was 2.0 mg/ mL for all samples.

The CD intensity of Fmoc-F-F **68** hydrogel was decreased during heating due to the disruption of self-assembly. A doubled positive maximum centred around 270 nm suggested

that, although to a lesser extent, self-assembly was still present after heating. In addition, no major differences were observed in absorbance intensity, which indicates that the hydrogelator did not have altered concentration *i.e.* increased solubility or precipitate from solution. This is consistent with the self-assembly being retained albeit in an altered form. The results for Cin-F-F **70** gel showed a significant decrease in CD intensity during and after heating, that could only suggest the disruption of self-assembly. Further to this the absorbance intensity increased significantly during heating as expected. From the findings, it was clear that the Fmoc-F-F **68** hydrogel had a much higher degree of thermal resistance than that of Cin-F-F **70** which was destroyed by heating and was not able to reform a gel with the cylindrical cell.

Phase transition temperature ($T_{gel\text{-}sol}$) measurements

Measurements of the phase transition temperature ($T_{sol\text{-}gel}$) showed that Fmoc-F-F **68** gel was no longer self-supporting between 75-80 °C, while the $T_{sol\text{-}gel}$ of Cin-F-F **70** hydrogel was between 45-50 °C. The results indicated that replacement of the Fmoc moiety with the cinnamoyl group formed weaker hydrogels, since less energy was required to cleave the self-assembled molecules. These results were consistent with the thermal studies performed by CD. The nature of Cin-F-F **70** gel was also confirmed to be soft and dynamic by the obtained values of the storage modulus G′ (see below). It is of note that the contribution of π-π interactions in the self-assembly were far lower for **70** than for **68**. $T_{sol\text{-}gel}$ was not measured for the Cin-D/L-F-F **70-93** hydrogel (epimeric mixture).

Stability tests

Stability tests of Fmoc-F-F **68** and Cin-F-F **70** hydrogels were undertaken under a range of different conditions (Figure 3.26) to assess potential use for culture application. In addition, Fmoc-F-F **68** hydrogel was not tested due to lack of material. Hydrogels Cin-F-F **70** and Cin-D/L-F-F **70-93** were prepared in triplicate following protocol **D**. To assess their stability, 1.0 mL of either water, PBS solution, cell culture medium (DMEM, Dulbecco's Modified Eagle Medium) or brine was carefully added onto the surface of the gels. The samples were heated at 37 °C for 12 hours and evaluated visually by the vial inversion.

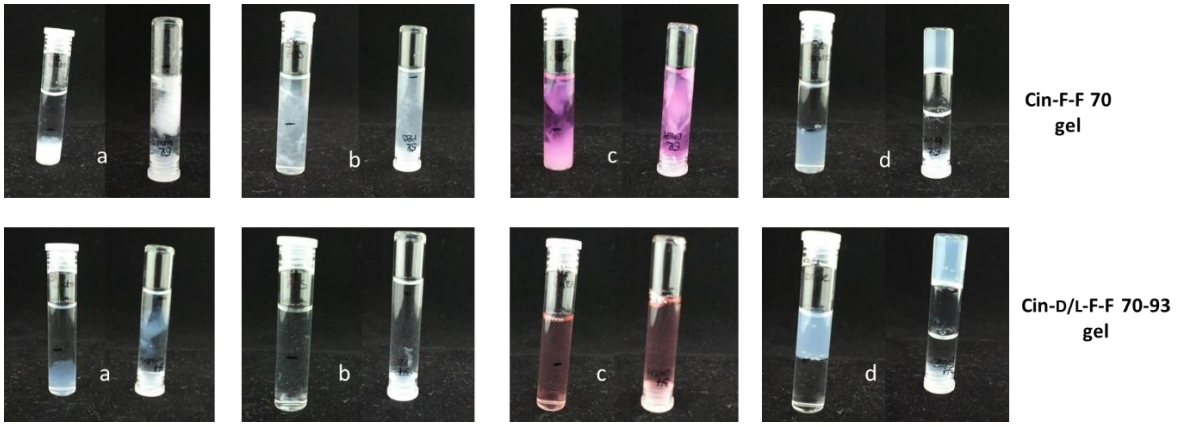

Figure 3.26 Stability tests of Cin-F-F 70 and Cin-D/L-F-F **70-93** hydrogels in (a) water, (b) PBS solution, (c) cell culture medium and (d) brine. Stability was assessed by vial inversion after 12 hours at 37 °C - both gels in brine passed the vial inversion test. Initial gels were prepared as per protocol **D** at a concentration of 2.0 mg/mL.

The results of the vial inversion method were qualitatively similar for both gels. Only the addition of brine allowed the gels to remain intact, whereas in all other cases the materials collapsed, yielding viscous free flowing solutions. Brine was found to penetrate both gels which remained intact even after a week. By contrast, water, PBS solution and cell culture medium caused partial disruption of the hydrogels almost immediately after addition to give a viscous, free flowing solution. Addition of brine increased the ionic strength of the gels and supported the self-assembly. Hydrogels are dynamic systems therefore they behave differently under different conditions. Addition of brine caused no swelling or shrinkage of the gels as confirmed by measuring their height. That presumably implied a dynamic equilibrium in the movement of water molecules from brine to gel and *vice versa* by an exchange of water molecules through the interface that separated gels from brine.

By contrast, addition of water, PBS solution and cell medium yielded viscous free-flowing flocculent solutions. That clearly implied the breaking of intermolecular interactions of the hydrogelators which led to the disruption of the gels.

FT-IR measurements

An antiparallel *β*-sheet supramolecular arrangement for the Fmoc-F-F **68** hydrogel, where gelation was achieved through the use of a pH trigger, has been reported based on its FT-IR spectrum.[27,30] Indeed, the observed sharp peak at 1625 cm^{-1} is characteristic of the presence of *β*-sheet structures while that at 1687 cm^{-1} is characteristic for the antiparallel arrangement of the *β*-sheets. Structurally similar hydrogelators bearing the diphenylalanine moiety

showed almost identical spectra, suggesting that it is not the type of the aromatic group attached at the *N*-terminus which is responsible for the molecular alignment but rather its relative spatial orientation.[40] The IR spectrum of Fmoc-F-F **68** hydrogel showed three peaks at 1692, 1634 and 1535 cm^{-1}, corresponding to the *C*-terminus C=O stretch and the two amide NC=O stretches respectively (amide I and II bands). Cin-F-F **70** gel showed similar peaks of which those, at 1652 and 1624 cm^{-1} were red shifted whereas that centred around 1544 cm^{-1} was blue shifted compared to the FT-IR spectrum of Fmoc-F-F **68** gel. The acquired FT-IR spectrum of Fmoc-F-F **68** hydrogel was consistent with the published data,[27,30] but that wasn't the case for that of Cin-F-F **70** (Figure 3.27). It is of note that there is no report in literature of a certain wavenumber shift that suggests a different interpretation from that of a *β*-sheet configuration for Cin-F-F **70** gel. It is the first time Cin-F-F **70** was synthetized and yielded a gel therefore in detail XRD and *in silico* studies need to be undertaken to interpret accurately the configuration of gelator **70** within the supramolecular matrix.

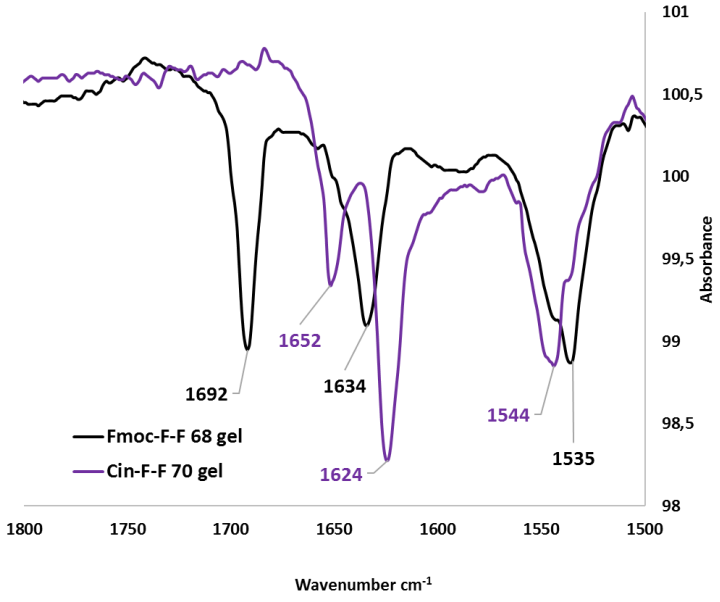

Figure 3.27 FTIR spectra of Fmoc-F-F **68** and Cin-F-F **70** hydrogels featuring the amide I and II regions. Both spectra were solvent subtracted. The hydrogels were prepared according to the standard protocols **B** and **D** respectively.

Fluorescence analysis

The recorded fluorescence spectrum of Fmoc-F-F **68** gel was different from the corresponding published data, being significantly blue shifted (reported λ_{max} 330 nm →

obtained λ_{max} 302 nm)[27,37] presumably due to the different gelation triggers employed. From comparison of the Fmoc-F-F **68** methanolic solution (true solution, no self-assembly present) and hydrogel, an increase in emission intensity and a small blue shift from 311 to 302 nm was noted for the gel. That could be explained by the possible formation of H-aggregates and the appearance of strong π-π interactions (Figure 3.28). The corresponding spectra of Cin-F-F **70** and Cin-D/L-F-F **70-93** gels had a negligible emission.

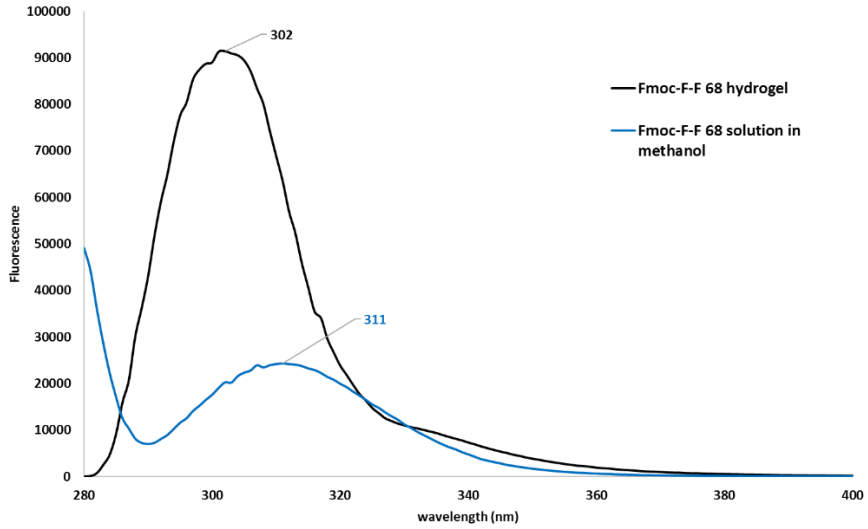

Figure 3.28 Emission spectra of the hydrogel and methanolic solution of Fmoc-F-F **68**.

Rheology measurements

Rheology studies of hydrogels **68**, **70** and **70-93** verified the viscoelastic properties of the materials. All measurements were undertaken on self-supporting hydrogels within the linear viscoelastic region in which the storage modulus (G′) and loss modulus (G″) are independent of the strain amplitude. Specifically, the obtained shear strain (γ%) was 0.03% for gel **68**, 0.05% for gel **70** and 0.03% for gel **70-93** (Figure 3.29).

Having measured the shear strain γ%, frequency sweep experiments were then undertaken within the linear viscoelastic region for each material. All measurements were performed in triplicate to acquire the storage G′ and loss G″ moduli (Figure 3.30). The storage G′ modulus had a greater value compared to loss G″ modulus in all cases, confirming the viscoelastic nature of the materials (gel state). No crossover points were observed indicating that all gels had similar elasticity. Finally, in terms of stiffness, hydrogel **I** was stiffer (G′ ~8697 Pa) followed by hydrogel **II** (G′ ~2263 Pa) and then hydrogel **III** (G′ ~156 Pa).

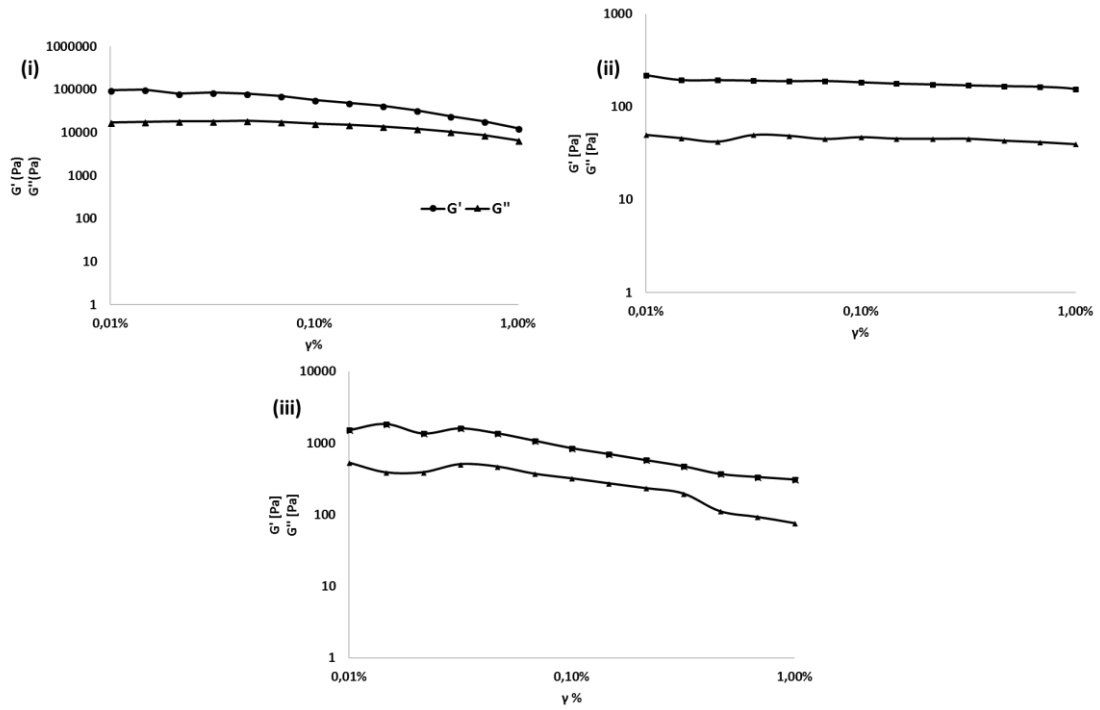

Figure 3.29 Amplitude sweep experiments at a fixed frequency of 1 Hz. Evaluation of the linear viscoelastic region of (i) Fmoc-F-F **68**, (ii) Cin-F-F **70** and (iii) Cin-D/L-F-F **70-93** hydrogels. All measurements were taken at a temperature of 25 °C.

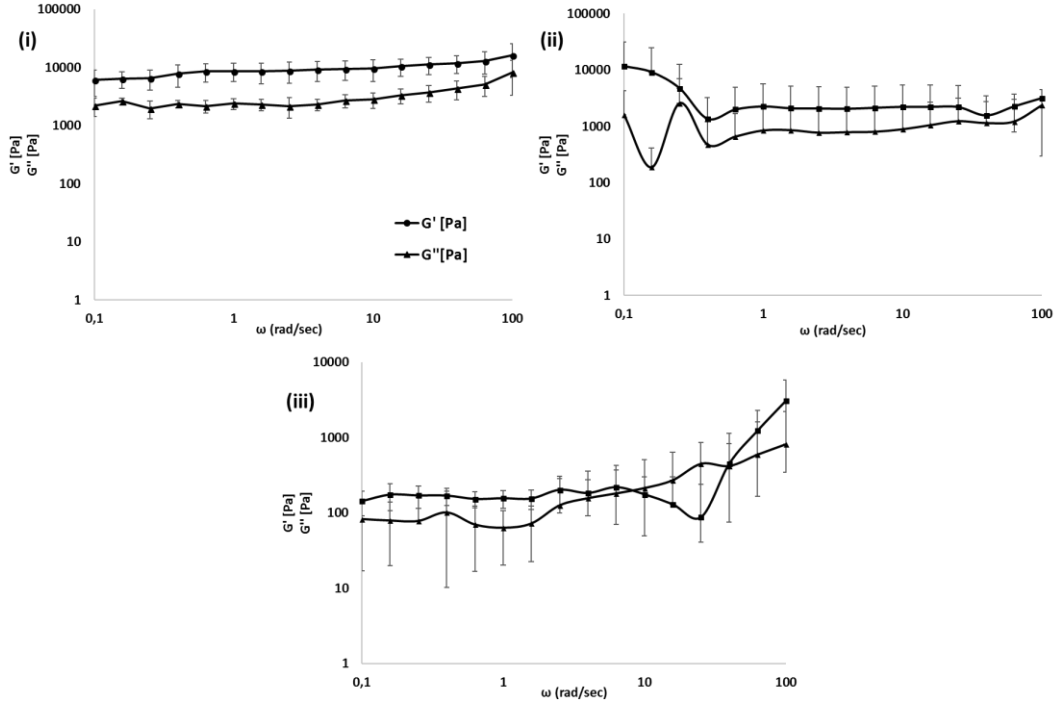

Figure 3.30 Frequency sweep experiments of the (i) Fmoc-F-F **68**, (ii) Cin-F-F **70** and (iii) Cin-D/L-F-F **70-93** hydrogels were performed from 0.1 rad/s to 100 rad/s under a 0.03% strain for **68**, 0.05% for **70** and 0.03% for **70-93**. All measurements were taken at a temperature of 25 °C..

Microscopy

Transmission and scanning electron microscopies (TEM/SEM) were used to determine the structural features of the fibres formed. The samples were diluted, as mentioned in the experimental section, and the dimensions of the fibres were measured using ImageJ software. Fmoc-F-F **68** hydrogel was composed of an overlapping mesh of flat ribbons yielding a thick supramolecular network, consistent with reported data (Figure 3.31).[27] The diameter of the ribbons was between 36-70 nm (Figure 3.31-c), while shear force tears could be observed for some ribbons at various points (red arrows). This was presumably as a result of disruption of the self-supporting nature of the gel by dilution and /or vortexing during the sample preparation.

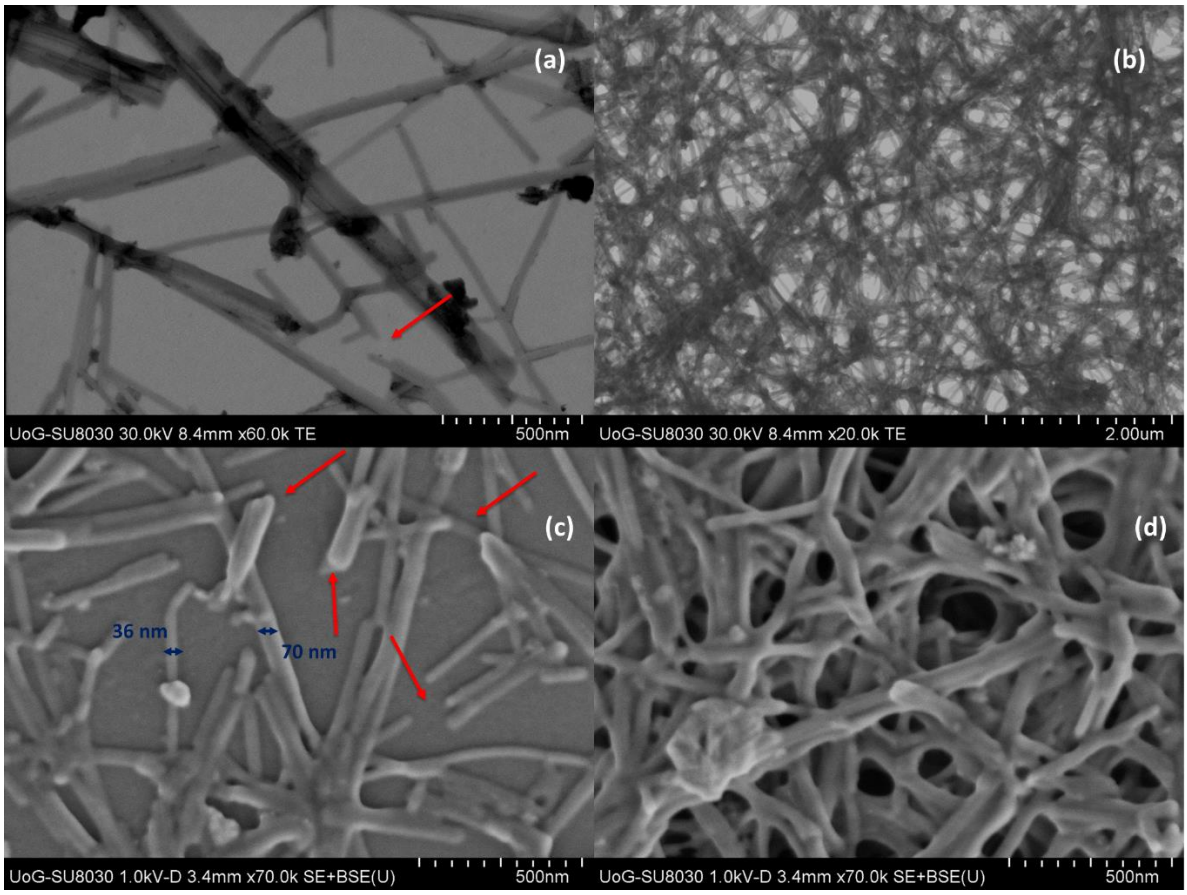

Figure 3.31 The microscopic structure of Fmoc-F-F **68** hydrogel. Transmission electron microscopy (a and b), scanning electron microscopy (c and d).

Cin-F-F **70** Hydrogel consisted of long fibers with a diameter of between 90-147 nm by SEM (Fig 3.32-a). These were connected to each other forming flat ribbons which adopted a helical structure. The length of the major turn of the helix (two-folds) was calculated as 1162

nm while the minor (one-fold) was 966 nm. The ribbons were able to form coiled coil formations yielding thicker bundles which can be clearly seen by SEM images (Figures 3.32-c and d). Shear force tears could be observed also for some ribbons at various points (red arrows).

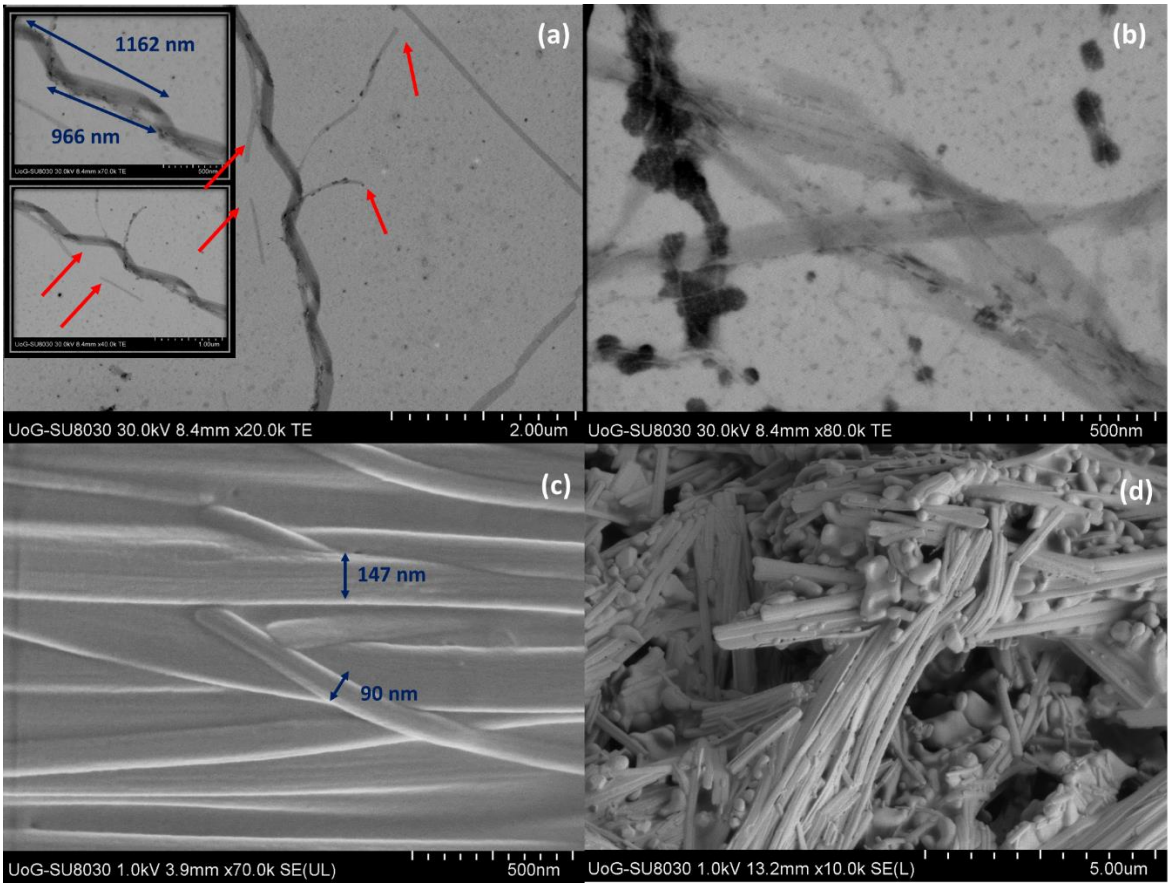

Figure 3.32 The microscopic structure of Cin-F-F **70** hydrogel. Transmission electron microscopy (a and b), scanning electron microscopy (c and d).

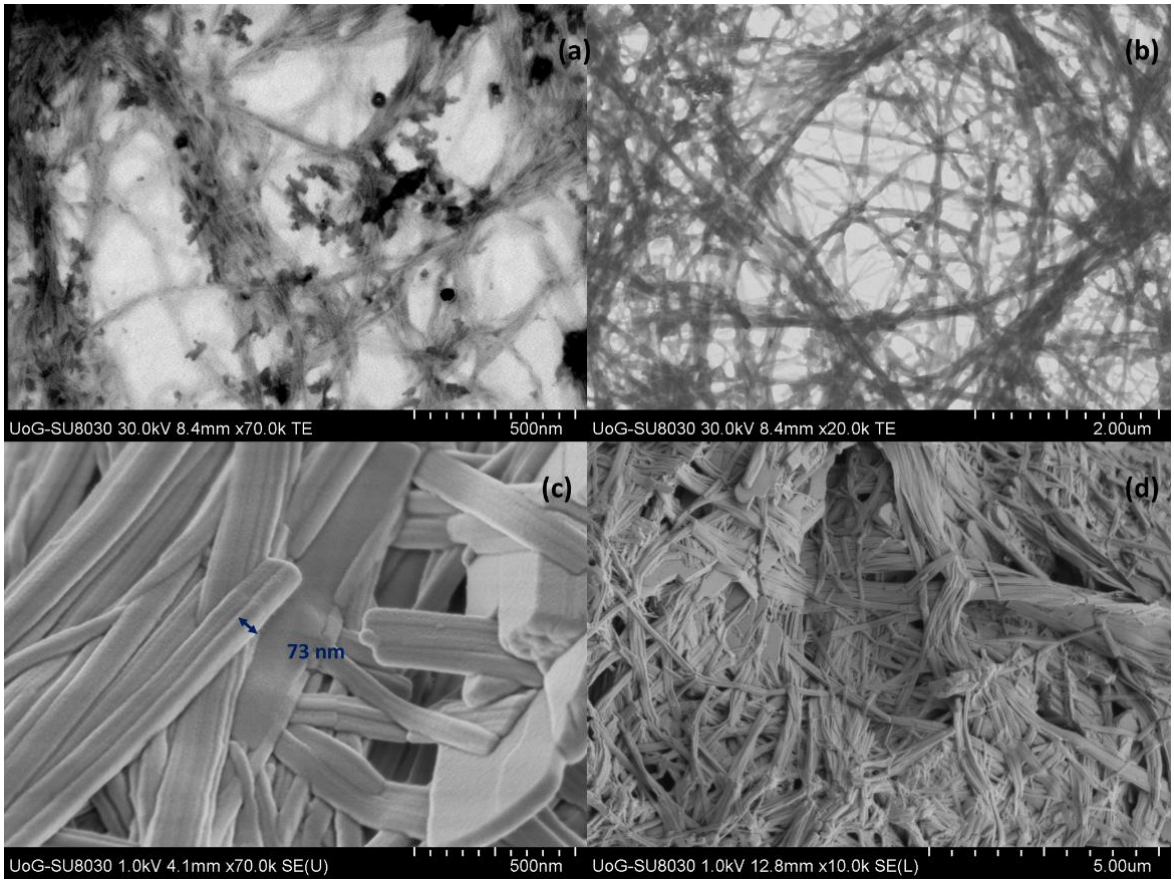

Figure 3.33 The microscopic structure of Cin-D/L-F-F **70-93** hydrogel. Transmission electron microscopy (a and b), scanning electron microscopy (c and d).

The hydrogel of epimeric mixture **70-93** consisted of long fibers with a diameter around 70 nm (Figure 3.33-c). In contrast to that of the pure epimer Cin-F-F **70**, although they formed flat ribbons when attached together, no helical structures were observed. In fact, the coiled coil formations of the ribbons yielded wider bundles which led to a similar supramolecular network to hydrogel **70** as can be seen in the SEM images are (Figures 3.33-c and d). Comparison of the hydrogels' micrographs verify the differences observed in CD and XRD studies mentioned above.

Summary

To explore the effects of different gelation triggers on self-assembly, one of the main representatives of the diphenylalanine family of aromatic peptide amphiphiles, Fmoc-F-F **68**, was used as a model gelator.

Fmoc-F-F **68** gelled PBS solution by sonication providing a self-supporting gel the viscoelastic properties of which were confirmed from measurements of the storage G′ and

loss G″ moduli. CD spectra showed that the handedness of the gel was due to self-assembly since a true solution of **68** yielded no CD signals. FT-IR measurements revealed two sharp peaks at 1692 and 1624 cm^{-1} which are characteristic of a β-sheet conformation. Additionally, by comparison of the UV-vis spectra of the hydrogel and its corresponding solution, a blue shift related to the gel was observed suggesting the formation of H-aggregates. Measurements of the phase transition temperature revealed that the gel was no longer self-supporting at 75-80 °C. Indeed, CD spectra after heating the gel at 85 °C showed that the initial self-assembly was partially disrupted while no reformation of the gel in its full extent was observed thereafter. Microscopy revealed an overlapping mesh of flat ribbons yielding a thick supramolecular network.

Comparison of the findings to the reported data confirmed that changing the gelation protocol affected the self-assembly of **68**. Although qualitatively similar, the spectroscopic data (CD, FT-IR, UV-vis) of hydrogel **68** appeared shifted, suggesting differences in its supramolecular network compared to the reported hydrogel.

Cin-F-F **70**, a structurally related analogue of dipeptide **68**, was tested to explore the effects of a different aromatic moiety on self-assembly. The results showed that the formed material was qualitatively different and had significantly different properties. In terms of rigidity, the obtained hydrogel from Fmoc-F-F **68** was stiffer than the Cin-F-F **70** gel. This was also observed from measurements of the phase transition temperature as it was found that gel **68** was disrupted at a higher temperature compared to gel **70**. CD and FT-IR spectroscopy showed significantly different spectroscopic profiles implying that the self-assembly of gels **68** and **70** was different. That was expected since the contribution of π-π interactions in the self-assembly were far lower for **70** than for **68**. Further to this the obtained micrographs revealed profound differences to the size, shape and entanglement of the formed fibres.

Finally, the epimeric mixture **70-93** yielded a hydrogel which was compared to that of the pure epimer Cin-F-F **70**. Rheology measurements showed that gel **70-93** was at least an order of magnitude weaker while its phase transition temperature was almost half the value of that of gel **70**. The CD spectrum of gel **70-93** showed negligible CD signals compared to gel **70** suggesting that epimers **70-93** in the given 2:1 ratio likely caused cancelation. Additionally, the absorbance data of gels **70** and **70-93** and those of their corresponding solutions suggested the formation of H-aggregates for **70** and J-aggregates for the epimeric mixture **70-93**. Differences in the supramolecular network were also identified by comparison of the

obtained micrographs. In contrast to helical fibrillar structures present in gel **70**, coiled coil formation of ribbons appeared in gel **70-93**.

3.4 Conclusions

A set of structurally related LMW compounds was assessed as potential hydrogelators followed by the preparation of their corresponding hydrogels and evaluation of their properties. The hydrogels were categorized as four groups based on the structural features of their constituent building blocks: (i) the Fmoc set of compounds, (ii) the indomethacin and diclofenac derivatives, (iii) the biotin-based compounds and (iv) the diphenylalanine analogues.

A range of techniques were employed to explore the macroscopic and microscopic properties of the formed materials. Therefore, gelation was assessed under different conditions. Stability tests, rheology studies and $T_{gel\text{-}sol}$ measurements were undertaken to assess the cohesion, stability, stiffness and elasticity of the gels. By CD spectroscopy the handedness of the supramolecular networks was assessed while reversibility of the gel-sol process was explored. From IR, NMR, UV-vis and fluorescence spectroscopy analysis, data were obtained regarding the gelators mode of self-assembly and the microenvironment of the chromophores. XRD was employed to evaluate the presence of polymorphism while TEM and SEM microscopy showed details of the morphology of the formed fibres within the supramolecular network.

Gelator GalNHFmoc **62** was used as a model sample for the optimization of techniques prior any characterization studies. Hydrogels prepared by the epimeric pair GalNHFmoc **62** and GlcNHFoc **63** were compared showing clear differences in their properties. The GlcNH-F-Fmoc **112** didn't yield a hydrogel in contract to its analogue GalNH-F-Fmoc **111** that gave a self-supporting gel. Gelation was optimized for the indomethacin and diclofenac derivatives however due to limited material no further characterization studies were undertaken. The biotin-based compounds were characterized as non-gelators since they fail to yield self-supporting hydrogels under different conditions.

The undertaken characterization work of the formed materials allowed us to answer the following three questions:

What did the characterization data show us?

The Fmoc-F-F **68** based gel was prepared following a different gelation protocol to that reported in bibliography and its characterization showed that it consists a material with different properties. To assess the effect of aromaticity on self-assembly, gel **68** was compared to that prepared from the Cin-F-F **70** analogue. Again, clear differences in the obtained data revealed that the two hydrogels were different materials. Further to this, gelation of the epimeric mixture **70-93** was explored. Comparison of gels **70** and **70-93** showed also differences in the macroscopic and microscopic properties of the gels.

What did we learn from the characterization process?

It is of note that hydrogels based on a single gelator *i.e.* GalNHFmoc **62** were prepared following different gelation protocols *e.g.* **A**, **B** and **C**. Due to practical reasons it was not possible to apply a certain protocol for a single compound towards different characterization techniques. The parameters and availability of the instruments used, *in situ* gelation in contrast to transferring materials, the volume of sample specimens that could be used and handling of gels as to preserve their self-assembly intact proved challenging. Therefore, extensive optimization work is needed to address such practical issues of gel preparation and handling for characterization purposes to achieve reliable and accurate results.

What is the outcome of the characterization work towards tissue culture applications?

Based on the obtained data, structural differences of the gelator molecules resulted in different modes of self-assembly leading to different supramolecular gels. Further to this, different gelation conditions when applied on a single gelator yielded also different materials. Therefore, by modifying chemically the structure of the molecular building blocks and/or inducing gelation under different conditions it is possible to obtain novel materials with desirable properties.

LMW hydrogels are to be used as cell culture substrates capable of mimicking the extracellular matrix. The microscopic and mechanical properties of the formed hydrogels are expected to have an immediate effect on cell viability and proliferation. By comparison of the hydrogels characterization and biocompatibility data we could therefore identify the optimum gelation conditions and structural motifs of the molecular building blocks for the preparation of efficient hydrogelators. To assess the biocompatibility of the formed materials

glioblastoma cancer cells have been cultured within the formed hydrogels and their metabolic activity has been assessed based on a colorimetric assay as described in chapter 5.

3.5 References

(1) Yu, G.; Yan, X.; Han, C.; Huang, F. Characterization of Supramolecular Gels. *Chem. Soc. Rev.* **2013**, *42* (16), 6697-6722.

(2) Goyal, N.; Cheuk, S.; Wang, G. Synthesis and Characterization of D-Glucosamine-Derived Low Molecular Weight Gelators. *Tetrahedron* **2010**, *66* (32), 5962-5971.

(3) Goyal, N.; Mangunuru, H. P. R.; Parikh, B.; Shrestha, S.; Wang, G. Synthesis and Characterization of pH Responsive D-Glucosamine Based Molecular Gelators. *Beilstein J. Org. Chem.* **2014**, *10*, 3111-3121.

(4) Draper, E. R.; Adams, D. J. Low-Molecular-Weight Gels : The State of the Art. *Chem.* **2017**, 390-410.

(5) Du, X.; Zhou, J.; Shi, J.; Xu, B. Supramolecular Hydrogelators and Hydrogels: From Soft Matter to Molecular Biomaterials. *Chem. Rev.* **2015**, *115* (24), 13165-13307.

(6) Mitra, R. N.; Das, D.; Roy, S.; Das, P. K. Structure and Properties of Low Molecular Weight Amphiphilic Peptide Hydrogelators. *J. Phys. Chem. B* **2007**, *111*, 14107-14113.

(7) Suzuki, M.; Yumoto, M.; Shirai, H.; Hanabusa, K. Supramolecular Gels Formed by Amphiphilic Low-Molecular-Weight Gelators of N^{α}-N^{ϵ}-Diacyl-L-Lysine Derivatives. *Chem. - A Eur. J.* **2008**, *14* (7), 2133-2144.

(8) Birchall, L. S.; Roy, S.; Jayawarna, V.; Hughes, M.; Irvine, E.; Okorogheye, G. T.; Saudi, N.; De Santis, E.; Tuttle, T.; Edwards, A. A.; et al. Exploiting CH-[Small Pi] Interactions in Supramolecular Hydrogels of Aromatic Carbohydrate Amphiphiles. *Chem. Sci.* **2011**, *2* (7), 1349-1355.

(9) Zanna, N.; Merlettini, A.; Tatulli, G.; Milli, L.; Focarete, M. L.; Tomasini, C. Hydrogelation Induced by Fmoc-Protected Peptidomimetics. *Langmuir* **2015**, *31* (44), 12240-12250.

(10) Sitsanidis, E. D.; Piras, C. C.; Alexander, B. D.; Siligardi, G.; Javorfi, T.; Hall, A. J.; Edwards, A. A. Circular Dichroism Studies of Low Molecular Weight Hydrogelators: The Use of SRCD and Addressing Practical Issues. **2018**, No. February, 1-11.

(11) Zuidema, J. M.; Rivet, C. J.; Gilbert, R. J.; Morrison, F. A. A Protocol for Rheological Characterization of Hydrogels for Tissue Engineering Strategies. *J. Biomed. Mater. Res. B Appl. Biomater.* **2014**, *102* (5), 1063-1073.

(12) Mammarella, E. J.; De Piante, D. A.; Rubiolo, A. C. Evaluation of Stress-Strain for Characterization of the Rheological Behavior of Alginate and Carrageenan Gels. *Brazilian J. Chem. Eng.* **2002**, *19* (4), 403-409.

(13) Yan, C.; Pochan, D. J. Rheological Properties of Peptide-Based Hydrogels for Biomedical and Other Applications. *Chem. Soc. Rev.* **2010**, *39* (9), 3528-3540.

(14) Piras, C. C. Low molecular weight gelators : synthesis and self - assembly of sugar amphiphiles. Medway School of Pharmacy, Universities of Greenwich and Kent, PhD Thesis, **2016**, 1-266.

(15) Grigoriou, S.; Johnson, E. K.; Chen, L.; Adams, D. J.; James, T. D.; Cameron, P. J. Dipeptide Hydrogel Formation Triggered by Boronic Acid-Sugar Recognition. *Soft Matter.* **2012**, *8* (25), 6788–6791.

(16) Fleming, S.; Ulijn, R. V. Design of Nanostructures Based on Aromatic Peptide Amphiphiles. *Chem. Soc. Rev.* **2014**, *43* (23), 8150-8177.

(17) Das, A. K.; Bose, P. P.; Drew, M. G. B.; Banerjee, A. The Role of Protecting Groups in the Formation of Organogels through a Nano-Fibrillar Network Formed by Self-Assembling Terminally Protected Tripeptides. *Tetrahedron* **2007**, *63* (31), 7432-7442.

(18) Joseph, J.; Jemmis, E. D. Red-, Blue-, or No-Shift in Hydrogen Bonds: A Unified Explanation. *J. Am. Chem. Soc.* **2007**, *129* (15), 4620-4632.

(19) Gronwald, O.; Sakurai, K.; Luboradzki, R.; Kimura, T.; Shinkai, S. Further Evidence for the Gelation Ability-Structure Correlation in Sugar-Based Gelators. *Carbohydr. Res.* **2001**, *331* (3), 307-318.

(20) Mathiselvam, M.; Loganathan, D.; Varghese, B. Synthesis and Characterization of Thiourea- and Urea-Linked Glycolipids as Low-Molecular-Weight Hydrogelators. *RSC Adv.* **2013**, *3* (34), 14528-14542.

(21) John, G.; Jung, J. H.; Masuda, M.; Shimizu, T. Unsaturation Effect on Gelation Behavior of Aryl Glycolipids. *Langmuir* **2004**, *20* (6), 2060-2065.

(22) Jung, J. H.; John, G.; Masuda, M.; Yoshida, K.; Shinkai, S.; Shimizu, T. Self-Assembly of a Sugar-Based Gelator in Water: Its Remarkable Diversity in Gelation Ability and Aggregate Structure. *Langmuir* **2001**, *17* (23), 7229-7232.

(23) Jung, J. H.; Shinkai, S.; Shimizu, T. Spectral Characterization of Self-Assemblies of Aldopyranoside Amphiphilic Gelators: What Is the Essential Structural Difference between Simple Amphiphiles and Bolaamphiphiles? *Chem. Eur. J.* **2002**, *8* (12), 2684-2690.

(24) Gao, D.; Xue, M.; Peng, J.; Liu, J.; Yan, N.; He, P.; Fang, Y. Preparation and Gelling Properties of Sugar-Contained Low-Molecular-Mass Gelators: Combination of Cholesterol and Linear Glucose. *Tetrahedron* **2010**, *66* (16), 2961-2968.

(25) Yan, N.; He, G.; Zhang, H.; Ding, L.; Fang, Y. Glucose-Based Fluorescent Low-Molecular Mass Compounds: Creation of Simple and Versatile Supramolecular Gelators. *Langmuir* **2010**, *26* (8), 5909-5917.

(26) Wang, G.; Cheuk, S.; Yang, H.; Goyal, N.; Narasimha Reddy, P. V.; Hopkinson, B. Synthesis and Characterization of Monosaccharide-Derived Carbamates as Low-Molecular-Weight Gelators. *Langmuir* **2009**, *25* (15), 8696-8705.

(27) Smith, A. M.; Williams, R. J.; Tang, C.; Coppo, P.; Collins, R. F.; Turner, M. L.; Saiani, A.; Ulijn, R. V. Fmoc-Diphenylalanine Self Assembles to a Hydrogel via a Novel Architecture Based on π-π Interlocked *β*-Sheets. *Adv. Mater.* **2008**, *20* (1), 37-41.

(28) Pal, A.; Dey, J. Rheology and Thermal Stability of PH-Dependent Hydrogels of N-Acyl-L-Carnosine Amphiphiles: Effect of the Alkoxy Tail Length. *Soft Matter.* **2011**, *7* (21), 10369-10376.

(29) Reddy, S. M. M.; Shanmugam, G.; Duraipandy, N.; Kiran, M. S.; Mandal, A. B. An

Additional Fluorenylmethoxycarbonyl (Fmoc) Moiety in Di-Fmoc-Functionalized L -Lysine Induces PH-Controlled Ambidextrous Gelation with Significant Advantages. *Soft Matter.* **2015**, *11*, 8126-8140.

(30) Tang, C.; Smith, A. M.; Collins, R. F.; Ulijn, R. V.; Saiani, A. Fmoc-Diphenylalanine Self-ASsembly Mechanism Induces Apparent PK a Shifts. *Langmuir* **2009**, *25* (16), 9447-9453.

(31) Skilling, K. J.; Kellam, B.; Ashford, M.; Bradshaw, T. D.; Marlow, M. Developing a Self-Healing Supramolecular Nucleoside Hydrogel. *Soft Matter.* **2016**, *12* (43), 8950-8957.

(32) Zelzer, M.; Ulijn, R. V. Next-Generation Peptide Nanomaterials: Molecular Networks, Interfaces and Supramolecular Functionality. *Chem. Soc. Rev.* **2010**, *39* (9), 3351-3357.

(33) Yan, X.; Zhu, P.; Li, J. Self-Assembly and Application of Diphenylalanine-Based Nanostructures. *Chem. Soc. Rev.* **2010**, *39* (6), 1877-1890.

(34) Ryan, D. M.; Nilsson, B. L. Self-Assembled Amino Acids and Dipeptides as Noncovalent Hydrogels for Tissue Engineering. *Polym. Chem.* **2012**, *3* (1), 18-33.

(35) Frederix, P. W. J. M.; Scott, G. G.; Abul-Haija, Y. M.; Kalafatovic, D.; Pappas, C. G.; Javid, N.; Hunt, N. T.; Ulijn, R. V; Tuttle, T. Exploring the Sequence Space for (Tri-)Peptide Self-Assembly to Design and Discover New Hydrogels. *Nat. Chem.* **2014**, *7* (1), 30-37.

(36) Draper, E. R.; Morris, K. L.; Little, M. A.; Raeburn, J.; Colquhoun, C.; Cross, E. R.; McDonald, T. O.; Serpell, L. C.; Adams, D. J. Hydrogels Formed from Fmoc Amino Acids. *CrystEngComm* **2015**, *17* (42), 8047-8057.

(37) Jayawarna, V.; Ali, M.; Jowitt, T. A.; Miller, A. F.; Saiani, A.; Gough, J. E.; Ulijn, R. V. Nanostructured Hydrogels for Three-Dimensional Cell Culture through Self-Assembly of Fluorenylmethoxycarbonyl-Dipeptides. *Adv. Mater.* **2006**, *18* (5), 611-614.

(38) Prashad, M.; Sutton, P.; Wu, R.; Hu, B.; Vivelo, J.; Carosi, J.; Kapa, P.; Liang, J. Process Research and Development of a MTP Inhibitor: Another Case of

Disappearing Polymorphs upon Scale-Up. *Org. Process Res. Dev.* **2010**, *14* (4), 878-882.

(39) Sagnella, S. M.; Conn, C. E.; Krodkiewska, I.; Moghaddam, M.; Drummond, C. J. Endogenous Nonionic Saturated Monoethanolamide Lipids: Solid State, Lyotropic Liquid Crystallineand Solid Lipid Nanoparticle Dispersion Behavior. *J. Phys. Chem. B* **2010**, *114* (4), 1729-1737.

(40) Martin, A. D.; Robinson, A. B.; Mason, A. F.; Wojciechowski, J. P.; Thordarson, P. Exceptionally Strong Hydrogels through Self-Assembly of an Indole-Capped Dipeptide. *Chem. Commun.* **2014**, *50* (98), 15541-15544.

4. SYNCHROTRON RADIATION CIRCULAR DICHROISM STUDIES OF LMW HYDROGELS: ADDRESSING PRACTICAL ISSUES

4.1 Introduction

Supramolecular hydrogels are viscoelastic, solid-like materials formed by a three-dimensional fibrous network derived from the non-covalent self-assembly of gelator molecules in water. The difference in light absorbance between left (LCPL) and right (RCPL) circularly polarized light (circular dichroism-CD) in such materials results from the chiral building blocks, however chirality may also be induced due to the configurational alignment of the formed fibers. Alternatively, the corresponding dichroic signal of molecular assemblies is related to the dichroism of their constituents. Indeed, the intrinsic chirality in LMW hydrogels arises from the diverse nature of their gelator molecules, many of which contain chiral components in their structure, the most common of which are carbohydrate- and amino acid-based moieties.[1–6]Although CD spectroscopy has been extensively used for the investigation of the conformation and configuration of chiral molecules, only a limited number of protocols and methods have been reported for the study of LMW hydrogels.[7–10] The work reported herein focuses on the development of a robust protocol to investigate the self-assembly of chiral hydrogelators *via* CD spectroscopy, the results of which have been published recently.[11]

Preliminary optimization by conventional CD spectroscopy using a Chirascan spectrophotometer (benchtop instrument), allowed a robust method of hydrogel sample preparation *in situ* within the cells. This was subsequently employed for synchrotron radiation circular dichroism (SRCD) to then develop a series of experiments for study of LMW hydrogels. Acquisition of SRCD spectra was undertaken using the facilities of the B23 beam line at Diamond Light Source, Oxfordshire. SRCD spectroscopy, when compared to conventional CD, provides a highly collimated cross section of beam light (250 μm) which gives enhanced spatial resolution, a higher photon flux in the far UV region (175-250 nm) and thus a lower signal-to-noise ratio compared to conventional CD spectrophotometers.

Each hydrogel has a characteristic CD profile due to the chirality of the building blocks and its higher order architecture (matrix) which reflects the asymmetry of the chromophores within the three-dimensional structure. By contrast, solvated gelator molecules (in true solutions) have a much weaker or negligible CD signal compared to that of their

corresponding gels and a slightly higher absorbance. This is because in solution (sol) the exciton coupling between the chromophores of the free moving gelator molecules is significantly weaker compared to that in the gel state (gel).

In solution, the anisotropy of chiral molecules gives rise to dichroism, however in highly order systems, in addition to the intrinsic chirality which defines the optical properties of the medium, there is also the contribution of optical artefacts generated by circular birefringence (CB), linear dichroism (LD) and linear birefringence (LB, see below). In contrast to benchtop instruments (conventional CD) which measure only the average of the hydrogel's chirality due to the large cross section of their beamlight (8 x 10 mm), SRCD spectroscopy allows measurements to be undertaken for several different sites (spots 1, 2 and 3) along the gel specimens, almost 0.5 mm in diameter, enabling the exploration of the hydrogels homogeneity (Figure 4.1). The use of a rotating platform, upon which the cuvette was placed, allowed acquisition of spectra in different rotations/orientations for a selected spot. This then allowed the evaluation of potential LD and LB contributions. Finally, as gel specimens were laid horizontally in the vertical sample chamber (module A, Figure 4.1),[12,13] the effects of potential gravitational movement of gels within the cuvettes were significantly reduced. Indeed, such effects could result in uneven thickness of the gels (concentration variations defined as variations in the topology of the supramolecular matrix) to give varied CD intensities.

Consequently, the aims of the research focused on addressing the following practical issues:

- the optimization of hydrogel preparation for SRCD analysis
- the identification of potential optical artefacts (LD and LB)
- the comparison of conventional CD and SRCD spectroscopy
- the evaluation of sample homogeneity
- the exploration of possible disruption of the hydrogel samples due to SRCD beam light;
- the evaluation of thermal disruption and reformation of hydrogels (sol-gel reversibility)

It is noted that for the assessment of potential LD and LB contributions, SRCD measurements on a single spot were obtained at rotations of 0° and 90°. Unfortunately, due to time constraints of beam time, measurements at 180° rotation for CB evaluation were not recorded.

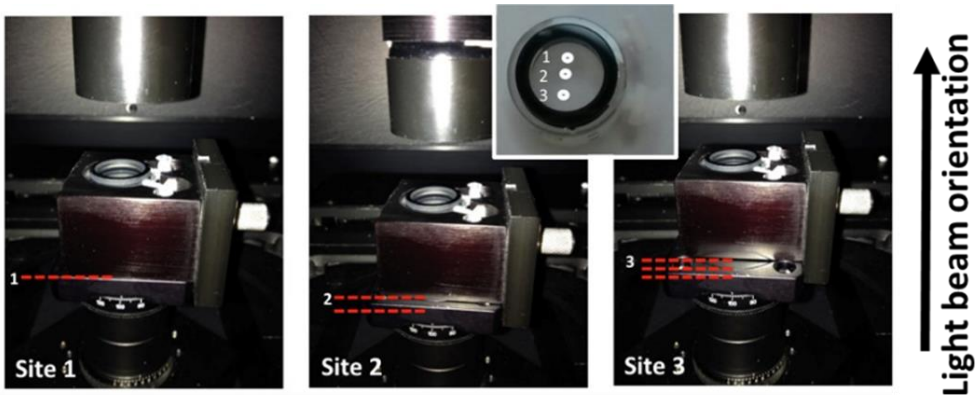

Figure 4.1 Horizontal positioning of gel specimens in sample chamber of module A, with a rotating platform and a cylindrical cell holder. SRCD spectra were acquired at three different sites (spots 1,2 and 3) for evaluation of homogeneity within the hydrogel.

A set of structurally related hydrogelators has been chosen to assess the chirality of their corresponding hydrogels (Figure 4.7). Based on the characterization results, structural differences of the molecular building blocks and different gelation triggers induce different modes of self-assembly. Therefore, a CD analysis of the specimens was expected to result different CD profiles due to the differences upon chirality of their supramolecular architecture. In addition, for the structurally related compounds, CD spectra were expected to be rather qualitatively similar due to the intrinsic chirality of the building blocks, however potential CD differences would strongly suggest that their molecular packing towards higher architectures would be different.

4.2 Fundamentals

Light is an electromagnetic radiation (transverse wave) consisting of an electric $\vec{E}$ and a magnetic $\vec{B}$ field which oscillate perpendicular to one another and to the direction of propagation. Linearly polarized light (LPL) is polarized in one direction only, in which the electric field vector oscillates within one plane (sinusoidal wave). However, for circularly polarized light (CPL) the electric field vector rotates about its propagation direction and retains a constant magnitude (Figure 4.2).

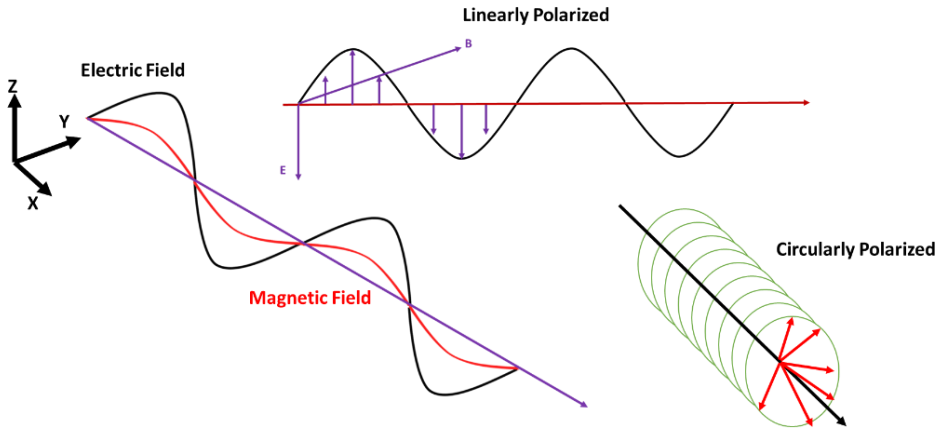

Figure 4.2 Schematic depiction of the oscillation of the electric field vector $\vec{E}$ in LPL and CPL.

Isotropy is defined as uniformity in all orientations. For example, isotropic radiation has the same intensity in all directions of measurement whereas anisotropy describes properties that vary systematically and are dependent on direction (Figure 4.3).

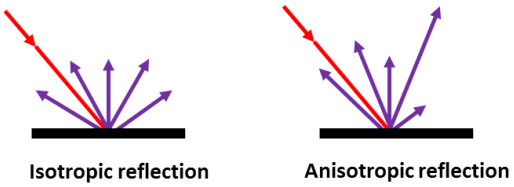

Figure 4.3 Schematic depiction of isotropic and anisotropic reflection of light.

In optics, the refractive index or index of refraction (n) of an optical medium describes how light or any other radiation propagates through that medium and is dimensionless. It is defined as n = c / v where c is the speed of light in vacuum and v is the phase velocity of light in the medium.

Birefringence (B) or double refraction is defined as the dependence of light refraction on light polarization. When a ray of unpolarized light is incident on the surface of a birefringent material, it splits into two polarized beams which propagate along different trajectories and with a different speed (normal and extraordinary rays). In other words, birefringence is the optical property of an optically anisotropic material, whose refractive index depends both on the polarization and direction of propagation of light. These materials are also named birefringent or birefractive (Figure 4.4)

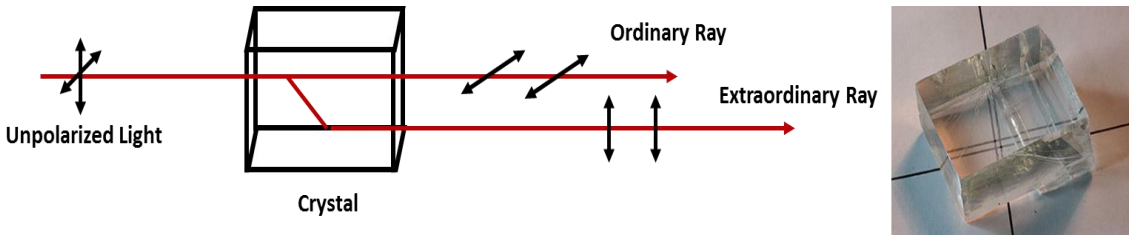

Figure 4.4 Schematic depiction of the optical property of a birefringent material.

Linear birefringence (LB) or linear double refraction is defined as the difference in refraction and the associated speed of light of linearly polarized light with orthogonal planes of polarization whereas circular birefringence (CB) or circular double refraction expresses the same refraction difference of both left and right circularly polarized light. The difference in the absorption (or emission) of linearly polarized light rays (orthogonal planes of polarization) is defined as linear dichroism (LD) while that of left and right circularly polarized light is defined as circular dichroism (CD).

When light or any other radiation interacts with matter, energetically favoured electronic transitions occur from the highest occupied molecular orbital (HOMO) to the lowest unoccupied molecular orbital (LUMO). The electron cloud redistribution gives rise to an electric dipole transition moment $\vec{\mu}$, while the electron rotation results in a magnetic transition dipole moment $\vec{m}$. The degree of alignment of the electric and magnetic transition dipole moments ($\vec{\mu}$, $\vec{m}$) with the electric and magnetic fields of the incident light ($\vec{E}$,$\vec{B}$) defines the degree of absorbance in optical media such as supramolecular gels. This dependence not only confers anisotropy upon soft materials, but also defines the dichroic effect as the difference in absorption depending on light polarization. Therefore, even though CD spectroscopy has been primarily used for the exploration of the secondary structure of biological macromolecules (macromolecular conformation), it can also prove a useful tool for the observation of the self-assembly in supramolecular materials (gelation process or sol-gel process) and the investigation of the reverse process (gel-sol) caused, for example, by disrupting thermally the self-assembly of the gels (Figure 4.5).

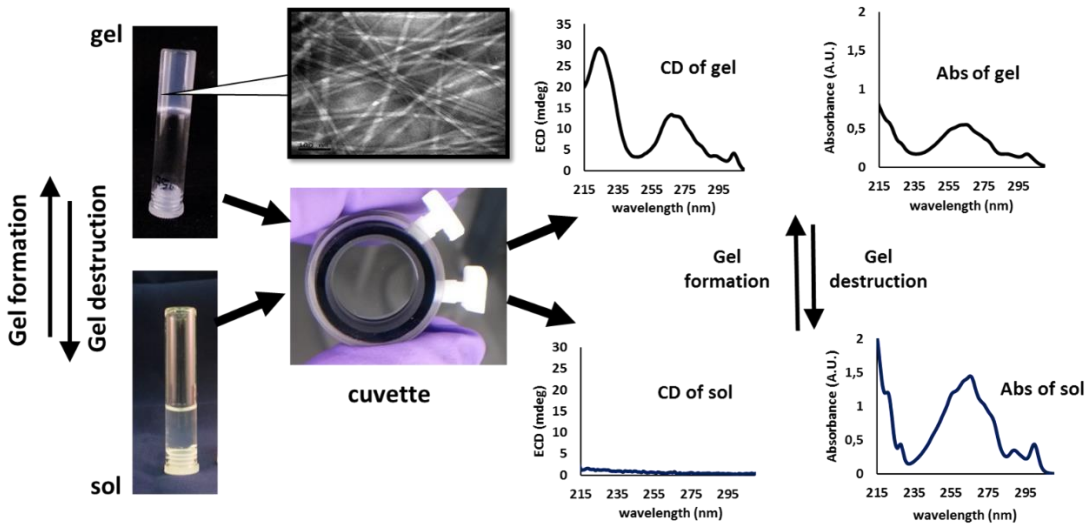

Figure 4.5 The use of CD for the study of supramolecular gels.

The part of a molecule which is responsible for its colour is defined as a chromophore. The observed color depends on the absorption of certain wavelengths of visible light and the emission or reflection of others. Based on their structure, chromophores can be distinguished as inherently achiral (carbonyl groups, double/triple bonds, sulfoxide groups *etc.*) and as inherently chiral (helicenes, biaryls, dienes, enones, *etc*.) The observed Cotton effects (CE) are based on "chiral" electronic perturbations during excitation. An electronic transition responsible for an absorbance band can be associated with either a positive or a negative CD band. In fact, CD spectroscopy depends on the magnitude and orientation of the chromophore's transition moments. Specifically, the observed CD signal results from the rotational strength $\vec{R}$, which refers to the corresponding electronic and magnetic dipole transition moments of the chromophores, $\vec{\mu}$ and $\vec{m}$, respectively. $\vec{R}$ is a signed quantity and defined as the scalar product of $\vec{\mu}$ and $\vec{m}$. Since $\vec{\mu}$ and $\vec{m}$ are vector quantities, both their magnitude and spatial orientation define $\vec{R}$. Therefore, for mirror image configurations (*e.g.* enantiomers), the rotational strength $\vec{R}$ will be of equal magnitude but opposite sign.

During the self-assembly process the molecular building blocks come into close proximity, causing their transition moments to interact. This phenomenon is known as exciton coupling. Especially in cases of conjugated systems with extended π orbitals, the molecules form supramolecular structures named H- or J-aggregates (Figure 4.6 (i)). The relative orientation of the molecules' transition moments mean that the formed dipoles acquire either a parallel or an antiparallel orientation. This results in the initial energy, E, of the individual molecules

being split into new energetic states, E′ and E″. In other words, when in close spatial proximity chromophores with similar exciton energies become excitons as their excited state is delocalized within the conjugated system (Figure 4.6 (ii)).

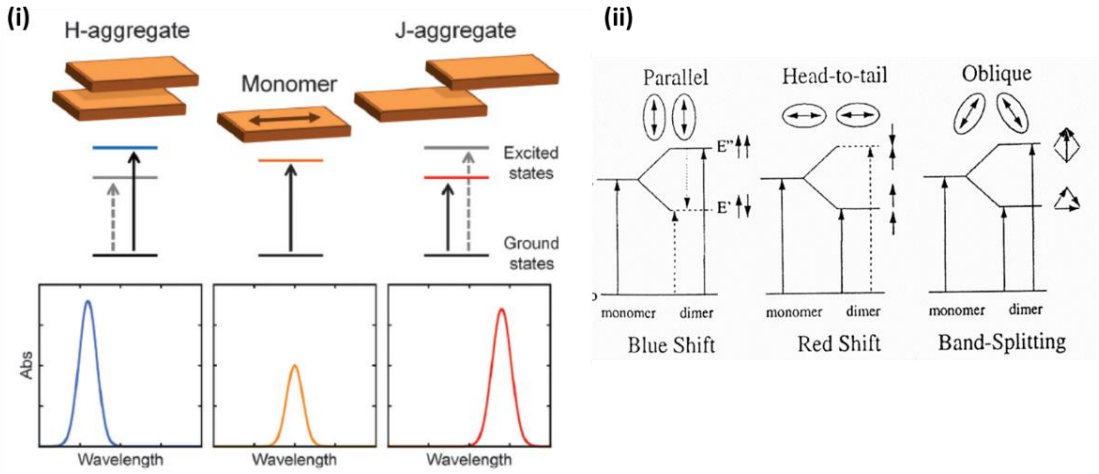

Figure 4.6 Observed shifts in UV-vis spectra of H and J-aggregates in relation to the corresponding monomer (i) and energetic states (ii) of dipole moments.[7]

A parallel orientation (H-aggregates) repels the conjugated chromophores and their dipole moments correspond to a higher energy state, whereas in antiparallel orientations (J-aggregates, head-to-tail) the attraction of dipole moments corresponds to lower energetic states. In terms of UV-vis absorption, such phenomena are interpreted *via* these energy transitions and are related to the observed wavelength maximum ($E = h\nu \rightarrow E = h / \lambda$). Therefore, high values of λ correspond to lower energy states, whereas decreased values of λ correspond to higher states. In relation to the absorbance spectrum of the monomers, H-aggregates will show a characteristic hypsochromic shift (blue shift), whereas J-aggregates will show a bathochromic shift (red shift) (Figure 4.6).[7,8] In terms of CD, exciton coupled chromophores result in a characteristic bisignate CD couplet (bisignate curve) centered around the absorbance λmax.

Finally, as mentioned by Berova and co-workers, there are three main situations that distinguish the appearance of CD spectra. Therefore, only one transition could be apparent in the CD spectrum (*i.e.* CD of saturated ketones in near-UV region) or two transitions could give rise to oppositely signed Cotton effects (as in the case of exciton coupling) or the chromophores that have a manifold of electronic transitions generate multiple bands (multiple CD signals).[8] In all cases, a general rule of CD spectroscopy is that the integral of

a CD spectrum over the whole wavelength range is equal to zero which in algebraic terms is described as:

$$\sum_{i,j}^{\text{all transitions}} \vec{R}i,j = 0$$

4.3 Materials and methods

4.3.1 Sample preparation

A set of LMW hydrogels was prepared for CD study using three Fmoc-protected hydrogelators: the enantiomeric monosaccharides GalNHFmoc **62** and GlcNHFmoc **63** and the Fmoc diphenylalanine derivative Fmoc-F-F **68** (Figure 4.7).

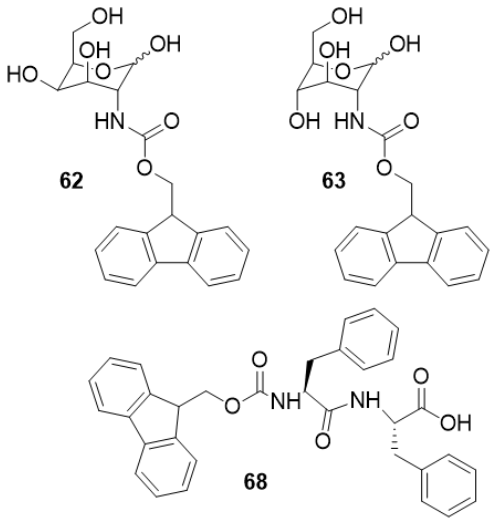

Figure 4.7 Hydrogelators GalNHFmoc **62**, GlcNHFmoc **63** and Fmoc-F-F **68**.

The two carbohydrate-based hydrogelators were synthesized as reported by Birchall *et al.*,[14] while dipeptide **68** was purchased from Biogelx (Newhouse, UK) and used without any further purification.

Extensive optimization of sample preparation and handling established that hydrogels were best formed *in situ* within a cylindrical cell. This avoided any alteration of their supramolecular structure by transfer or handling, such as with the use of demountable cells. Therefore, all gels were prepared at Diamond Light Source, a day prior to measurement, within cylindrical non-demountable cells and were left to gel overnight before commencing any SRCD/CD measurements. The gelation process employed was the same as protocols **A**

and **B** reported in chapter 3; gelation was triggered either by sonication or thermally (heating and cooling cycles) to yield hydrogel specimens **A-E** (Table 4.1).

Table 4.1 Gelation conditions for the preparation of hydrogel specimens **A-E**. The minimum gelation concentration for all gels was 2.0 mg / mL.

Hydrogelator	**Solvent**	**Gelation trigger**	**Hydrogel**
GalNHFmoc **62**	water	Thermal	**A**
	PBS	Sonication	**B**
	PBS	Thermal	**C**
GlcNHFmoc **63**	water	Thermal	**D**
Fmoc-F-F **68**	PBS	Sonication	**E**

2.0 mg of each gelator were weighed into vials and suspended either in 1.0 mL of water (Romil, water PUROM, high purity process solvent for preparative HPLC) or phosphate-buffered saline (PBS) solution. PBS solution was prepared by dissolving one PBS tablet (Sigma Aldrich) in 100 mL of purified water.

Hydrogels **B** and **E** were gelled by sonication only. Suspensions of hydrogelators **62** and **63** in PBS solution were first sonicated in vials, then pipetted into the cells and left to gel overnight. Hydrogels **A**, **C** and **D** were gelled thermally. The corresponding suspensions of **62** and **63** in water or PBS solution were sonicated in vials and transferred into the cells, which were then progressively heated in a block heater (55 to 95 °C) by raising the temperature every 10 minutes by 10°C. The cells were then cooled down in steps of 20 °C per hour to reach room temperature, then left overnight to allow gelation, prior to the start of measurement.

Solutions of hydrogelators **62**, **63** and **68** were also prepared in methanol at a concentration of 0.2 mg/mL. The use of methanol yielded true solutions free from light scattering. To allow suitable UV transparency, dilution was necessary to avoid signal saturation.

4.3.2 Experimental and data acquisition

Potential disruption of supramolecular hydrogels by SRCD beam light was evaluated prior to any study of specimens **A-E** by the use of soft and hard irradiation experiments. A hydrogel of **62** in water was used as a model sample; it was gelled thermally within a rectangular non-demountable cell (0.5 mm path length). Soft irradiation SRCD tests used the following parameters: wavelength range of 210-340 nm, temperature 23°C, 12 scans, slit opening 1.0 mm, interaction with the beam light (time per point) of 1 second. Hard irradiation SRCD tests used the following parameters: wavelength range of 210-340 nm, temperature 23 °C, 4 scans, slit opening 1.0 mm, interaction with the beam light (time per point) of 4 seconds.

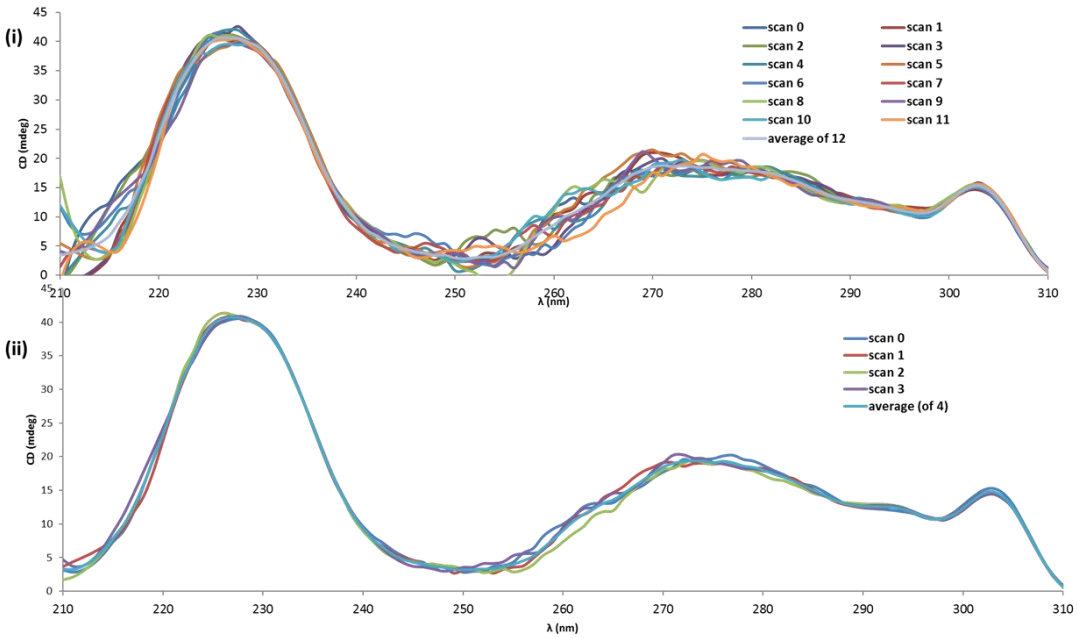

Figure 4.8 CD spectra obtained by soft (i) and hard (ii) SRCD irradiation experiments of GalNHFmoc **62** hydrogel.

Gelation was confirmed by comparing the CD intensity of the methanolic solutions with that of the corresponding hydrogel samples. Additionally, comparison of the CD of the methanolic solutions to a heated gel could confirm disruption of the gel. Indeed, in true solutions, the intermolecular interactions are disrupted due to the dissolution of the building blocks by the organic solvent, whereas in thermally treated hydrogels disruption of the intermolecular interactions resulted from Brownian motion. In both cases where the interactions are disrupted, a negligible CD signal was expected when compared to that of the initial gels and those reformed after thermal disruption.

To avoid signal saturation of the hydrogel samples, several path lengths were used (0.5, 0.2 and 0.1 mm) as dilution of hydrogel samples **A**-**E** was not possible since this would disrupt their self-assembly. For this reason, the minimum gelation concentration of each sample was used. Evaluation of the appropriate path length of cell (*i.e*. far UV cut off) and, thus, the appropriate wavelength range, was achieved by measuring the absorbance of each sample in a Chirascan spectrophotometer prior to any SRCD measurement. The absorbance spectrum of spot 2 for all gel specimens was measured and the corresponding CD spectra were truncated where the absorbance exceeded 1.0 AU. The wavelength range (spectral cut-off) for SRCD spectra was based on both (i) the known absorbance of spot 2 by the Chirascan and (ii) the obtained PMT (HV) spectrum (cut off above 600 V) which was recorded for each spot (1, 2 and 3) of the samples on the SRCD instrument at module A.

To ascertain if any potential LD and LB contributions were present, SRCD measurements of spot 2 at two different orientations (0° and 90°) were undertaken. This was achieved by use of a rotating platform upon which the cell holder was placed (Figure 4.1). Homogeneity checks of the hydrogels consisted of comparison of SRCD spectra obtained at three different sites of the same sample (spots 1, 2 and 3). CD measurements using the Chirascan spectrophotometer and module A of the same sample allowed subsequent comparison of conventional CD and SRCD spectra of the samples. Any potential differences in the obtained CD profiles were primarily attributed to the difference of the cross-sectional area of the beam light of each instrument.

For the evaluation of the thermal disruption (gel-sol) and reformation (sol-gel) of hydrogels, gel specimens were heated for 30 minutes at 85 °C using a Peltier thermostated cell holder. To allow reformation of the gels, the samples were left at room temperature overnight. CD spectra were acquired before, during and after heating (hourly intervals) to evaluate the reversibility of the self-assembly process.

Finally, the obtained CD spectra for all measurements were baseline corrected. CD spectra of water, PBS solution and methanol were recorded prior to any measurement of the gel specimens, using the same cell, *i.e*. type and path length. The CD spectrum of the solvent was then subtracted from that of the corresponding spectrum.

4.4 Results and discussion

Fmoc-F-F **68** is one of the most well-known gelators and its corresponding gels have been extensively studied.[15,16] However, during the current project its gelation was triggered by sonication only rather than using the reported trigger of sequential change in pH. Therefore, hydrogel **E** can be considered a different material relative to those already reported in literature. Indeed, the free carboxylic group (COO^-) is responsible for its ionic character when pH is changed, while when gelation is triggered by sonication the acid could be in COOH form thus the organization of supramolecular interactions may differ *e.g.* achieved by a combination of π-π stacking and H-bonding. By contrast, the thermally induced self-assembly of carbohydrate-based hydrogels **62**, **63** reported here is based on CH-π interactions, as indicated by Birchall and co-workers.[14] From review of literature, no SRCD studies have been reported for hydrogel samples **A**-**E** except for the recently published current project.[11]

4.4.1 Evaluation of LD and LB contributions in SRCD spectra

To evaluate the contribution of LD and LB to the SRCD spectra, measurements were acquired on spot 2 of each sample at two different orientations. The obtained spectra of gel specimens **A**-**E** are given below (Figure 4.9).

According to the data obtained, the SRCD profiles of galactosamine-based **62** hydrogels **A**-**C** showed no significant LD or LB contributions. Specifically, the SRCD spectra of sample **A** were orientation independent and superimposable, indicating the absence of any optical artefacts. In contrast, samples **B** and **C** were orientation dependent, as their CD profiles were not identical upon rotation (Figure 4.9-ii and iii). Although no shifts were present, a difference in intensity was observed. Therefore, to verify whether or not the two orientation-dependent spectra resulted from a different supramolecular structure or to optical artefacts, further data processing was attempted.

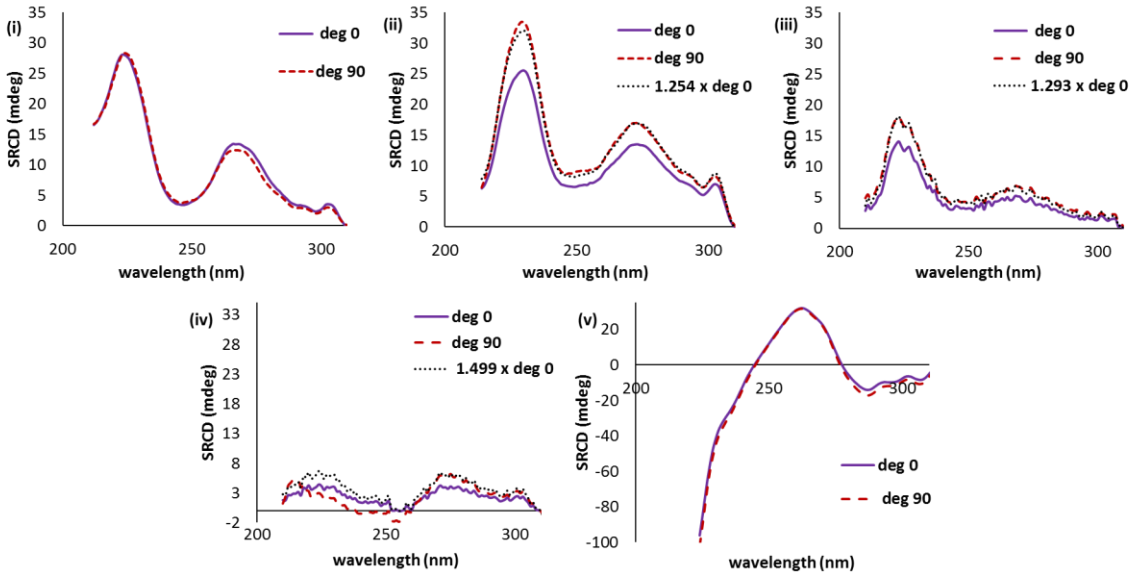

Figure 4.9 Evaluation of LD and LB contribution. SRCD spectra were obtained at 0° and 90° orientations. (i) hydrogel **A** of **62** in water triggered thermally (0.1 mm PL cell); (ii) hydrogel **B** of **62** in PBS triggered by sonication (0.2 mm PL cell); (iii) hydrogel **C** of **62** in PBS triggered thermally (0.1 mm PL cell); (iv) hydrogel **D** of **63** in water triggered thermally (0.2 mm PL cell); (v) hydrogel **E** of **68** in PBS triggered by sonication (0.1 mm PL cell).

By multiplying the two spectra by a numerical factor, it was possible to superimpose the spectra. This indicated that the CD differences upon orientation could be attributed to concentration variations within the gel's matrix and not due to LD or LB. It is noted that the term "concentration variations" is equal to the term "variations in the topology of the supramolecular matrix". The matrix concentration at the same spot of a single specimen had to remain constant upon rotation though. In fact, as the cells were laid horizontally on the sample holder in module A, no such differences due to thickness variations were expected since any gravitational movement of the gels within the cells was impossible. Alternatively, thickness variation was expected due to the very short path length as gelation in the cell may not be completely uniform. Further to this, the non-superimposable spectra could be explained by the ellipsoidal shape of the beam light cross section, which sampled a slightly different area of 'spot 2' upon rotation.

Overall the CD profiles of hydrogels **C** (gelled in PBS thermally), **A** (gelled in water thermally) and **B** (gelled in PBS by sonication) were similar for maxima and minima suggesting that similar interactions (exciton coupling) were occurring, however there was a marked change in intensity (reduced signal intensity of hydrogel **C**, Figure 4.9-iii). The intensity is indicative of the extent of conformational ordering, *i.e.* self-assembly and thus

gelation. It is clear that gelation thermally in water (hydrogel **A**) or in PBS by sonication (hydrogel **B**) gives the greatest CD intensity and thus presumably self-assembly by contrast to hydrogel formed in PBS thermally (hydrogel **C**).

The spectra of hydrogel **D** (from the glucosamine-based gelator **63**) were very weak compared to that of specimens **A**-**C** (Figure 4.9-iv). Previous gelation experiments (gelation was assessed by vial inversion method) showed that the hydrogel **D** samples were much weaker (soft and dynamic gels) compared to the stiffer hydrogels **A**-**C** produced by the epimeric gelator **62**. The CD spectra therefore indicated a lesser extent of assembly. The intensity differences between hydrogels **A**-**D** were apparent by both conventional and SRCD spectroscopy. Although hydrogel **D** was weaker under the given gelation conditions, a different gelation protocol reported by Birchall *et al.* showed the opposite, *i.e.* hydrogels prepared from **63** were stiffer than those generated from its epimer **62**.[14] These observations not only confirm the dynamic nature of supramolecular materials, but further suggest that different gelation triggers can direct the extent of molecular packing, *i.e.* to form different higher order architectures which are responsible for the diversity of the material's microscopic and macroscopic properties. In other words, different gelation triggers yield different gels.

Finally, the obtained SRCD spectra of hydrogel **E** were identical and superimposable. Therefore, the two non-orientation depended CD profiles confirmed the absence of LD and LB contributions. Interestingly, when a different gelation trigger (pH change) was applied to the hydrogelator Fmoc-FF **68** the reported spectra were consistent with those presented herein (Figure 4.9-v)[15,16]. This observation suggests a similar molecular packing despite the fact that two different gelation triggers were used. This is in marked contrast to gelators **62** and **63**, where altering their gelation conditions gave significant changes in the macroscopic properties of the resulting gels.

4.4.2 Evaluation of hydrogel homogeneity

Two features were considered for evaluation of sample homogeneity, that of the self-assembly itself and the consistency of the matrix topology formed. Therefore, by comparison of the CD spectral features of different 'spots' of the hydrogel sample, it was possible to assess the homogeneity of gels **A-E** and then correlate the CD profiles to either different molecular packings and/or differences in the matrix concentration/topology. SRCD measurements, taken at three different sites for each gel (spots 1,2 and 3) (as indicated in

Figure 4.1), showed almost identical CD profiles for spots 1 and 2, while spot 3 did not give comparable spectra (Figure 4.10).

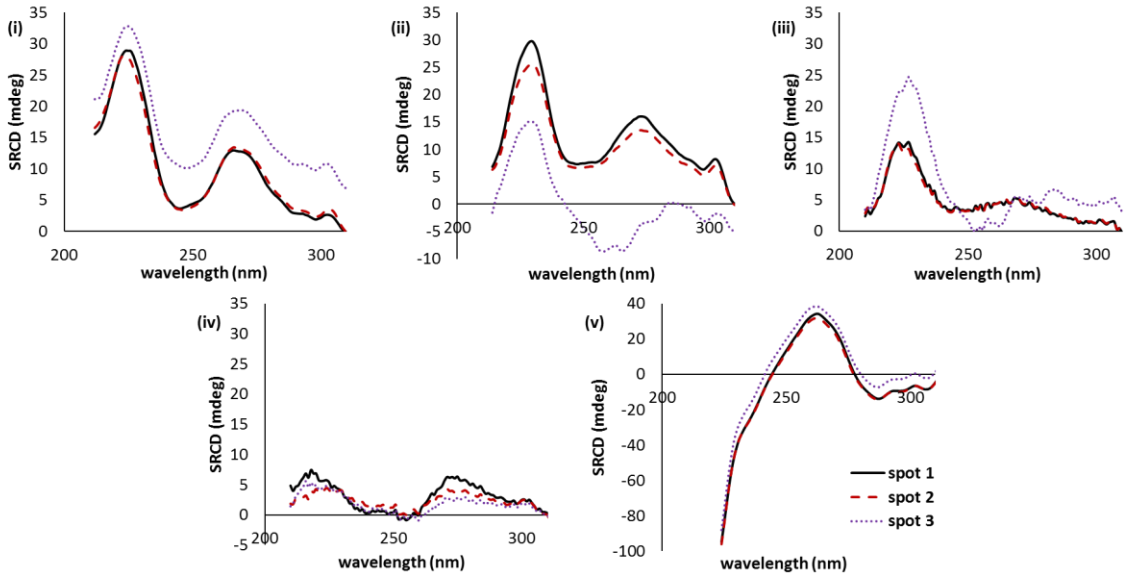

Figure 4.10 Evaluation of hydrogel homogeneity. (i) hydrogel **A** of **62** in water triggered thermally (0.1 mm PL cell); (ii) hydrogel **B** of **62** in PBS triggered by sonication (0.2 mm PL cell); (iii) hydrogel **C** of **62** in PBS triggered thermally (0.1 mm PL cell); (iv) hydrogel **D** of **63** in water triggered thermally (0.2 mm PL cell); (v) hydrogel **E** of **68** in PBS triggered by sonication (0.1 mm PL cell).

Hydrogel **A** (Figure 4.10-i) appeared to have similar homogeneity across sample sites 1-3 as the spectra of spots 1 and 2 were identical, while that of spot 3, although qualitatively comparable, differed in intensity. A similar trend was observed for hydrogel **B** (Figure 4.10-ii), although the CD of spot 3 was rather distorted around 260 nm. The results for hydrogel **C** (Figure 4.10-iii) were similar to those of **B**, while for hydrogel **D** (Figure 4.10-iv) all spectra were comparable in the near UV region but could only be described as inconsistent across the entire wavelength range. Finally, hydrogel **E** (Figure 4.10-v) gave identical spectra at spots 1 and 2, while that of 3, after offset, appeared comparable to the first two.

Due to the observed CD inconsistencies of spot 3 versus spots 1 and 2, the recorded PMT (photomultiplier tube) plots of HV (high voltage) for all sites 1-3 were checked (Figure 4.11). Indeed, for hydrogels **B** and **C** (Figure 4.11-ii and iii) the significant variation in PMT (HV) for spot 3 suggested that this site was too close to the cell wall, resulting in masking of the incident beam light. However, for hydrogels **A**, **D** and **E**, although PMT (HV) plots of spot 3 were consistent with those of spots 1 and 2, their corresponding SRCD spectra were

inconsistent. Therefore, for hydrogels **A**, **D** and **E**, the different SRCD spectra obtained for spot 3 are thus interpreted as a lack of homogeneity in the hydrogel sample in the cell.

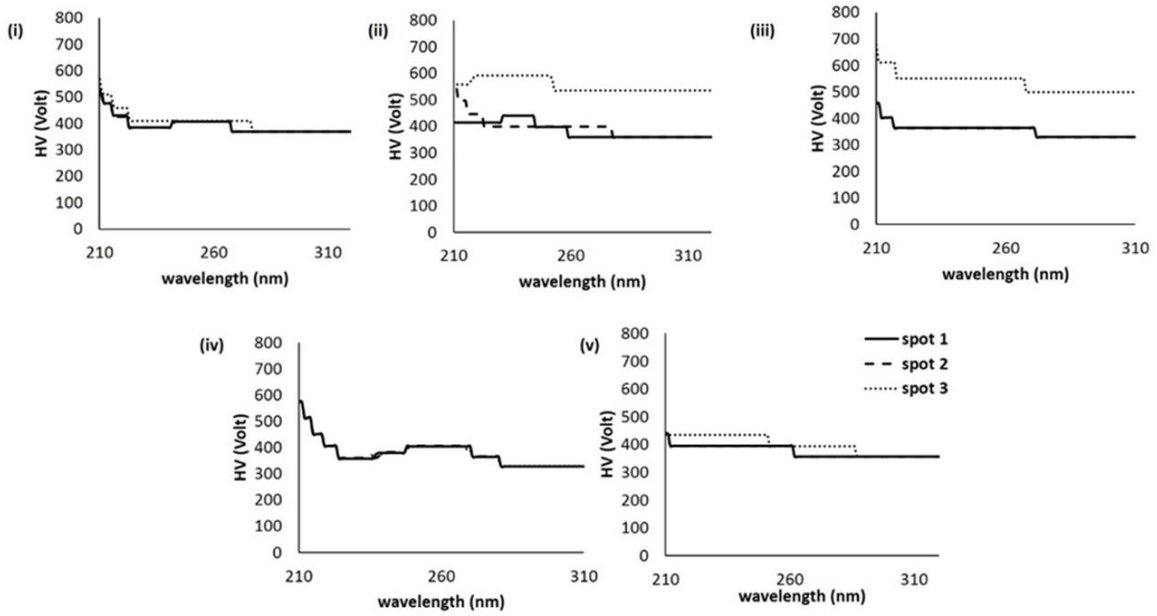

Figure 4.11 The PMT plots of HV for each of the SRCD spectra obtained from different sites/spots in a hydrogel sample. (i) GalNHFmoc hydrogel **A** in water triggered thermally (0.1 mm PL cell); (ii) GalNHFmoc hydrogel **B** in PBS triggered by sonication (0.2 mm PL cell); (iii) GalNHFmoc hydrogel **C** in PBS triggered thermally (0.1 mm PL cell); (iv) GlcNHFmoc hydrogel **D** in water triggered thermally (0.2 mm PL cell); (v) Fmoc-F-F hydrogel **E** in PBS triggered by sonication (0.1 mm PL cell).

Supramolecular hydrogels are highly dynamic systems in nature and their matrix topology can be affected by the shape and volume of the vessel in which they were formed. Therefore, the observed variations of the matrix topology at spot 3, closer to the cell wall, were colloquially described as a "wall effect". Unfortunately, due to the nature of sampling and technical restrictions it was not possible to further evaluate the molecular packing of the samples near the cell wall. To better facilitate future studies, new experimental procedures will need to be developed for the detailed X-Y mapping of the gels, in order to map more effectively sample sites adjacent to the cell wall.

4.4.3 Comparison of conventional and SRCD spectroscopy

CD spectra were acquired using both benchtop instruments (Chirascan spectrophotometers) and by SRCD instrumentation at Diamond Light Source. The use of the B23 beam line at Diamond Light Source (for SRCD measurements) provided spectral features with an

enhanced resolution due to the greater intensity of synchrotron beam light (greater photon flux) and thus reduced the signal-to-noise ratio compared to conventional instruments – especially in the far-UV region. The smaller cross-sectional area (*ca.* 250 μm) of the synchrotron beam, in contrast to that of the Chirascan instrument, which covers on average a 16-mm diameter area, is also beneficial for signal-to-noise and allows multi-site sampling.

It is of note that conventional CD measures the average chirality of the supramolecular network (*i.e.* samples the whole cell area simultaneously) whereas SRCD allows measurement of multiple sites (*i.e.* selected regions such as spots 1, 2 and 3). Therefore, this study demonstrated that the homogeneity of gel specimens **A**-**E** would be better assessed by comparison of SRCD and conventional CD, *i.e.* if a difference could be seen by sampling a larger area relative to a smaller one (Figure 4.12). Indeed, any similar spectral features, in terms of intensity and sign, would therefore indicate a consistency of matrix topology, thus confirming the homogeneity of the samples.

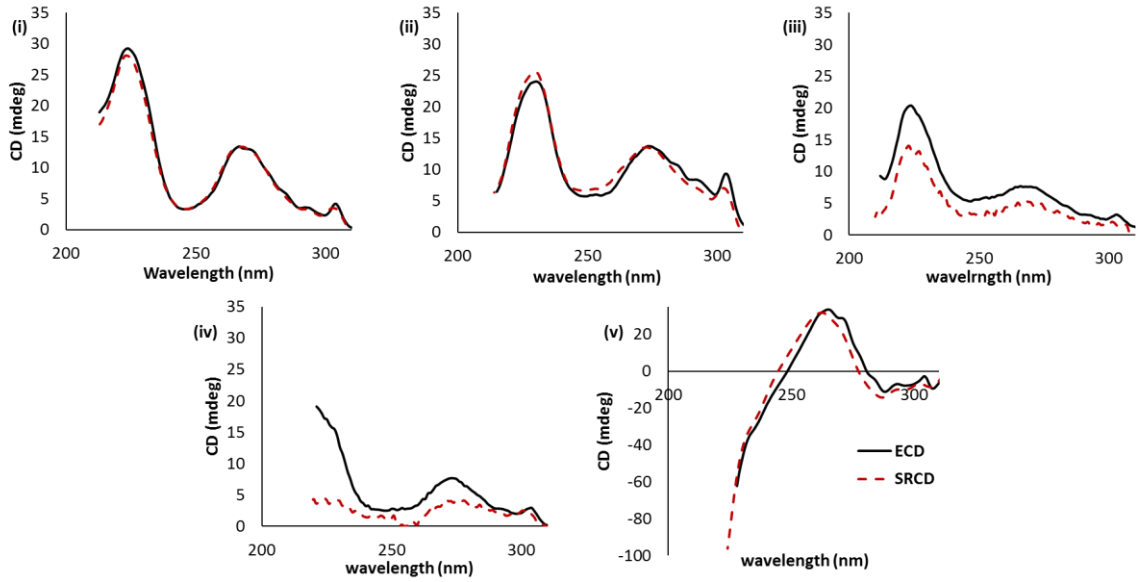

Figure 4.12 Comparison of conventional (ECD) and SRCD spectra. (i) hydrogel **A** of **62** in water triggered thermally (0.1 mm PL cell); (ii) hydrogel **B** of **62** in PBS triggered by sonication (0.2 mm PL cell); (iii) hydrogel **C** of **62** in PBS triggered thermally (0.1 mm PL cell); (iv) hydrogel **D** of **63** in water triggered thermally (0.2 mm PL cell); (v) hydrogel **E** of **68** in PBS triggered by sonication (0.1 mm PL cell).

In terms of signal intensity and sign, both the conventional and SRCD spectra, together with absorbance spectra (Figure 4.13) appeared qualitatively similar for hydrogels **A**, **B** and **E**, suggesting they were homogeneous. In fact, the observed higher absorbance intensity in

conventional spectroscopy can be interpreted as being due to the greater extent of self-assembly that the instrument can sample relative to the smaller sampling area of SRCD.

The greatest differences in CD intensity were observed in hydrogel samples **C** and **D** (Figure 4.12-iii and iv). The SRCD spectra acquired at different sample sites for hydrogel **C** (Figure 4.10-iii) gave identical profiles for spots 1 and 2, but spot 3 was distorted, presumably due to masking of the beamlight. Conventional CD appeared qualitatively similar to SRCD, differing only in intensity. Therefore, as both spectral features were comparable, hydrogel **C** was characterized as homogeneous. In contrast, hydrogel **D** was already known to be a dynamic soft material with a lesser extent of self-assembly compared to the other specimens. Considering the difference in sampling areas upon which incident light reaches, the observed inconsistencies of the obtained CD profiles were expected and, thus, sample **D** was characterized as heterogeneous.

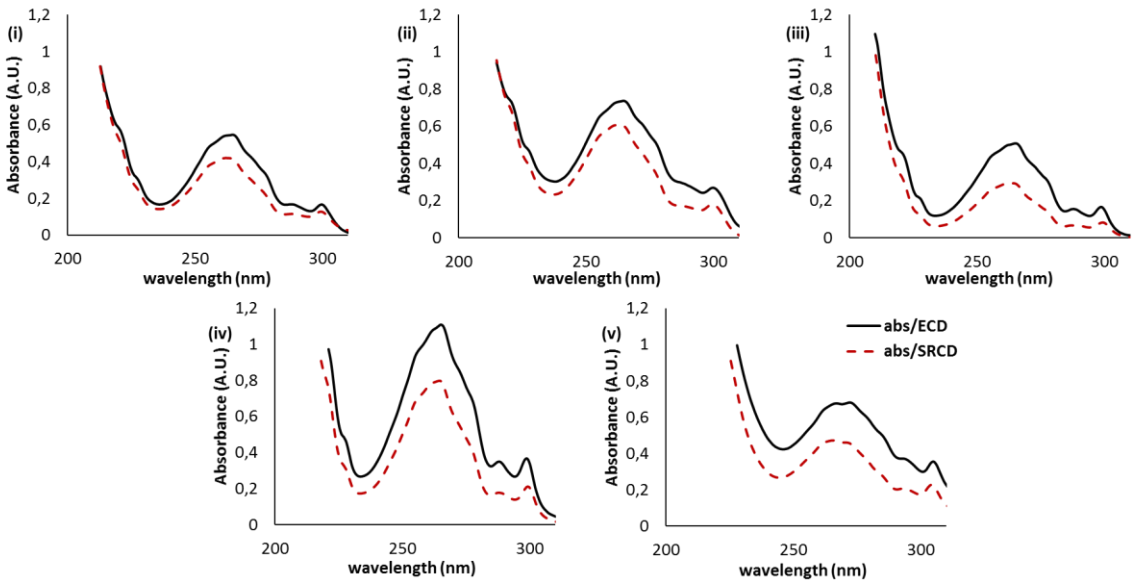

Figure 4.13 Comparison of the absorbance spectra from CD (Chirascan) and SRCD instruments showing the spectral differences arising from differing cross sectional areas of the beam. (i) hydrogel **A** of **62** in water triggered thermally (0.1 mm PL cell); (ii) hydrogel **B** of **62** in PBS triggered by sonication (0.2 mm PL cell); (iii) hydrogel **C** of **62** in PBS triggered thermally (0.1 mm PL cell); (iv) hydrogel **D** of **63** in water triggered thermally (0.2 mm PL cell); (v) hydrogel **E** of **68** in PBS triggered by sonication (0.1 mm PL cell).

4.4.4 Thermal studies

The reversibility of the self-assembly process (gel-sol-gel reversibility) was assessed by thermal disruption of the formed hydrogels and subsequently allowing the gelation to

reoccur. Therefore, hydrogel specimens **A**, **B** and **E** were studied as a function of temperature with comparison of the CD spectra obtained before, during and after heating. Due to the large cross-sectional beamlight area in conventional CD, it was observed that the reformation of thermally broken hydrogels was better monitored by benchtop CD rather than SRCD.

The absorbance spectra of the gels were expected to be similar to those of the "broken gels", with no major differences in intensity. However, a collapsed CD spectrum (negligible signal) should be observed for all thermally destroyed hydrogels (Figures 4.15 and 4.16). Compared to the corresponding CD profile of the initial unheated hydrogels, the collapsed CD would indicate the presence of cancellation due to opposite chirality or different sample orientation, with electronic transitions perpendicular to the direction of propagation of incident light. On heating, the supramolecular network is disrupted, as the non-covalent interactions responsible for the coherence of the formed matrix are now broken. The CD spectrum of a broken gel would thus become like an oriented one, resembling that of its corresponding solution. Such a case is illustrated in figure 4.14 for the GalNHFmoc **62**-based hydrogel **A** by comparison of the CD spectra (Figure 4.14-left) acquired before heating (initial gel), after heating (thermally destructed gel) and that of its corresponding methanolic solution. By contrast, the given absorbance (Figure 4.14-right) of the broken gel and the solution of gelator **62** has a greater intensity compared to the initial gel **A** (Figure 4.14 right). This is due to the increased solubility of hydrogelator **62**, resulting from the elevated temperature, which leads to its increased concentration in the sol state.

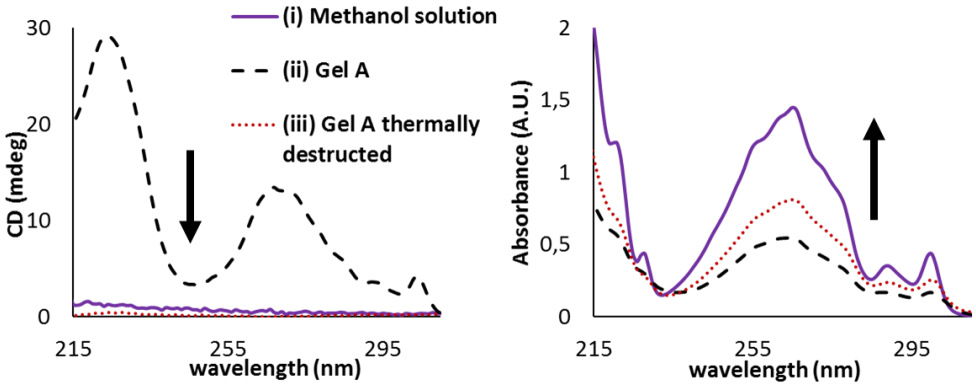

Figure 4.14 CD (left) and absorbance (right) spectra of GalNHFmoc **62** as a MeOH solution and as a hydrogel before and after heating in a cylindrical non-demountable cell (PL 0.1 mm): (i) solution in MeOH (3.0 mg/mL); (ii) hydrogel **A** in water (2.0 mg/mL), thermally triggered - initial gel; (iii) hydrogel **A** in water (2.0 mg/mL), thermally triggered – after thermal destruction.

Through comparison of the CD spectra during the gel-sol-gel process (Figure 4.15-i and ii), it was found that the thermally destroyed, carbohydrate-based hydrogels **A** and **B** were able to change from their initial CD profiles to a negligible CD signal, similar to that of their corresponding methanolic solutions (see appendix). However, the thermally destroyed hydrogel **E** (Figure 4.15-iii) did not revert to a negligible CD spectrum, suggesting that its self-assembly persisted to some extent after heating.

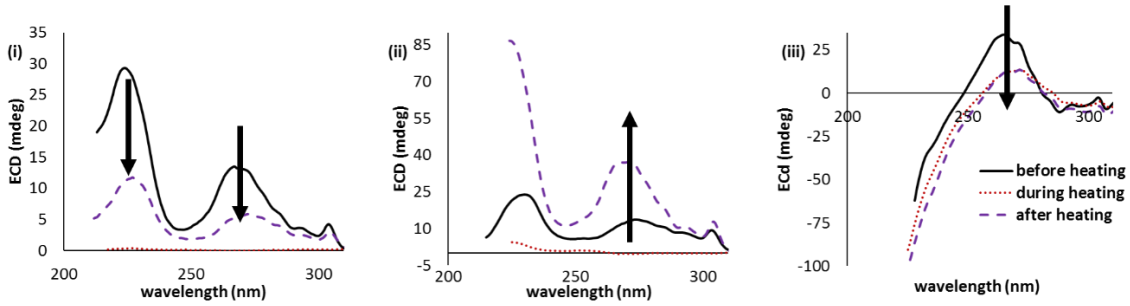

Figure 4.15 Thermal studies - evaluation of the reversibility of gelation. (i) hydrogel **A** of **62** in water triggered thermally (0.1 mm PL cell); (ii) hydrogel **B** of **62** in PBS triggered by sonication (0.2 mm PL cell); (iii) hydrogel **E** of **68** in PBS triggered by sonication (0.1 mm PL cell).

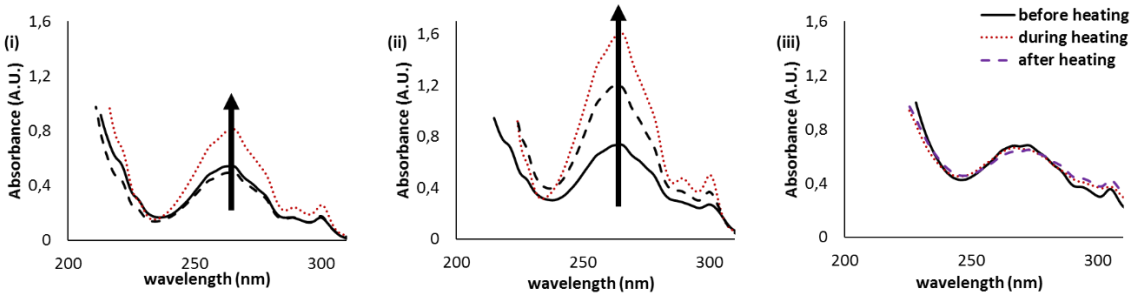

Figure 4.16 The absorbance spectra for the thermal studies of hydrogels to ascertain the contribution of the self-assembly to the spectrum and the reversibility of gelation. (i) hydrogel **A** of **62** in water triggered thermally (0.1 mm PL cell); (ii) hydrogel **B** of **62** in PBS triggered by sonication (0.2 mm PL cell); (iii) hydrogel **E** of **68** in PBS triggered by sonication (0.1 mm PL cell).

Further to this, the observed variations in CD signal intensity before and after heating, could be attributed to the difference of the thermal disruption process compared to the initial gelation method (see figure 4.15 arrows). Differences in gelation conditions can have a profound effect on self-assembly. Indeed, the initial CD signal after the gel-sol-gel process was increased for hydrogel **B** and decreased for specimens **A** and **E**. Hydrogel **A** was initially gelled by a controlled heating/cooling rate, whereas gelation of hydrogels **B** and **E** was triggered by sonication only. Specifically, the increased intensity observed for hydrogel **B**

could suggest either that *in situ* gelation did not fully occur during the first sol-gel cycle and/or that the extent of self-assembly increased during the second sol-gel cycle or the type of self-assembly could have changed (*i.e.* kinetic vs thermodynamic).

4.5 CD alterations due to self-assembly differences

The project clearly demonstrates that gelator molecules have different tolerances for gelation triggers and their corresponding environments. Indeed, GalNHFmoc **62** proved to be the most versatile and robust hydrogelator, as it gelled both water and PBS solution, either by sonication only or by a controlled heating/cooling process, yielding hydrogels **A**, **B** and **C** (Figure 4.17).

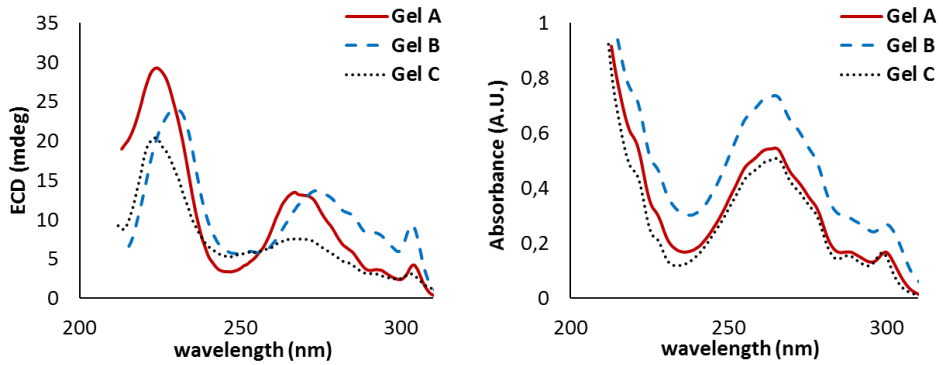

Figure 4.17 Conventional CD (left) and absorbance (right) spectra of hydrogels of GalNHFmoc **62** prepared by different gelation conditions. Gel **A** in water triggered thermally (0.1 mm PL cell); Gel **B** in PBS triggered by sonication (0.2 mm PL cell); Gel **C** in PBS triggered thermally (0.1 mm PL cell). All samples were gelled in the cell (0.1 mm PL) at a concentration of 2.0 mg/mL.

The spectral features of samples **A-C** appeared qualitatively similar (two positive CD bands at *ca.* 220 and 270 nm), although hydrogel **B** was slightly red shifted and differed also in absorbance (higher intensity). Such variations suggest that, under different gelation conditions (gelation triggers and solvent used), different modes of self-assembly could lead to different molecular packing. Additionally, simple modifications of the structure of the gelator molecules are also responsible for different gelation behaviours. For example, the carbohydrate-based gelators **62** and **63**, although differing only in one chiral centre, yielded hydrogels with different microscopic and macroscopic properties. Hydrogels from **63** were dynamic and soft in nature, presumably due to a lesser extent of self-assembly compared to its epimer **62**.

4.6 Conclusions

The combined use of conventional CD and SRCD spectroscopy provided a wealth of information about LMW hydrogels. Specifically, SRCD proved advantageous, compared to conventional CD, due to the collimated beam which gave a small cross-sectional area for the beam which allowed the evaluation of the specimens' homogeneity by multisite sampling. Data acquisition of a single site in two different orientations showed that there were no significant LD and LB contributions to SRCD spectra with the exception of GlcNHFmoc **63** based hydrogel (which was known for its soft nature, as confirmed by the vial inversion method). The nature and extent of homogeneity of the tested gel specimens was assessed *via* SRCD analysis using multisite sampling combined with comparison to conventional CD spectra. The observed differences in homogeneity of the peptide-based hydrogel **E**, compared to the carbohydrate-based hydrogels **A**-**D,** could be attributed to a different mode of self-assembly related to its ionic character. In addition, a high CD signal was attributed to the greater extent of self-assembly measured by conventional CD relative to a smaller sampling area analyzed by SRCD. Thermal studies showed that the Fmoc-peptide based hydrogel maintained, to some extent, it's self-assembly after 30 minutes of heating and that the CD intensity was altered for some gel specimens after the second sol-gel cycle.

In conclusion, the above methods described can be successfully used for quality control to assess gelation and to obtain the required specifications and properties of the formed gels. Since only a limited number of protocols and methods have been reported for the study of LMW hydrogels, the work reported herein describes for the first time a robust protocol to investigate the self-assembly of chiral hydrogelators *via* CD spectroscopy, the results of which have been published recently by our group.[11]

4.7 References

(1) Du, X.; Zhou, J.; Shi, J.; Xu, B. Supramolecular Hydrogelators and Hydrogels: From Soft Matter to Molecular Biomaterials. *Chem. Rev.* **2015**, *115* (24), 13165-13307.

(2) Liu, J.; Sun, Z.; Yuan, Y.; Tian, X.; Liu, X.; Duan, G.; Yang, Y.; Yuan, L.; Lin, H. C.; Li, X. Peptide Glycosylation Generates Supramolecular Assemblies from Glycopeptides as Biomimetic Scaffolds for Cell Adhesion and Proliferation. *ACS Appl. Mater. Interfaces* **2016**, *8* (11), 6917-6924.

(3) Yoza, K.; Amanokura, N.; Ono, Y.; Akao, T.; Shinmori, H.; Takeuchi, M.; Shinkai,

S.; Reinhoudt, D. N. Sugar-Integrated Gelators of Organic Solvents-Their Remarkable Diversity in Gelation Ability and Aggregate Structure. *Chem. Eur. J.* **1999**, *5* (9), 2722-2729.

(4) Smith, D. K. Lost in Translation? Chirality Effects in the Self-Assembly of Nanostructured Gel-Phase Materials. *Chem. Soc. Rev.* **2009**, *38* (3), 684-694.

(5) Amdursky, N.; Stevens, M. M. Circular Dichroism of Amino Acids: Following the Structural Formation of Phenylalanine. *ChemPhysChem* **2015**, *16* (13), 2768-2774.

(6) Jung, J. H.; Rim, J. A.; Han, W. S.; Lee, S. J.; Lee, Y. J.; Cho, E. J.; Kim, J. S.; Ji, Q.; Shimizu, T. Hydrogel Behavior of a Sugar-Based Gelator by Introduction of an Unsaturated Moiety as a Hydrophobic Group. *Org. Biomol. Chem.* **2006**, *4* (10), 2033-2038.

(7) Pescitelli, G.; Di Bari, L.; Berova, N. Application of Electronic Circular Dichroism in the Study of Supramolecular Systems. *Chem. Soc. Rev.* **2014**, *43* (15), 5211-5233.

(8) Pescitelli, G.; Di Bari, L.; Berova, N. Conformational Aspects in the Studies of Organic Compounds by Electronic Circular Dichroism. *Chem. Soc. Rev.* **2011**, *40* (9), 4603-4625.

(9) Berova, N.; Di Bari, L.; Pescitelli, G. Application of Electronic Circular Dichroism in Configurational and Conformational Analysis of Organic Compounds. *Chem. Soc. Rev.* **2007**, *36* (6), 914-931.

(10) Yu, G.; Yan, X.; Han, C.; Huang, F. Characterization of Supramolecular Gels. *Chem. Soc. Rev.* **2013**, *42* (16), 6697-6722.

(11) Sitsanidis, E. D.; Piras, C. C.; Alexander, B. D.; Siligardi, G.; Javorfi, T.; Hall, A. J.; Edwards, A. A. Circular Dichroism Studies of Low Molecular Weight Hydrogelators: The Use of SRCD and Addressing Practical Issues. *Chirality* **2018**, 1-11.

(12) Hussain, R.; Jávorfi, T.; Siligardi, G. Circular Dichroism Beamline B23 at the Diamond Light Source. *J. Synchrotron Radiat.* **2012**, *19* (1), 132-135.

(13) Hussain, R.; Jávorfi, T.; Rudd, T. R.; Siligardi, G. High-Throughput SRCD Using Multi-Well Plates and Its Applications. *Sci. Rep.* **2016**, *6*, 1-6.

(14) Birchall, L. S.; Roy, S.; Jayawarna, V.; Hughes, M.; Irvine, E.; Okorogheye, G. T.; Saudi, N.; De Santis, E.; Tuttle, T.; Edwards, A. A.; et al. Exploiting CH-π Interactions in Supramolecular Hydrogels of Aromatic Carbohydrate Amphiphiles. *Chem. Sci.* **2011**, *2* (7), 1349-1355.

(15) Smith, A. M.; Williams, R. J.; Tang, C.; Coppo, P.; Collins, R. F.; Turner, M. L.; Saiani, A.; Ulijn, R. V. Fmoc-Diphenylalanine Self Assembles to a Hydrogel via a Novel Architecture Based on π-π Interlocked β-Sheets. *Adv. Mater.* **2008**, *20* (1), 37-41.

(16) Zhou, M.; Smith, A. M.; Das, A. K.; Hodson, N. W.; Collins, R. F.; Ulijn, R. V.; Gough, J. E. Self-Assembled Peptide-Based Hydrogels as Scaffolds for Anchorage-Dependent Cells. *Biomaterials* **2009**, *30* (13), 2523-2530.

5. BIOCOMPATIBILITY STUDIES OF LMW HYDROGELS

5.1. Introduction

The current research project was aimed at the preparation of supramolecular hydrogels to be used as functional biomaterials, capable of mimicking the extracellular matrix (ECM) and encapsulating cells within their three-dimensional fibrous network. Part of this work has involved the preliminary evaluation of the hydrogels' biocompatibility, *i.e.* exploring their cytotoxicity towards and their impact on the proliferation of mammalian cells. The cells, after implantation on the surface of the gel samples (two-dimensional cell culture), were expected to either adhere to or migrate within the inner fibrous network. Within a biocompatible environment, the cells' phenotype should not change, their metabolic activity should function normally and proliferation should be observed during the first 24 hours. The performed biocompatibility studies focused on the effect of the following on cell proliferation: structural features of the hydrogelators and the matrix topology of their corresponding gels. It was expected to obtain different biocompatibility profiles since the formed hydrogels showed different macroscopic and microscopic properties. For clarity reasons, hydrogel specimens were categorized according to the structural features of their corresponding gelator molecules (building blocks).

The first set of samples consisted of gels prepared from the Fmoc-based hydrogelators (GalNHFmoc **62**, GlcNHFmoc **63**, GalNH-F-Fmoc **111** and Fmoc-F-F **68**). The second set was prepared from the cinnamoyl capped diphenylalanine peptides (Cin-F-F **70** and the epimeric mixture Cin-L/D-F-L-F **70/93**). The third set consisted of hydrogelators bearing the diclofenac moiety (GalNH-Diclofenac **113**, GlcNH-Diclofenac **114**) and the fourth set comprised the indomethacin-based hydrogelators (GalNH-Indomethacin **115**, GlcNH-Indomethacin **116**) (Figure 5.1).

According to literature,[1–4] special characteristics of the biomaterials inner structure (matrix topology) such as the shape, size and alignment of fibres, are responsible either for cell death (apoptosis) or proliferation. The cells' viability depends on whether or not the fibrous three-dimensional network emulates the functionality of the mammalian ECM. Indeed, the development of non-covalent intermolecular interactions, such as H-bonds, π-π interactions, electrostatic forces and the presence of hydrophobic and hydrophilic domains, defines the

matrix topology of the formed fibrous network. This then determines the properties of the hydrogels, such as stiffness, functionality and biocompatibility[5–7].

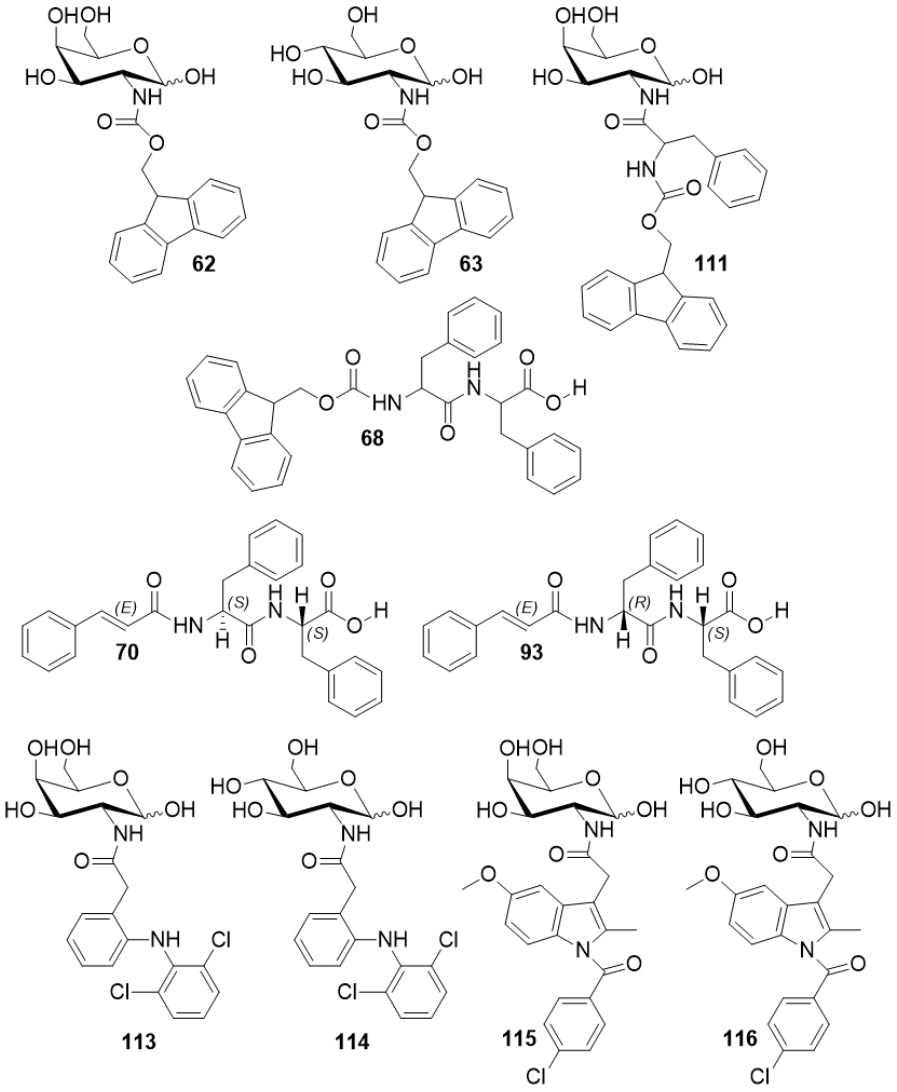

Figure 5.1 Chemical structures of the hydrogelator molecules.

5.2 Experimental design-practical considerations

In an effort to evaluate the cytotoxic effects of the above hydrogelators, a concentration dependent test had to be undertaken. Therefore, stock solutions of the hydrogelators in DMSO were initially prepared followed by serial dilutions using either water or PBS solution. It is of note that, solutions had to be prepared with the aim to achieve final concentrations of the hydrogelators within the cell culture, to be around the ordinary limits of cytotoxicity studies (0.05-0.5 mM)[8–10] and the final concentration of DMSO as 1% v/v. However, due to the hydrogelators amphiphilic nature their solubility in water, PBS solution, cell medium and DMSO was poor and this approach had to be withdrawn.

Instead of using solutions, cytotoxicity was evaluated by testing broken hydrogels formed either in water or PBS solution. However, Cin-F-F **70** did appear to be soluble in DMSO within the permitted range of concentrations which allowed the use of its solutions for a concentration depended cytotoxicity study followed by a live-dead staining assay (fluorescence microscopy).

Having already characterized the structural features of the synthesized hydrogelators and their mode(s) of self-assembly, it was important to proceed with the preliminary biocompatibility evaluation of their corresponding hydrogels. The results were expected to be influenced by the microenvironment in which the cells were growing. Different microenvironments were informed by the differences in the supramolecular cohesion of each gel, as directed by the standard gelation protocol for each hydrogelator as well as the chemical structure. The main goal was to investigate if different supramolecular networks would affect the viability of the same cell line. In addition, the stability and stiffness of all hydrogel samples under the used cell culture conditions had to be explored.

Before conducting any tests on the hydrogels, it was necessary to first identify a suitable cell line to be a model for the biological studies. There is a plethora of examples in the literature referring to encapsulated cell types being used when evaluating the biocompatibility of supramolecular scaffolds.[11–14] Specifically, for those materials used in regenerative medicine applications, cell types are selected in accordance to the chosen tissue to be engineered. Alternatively, for studies regarding the treatment of diseases related to secreted therapeutic proteins, both the cell type and the tissue affected play a significant role in biological studies.[15] In other cases, the nature of the biomaterial can influence the proliferation of different cell types, as reported by Suuronen and co-workers in the example of heart repair and regeneration after myocardial infraction.[16] Finally, supramolecular biomaterials can also be used as targeted therapeutic agents, especially if triggering of gelation is cell specific.[17]

For all experiments reported herein, the glioblastoma cancer cell line U87MG was used. Glioblastoma multiforme (GBM) is the most common and aggressive primary brain tumor in adults. Recent studies revealed that the spread of single GBM cells into the brain's parenchyma, causing metastasis, is due to the intracellular interactions with the microenvironment of the tumor.[18,19] In fact, the cell proliferation and infiltration are based on signaling pathways and the expression of proteins which are stimulated by the presence of primary components of the brain's ECM, such as collagen and hyaluronic acid. Another

example of this interplay between the supramolecular scaffold of brain tissue and GBM cells is that they rarely metastasize in other organs as they do not invade into the walls of blood vessel.[19]

Since differences in the chemical structure of the hydrogelator molecules leads to a unique self-assembly mode and thus a specific matrix topology of their supramolecular hydrogels (different microenvironments), the ability of the encapsulated GBM cells to grow and proliferate within each hydrogel was expected to be different.

5.3 Materials and methods

Human glioblastoma cell line U87MG (ATCC, HBT-14, grade IV WHO classification) was purchased from American Type Culture Collection (ATCC Manassas, VA, USA).

U87MG cells were maintained in a fully supplemented (complete) DMEM medium (Dulbecco's Modified Eagle Medium) with 10% FBS (Fetal Bovine Serum), 1% Antibiotic/Antimicotic and 1% sodium pyruvate. DMEM, Antibiotic/Antimicotic and FBS were purchased from Gibco by Life Technologies. Sodium pyruvate was purchased from Sigma Aldrich.

Cell splitting: The cell culture medium, Ca^{2+}/ Mg^{2+}-free Dulbecco's Phosphate Buffered Saline (DPBS), was removed from the original cell culture and the adhered layer of U87MG cells was washed once with DPBS (10 mL) to remove any serum containing trypsin inhibitors. Addition of trypsin-EDTA solution (2 mL) and incubation of the flask at 37 °C under a 5% CO_2 atmosphere for 5 minutes resulted in the dispersion of the cells, which were then further diluted by adding 10 mL of complete DMEM medium and were gently aspirated with a pipette. The cell suspension was centrifuged for 5 minutes (125 rpm) and the formed pellet was re-suspended in complete DMEM medium (10 mL).

Cell counting: The cell suspension (30 μL) was transferred to an Eppendorf tube and mixed with trypan blue solution (30 μL). Aliquots of the dark blue mixture (10 μL) were then pipetted into each chamber of a hemocytometer and cells were counted under an inverted phase light microscope (20x magnification).

Preparation of hydrogels: For each hydrogelator, gels were prepared in a vial as per the standard protocol(s) (see chapter 3), either in water or PBS solution, and were left undisturbed at room temperature overnight. 50 μL of each gel was transferred by

micropipette into each well of a 96-well flat-bottomed plate and sterilized under UV light irradiation for three hours. Before cell seeding, the plate was placed in an incubator at 37 °C under 5% of CO_2 atmosphere for at least half an hour.

Cell seeding[10]: 100 μL of the cell suspension in complete DMEM medium, containing the appropriate number of cells, were pipetted on top of the gel surface (Figure 5.2). For both cytotoxicity and proliferation studies, 5000 cells were transferred into each well. That was due to the small surface area of the wells and the steep gradient of the calibration curve (Figure 5.2). The cells would need a larger area to attach if more than 5000 and it would be difficult to calculate their number as above 10000 the gradient of the calibration curve was not that steep. Buffer exchange of the gels with complete DMEM medium was not undertaken before the seeding of cells as it was noticed that the gels were breaking.

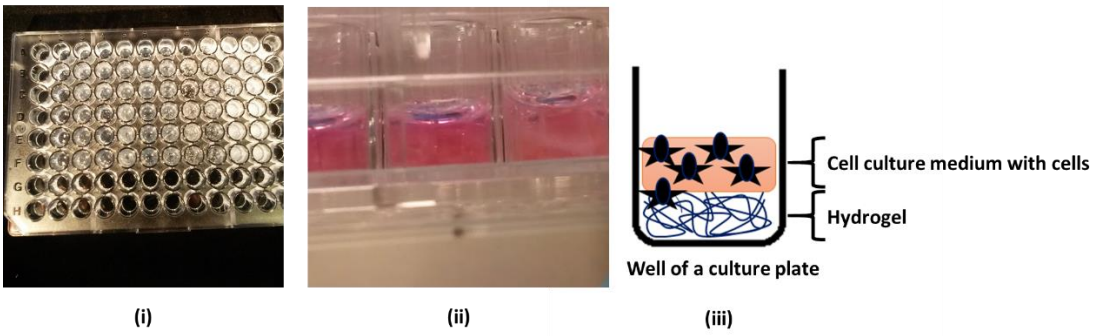

Figure 5.2 Cell culture using a 96 well flat bottom plate (i) transferring of gels into the wells (ii) addition of cell culture medium and cells upon the gels surface (iii) schematic depiction of the cell culture.

Cell viability and proliferation tests: The time points for both the cytotoxicity and proliferation studies were set as 24 and 48 hours for each sample. The number of metabolically active cells was assessed by using a CellTiter 96 AQ_{ueous} One Solution Proliferation Assay (MTS assay, Promega). MTS solution (20 μL) was pipetted into each well and the plate was left in the incubator for one hour at 37°C. Subsequently, the absorbance at 490 nm was measured using a Tecan Infinite 200 Pro multifunctional microplate reader after the plate had been shaken for 5 seconds (orbital orientation). The approximate number of viable cells was estimated using a calibration curve that was previously generated using the standard MTS assay protocol (Figure 5.3).

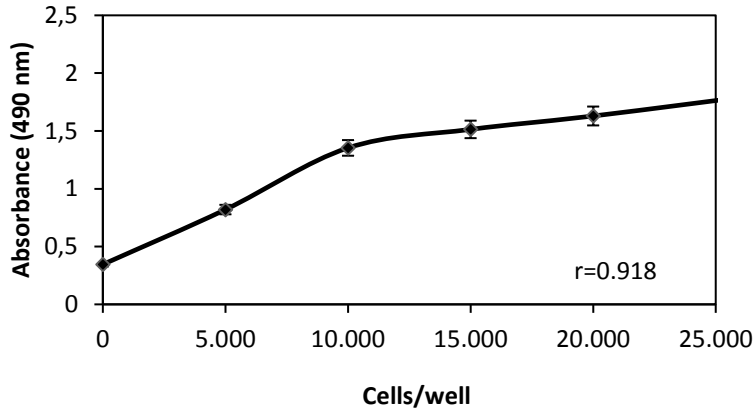

Figure 5.3 Calibration curve for U87MG cells obtained by the standard MTS assay protocol.

The cytotoxicity of the cells in gel samples (measured as percent of viable cells) was calculated by comparison of the number of untreated cells from the positive control. Untreated cells were incubated for an hour before addition of MTS solution. The incubation time with MTS solution was one hour. All experiments were performed in triplicate.

Live-dead staining: Evaluation of the cell viability was performed by a fluorescent live-dead assay (Invitrogen). The tested samples consisted either of gels or the hydrogelators solutions over a range of concentrations. In each well of a 96-well flat-bottomed plate, a solution of 4.0 μL of ethidium homodimer-1 (EthD-1) and 2.0 μL of calcein AM were added and the plate was left to rest for 20 minutes at room temperature. The cells were then viewed under an EVOS Floid cell imaging station fluorescent microscope (20x magnification). Viable cells were stained green while dead cells appeared red. Photographs were taken from four different sites of each well.

5.4 Results and discussion

In order to determine the optimal incubation time for treated and untreated cells (cells in gels and positive control respectively) and to establish a cell viability protocol suitable for all hydrogel samples, a colorimetric assay (MTS) was employed. Absorbance measurements were performed at 490 nm at intervals of 4, 8, 24 and 48 hours, using a model hydrogel **A** prepared from GalNHFmoc **62** in PBS solution. Therefore, 5000 cells were initially pipetted into each well (time t_o) while the number of cells was calculated based on the calibration curve for untreated cells (Figure 5.4). All measurements were performed based on the standard MTS colorimetric assay.

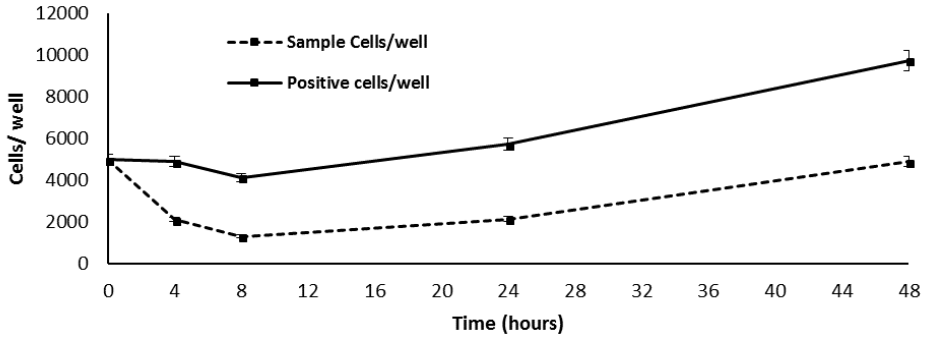

Figure 5.4 Initial monitoring of viable cells at different time intervals for treated and untreated cells.

From the findings, it was clear that by 8 hours of incubation a decrease in cell numbers occurred for both untreated and treated cells, possibly due to the trypsination of cells prior to addition in the wells. Moreover, incubation periods of 24 and 48 hours resulted in a clear increase in cell numbers, especially for the positive control, as within this timeframe they had adhered on the surface of the well (positive control) or the surface of hydrogel **A** (treated cells). This suggested that since the initial trypsinized cells of the positive control required at least 48 hours of incubation to reach numbers two folds greater than the initial population, all measurements had to be performed at two time intervals, *i.e.* 24 and 48 hours, for all gel samples.

Biocompatibility studies commenced with hydrogels made from the Fmoc-protected set of hydrogelators GalNHFmoc **62**, GlcNHFmoc **63**, GalNH-F-Fmoc **111** and Fmoc-F-F **68**. All hydrogels were prepared in vials as per the standard protocol (Table 5.1) and pipetted into the wells the next day. The obtained results after 24 and 48 hours of incubation are shown below (Figure 5.5).

Table 5.1 Gelation conditions for each compound of the Fmoc-protected set of hydrogelators. All gels were prepared in PBS solution.

Compound	**Gelation method**	**Concentration (mg/ mL)**	**Gel**
GalNHFmoc **62**	Sonication only	2.0	**A**
GlcNHFmoc **63**	Heating/cooling	3.0	**B**
GalNH-F-Fmoc **111**	Heating/cooling	2.0	**C**
Fmoc-F-F **68**	Sonication only	2.0	**D**

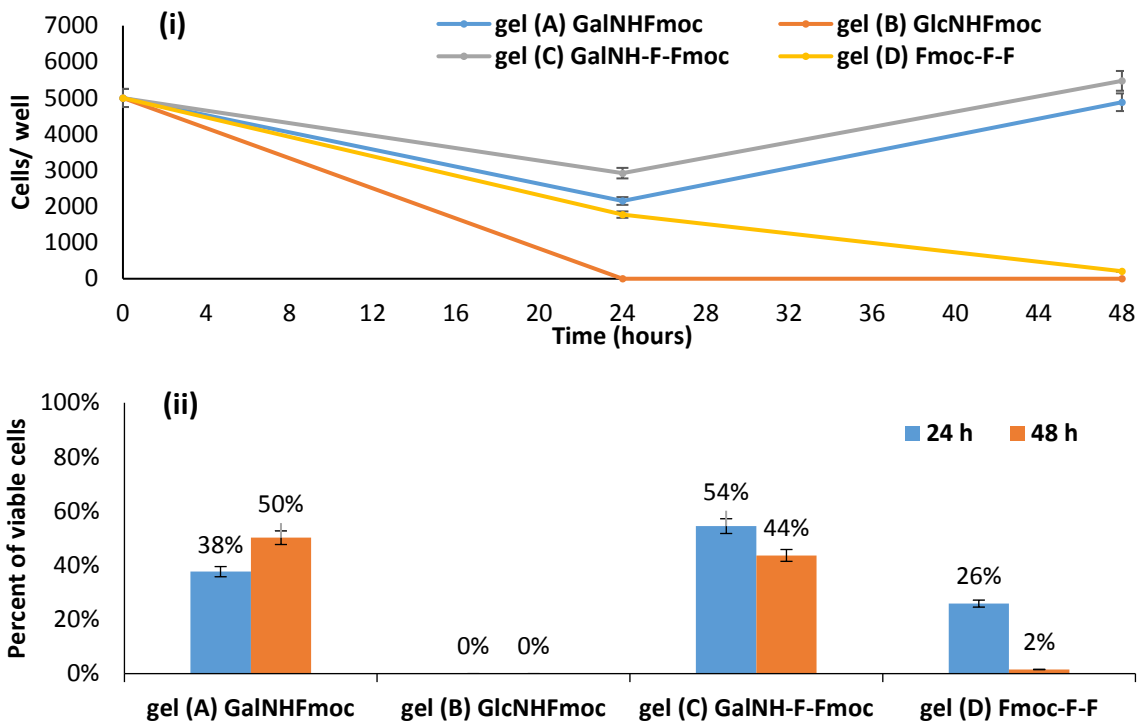

Figure 5.5 (i) Proliferation profiles and (ii) percentage of viable cells of hydrogel samples **A**-**D**. Measurements were performed after 24 and 48 hours of incubation using the standard MTS colorimetric assay.

Based on the obtained data, hydrogel **B** (GlcNHFmoc **63**) was the most cytotoxic since all cells died within 24 hours. Furthermore, hydrogels **A** and **C** (from GalNHFmoc **62** and GalNH-F-Fmoc **111**) showed differences in the percentage of viable cells after 24 and 48 hours. It was clear that, for hydrogel **A**, cell proliferation improved over the second day, in contrast to the behavior with hydrogel **C**. The results indicate that the structural differences of the hydrogelators and/or their resulting supramolecular scaffolds affected the microenvironment in which the cells were growing and thus directly affected their viability.

It is worth mentioning that for the hydrogelators, different gelation triggers can yield different modes of self-assembly, leading to different matrix topologies. Such variations in the supramolecular inner structure can potentially affect cell viability. For example, as reported by Ulijn *et al.*[20] an Fmoc-F-F **68** based hydrogel triggered by pH changes had a different biocompatibility profile for chondrocyte cells (high cell viability) compared to the above data regarding GBM cells (low cell viability). For the latter Fmoc-F-F gel **D**, in which gelation was triggered by sonication only, both viability and proliferation were disappointing for the GBM cells, especially after the second day when compared to the published data. Since different cell types can proliferate to a different extent, it would have been useful to

further evaluate these two key factors, *i.e.* the use of different cell types and different gelation triggers; however, such experiments were not performed due to limited resources.

Images of GBM cells were taken using an inverted light microscope (20x magnification) to correlate their morphology with the observed biocompatibility profiles for hydrogels **A**-**D**. Images were taken after 24 (**1**) and 48 (**2**) hours of incubation time (Figure 5.6). The untreated cells (positive control **P**), at both time intervals, adhered to the surface of the well and proliferated satisfactorily (**P_1, P_2**). For hydrogel **A**, the same elongated, star-shaped morphology shown by the positive control was observed; adhesion and proliferation were also present (**A_1, A_2**). However, this was not the case for hydrogel **B**, where spherical cells were present and appeared to be dead within 24 hours (**B_1, B_2**). Hydrogel **C**, even though favoring adhesion, did not support proliferation (viability 48 h < viability 24 h). Even so, no major differences were observed regarding the morphology of the cells (**C_1, C_2**), compared to the positive control (**P_1, P_2**). Furthermore, spherical cells were present in hydrogel **D** after the first 24 hours; these did not proliferate as confirmed by the cytotoxicity data (**D_1, D_2**) (Figure 5.6).

The next set of experiments were performed with hydrogels derived from the indomethacin and diclofenac containing compounds. Samples were prepared according to the appropriate gelation protocol for each gelator (see chapter 3) while GBM cancer cells were cultured under the same conditions as those used for the Fmoc-based set of hydrogels (Table 5.2).

Table 5.2 Hydrogels based on the indomethacin and diclofenac set of compounds. All hydrogels were prepared in water at a concentration of 3.0 mg/mL following the standard heating/cooling protocol (see chapter 3, section 3.2).

Compound	Gel
GalNH-Indomethacin **115**	**E**
GlcNH-Indomethacin **116**	**F**
GalNH-Diclofenac **113**	**G**
GlcNH-Diclofenac **114**	**H**

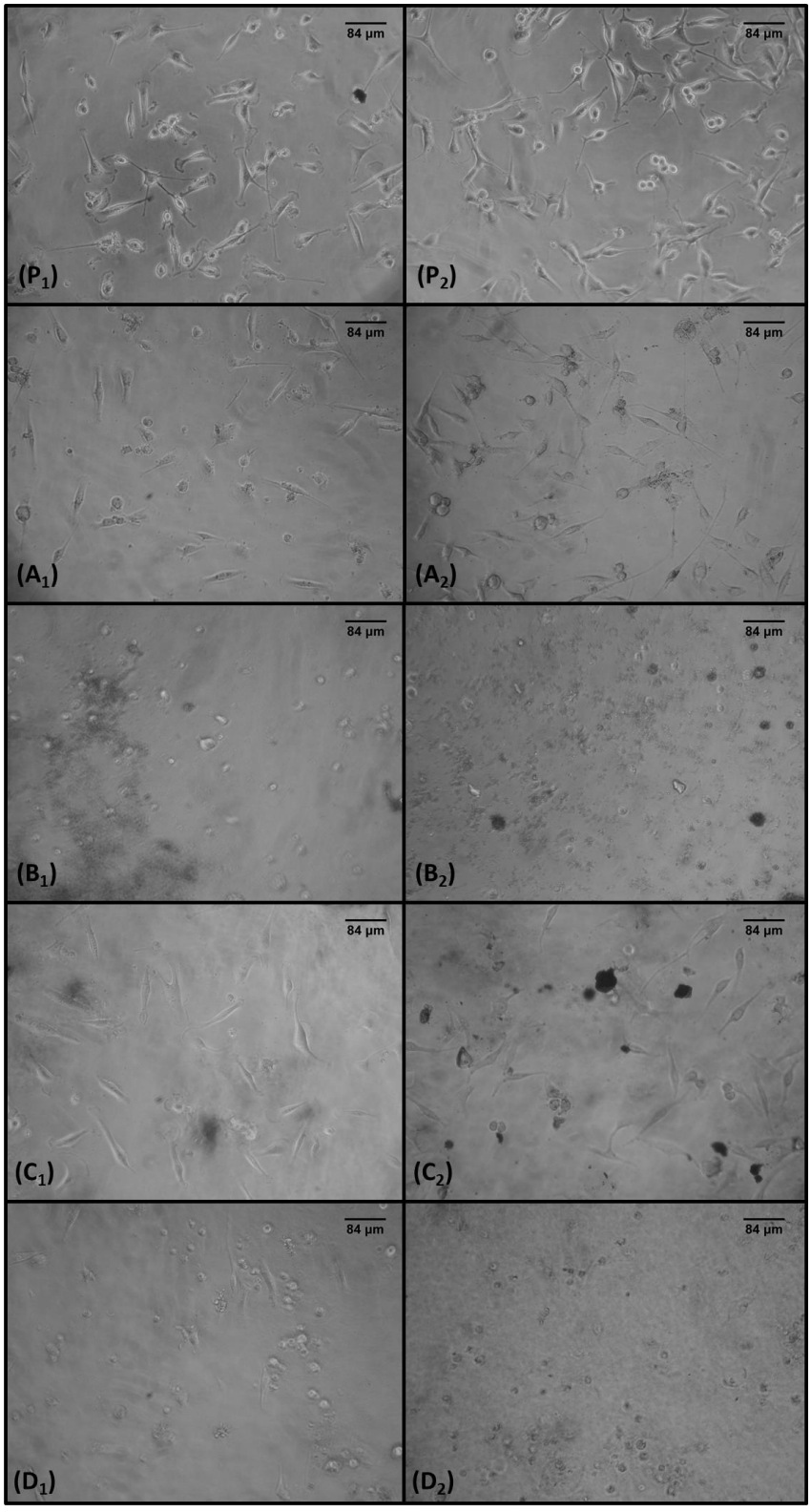

Figure 5.6 Morphology of GBM cells. Images were taken after 24 (1) and 48 (2) hours of incubation time. Positive control (**P**$_1$, **P**$_2$); GalNHFmoc hydrogel **A** (**A**$_1$, **A**$_2$); GlcNHFmoc hydrogel **B** (**B**$_1$, **B**$_2$); GalNH-F-Fmoc hydrogel **C** (**C**$_1$, **C**$_2$); Fmoc-F-F hydrogel **D** (**D**$_1$, **D**$_2$). Scale bars represent 84 µm. Images were processed using ImageJ software.

Both compounds bearing the indomethacin moiety (**115** and **116)**, yielded the corresponding self-supporting hydrogels **E** and **F** as confirmed by the vial inversion method. However, for the diclofenac-based compounds, hydrogel **H** (GlcNH-Diclofenac **114**) was a stiff self-supporting gel while hydrogel **G** (GalNH-Diclofenac **113**) was characterized as a viscous partial gel. From the data (Figure 5.7), it was clear that the indomethacin-based hydrogels **E** and **F** showed better cell viability and proliferation profiles compared to those based on diclofenac (**G** and **H**), which were more cytotoxic. Interestingly, an increase in proliferation was observed after the second day for hydrogel **E** compared with hydrogel **F**, even though its cytotoxicity was observed to be greater within the first 24 hours (Figure 5.7).

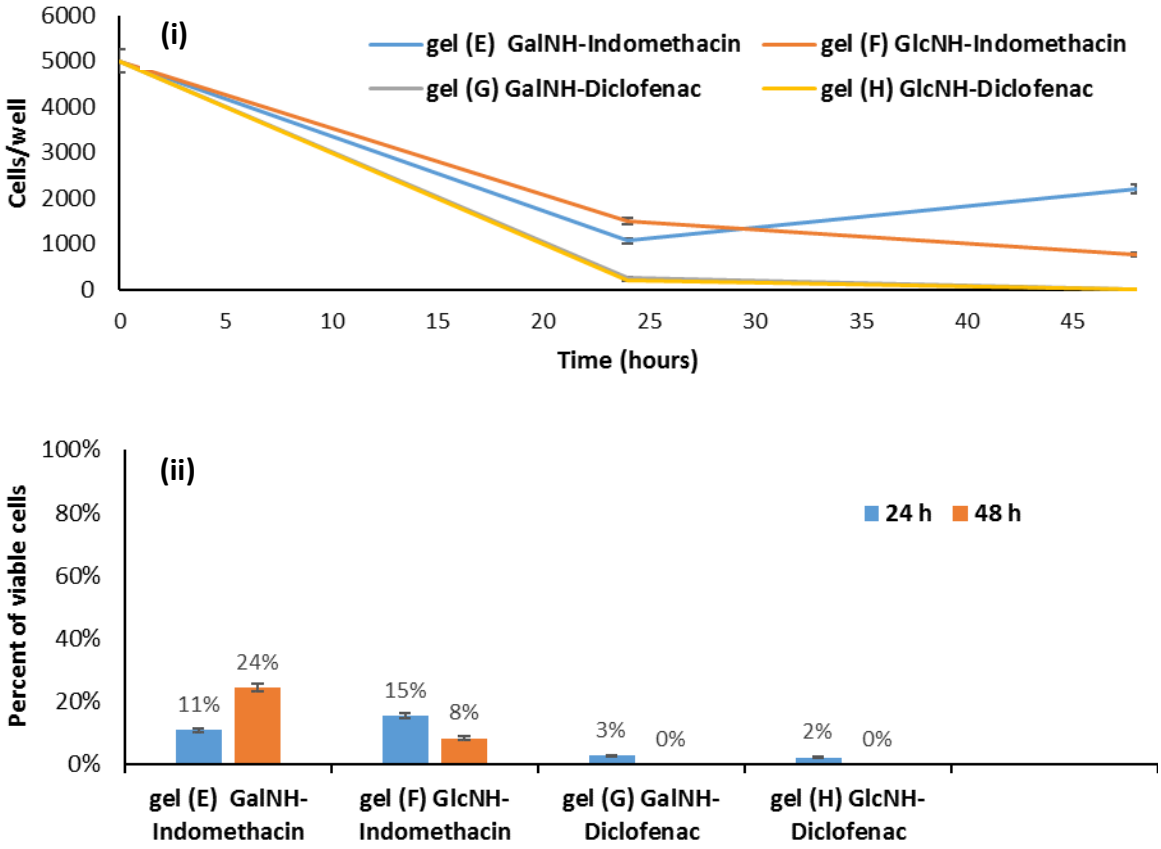

Figure 5.7 (i) Proliferation profiles and (ii) percentage of viable cells of hydrogel samples **E-H**. Measurements were performed after 24 and 48 hours of incubation time using the standard MTS colorimetric assay.

Such an observation suggests that, under the cell culture conditions used, the supramolecular network of sample **E** was not stable. Indeed, the increased ionic strength caused by the cell culture medium (contained salts), in addition to a high temperature (37 °C) could possibly induce swelling and breakage of the gels. Since these potential changes in the hydrogel's

matrix topology appeared to affect cell viability, such macroscopic alterations had to be explored further. Unfortunately, a shortage of materials (hydrogelators **113**, **114**, **115**, **116**) did not allow for any stability studies of hydrogel samples **E-H** to be undertaken in the given cell culture conditions. Finally, images of the treated cells were collected to compare their morphologies with those of the positive control and to identify potential changes from the normal phenotype (Figure 5.8).

Within the first 24 hours, GBM cells grown in sample hydrogel $\mathbf{E_1}$ were spherical in shape compared to untreated cells, while after the second day $\mathbf{E_2}$, as their population increased, their morphology more closely resembled that of the positive control. This observation suggested that from the initial trypsinized cells, those that survived adjusted to the microenvironment of hydrogel **E** and adhered to its surface. In addition, instead of the elongated star-shaped cells (untreated cells $\mathbf{P_1}$, $\mathbf{P_2}$), spherical cells which were much larger were present in sample $\mathbf{F_1}$ after the first day, compared to those observed after the second day $\mathbf{F_2}$. For the diclofenac-based hydrogels **G** and **H**, smaller spherical shaped cells were detected after both time intervals. Subsequently, within sample **H**, a network of small sharp rods was observed; these could be responsible for the cell death, as they could damage the membrane by puncturing/penetration. These rods could be potential crystals since addition of the cell medium on the gels could trigger crystallization. A similar case was reported for an Ind-F-F **69** based hydrogel where the presence of salts in the cell culture medium caused the breaking of the large fibres into sharp smaller proto-fibres causing cell apoptosis.[10,21]

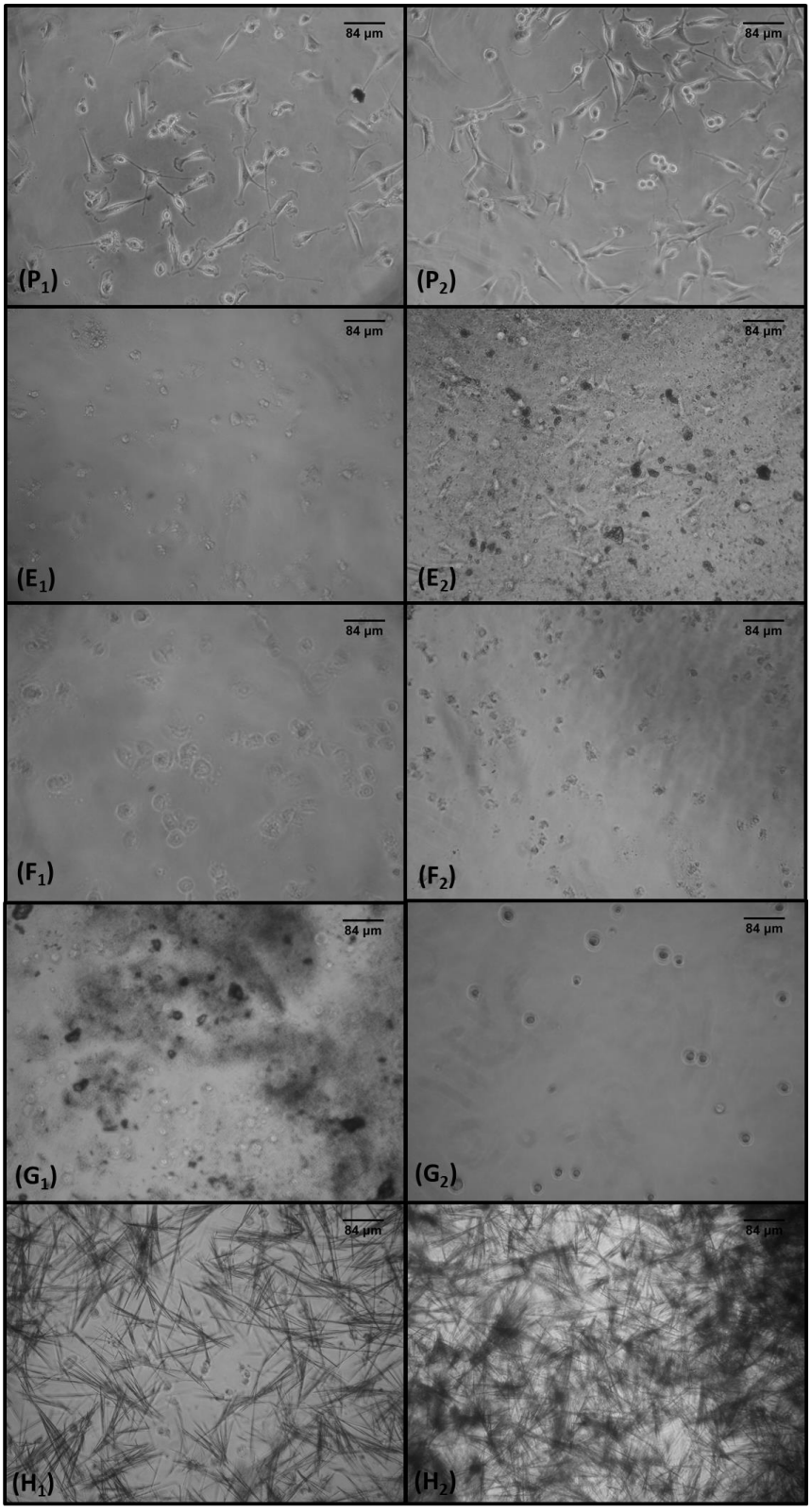

Figure 5.8 Morphology of GBM cells. Images were taken after 24 (1) and 48 (2) hours of incubation time. Positive control (**P1**, **P2**); GalNH-Indomethacin hydrogel (**E1**, **E2**); GlcNH-Indomethacin hydrogel (**F1**, **F2**); GalNH-Diclofenac hydrogel (**G1**, **G2**); GlcNH-Diclofenac hydrogel (**H1**, **H2**). Scale bars represent 84µm. Images were processed using ImageJ software.

Before commencing tests on the last set of hydrogels, a concentration-based cytotoxicity study was undertaken for compound Cin-F-F **70**. Since **70** was soluble in DMSO, serial dilutions of the initial stock solution with PBS resulted in solutions within the permitted range of concentrations for cytotoxicity studies (0.05-0.5 mM) (Table 5.3). These tests aimed to identify the maximum concentration at which GBM cells could remain alive for 48 hours under the given cell culture conditions.

Table 5.3 Cin-F-F **70** solutions in PBS/DMSO. The final concentration of DMSO is less than 1% v/v. Solutions (ii) and (iii) are within the permitted range of concentrations whereas solution (i) is intentionally more concentrated.

Solution of Cin-F-F 70	**Concentration (% w/v)**	**Concentration (mM)**
(i)	0.1	2.26
(ii)	0.01	0.23
(iii)	0.001	0.023

For each sample solution (i-iii), the standard colorimetric assay (MTS) was used to evaluate cell viability (Figure 5.9), while a live-dead assay (fluorescence microscopy) was undertaken to confirm the obtained results (Figures 5.10 and 5.11). Measurements taken after 24 and 48 hours of incubation indicated that sample solution (i) was cytotoxic in comparison to samples (ii) and (iii), in which cell viability was > 80%. It should be noted that the decrease in cell viability after 48 hours for samples (ii) and (iii) can be attributed to the small surface area of the 96-well flat-bottomed plate used. Additionally, no differences in cell morphology were observed within 48 hours.

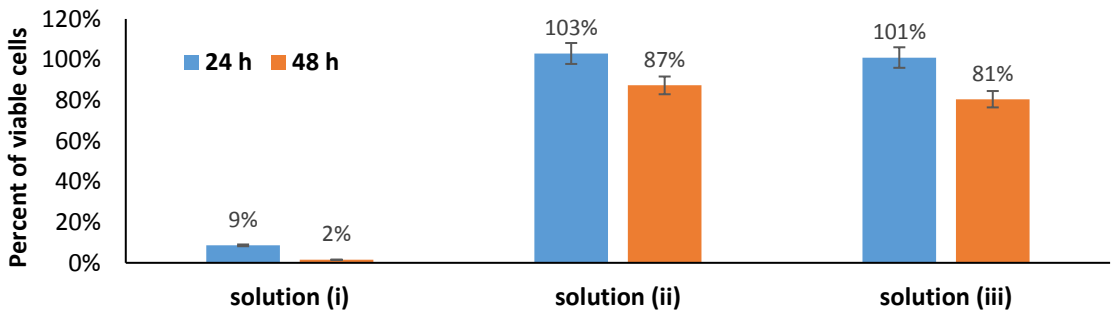

Figure 5.9 Percentage of viable cells for sample solutions (i)-(iii).

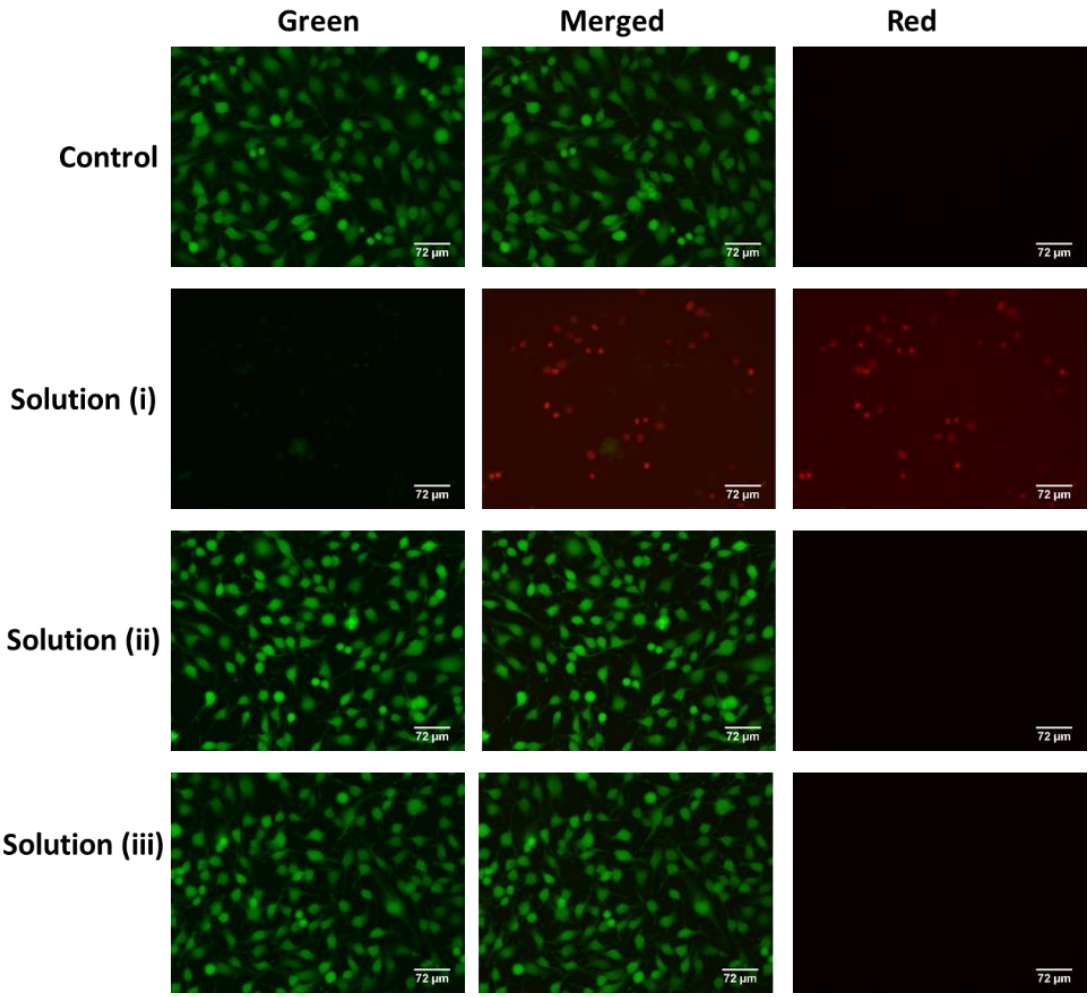

Figure 5.10 Comparison of solutions (i)-(iii) after 24 hours of incubation time. Green staining indicates live cells and red staining indicates dead cells. Scale bar represents 72 µm. Images were processed using ImageJ software.

Hydrogel samples of gelator Cin-F-F **70** (hydrogel **I**) and its epimeric mixture Cin-D/L-F-L-F **70/93** (hydrogel **J**) were prepared in PBS solution using the same concentration and following the gelation protocols shown in Table 5.4.

Table 5.4 Hydrogels based on Fmoc-F-F **68**, Cin-F-F **70** and the epimeric mixture Cin-D/L-F-L-F **70/93**. All hydrogels were prepared in PBS solution at a concentration of 2.0 mg/mL following the appropriate gelation protocol for each compound (see chapter 3, section 3.2).

Compound	Gelation method	Gel
Fmoc-F-F	Sonication only	**D**
Cin-F-F	Heating/sonication	**I**
Cin-D/L-F-L-F	Heating/sonication	**J**

Cytotoxicity experiments were aimed at the detection of potential differences in the biocompatibility profiles of hydrogel samples **I** and **J** due to the different stereochemistries of their building blocks. In addition, comparing the data obtained with those of hydrogel **D** (from Fmoc-F-F **68**) might explain differences in cell viability resulting from the substitution of the Fmoc group by the cinnamoyl moiety. According to the obtained viability and proliferation data, all three gels were highly cytotoxic (Figure 5.12).

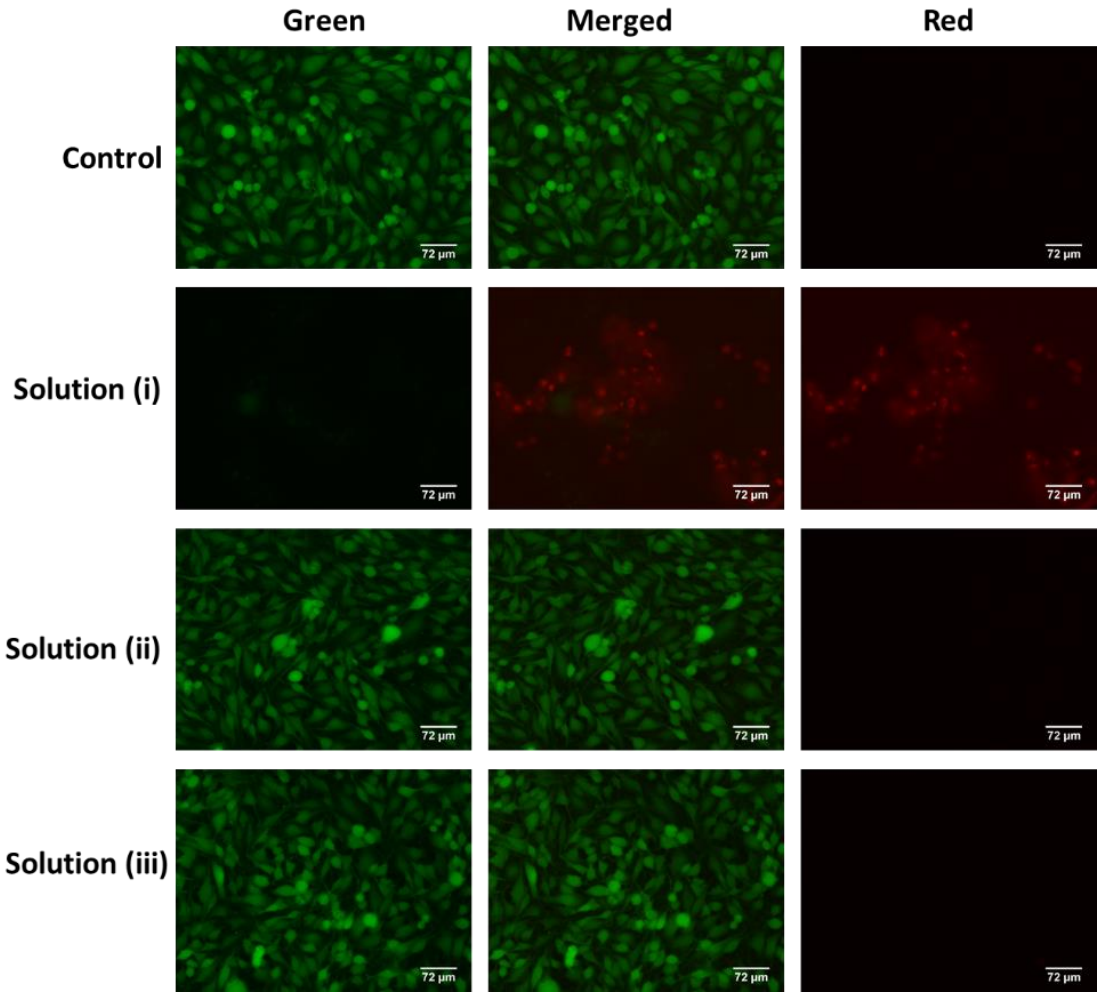

Figure 5.11 Comparison of solutions (i)-(iii) after 48 hours of incubation time. Green staining indicates live cells and red staining indicates dead cells. Scale bar represents 72 µm. Images were processed using ImageJ software.

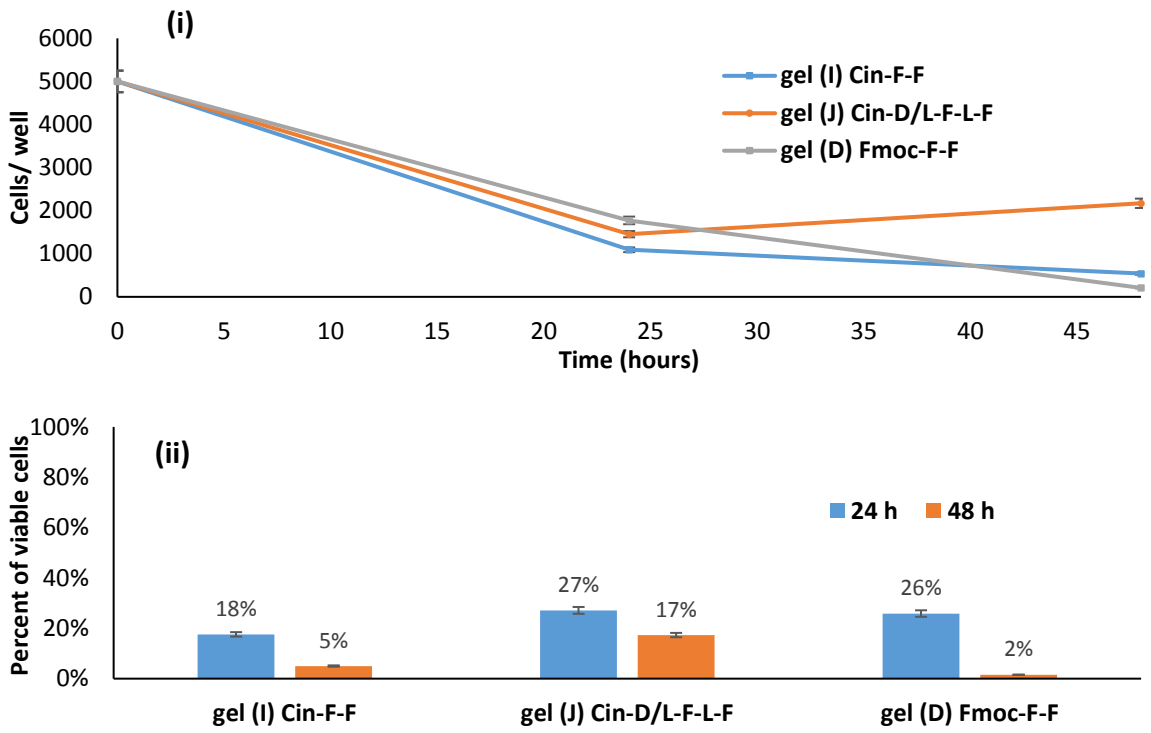

Figure 5.12 (i) Proliferation profiles and (ii) percentage of viable cells of hydrogel samples (**I**, **J** and **D**). Measurements were performed after 24 and 48 hours of incubation time using the standard MTS colorimetric assay.

In all cases, the lowest percentage of viable cells was observed after 48 hours of incubation. A difference in cytotoxicity between day one and day two was more intense for hydrogels **D** (from Fmoc-F-F **68**) and **I** (from Cin-F-F **70**), but not for hydrogel **J** (from Cin-D/L-F-L-F **70/93**). It was clear that the stereochemical differences of the cinnamoyl-based building blocks affected the hydrogels' cytotoxicity. The microenvironment in which the cells were growing was not the same in samples **I** and **J**, presumably because their supramolecular systems were different. This was also supported by comparison of the SEM images of their xerogels (see chapter 3, section 3.3). The substitution of the Fmoc moiety by cinnamic acid affected the viability of cells, as can be seen after 48 hours of incubation. This observation suggests that by introducing structural changes on the gelator scaffold, it may be possible to control their biocompatibility.

Images of treated cells were collected under an inverted light microscope for evaluation of their morphology (Figure 5.13). For all three hydrogels (**I**, **J** and **D**), spherical cells (indicative of dead cells) were observed which were different in size. Sample **J** encapsulated the biggest cells compared to the other two samples. Cell clusters were present in sample **I**, while in the other two gels, the cells appeared to be almost evenly dispersed (Figure 5.13).

For the enantiopure hydrogel **I** a live-dead assay (fluorescence microscopy) was performed to verify the colorimetric assay data (MTS) reported above. Therefore, the same procedure was followed regarding sample preparation, cell seeding and incubation conditions as described previously. The data obtained were reproducible and verified cell apoptosis after both time intervals, as shown below (Figure 5.14).

The data revealed that Cin-F-F **70** solution was cytotoxic above 0.23 mM. However, the minimum gelation concentration required to prepare its corresponding hydrogel **I** is 2.0 mg/mL (4.5 mM) which is above the given "biocompatible concentration value". This suggests that the increased concentration of Cin-F-F **70** is responsible for the cell apoptosis observed. It is of note that in the gel state the free hydrogelator **70** concentration is not actually 4.5mM but a much smaller number as the rest is tied up (albeit dynamically) in the supramolecular assembly.

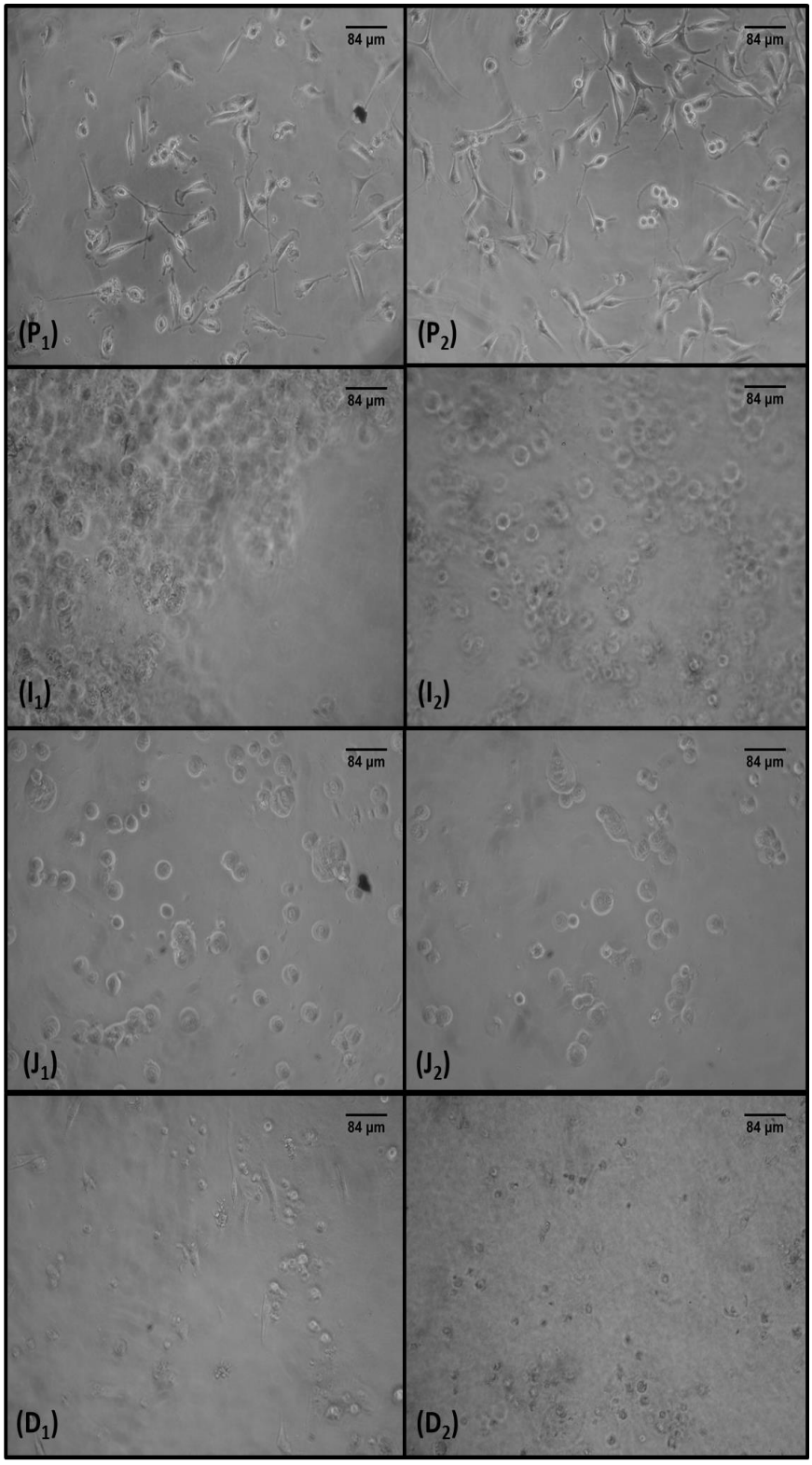

Figure 5.13 Morphology of GBM cells. Images were taken after 24 (1) and 48 (2) hours of incubation time. Positive control (**P**$_1$, **P**$_2$); Cin-F-F hydrogel (**I**$_1$, **I**$_2$); Cin-D/L-F-L-F hydrogel (**J**$_1$, **J**$_2$); Fmoc-F-F hydrogel (**D**$_1$, **D**$_2$). Scale bar represents 84 µm. Images were processed using ImageJ software.

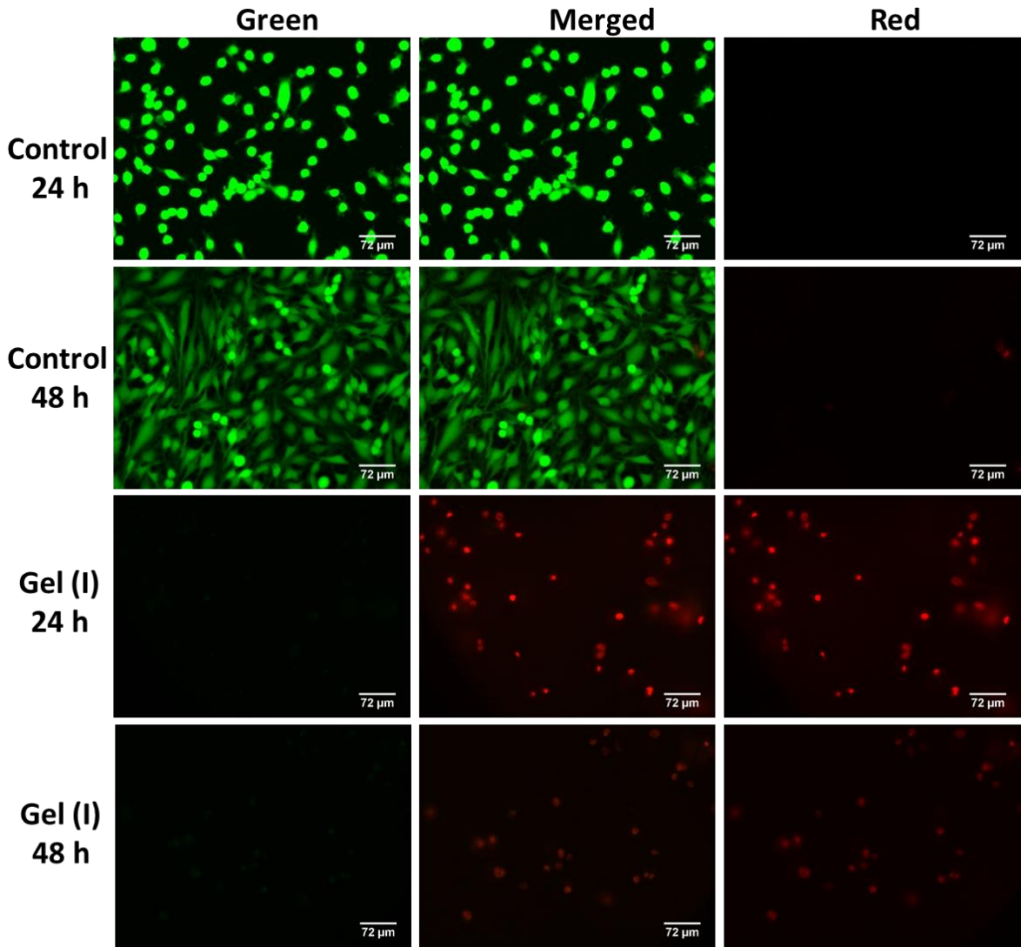

Figure 5.14 Comparison of hydrogel **I** cytotoxicity profiles after 24 and 48 hours of incubation time. Green staining indicates live cells and red staining indicates dead cells. Scale bar represents 72 µm. Images were processed using ImageJ software.

5.5 Conclusions

In all cases, the percentage of viable cells was below 80% after 24 and 48 hours of incubation, indicating that all the hydrogels **A**-**J** were cytotoxic. A question that arises is what might be responsible for the high cytotoxicity? The compounds themselves or their supramolecular networks? Unfortunately, the hydrogelators' poor solubility did not allow the performance of concentration-based cytotoxicity studies, except in the case of compound Cin-F-F **70** which was soluble in DMSO.

In addition, the self-assembly for all hydrogel samples was disrupted as they were pipetted from their vials into the wells prior to seeding with cells. The presence of fibres in each well was unquestionable, however, under the described cell culture conditions, the gels were expected to swell and yield viscous solutions containing both intact and broken fibres,

undissolved salts (present in cell medium) and gelator molecules. The increased cell viability observed after 48 hours of incubation with the GalNHFmoc hydrogel **A** (50%) and the decreased cell viability observed with the GalNH-F-Fmoc hydrogel **C** (44%) indicate that any potential changes in the gel's supramolecular network could affect the cell viability.

Further investigation is required into the influence of the sample handling and preparation with respect to the cell viability and proliferation. The detection of any potential architectural alterations of the gel samples under the given incubation conditions also needs to be evaluated. Finally, repeating the experiments by using a series of different cell lines (*i.e.* adherent and non-adherent cells) would reveal if the cytotoxicity exhibited by the gels is cell specific.

5.6 References

(1) Newcomb, C. J.; Sur, S.; Ortony, J. H.; Lee, O.-S.; Matson, J. B.; Boekhoven, J.; Yu, J. M.; Schatz, G. C.; Stupp, S. I. Cell Death versus Cell Survival Instructed by Supramolecular Cohesion of Nanostructures. *Nat. Commun.* **2014**, *5*, 1-10.

(2) Collier, J. H.; Messersmith, P. B. Self-Assembling Polymer-Peptide Conjugates: Nanostructural Tailoring. *Adv. Mater.* **2004**, *16* (11), 907-910.

(3) O'Leary, L. E. R.; Fallas, J. A.; Bakota, E. L.; Kang, M. K.; Hartgerink, J. D. Multi-Hierarchical Self-Assembly of a Collagen Mimetic Peptide from Triple Helix to Nanofibre and Hydrogel. *Nat. Chem.* **2011**, *3* (10), 821-828.

(4) Hartgerink, J. D. Self-Assembly and Mineralization of Peptide-Amphiphile Nanofibers. *Science (80-.).* **2001**, *294* (5547), 1684-1688.

(5) Pashuck, E. T.; Cui, H.; Stupp, S. I. Tuning Supramolecular Rigidity of Peptide Fibers through Molecular Structure. *J. Am. Chem. Soc.* **2010**, *132* (17), 6041-6046.

(6) Goldberger, J. E.; Berns, E. J.; Bitton, R.; Newcomb, C. J.; Stupp, S. I. Electrostatic Control of Bioactivity. *Angew. Chemie - Int. Ed.* **2011**, *50* (28), 6292-6295.

(7) Sur, S.; Newcomb, C. J.; Webber, M. J.; Stupp, S. I. Tuning Supramolecular Mechanics to Guide Neuron Development. *Biomaterials* **2013**, *34* (20), 4749-4757.

(8) Miwa, M.; Ura, M.; Nishida, M.; Sawada, N.; Ishikawa, T.; Mori, K.; Shimma, N.; Umeda, I.; Ishitsuka, H. Design of a Novel Oral Fluoropyrimidine Carbamate,

Capecitabine, Which Generates 5 Fluorouracil Selectively in Tumours by Enzymes Concentrated in Human Liver and Cancer Tissue. *Eur. J. Cancer* **1998**, *34* (8), 1274-1281.

(9) Guichard, S. M.; Macpherson, J. S.; Mayer, I.; Reid, E.; Muir, M.; Dodds, M.; Alexander, S.; Jodrell, D. I. Gene Expression Predicts Differential Capecitabine Metabolism, Impacting on Both Pharmacokinetics and Antitumour Activity. *Eur. J. Cancer* **2008**, *44* (2), 310-317.

(10) Martin, A. D.; Robinson, A. B.; Mason, A. F.; Wojciechowski, J. P.; Thordarson, P. Exceptionally Strong Hydrogels through Self-Assembly of an Indole-Capped Dipeptide. *Chem. Commun.* **2014**, *50* (98), 15541-15544.

(11) Storrie, H.; Guler, M. O.; Abu-Amara, S. N.; Volberg, T.; Rao, M.; Geiger, B.; Stupp, S. I. Supramolecular Crafting of Cell Adhesion. *Biomaterials* **2007**, *28* (31), 4608-4618.

(12) Zhou, M.; Smith, A. M.; Das, A. K.; Hodson, N. W.; Collins, R. F.; Ulijn, R. V.; Gough, J. E. Self-Assembled Peptide-Based Hydrogels as Scaffolds for Anchorage-Dependent Cells. *Biomaterials* **2009**, *30* (13), 2523-2530.

(13) Tan, J.; Gemeinhart, R. A.; Ma, M.; Mark Saltzman, W. Improved Cell Adhesion and Proliferation on Synthetic Phosphonic Acid-Containing Hydrogels. *Biomaterials* **2005**, *26* (17), 3663-3671.

(14) Caliari, S. R.; Burdick, J. A. A Practical Guide to Hydrogels for Cell Culture. *Nat. Methods* **2016**, *13* (5), 405-414.

(15) Hunt, N. C.; Grover, L. M. Cell Encapsulation Using Biopolymer Gels for Regenerative Medicine. *Biotechnol. Lett.* **2010**, *32* (6), 733-742.

(16) Lister, Z.; Rayner, K. J.; Suuronen, E. J. How Biomaterials Can Influence Various Cell Types in the Repair and Regeneration of the Heart after Myocardial Infarction. *Front. Bioeng. Biotechnol.* **2016**, *4* (July), 62, 1-17.

(17) Pires, R. A.; Abul-Haija, Y. M.; Costa, D. S.; Novoa-Carballal, R.; Reis, R. L.; Ulijn, R. V.; Pashkuleva, I. Controlling Cancer Cell Fate Using Localized Biocatalytic Self-Assembly of an Aromatic Carbohydrate Amphiphile. *J. Am. Chem. Soc.* **2015**, *137*

(2), 576-579.

(18) Ananthanarayanan, B.; Kim, Y.; Kumar, S. Elucidating the Mechanobiology of Malignant Brain Tumors Using a Brain Matrix-Mimetic Hyaluronic Acid Hydrogel Platform. *Biomaterials* **2011**, *32* (31), 7913-7923.

(19) Wang, C.; Tong, X.; Yang, F. Bioengineered 3D Brain Tumor Model To Elucidate the E Ff Ects of Matrix Sti Ff Ness on Glioblastoma Cell Behavior Using PEG-Based Hydrogels. *Mol. Pharm.* **2014,** *11*, 2115-2125.

(20) Jayawarna, V.; Ali, M.; Jowitt, T. A.; Miller, A. F.; Saiani, A.; Gough, J. E.; Ulijn, R. V. Nanostructured Hydrogels for Three-Dimensional Cell Culture through Self-Assembly of Fluorenylmethoxycarbonyl-Dipeptides. *Adv. Mater.* **2006**, *18* (5), 611-614.

(21) Sagnella, S. M.; Conn, C. E.; Krodkiewska, I.; Moghaddam, M.; Drummond, C. J. Endogenous Nonionic Saturated Monoethanolamide Lipids: Solid State, Lyotropic Liquid Crystallineand Solid Lipid Nanoparticle Dispersion Behavior. *J. Phys. Chem. B* **2010**, *114* (4), 1729-1737.

6. CONCLUSIONS AND FUTURE WORK

The PhD research project focused on the development of novel LMW hydrogels as functional biomaterials with potential for tissue culture application. Several LMW compounds were synthesized and their gelation behaviour was assessed – this led to identification of new hydrogelators and improved synthesis and gelation of known hydrogelators. Different gelation protocols were tested and various techniques were employed to characterize the properties of the materials obtained. Since the main findings are described in detail within specific chapters of the current thesis, this section summarizes the obtained outcomes and suggests future experimental work.

A set of structurally related compounds was synthesized as described in **chapter 2**. Based on their structural features, the three sets of potential hydrogelators were classified as fluorenylmethyloxycarbonyl (Fmoc-), biotinylated and diphenylalanine analogues. Further material of the known hydrogelators **62** and **63** was prepared. The Fmoc-protected glycopyranosylamine compounds **64** and **65** were obtained in 26% and 19% yield respectively over three steps. The biotinylated derivatives of galactosamine **66** (36% yield) and glucosamine **67** (90% yield) were synthesized over one step by coupling biotin with the corresponding amino sugars. The cinnamoyl-capped diphenylalanine **70** was obtained in 29% yield over four steps while a different synthetic route led to the formation of the epimeric mixture **70-93** in a 2:1 ratio. Finally, the indole-protected analogue **69** couldn't be purified.

The amphiphilic nature of the synthesized compounds resulted in a challenging isolation and purification process. Therefore, for the carbohydrate derivatives it is proposed to alter the synthetic protocols employed and introduce certain protecting groups on the sugar moiety to achieve better solubility and thus ease purification. In addition, methylation of the anomeric OH group could yield pure anomers allowing evaluation of potential anomeric effects towards the self-assembly process, if the methyl glycosides are successful gelators.

During the synthesis of the diphenylalanine derivatives **70** and **69** both epimerization and purification issues had to be addressed. Hence, a new synthetic approach would form the salts instead of the free acids of **70** and **69** which could ease purification. Acidification of the obtained salts would yield eventually the free acids. Alternatively, a solid phase synthesis instead of a solution phase would hinder formation of epimers and lead to better yields.

Chapter 3 describes a variety of techniques to assess gelation and evaluate the properties of the hydrogels. From the findings it was clear that structural changes of the gelator molecules affected both gelation success and the properties of the formed materials. Further to this, by employing different gelation triggers for a single compound, different materials were formed.

The epimeric compounds GalNHFmoc **62** and GlcNHFmoc **63** yielded hydrogels with different properties. In addition, by changing the position of the Fmoc group on the sugar scaffold (analogues **64** and **65**) gelation was found to be unsuccessful. Incorporation of the biotin group instead of the aromatic Fmoc moiety (compounds **66** and **67**) was also found to not support gelation despite previous results by a colleague. Different gelation triggers resulted in different materials as studies of Fmoc-F-F **68** hydrogelator verified. This was also seen when using different solvent for gelation *i.e.* GalNHFmoc **62** in water and PBS solution since the corresponding hydrogels showed spectral differences by CD. Finally, incorporation of cinnamic acid instead of the Fmoc moiety to the diphenylalanine scaffold, resulted in the Cin-F-F **70** analogue which hydrogel had altered macroscopic and microscopic properties compared to **68**. Further to this, the epimeric mixture **70-93** yielded a hydrogel with different properties to the hydrogel originated from enantiopure **70**.

Optimization of sample preparation and handling allowed CD studies to be performed in a manner that avoided any possible alteration of the supramolecular structure of the gels. Further optimization though is needed to preserve self-assembly while acquiring IR, NMR and fluorescence data. Additionally, in-depth rheology studies should be employed to explore reversibility of the gel-sol process in addition to effect of concentration on stiffness. *In silico* studies based on the obtained XRD data could also provide valuable information regarding the orientation and configuration of hydrogelator **70** within the formed supramolecular network. Finally, it would be interesting to assess gelation of the given compounds by pH change and by solvent switch methodologies.

The current work contributed to the establishment of a protocol for the evaluation of LMW hydrogels by SRCD spectroscopy, which was recently published. The aims of the research, as described in **chapter 4** were (i) the optimization of hydrogel preparation for SRCD analysis, (ii) the identification of potential optical artefacts (LD and LB), (iii) the comparison of conventional CD and SRCD spectroscopy, (iv) the evaluation of sample homogeneity, (v) the exploration of possible disruption of the hydrogel samples due to SRCD beam light and

(vi) the evaluation of sol-gel reversibility. Due to time restrictions spectra were not assessed for potential circular birefringence (CB) artefacts. Therefore, acquisition of CD spectra at two different orientations (0° and 180°) over a single spot needs to be undertaken. Further to this, to better facilitate future studies, new experimental procedures will need to be developed for the detailed X-Y mapping of the gels, in order to map more effectively sample sites adjacent to the cuvette wall.

A preliminary biocompatibility study of the formed hydrogels is described in **chapter 5.** To assess cytotoxicity of hydrogelators, a concentration-based study was attempted. However, their amphiphilic nature resulted in poor solubility within a given range of permitted concentrations. Therefore, to evaluate if their supramolecular network was cytotoxic, broken hydrogels were used. The findings showed that all hydrogels were cytotoxic since the percentage of viable cells was below 80% after 24 and 48 hours of incubation.

In contrast to the 96-well flat bottom plate, experiments need to be repeated using cell culture plates with inserts. Preparation of hydrogels in inserts has been already evaluated and found to yield self-supporting hydrogels. Additionally, exploring potential alterations of the self-assembly under the given cell culture conditions could prove fundamental for cell viability. Hydrogels are dynamic systems and therefore behave differently under different conditions. Therefore, gelation of hydrogelators using cell culture medium containing cells should be performed. This will allow evaluation of cell viability within 3D cultures in comparison to 2D cultures. Finally, the experiments need to be repeated using a series of different cell lines (*i.e.* adherent and non-adherent cells) to explore if cytotoxicity is exhibited by the gels or is cell specific.

Overall, the work presented herein has significantly progressed research endeavours in the field of LMW hydrogelators and has established methodologies which can be followed for synthesis of the hydrogelators reported herein and developed and optimised methods for characterisation of the corresponding materials. Perhaps most significantly, the stability studies and preliminary biocompatibility studies has established the basis from which progress can be made towards cell culture application.